UNIVERSITAT POLITÈCNICA DE VALÈNCIA

DEPARTAMENTO DE TECNOLOGÍA DE ALIMENTOS

CENTRO DE RECONOCIMIENTO MOLECULAR Y DESARROLLO TECNOLÓGICO

Encapsulation of Folic Acid in Mesoporous Silica Supports: A Nutritional and Technological Approach

PhD THESIS

Submitted by

Édgar Pérez Esteve

PhD Supervisors:

Prof. José Manuel Barat Baviera
Prof. Ramón Martínez Máñez

Valencia, November 2015

JOSÉ MANUEL BARAT BAVIERA, PhD in Food Technology and Professor at the *Universitat Politècnica de València*, and RAMÓN MARTÍNEZ MÁÑEZ, PhD in Chemistry and Professor at the *Universitat Politècnica de València*

CERTIFY:

That the work *"***Encapsulation of Folic Acid in Mesoporous Silica Supports: A Nutritional and Technological Approach"** has been developed by Édgar Pérez Esteve under their supervision in the Departamento de Tecnología de Alimentos and the Centro de Reconocimiento Molecular y Desarrollo Tecnológico (IDM) of the *Universitat Politècnica de València*, as a Thesis Project in order to obtain the degree of PhD in Food Technology at the *Universitat Politècnica de València.*

Valencia, 2nd November 2015.

Prof. José Manuel Barat Baviera Prof. Ramón Martínez Máñez

“Si puedes soñarlo, puedes hacerlo”

Walt Disney

Acknowledgements

Agradecimientos

Una vez leí:
"Si quieres llegar rápido viaja solo;
si quieres llegar lejos viaja acompañado".
A partir de ese momento escogí viajar acompañado. Por eso, llegados al final de este viaje sólo puedo estar agradecido por todos los que de una manera u otra han viajado conmigo en ésta, mi gran aventura.

Me gustaría expresar mis más sinceros agradecimientos a mis directores de tesis, **José Manuel Barat** y **Ramón Martínez**, por ofrecerme la oportunidad de trabajar en una línea de investigación tan innovadora e interesante. Muchas gracias por vuestras enseñanzas, dedicación y apoyo.

Agradezco también todo el tiempo dedicado por los profesores **Félix Sancenón** y **Loles Marcos**. Sin esperar nada a cambio, siempre habéis tenido tiempo para responder todas mis dudas de nutricionista que necesitaba saber de química.

Gracias a **Ana Fuentes** por acogerme desde el primer día y por enseñarme que la ciencia no es nuestro trabajo, es nuestro idioma.

Gracias a **Harmen H. J. de Jongh** por abrirme las puertas de su grupo de investigación en la Universidad de Wageningen para poder realizar la estancia de investigación.

Gracias como no a los **compañeros y compañeras** de todos estos años. Juntos hemos aprendido, crecido, avanzado, pero sobre todo compartido el verdadero valor de la amistad. Sabéis quienes sois; no necesitáis que os nombre.

Gracias a todos los que habéis participado activamente en el trabajo presentado en esta tesis. En especial gracias a **Andrea Bernardos** y **María Ruiz** por haberme permitido trabajar con vosotras como si sólo fuéramos uno. A **José A. Espino** por su creatividad y cariño puesto para ilustrar esta tesis y su portada.

A todos mis **amigos** por estar siempre ahí, por escucharme en los momentos de agobio y por acompañarme en la celebración de los éxitos.

Por último gracias a mi **familia**, porque aunque a veces no entendáis este mundo de la investigación, con cada gesto de apoyo hacia lo que hago permitís que siga adelante.

Resumen

La presente tesis doctoral que lleva por título “Encapsulación de ácido fólico en soportes porosos de óxido de silicio: una aproximación nutricional y tecnológica” está centrada en el desarrollo de nuevos sistemas inteligentes de liberación controlada de ácido fólico para aplicaciones nutricionales.

La primera parte de la tesis muestra la encapsulación de ácido fólico en matrices porosas de óxido de silicio funcionalizadas con poliaminas desde una aproximación nutricional. En ella se ha evaluado la influencia del método de cargado y del tipo de soporte de óxido de silicio utilizado (MCM-41, SBA-15, UVM-7 y Hollow Silica) en la eficacia de encapsulación de ácido fólico. En esta primera parte, también se ha evaluado la influencia de la morfología y el sistema de poros de los diferentes soportes en el perfil de liberación del ácido fólico desde los mismos. Los estudios de liberación de ácido fólico desde los diferentes soportes a diferentes valores de pH han demostrado que los sistemas diseñados son capaces de modular inteligentemente la liberación de ácido fólico en función del pH del medio (inhibición de la liberación a pH ácido -estómago-; liberación controlada a pH neutro -intestino-).

Esta capacidad convierte a los sistemas liberación desarrollados en una alternativa excelente a la fortificación directa para modular exitosamente la bioaccesibilidad del ácido fólico a lo largo del tracto gastrointestinal. Por otra parte, se ha evaluado la estabilidad de los soportes durante un proceso de digestión *in vitro*, demostrando que si bien algunos soportes pueden ser atacados durante la digestión, la funcionalización con moléculas que actúan como puertas moleculares previene dicho ataque. Por último, los estudios de viabilidad celular llevados a cabo en cuatro tipos de líneas celulares demuestran que ni los soportes, ni los productos de degradación de los mismos durante el proceso de digestión *in vitro* promueven ningún tipo de toxicidad inespecífica.

Resumen

En la segunda parte se ha evaluado la influencia de la adición de diferentes soportes de óxido de silicio a dos matrices alimentarias, geles de gelatina y yogures. Esta aproximación tecnológica ha permitido conocer que la capacidad de estos sistemas inteligentes para liberar controladamente el ácido fólico a lo largo de un proceso de digestión *in vitro* se mantiene incluso tras su incorporación en yogures batidos. Por otra parte, se ha comprobado que el efecto de las matrices sobre las propiedades físicas de los geles, es dependiente tanto del tamaño de las partículas, como de su funcionalización y concentración. Por último, se ha comprobado que debido a la optimización del cargado de ácido fólico alcanzada en la primera parte de la tesis, se puede lograr una fortificación de un yogur con el 100% de la cantidad diaria recomendada de ácido fólico con una cantidad tan pequeña de sistema que ni las propiedades físico-químicas del yogur, ni la viabilidad bacteriana se ven comprometidas.

En resumen, se puede concluir que la presente tesis ha abordado de una manera global la encapsulación de ácido fólico en matrices porosas de óxido de silicio para ser utilizados en aplicaciones nutricionales incluyendo estudios de optimización de cargado, estudios de liberación en función del pH, digestiones *in vitro*, estudios de estabilidad de las matrices utilizadas, estudios de biocompatibilidad, así como estudios de la influencia de la adición de estos sistemas inteligentes en matrices alimentarias. Los resultados obtenidos han puesto de manifiesto que los sistemas inteligentes de liberación de ácido fólico desarrollados abren la puerta a una nueva manera de fortificar los alimentos sin comprometer sus características físico-químicas.

Resum

La present tesi doctoral, que porta per títol "Encapsulació d'àcid fòlic en suports porosos d'òxid de silici: una aproximació nutricional i tecnològica" està centrada en el desenvolupament de nous sistemes intel·ligents d'alliberament controlat d'àcid fòlic per a aplicacions nutricionals.

La primera part de la tesi mostra l'encapsulació d'àcid fòlic en matrius poroses d'òxid de silici funcionalitzades amb poliamines des d'una aproximació nutricional. En esta part, s'ha avaluat la influència del mètode de carrega i del tipus de suport d'òxid de silici que s'ha emprat (MCM-41, SBA-15, UVM-7 i Hollow Silica) en l'eficàcia de l'encapsulació d'àcid fòlic. En esta primera part, també s'ha avaluat la influència de la morfologia i el sistema de porus dels diferents suports en el perfil d'alliberament de l'àcid fòlic des dels mateixos. Els estudis d'alliberament d'àcid fòlic des dels diferents suports a diferents valors de pH han demostrat que els sistemes dissenyats són capaços de modular intel·ligentment l'alliberament d'àcid fòlic en funció del pH del medi (inhibició de l'alliberament a pH àcid -estómac-; alliberament controlat a pH neutre -intestí-).

Esta capacitat fa dels sistemes desenvolupats una excel·lent alternativa a la fortificació directa per a modular amb èxit la bioaccessibilitat de l'àcid fòlic a través del tracte gastrointestinal. D'altra banda, s'ha avaluat l'estabilitat dels suports en un procés de digestió *in vitro*, demostrant que mentre que les partícules menudes poden ser atacades durant la digestió, la funcionalització amb molècules orgàniques que actuen com a portes moleculars prevé aquest atac. Per últim, els estudis de viabilitat cel·lular duts a terme en quatre tipus de línies cel·lulars demostren que ni els suports, ni els productes de degradació dels mateixos durant el procés de digestió *in vitro* promouen cap tipus de toxicitat inespecífica.

En la segona part, s'ha avaluat la influència de l'addició de diferents suports d'òxid de silici a dos matrius alimentàries, gels de gelatina i iogurts. Esta aproximació tecnològica ha permés conéixer que la capacitat d'aquests sistemes intel·ligents per alliberar controladament àcid fòlic durant un procés de digestió *in vitro* es manté fins i tot després de ser incorporats en iogurts batuts. D'altra banda, s'ha comprovat que l'efecte de les matrius sobre les propietats físiques dels gels, és dependent tant de la grandària de les partícules, com de la seua funcionalització i concentració.

Per últim, s'ha comprovat que a causa de l'optimització del carregat d'àcid fòlic assolida en la primera part de la tesi, es pot aconseguir una fortificació d'un iogurt amb el 100% de la quantitat diària recomanada d'àcid fòlic amb una quantitat tan baixa del sistema que ni les propietats físico-químiques del iogurt, ni la viabilitat bacteriana se'n veuen compromeses.

En resum, es pot concluir que en la present tesi s'ha abordat d'una manera global l'encapsulació d'àcid fòlic en matrius poroses d'òxid de silici per a ser utilitzades en aplicacions nutricionals i alimentàries, que inclouen estudis d'optimització de carregat, estudis d'alliberament en funció del pH, digestions *in vitro*, estudis d'estabilitat de les matrius utilitzades, estudis de biocompatibilitat, així com estudis de la influència de l'addició d'aquests sistemes en matrius alimentàries. Els resultats obtinguts han posat de manifest de forma positiva que els sistemes intel·ligents d'àcid fòlic que s'han desenvolupat obrin una porta a una nova manera de fortificar els aliments sense comprometre les seues característiques físico-químiques.

Abstract

The present PhD thesis, entitled “Encapsulation of folic acid in silica porous supports: a nutritional and technological approach”, focuses on the development of new smart systems for the controlled delivery of folic acid for nutritional applications.

The first part of the thesis shows folic acid encapsulation in polyamine-functionalized silica porous matrices from a nutritional approach. The first part evaluates not only the influence of the loading method and the type of silica support employed (MCM-41, SBA-15, UVM-7 and Hollow Silica) on the efficiency of folic acid encapsulation, but also the influence of the morphology and porous system on the folic acid delivery profile from different supports. Folic acid release studies from different supports with various pH values have demonstrated that the designed systems are capable of smartly modulating the delivery of the folic acid dependent on the pH of the medium (inhibition of the release at an acidic pH -stomach-, controlled release at a neutral pH -intestine-).

This capacity makes these developed delivery systems an excellent alternative to direct fortification to successfully modulate the bioaccessibility of folic acid along the gastrointestinal tract. The stability of the supports during an *in vitro* digestive process was evaluated, and demonstrated that not only small particles can be attacked during the digestion process, but also the functionalization with organic molecules, which act as molecular gates, prevents this attack. Finally, the cell viability studies carried out with four different cell lines revealed that neither the supports nor their degradation products caused any specific toxicity during the *in vitro* digestive process.

Abstract

The second part evaluates the influence of adding different silica supports to two food matrices: gelatin gels and yoghurts. This technological approach enabled us to know that the capacity of these smart systems to deliver folic acid in a controlled manner during an *in vitro* digestive process is mantained even after their incorporation in stirred yoghurt. The effect of the matrices on the gel's physical properties depends on the particle size, functionalization and concentration.

Finally, this thesis tested that the optimization of folic acid loading, achieved in the first part of the thesis, allowed the fortification of yoghurt with 100% of the dietary reference intake of folic acid with a very low amount of the system. This fortification affected neither the physico-chemical properties of the yoghurt, nor bacterial viability.

In summary, it was concluded that the present thesis globally deals with folic acid encapsulation in silica porous matrices to be used in nutritional and food applications, which include the optimization of loading, release studies at diferent pH, *in vitro* digestions, stability studies of the employed matrixes, biocompatibility studies, and studies into the influence of their addition to food matrixes. The obtained results positively demonstrate that the developed smart folic acid delivery systems open up a new way of fortifying food without endangering the physico-chemical properties of the food to which they are added.

TABLE OF CONTENTS

1. PREAMBLE

This PhD thesis forms part of the project "***Improvement of the stability and control release of biomolecules by using microcapsules functionalized with molecular gates*** (AGL2012-39597-C02-01)", funded by the 2013-2016 National Research Plan of the Spanish Ministry of Economy and Competitiveness.

Protecting bioactive molecules is a subject of much interest in food technology. To date, scientific studies have concluded that the functional activity of a molecule, demonstrated by *in vitro* models, does not guarantee the same biological effects in the human body, mainly as a result of the transformations that this compound undergoes during processing, conservation, and even during digestion. Sometimes, handling some bioactive components is extremely complicated. Other times the bioactive molecule is simply not compatible with the food matrix in solubility or sensory properties terms. This has led to increased interest in protecting certain bioactive molecules so they can be easily consumed, and effectively absorbed and assimilated in the body.

In this context, the main objective of the project is to improve the stability and the release of bioactive substances of nutritional interest by encapsulating them in hybrid materials based on porous or hollow silicon oxide matrices, functionalized with organic molecules that act as a molecular gates. The aforementioned molecular gates should be able to maintain the substances of interest confined, and to release them in the intestinal tract, possibly at a controlled rate.

This main objective of this project is subdivided into several specific objectives:

1. To obtain suitable carriers (MCM-41, SBA-15, UVM-7, Hollow Silica, and other low-cost porous materials) capable of being used in the preparation of different encapsulation systems.
2. To functionalize carriers with organic molecules capable of hindering or allowing cargo delivery in a controlled and triggered manner (molecular gates).
3. To optimize the loading process of three bioactive molecules: folic acid, caprylic acid and garlic extracts.
4. To study the release rate of the encapsulated bioactive molecules in the presence of different triggering stimuli.
5. To examine the stability of the encapsulated bioactive molecules in the presence of different environments.
6. To evaluate the biocompatibility of the developed smart delivery systems using both cell cultures and the nematode *Caenorhabditis elegans.*
7. To assess the compatibility of the delivered smart delivery systems with different food matrices.

The doctoral thesis "Encapsulation of folic acid in porous silica supports: a nutritional and technological approach" is the first doctoral thesis developed as part of this framework.

2. OBJECTIVES

The main objective of this PhD thesis was to design, fabricate and evaluate different porous silica supports capped with molecular gates responsive to changes in pH to act as smart delivery systems (SDS) able to modulate the bioaccessibility of folic acid (FA) along a digestion procedure when incorporated in food matrixes.

To achieve this main objective, the following partial objectives were set:

1. The study of the possibilities of mesoporous silica particles to develop SDS capable of controlling and targeting the release of bioactive molecules in the gastrointestinal tract.
2. The synthesis and characterization of different porous silica supports with different morphologies and porous systems.
3. The optimization of the loading procedure to obtain SDS capable of delivering large amounts of FA with a minimum amount of support.
4. The evaluation of the capability of the developed SDS to modulate FA delivery according to pH (i.e. hinder release at an acid pH and allow a sustained release at a neutral pH).
5. The *in vitro* evaluation of the biocompability of the developed SDS.
6. The evaluation of the stability of the developed SDS during simulated in vitro digestion.
7. The determination of the effect of incorporating the developed SDS into different food matrices.

To reach these objectives, the present thesis was divided into two different approaches:

a. ***The nutritional approach.*** It was addressed to evaluate all the aspects related to the development of SDS (including their stability in the gastrointestinal tract) capable of loading large amounts of FA and delivering it in a controlled manner to solve current nutritional problems.

b. ***The technological approach.*** It addressed the study of the influence of genuinely adding the developed SDS to food matrices in terms of the delivery efficiency and modification of the physico-chemical properties.

3. GENERAL INTRODUCTION[1]

[1]General Introduction is based on the article: Pérez-Esteve, É., Ruiz-Rico, M., Martínez-Máñez, R., & Barat, J. M. (2015) Mesoporous silica-based supports for the controlled and targeted release of bioactive molecules in the gastrointestinal tract. *Journal of Food Science* (DOI: 10.1111/1750-3841.13095).

1. Mesoporous silica particles as encapsulation supports

Mesoporous silica particles (MSPs) are structures of silicon dioxide (SiO_2) which are arranged so that they create pores of 2-50 nm (Zhao, 2006). The first described porous silica with a uniform pore size, called folded sheet mesoporous material (FSM-16), was reported by Kuroda and co-workers in 1990 (Yanagisawa *et al*., 1990). A few years later, in 1992, researchers of the Mobil Company reported the synthesis of a family of mesoporous silica materials called M41S (Beck *et al.*, 1992), which include hexagonal MCM-41, cubic MCM-48 and lamellar MCM-50.

Since their discovery, applications of MSPs have grown exponentially as a result of their unique properties. Specifically, MSPs have demonstrated to have huge applications in the food sector, where they could be employed as catalysts in the synthesis of nutrients and bioactive molecules (Márquez-Ávarez *et al*., 2004), in sensor technology (Climent *et al*., 2009) and also as carriers in the design of smart delivery systems (Bernardos *et al*., 2008, Pérez-Esteve *et al*., 2015). Of these applications, the design of smart delivery systems is viewed as challenging given the possibility of improving the handling and utilization of different bioactive molecules or functional ingredients, and the subsequent formulation of functional food (Bernardos & Kourimská, 2013).

Although there is neither a regulatory nor a standard definition of "functional foods" (Aryee & Boye, 2015), this term refers to the foods and food components that may offer health benefits beyond basic nutrition (Bech-Larsen & Grunert, 2003). The terms food components and bioactive ingredients with beneficial biological activity include basic nutrients (i.e. carbohydrates, proteins, lipids, vitamins, minerals, etc.), bioactive components (i.e., omega-3 fatty acids, amino acids and peptides, and phytochemicals), sensory appeal compounds (i.e. organic acids, flavors and pigments), as well as pre- and probiotics, healthy oils, spices and herbs (Fang & Bhandari, 2012).

Despite the increase in functional products in markets and the scientific literature, the incorporation of these functional ingredients into existing food formulations is still viewed as challenging. On the one hand, most studies on the functionality of food compounds have been done *in vitro*, which thus excludes studying changes in potential active compounds during food processing, storage, ingestion and interaction with gut microflora. On the other hand, some bioactive components are most complicated to be handled or are not compatible with the food matrix in terms of solubility (lipophilic compounds), sensorial properties (i.e. fish oils or garlic extracts), or are very susceptible to degradation (vitamins, antioxidants). The desire to overcome these limitations has increased the interest in the encapsulation of bioactive components because after encapsulation, they could be released in a particular site-of-action of the digestive tract and/or be absorbed in their native form, which thus avoids problems related to instability or to unpleasant sensory properties (McClements, 2012).

Typically, food applicable encapsulating systems are based on carbohydrates, proteins or lipids (Fathi *et al*., 2012; Wang *et al*., 2012; Fathi *et al*., 2014). However, these systems exhibit low structure stability while food is processed and stored, a poor capability to control the release rate or to provide a targeted delivery, and a very poor effect on the protection of the encapsulated substance while it passes through the stomach. Some of these problems could be avoided if mesoporous silica particles (MSPs) are used as encapsulating supports. Compared to other organic polymer-based carriers, MSPs are more stable, rigid and biocompatible. They also better resist the harsh conditions of the stomach and microbial attack. MSPs are also able to protect entrapped guest molecules against enzymatic degradation or denaturation induced by pH or temperature (Arcos & Vallet-Regí, 2013).

This introduction critically assesses the possible use of mesoporous silica materials to design site-specific smart delivery systems capable of encapsulating, protecting, transporting and releasing bioactive molecules in a controlled fashion in the gastrointestinal tract (GIT).

2. Requirements for folic acid encapsulation and controlled release

2.1 Folic acid: history, chemical structure and physic-chemical properties

Folates have been and remain a subject of unending research. Despite being one of the most studied dietary compounds, their multiple roles in metabolism and the controversy on whether their nutritional supplementation has on the population leaves a number of research gaps to be filled.

Folates received their name in 1941 when were isolated from spinach (folium is the latin word for leaves) and were shown to be growth factors for *Streptococcus lactis*. In 1962, Victor Herbert used self-experimentation to prove that dietary folate deficiency could cause megaloblastic anaemia. From that study, he developed his hypothesis for the sequential stages in the development of folate deficiency and dietary reference intake (Golding, 2014).

Folate (also known as vitamin B9, folacin and folinic acid) is a generic term for a water-soluble group of vitamins including folic acid (FA) and naturally occurring folates. In general, FA refers to the oxidized form, which is almost non-existent in plant and animal foods but is present in supplements and fortified foods; folate refers to the reduced forms, such as 5-methyltetrahydrofolate, 5-formyltetrahydrofolate, 10-formyltetrahydrofolate which are present in food and biological tissues (Ginting & Arcot, 2004).

All the folates have in common the pteroylmonoglutamic acid (PteGlu or PGA) structure composed by a bicyclic 6-methylpterin ring connected by a methylene bond to a residue of *p*-amino benzoic acid, linked at the same time to a single molecule of L-glutamic acid by an amide bond (**Fig 1**). The different folates differ in the pteridine ring, which can have different reduced forms and various types of substitutions, and the *p*-aminobenzoglutamate residue that can be linked to the peptide bond a variable number of glutamate residues (Vora *et al*., 2002) being the most common in the organism the mono-, penta- and hexa-glutamates (Mataix, 2002). Nearly 80% of natural folates in foods exist as polyglutamates.

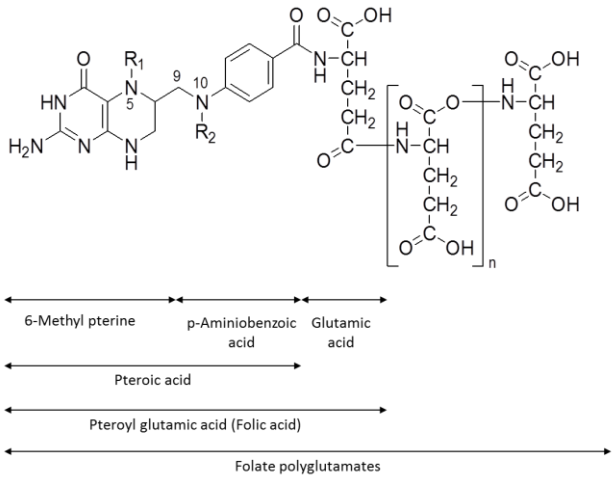

R_1	R_2	Folate species
H	H	THF
CHO	H	5-formyl-THF
H	CHO	10-formyl-THF
CH_3	H	5-methyl-THF
$-CH_2-$		5,10-methylene-THF
=CH-		5,10-methenyl-THF

Figure 1. Chemical structures of folic acid and folates

FA is tasteless, odourless and displays a yellow-orange crystalline appearance in the solid state. Despite being considered a hydrosoluble vitamin, its solubility in water is only 1.6 mg L^{-1}, increasing its solubility in weak acid and alkaline solutions. It is insoluble in alcohol, acetone, ether and chloroform. FA is a photosensitive compound that is degraded in aqueous solution by sunlight, ultraviolet and visible light (Akhtar *et al*., 2003). The susceptibility of FA to cleavage under acidic conditions and high temperatures has long been established. However, the degree and rate of destruction has been shown to be influenced by the pH of the medium, reducing agents in the buffer, folate derivatives, type of buffer, and food system. Under neutral to alkaline conditions, FA displays increased solubility, and stability particularly in solutions of alkali hydroxides and carbonates, as well as a limited number of organic solvents. In aqueous solution, FA is stable at 100 °C for 10 h in a pH range of 5.0-12.0 when protected from light, but becomes increasingly unstable as the pH decreases below 5.0 (Cheung *et al*., 2008).

2.2 Folic acid in human nutrition

Folate intake is vital in human subjects for normal cell division, homeostasis, proper growth, prevention of anaemia, and also for normal foetal development. Its importance is related to the role of folate coenzymes in nucleic acid (DNA and RNA) synthesis, synthesis of the amino acid methionine from homocysteine, and in the shuttling, oxidation and reduction of one-carbon units required for normal metabolism and regulation (Wagner, 1995).

Folate requirements have historically been defined as the quantity of intake necessary to prevent a severe deficiency with clinical symptoms. More recently, the focus has shifted to identifying intakes associated with maintenance of normal one-carbon transfer reactions as described above (Bailey & Gregory, 1999). In the USA, the Dietary Reference Intake (DRIs) for FA is stablished as 400 μg folate per day in adults and 600 μg folate per day in pregnant women (USDA, 2010). In Europe, the European Food Safety Authority (EFSA) recommends a daily intake of 200-400 μg folate per day for adults and an additional 400 μg folate per day (ESFA, 2009) in pregnant women. Because the bioavailability of synthetic FA is approximately twice that of folate found in food, the dietary folate equivalent (DFE) system established the relationship between dietary folate and FA from supplements. One DFE is defined as 1 μg of dietary folate, 0.6 μg of FA from fortified food or as a supplement taken with meal, or 0.5 μg of of a supplement taken on an empty stomach (Suitor & Bailey, 2000).

An adequate folate status during pregnancy prevents birth defects (Branum *et al*., 2013). In other life stages, an optimal folate status may provide health benefits in the general population by preventing cardiovascular diseases (Lucock, 2000; Choi & Mason, 2002; Pitkin, 2007), Alzheimer (Clarke *et al*., 1998), atherosclerosis (Hoag *et al*., 1997), or a disruption of the nucleotide biosynthesis which can result in colon and colorectal cancer (Choi & Mason, 2002; Stover, 2004).

Folates can only be synthetized by microorganisms and plants. Thus, humans depend on a variety of dietary sources for the vitamin, including liver, egg yolk, fresh, dark green and leafy vegetables such us spinach or broccoli, beans such as lentils, citrus fruits, wheat germ, and yeasts (Hau Fung Cheung *et al*., 2009; Lubecka-Pietruszewska *et al*., 2012). Folates synthesised by intestinal bacteria do not contribute significantly to folate nutrition in humans because bacterial folate synthesis is usually restricted to the large intestine (colon), whereas absorption occurs mainly in the upper part of the small intestine (jejunum) (Spitzer, 2007).

In the diet, folate exists in the form of mono- (10%) and polyglutamates (90%). Before absorption, folate polyglutamates are hydrolysed to folate monoglutamates. This digestion process occurs mainly in the proximal part of the small intestine where the enzyme folylpoly-glutamate carboxypeptidase (EC 3.4.17.21) present in the enterocyte brush border transform polyglutamates to the corresponding monoglutamate forms (Said, 2011).

FA and reduced monoglutamates are then absorbed mainly in the proximal small intestine (jejunum) by a saturable, carrier-mediated, pH and energy-dependent transport mechanism which, unlike other epithelial tissues, appears to be unique in its lack of hierarchy of transport, having a similar affinity for both oxidised (e.g. FA) and reduced folate forms. Absorption of FA is almost 100% when consumed under fasting conditions. When FA is consumed with a portion of food, bioavailability is estimated from experimental data to be 85% compared with free FA. The bioavailability of food folates is variable and incomplete, and has been estimated to be no more than 50% that of FA (Spitzer, 2007).

After absorption, FA has to be transformed into the biologically active folate. The process occurring within the intestinal mucosal cells involves the conversion of FA into dihydrofolate and a subsequent reduction to the 5-methyltetrahydrofolate by the enzyme dihydrofolate reductase. Absorbed folates are subsequently transferred via the mesenteric veins to the hepatic portal vein and carried to the liver where they are stored or removed (Wright *et al*., 2007).

From the liver, folates are widely distributed in tissues, most of them as polyglutamate derivatives. The process is summarized in **Figure 2**.

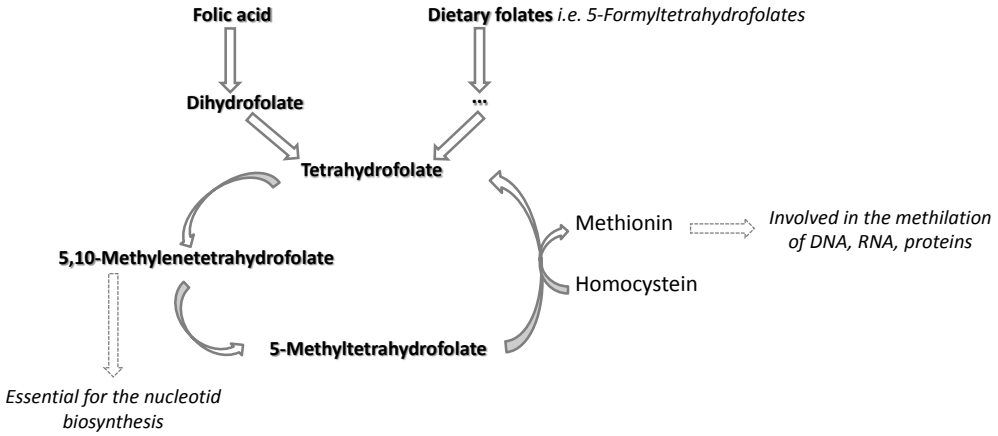

Figure 2. Folate-folic acid metabolic pathway in mammalian cells

2.3 Folate deficiency and disease prevention

Folate deficiency has been demonstrated to initiate an onset of several diseases and disorders in humans. Early symptoms of folate deficiency are non-specific and may include tiredness, irritability and loss of appetite. Severe folate deficiency leads to megaloblastic anaemia, cancers, and increased plasma homocysteine concentration, the latter being associated with an elevated risk of cardiovascular disease. Deficiency during pregnancy may result in premature birth, infant low birth weight and foetal growth retardation. In children, growth may be retarded and puberty delayed (Moat *et al*., 2004; Reynolds, 2006; Spitzer, 1997).

The most important factor contributing to folate deficiency is insufficient dietary intake. Although folates are widely distributed in food, they are in relative low density and moreover, are very sensitive to physical factors such as temperature, pressure, and exposure to light. This provokes losses of folate during food processing and home preparation by oxidation, leaching by aqueous cooking media, or both (Gregory, 2007).

Other factors contributing to folate deficiency are defective absorption generated by intestinal diseases, drug intake or hereditary folate malabsorption; acquired metabolic impairments (i.e presence of dihydrofolate reductase inhibitors, alcohol or sulfasalazine); genetic metabolic impairments (i.e deficiency of methylenetetrahydrofolate reductase or glutamate formiminotransferase, polymorphism in methylenentretrahydrofolate reductase); and increased requirements, such as hemodialysis, prematurity, pregnancy and lactation (Combs, 2008).

Folate deficiency is very common in many parts of the developing world and is a part of the wider problem of poverty and malnutrition (Talaulikar & Arulkumaran, 2001). In developed countries, nutritional folate deficiency may be encountered above all in economically underprivileged groups. Reduced folate intake is also often seen in people on special diets (i.e. weight-reducing diets). Disorders of the stomach (i.e. celiac disease, sprue, Crohn's disease) may lead to folate deficiency as a result of malabsorption. Folate deficiencies also occur in conditions with a high rate of cell turnover such as cancer, certain anaemias and skin disorders. This is also the case during pregnancy and lactation, due to rapid tissue growth occurring in pregnancy and to losses through the milk in lactation. People undergoing drug treatment (i.e. epilepsy, cancer or an infection) are at high risk of developing a folate deficiency, as are patients with renal failure who require regular haemodialysis as folate is loosely bound to proteins in serum and thus is lost from body. Finally, acute folate deficiencies have been reported to occur within a relatively short time in patients undergoing intensive care, especially those on total parenteral nutrition (Spitzer, 1997).

The 400 μg per day of dietary folate equivalents recommended for adults are best provided by a healthy diet with plenty of vegetables and other foods rich in folate such as wholemeal products, which are independently associated with a reduced risk of cardiovascular disease and cancer. However, the recommendations are not easily achieved because people are not willing to change their diet. In these cases, recommendations can be also met by taking FA from foods fortified (on a voluntary or mandatory basis), supplements, or both. When planning a pregnancy, benefits of FA in prevention of neural tube defects has been pointed out since 1992, leading many health organisations to issue recommendations for women to maintain a healthy diet and take FA supplements (Eichholzer and others 2006). In this context, in 1998, the USA implemented mandatory FA fortification to reduce neural tube defects (Lucock and Yates, 2009). Many other countries such as Canada and UK have joined this mandatory proposal with the objective of ensuring a 400 μg intake for adults and an additional 200 μg for pregnant women.

2.4 Encapsulation of folic acid: towards enhancing its bioavailability

Although there is irrefutable evidence of the benefits of FA supplementation to reduce neural tube defects, homocysteine blood levels, certain cancers, etc., recent studies suggest that a massive exposure to high lybioavailable FA is a double-edged sword (Lucock & Yates, 2009).

Although folate is safe and almost free of toxicity, there is concern that high doses of FA may mask symptoms of vitamin B12 deficiency, primarily in the elderly population, and may lead to progression of neurological symptoms (Cornell *et al*., 2009). Moreover, some data suggest the possibility that high FA intakes may be associated with increased risks of cancer. A possible role of FA in

cancer development is supported by biologically plausible mechanisms. Folate is essential in biological methylation reactions and nucleotide synthesis and impairment of these processes are thought to be involved in cancer development (ESFA, 2009). Some authors also report that excess of FA may affect cognitive and immune function and interfere in anti-folate chemotherapy (Wright *et al*., 2007).

Recent studies suggest that these side-effects might be related to the presence of unmetabolized FA in blood. Humans have a reduced dihydrofolate reductase activity and a poor ability to reduce FA. Thus, oral doses of FA of about 260-280 µg (589-634 nmol) have been reported to lead to the direct appearance of untransformed FA in the systemic circulation (Lucock & Yates, 2009).

As stated, controlling FA dosage and modulation of FA bioavailability (i.e. by adjusting its bioaccessibility along the gastrointestinal tract) appear to be essential to keep positive effects of fortification while avoiding problems related to massive exposition. For this purpose, design of smart delivery systems to encapsulate, transport and dosage FA in the small intestine sustainably over time is a challenge for current nutrition science. An adequate smart delivery system for FA encapsulation should be able to encapsulate a large amount of FA, protect it from degradation, hinder its release during its pass through the stomach and gradually deliver the cargo during its pass through the intestine.

3. Fabrication of gated MSPs

3.1 Synthesis and features of the inorganic support

MSPs are synthesized using two main elements: a) a template whose function is to direct the construction of the high ordered (crystalline) porous net; b) a polymeric precursor which self-organizes around the template and, upon polymerization, builds up the final rigid structure. Synthesis starts with the polymerization, in an aqueous solution, of the inorganic siliceous precursor (i.e. tetraethyl orthosilicate) around surfactant micelles (i.e. *N*-cetyltrimethylammonium bromide -CTABr-). The mesoporous inorganic scaffold obtained under these conditions presents cylindrical unidirectional empty channels of approximately 3 nm in diameter (when CTABr is used as a surfactant), arranged in a hexagonal distribution. Mesoporous materials are obtained by the subsequent removal of the surfactant by extraction with appropiate solvents or by aerobic high temperature calcination (500-600 °C) (Hoffman *et al.*, 2006). **Figure 3** schematically represents the complete synthesis procedure.

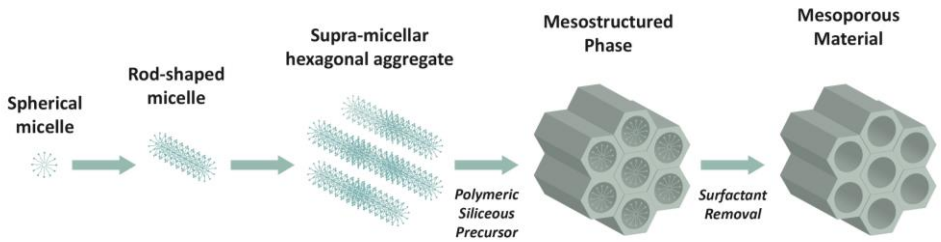

Figure 3. Schematic representation of the synthesis of mesoporous silica particles by *structure-directing agents.*

Minor changes in the synthesis route make it possible to modify final key features in the solid to produce other types of mesoporous silica, such as hexagonal mesoporous silica (HMS) (Tanev & Pinnavaia, 1995), Michigan State University material (MSU) (Bagshaw *et al.* 1995), Santa Barbara Amorphous Silica (i.e. SBA-15) (Zhao *et al.* 1998 a,b), Technische Universiteit Delft material (i.e. TUD-1) (Jansen *et al.* 2001), Universidad Valencia Material (i.e. UVM-7) (el

Haskouri *et al.* 2002), and a wide variety of hollow silica spheres (Li *et al.* 2004; Zhang *et al.* 2009; Cao *et al.* 2013). TEM and FESEM pictures of some of these particles are provided in **Figure 4**.

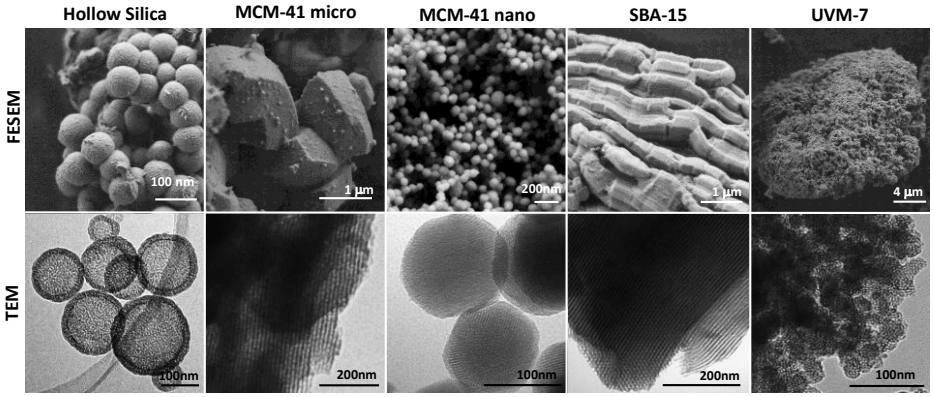

Figure 4. TEM and FESM images of different mesoporous silica particles.

Given the potential application of MSPs to develop oral controlled delivery systems, different attempts to synthesize MSPs from food-like precursors have been successfully made. On the one hand, rice husk ashes have been employed as a silica source for the synthesis of different mesoporous silicas (Jang *et al.*, 2009; Bhagiyalakshmi, 2010). On the other hand, polyglycerol esters of fatty acids, myristic acid ester of pentaglycerol and oleic acid have also been employed as food grade structures directing agents (Kapoor *et al.*, 2010; Han *et al.*, 2011; Ishii *et al.*, 2012).

In any case, different MSPs share their composition, which is based on a SiO_2-network, an ordered mesostructure and the presence of silanol groups on the particle surface. Some differ from others in size, shape, porous size and volume, specific surface area and density of silanol groups on the surface to provide different surface charges (Pérez-Esteve *et al.*, 2014). The morphology and porosity of different MSPs are determined by processing parameters: type of surfactant template, silica source, pH, temperature, aging time, additives, and solvents (Kierys *et al.*, 2010). The textural properties of different MSPs have been previously reviewed and compared in different publications (Wang *et al.*, 2011; Wright, 2008).

In general, MSPs stand out for being supports that can be synthesized with a controlled size from 50 nm to a few microns. This range in size is important in scope. While small MSPs can cross epitheliums and can be distributed in the body to be non-specifically internalized by certain cells, oversized particles cannot easily cross physical membranes in the body. As particle size has been demonstrated to play a key role in the distribution and behavior of particles in living systems, large particle sizes are preferred for developing orally administrated controlled release devices (Arcos &Vallet-Regí 2013).

MSPs can also be synthesized with uniform tunable porosity. Pore size can be tailored between 2-10 nm (Aznar *et al.*, 2009a). The presence of a mesoporous network provides large surface areas (700-1000 $m^2\ g^{-1}$) and a great loading capacity due to large pore volumes (0.6-1 $cm^3\ g^{-1}$) (Colilla *et al.*, 2013). Pore size, pore volume and a proper surface charge are essential for encapsulating a sufficiently large amount of a certain bioactive component and for efficiently retaining it during storage. Adsorption of bioactive molecules into mesoporous silica is governed by size and charge selectivity. Only the molecules with a size smaller than the porous size of the silica support can be entrapped by the porous structure (Arcos *et al.*, 2013). Other factors that determine adsorption and the release kinetics of a bioactive compound in a certain media are pore length and pore ordering (Izquierdo-Barba *et al.*, 2009a; Burguete *et al.*, 2012), particle morphology (Manzano *et al.*, 2008), surface area (Balas *et al.*, 2006), macroscopic form (Izquierdo-Barba *et al.*, 2009b) and modification or functionalization of the silica surface with functional groups (Nieto and others 2008).

Finally, the surface of MSPs can be easily functionalized with molecular/supramolecular ensembles to develop gated MSPs that show “zero delivery” and are capable of releasing their cargo on-command in response to specifically designed external stimuli (Mondragón *et al.*, 2014). These unique features of MSPs make them excellent candidates for developing smart delivery systems.

3.2 Functionalization of MSPs to develop triggered delivery systems

The surface of MSPs presents a high concentration of structural defects in the form of silanol (Si-OH) groups that can easily react with trialkoxysilane derivatives ($(R'O)_3$-Si-R) and allow the possibility of generating organic-inorganic hybrid materials (Vinu *et al.,* 2005).

In this area, one appealing concept is the development of molecular gates. Molecular or supramolecular gates are defined as nanoscopic supramolecular-based devices that are attached to certain solid supports, in which mass transport can be triggered by a target external stimulus that can control the state of the gate (closed or open) at will (Aznar *et al.,* 2009). In particular, and depending on the type of stimulus applied, it is possible to modify the properties of anchored molecules (i.e. polarity, conformation, size, interaction with other species, bond hydrolysis etc.) which, in turn, results in controlled delivery (Coll *et al.,* 2007; Casasús *et al.,* 2008; Aznar *et al.,* 2009b; Bernardos *et al.,* 2012). A schematic representation of a gate-like superstructure is shown in **Figure 5**.

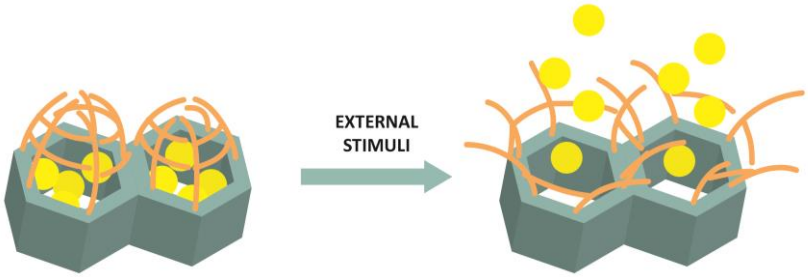

Figure 5. Representation of a nanoscopic molecular gate system working principle

As observed, smart delivery systems based on gated MSPs contain two components: a suitable inorganic support which acts as a nanocontainer (for loading the cargo); a switchable "gate-like" ensemble capable of being opened or closed when certain external stimuli are applied. Both components are important, and their selection determines the controlled release performance of the hybrid support (Bernardos *et al.,* 2010; Burguete *et al.,* 2012). The first example of a molecular gate was reported by Fujiwara and co-workers in 2003 (Mal *et al.,* 2003). Since then, a number of gated systems that have used mesoporous silica supports which respond to a wide variety of stimuli have been described (Aznar *et al.,* 2009a; Coll *et al.,* 2013; Arcos & Vallet-Regí, 2013).

4. Design of site-specific delivery systems that act along the gastrointestinal tract through gated MSPs

As previously stated, the encapsulation and later administration of bioactive molecules at a particular site-of-action of the digestive tract (mouth, stomach, intestine or colon) offers huge possibilities to develop new functional foods or medical therapies. Hence the design of systems capable of controlling the release of basic nutrients, bioactive components, sensory appeal compounds, and pre- and probiotics, and even drugs, is a very challenging strategy that can be easily achieved by using capped MSPs.

When designing a site-specific delivery system based on hybrid organic-inorganic supports, there are two factors that should be taken into account. On the one hand, the porous system of the inorganic support should be able to entrap the target molecule. On the other hand, the capping molecule should be responsive to a triggering stimulus that is present in a particular cavity of the gastrointestinal tract. Moreover, the capping molecule must remain unchanged in the cavities that proceed. An overview of these stimuli is provided in **Figure 6**.

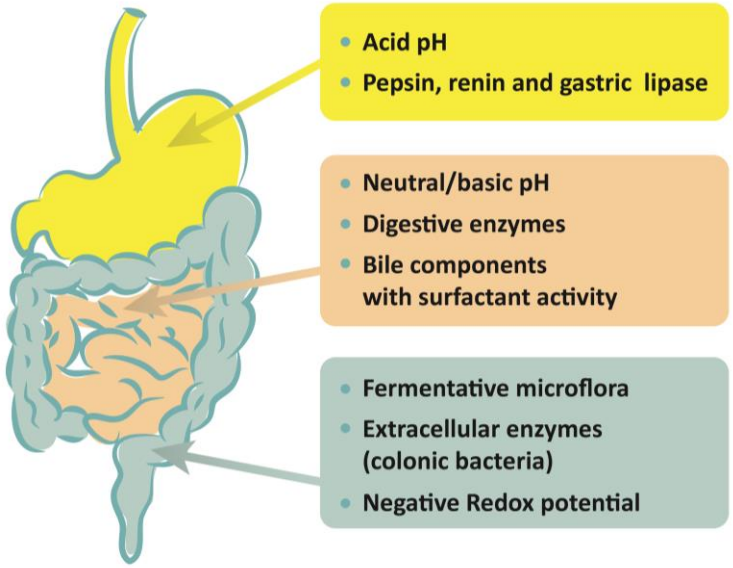

Figure 6. Summary of chemical and biological stimuli able to trigger caped-MSPs during digestion

4.1 A brief physicochemical description of the digestive system

This section describes the suitable stimuli found along the gastrointestinal tract that could be employed in developing site-specific delivery systems and all the approaches developed to date to design molecular gates responsive to these stimuli.

4.1.1 Mouth

Gastrointestinal tract activity begins in the mouth where the ingested food is chewed and mixed with saliva to allow bolus formation and to enhance taste (Humphrey & Williamson, 2001; Chen, 2009). Saliva is a complex heterogeneous clear fluid (pH 5.6-7.6) that consists in roughly 98% water and 2% organic and inorganic substances, including electrolytes, mucus, glycoproteins, proteins, antibacterial compounds, enzymes, and others (Levine *et al.*, 1987).

Of all the enzymes contained in saliva, α-amylase is the most important. The interaction of amylase with starch-based ingredients produces a breakdown of starch into simpler sugars (i.e. maltose and dextrins), which can be further broken down in the small intestine. Salivary *α*-amylase is most active at its optimum pH of 7.4, and is inactivated in the stomach because of gastric acid. Thus, even though enzyme interaction begins almost immediately after food ingestion, its contribution to full starch breakdown is relatively insignificant. Most starch digestion results from pancreatic amylase rather than from salivary amylase (Chen, 2009). Salivary glands also secrete salivary lipase that starts the degradation of dietary triglycerides into fatty acids and diglycerides that start with fat digestion. However, salivary lipase does not play a digestive role in adult humans. Recent studies have suggested that it only plays a role in fat taste and texture perception (Drewnowski & Almiron-Roig, 1997).

The residence time in the oral cavity is short, and varies by 2-5 min depending on saliva swallowing and water intake. Thus the main suitable triggering stimuli in the buccal cavity are pH (neutral) and presence of α-amylase and salivary lipase. However, due to the short residence time and low enzyme activity, the influence of the mouth on the action of molecular gates could be considered negligible.

4.1.2 Stomach

Once food is swallowed, it passes into the stomach. In the stomach, food stuffs encounter gastric juice secretion. Gastric juice provides a harsh environment characterized by a very acid media (pH 1-2) that is rich in electrolytes, proteases (pepsin, renin and gastric lipase) and lipases (Chiras, 2015). Microflora in the stomach is predominantly Gram-positive and aerobic, and the bacterial concentration is usually $<10^3$ colony-forming units (CFU) mL^{-1} (Campieri & Gionchetti, 1999). The redox potential in the stomach is +150 mV (Friend, 1992). The residence time of food in the stomach depends on the digestibility of meals; while light meals based on carbohydrates may be ready to pass into the small intestine through the pyloric valve in 2 h, heavy meals that contain proteins and fats may require up to 6 h to perform the same action. After this period, proteins are transformed into large polypeptides, and about 10-30% of dietary fat has been hydrolyzed (Krohn *et al.*, 2008). The digestion process is thus completed in the small intestine.

4.1.3 Small intestine

In the small intestine, the hydrolysis of all the majority food structures and macronutrients occurs by the combined action of small intestine and accessory organs (pancreas and liver) secretions.

Once the chyme arrives to the duodenum, the pancreas secretes pancreatic juice. Pancreatic juice is a liquid that contains water, sodium chloride, sodium bicarbonate and a number of digestive enzymes (i.e. amylases, lipases, proteases, ribonucleases and deoxyribonucleases) that help finish the digestive process that started in the stomach. Sodium bicarbonate neutralizes the high acidity of the

chyme. In this manner, the duodenum pH is 6.0 (within the 5.7-6.2 range) and gradually increases through the small intestine to pH 7.5 (within the 7.3-7.7 range) (Fallingborg, 1999). This difference with the stomach pH allows the design of pH-responsive devices. The enzymatic profile of pancreatic juice is completed by enzymes of microvilli that constitute the brush border (i.e. saccharidases, peptidases and nucleases). Working together, both types of enzymes are able to hydrolyze almost all large molecules into absorbable food components.

The duodenum also receives a fluid though the bile duct which is produced in the liver and stored in the gallbladder, and is known as bile. Bile is composed of water, cholesterol, lecithin (a phospholipid), bile pigments (with no digestive function), bile salts (sodium glycocholate and sodium taurocholate) and bicarbonate ions. The powerful surfactant activity of bile components helps with the digestion and adsorption of lipophilic components.

Regarding microflora, the proximal small bowel is similar to that of the stomach. The bacterial concentration is 10^3-10^4 CFU mL^{-1}. However, the distal ileum is able to support anaerobic bacterial flora. Consequently, the concentration of microorganisms increases in the distal ileum to levels of 10^5-10^9 CFU mL^{-1} and the redox potential in the small intestine lowers from -50 mV in the duodenum or jejunum to -150 mV in the ileum (Friend, 1992; Campieri & Bionchetti, 1999).

After this complete digestive process, which lasts between 2-5 h, most food structures have been disintegrated into absorbable molecules. Undigested food remains pass through the ileocaecal valve to the large intestine.

4.1.4 Large intestine

The large intestine, which comprises the caecum, colon and rectum, is the last part of the digestive tract. Its main functions are to absorb the water and electrolytes that escape from absorption in the small intestine, and to store and remove feces during defecation. Understanding the last part of the GIT offers different possibilities to design triggered responsive MSPs for controlled release in the large intestine.

The large intestine pH varies according to the food ingested. In general, the pH in the ascending colon is 6-7.1 due to fermentation processes, and varies along the large intestine length. The transverse colon exhibits a pH of 7.4, descending colon, pH 7.5, sigmoidal colon, pH 7.4, and rectum, pH 7.2. The shallow pH gradient between the small intestine and the colon does not allow the design of colonic delivery drug carriers based on pH changes (Milabuer *et al.*, 2010).

However, the large intestine is the natural habitat for a huge microbial community. The colon contains 10^{11} to 10^{12} CFU mL^{-1}. Predominant species include *Bacteroides*, *Bifidobacterium* and *Eubacterium*. Anaerobic gram-positive cocci, as well as *Clostridium*, enterococci, and various species of *Enterobacteriaceae* are also present. The final digestion stage can be considered to be carried out by a wide variety of metabolic processes, including fermentation, enzyme-mediated reactions, and the reduction of a wide range of organic functional groups. Among the different extracellular enzymes produced by colonic bacteria, azoreductases, oxidoreductases, ureases, dextranases and a number of saccharidases capable of breaking indigestible carbohydrates, stand out.

The total metabolic and bacterial activity in the large intestine generates a characteristic redox potential (-200 mV) that can be used as a highly selective mechanism for targeting in the colon (Friend, 1992; Chourasia & Jain, 2003). The residence time in the large intestine ranges from 2-72 h. In most individuals, mouth-to-anus transit times are usually longer than 24 h. More detailed information is provided in **Table 1**.

Table 1. Summary of digestive stimuli suitable for the design of triggered MSPs-based delivery systems.

	Chemical		Enzymatic		
		Enzyme	Substrate	Origin
Mouth	Neutral pH	α-amylase (ptyalin)	Starch	Salivary glandules
		Salivary lipase	Triacylgliceride	Salivary glandules
Stomach	Acid pH (H^+ species)	Gastric lipase	Triacylgliceride	Gastric chief cells
		Pepsin	Proteins and polipeptids	Gastric chief cells
		Renin	Casein	Gastric chief cells
Small intestine	Neutral/basic pH	Chymotrypsin (endopeptidase)	Proteins (endopeptidase)	Pancreas
	Bile acids (cholic and deoxycholic acid)	Carboxypeptidase A & B (exopeptidase)	Proteins	Pancreas
	Phospholipids	Cholesterol esterase	Cholesterol esters	Pancreas
		Colipase	Favours the action of the lipase	Pancreas
		Deoxyribonuclease	Deoxyribonucleic acid (DNA)	Pancreas
		Elastase	Elastin fibres	Pancreas
		β-fructofuranosidase (Sucrase or Isomaltase)	Sucrose	Brush border
		Pancreatic α-amylase	Starch	Pancreas
		Pancreatic lipase	Fat and triglycerides	Pancreas
		Phospholipase A2	Phospholipids	Pancreas
		Ribonuclease	Ribonucleic acid (RNA)	Pancreas
		Trypsin (Endopeptidase)	Proteins	Pancreas
		β-1-4 galactosidase (Lactase)	Lactose	Brush border
		α-glucosidase (Maltase)	Maltose	Brush border
		α-limit dextrinase	Limit dextrines	Brush border
		Nucleosidase	Nucleosides	Brush border
		Peptidases	Small peptides	Brush border and mucosal cells

Table 1. *Continuation.*

Chemical		Enzymatic		
		Enzyme	Substrate	Origin
Large intestine	Basic pH	α-L-arabinosidase	α-L-arabinofuranosides, arabinoxylans and arabinogalactans	Colonic bacteria
	Redox potential	Azoreductases	Azo (N=N) bonds	Colonic bacteria
		Dextranase	Dextran	Colonic bacteria
		β-D-galactosidase	β-D-galactosides (i.e. galactooligosaccharides)	Colonic bacteria
		β-D-glucosidase	β-glucosides (i.e. cellulose and hemicellulose)	Colonic bacteria
		β-glucuronidase	β-D-glucuronic acid residues	Colonic bacteria
		Oxidoreductase	Transfer of electrons (i.e. pyruvate oxidation)	Colonic bacteria
		Polysaccharidases	Indigestible polysaccharides (i.e. amylose, chitosan, dextrans…)	Colonic bacteria
		Urease	Urea	Colonic bacteria
		β-D-xylosidase	β-D-xylans, xylobiose	Colonic bacteria

4.2 Strategies to develop site-specific smart delivery devices

After discussing the most significant digestive stimuli that could be used to design capped MSPs for controlled release purposes in the gastrointestinal tract, the current MSP-based systems that can be opened using these triggering principles are presented in this section.

4.2.1 pH-responsive molecular gates

The first strategy to develop pH-responsive gated materials is based on using ionizable simple molecules anchored to the material surface, which undergo conformational and/or solubility changes in response to environmental pH variation, which modifies its conformation. Based on this approach, Martínez-Máñez and co-workers developed the first pH-driven molecular gate in 2004 (Casasús *et al.,* 2004). Their mechanism was based on the protonation/deprotonation processes of polyamines grafted onto the pore outlets of the mesoporous inorganic scaffolds. At an acid pH, the columbic repulsions between the protonated amino groups hinders pore access (gate closed), while at a neutral pH, unprotonated amines tend to interact with each other, which favors pore access (gate open). **Figure 7** illustrates the action mechanism of this reversible smart delivery system. Bearing in mind all these concepts, Bernardos *et al,* (2008), developed the first controlled release system mediated by a gastrointestinal stimulus. Given the objective of protecting riboflavin from acidic stomach conditions and of releasing the load in the intestine, these authors encapsulated vitamin riboflavin in an MCM-41 type support and functionalized its surface with the described pH-controlled gate-like scaffolding. They found a zero release under the stomach-like conditions (acid pH, gate closed) and a time-modulated delivery under the intestine-like conditions (neutral pH, gate open).

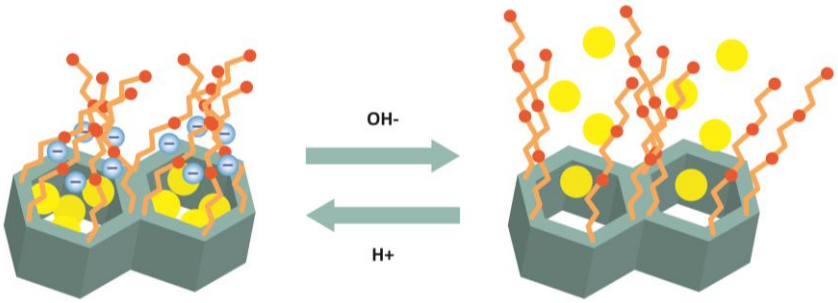

Figure 7. Schematic representation of a pH driven molecular gate-like material based in the use of polyamines.

A second strategy involves modifying the chemical interactions among the molecules covalently anchored to the surface of the mesoporous silica as a result of changes in pH. Following this approach, Lee *et al.* (2008) described the use of mesoporous silica nanoparticles loaded with sulfasalazine (an anti-inflammatory prodrug used for bowel disease) and functionalised with trimethylammonium functional groups via direct co-condensation of a trimethylammonium silane. At acidic conditions, the cargo remained inside the voids of the porous support. However, at neutral conditions deprotonation of silanol groups generated a strong electrostatic repulsion that triggered a sustained release of the loaded molecules.

The third strategy comprises the design of devices capped with molecules anchored with acid-sensitive bonds whose cleavage enables the release of cargo molecules. Bearing in mind this principle, Zhao *et al.* (2010) developed a pH-responsive nanoparticle able to be opened under acid conditions. The design strategy involved the use of mesoporous silica nanoparticles loaded with rhodamine B and functionalized with β-cyclodextrins through imine double bonds. The β-cyclodextrin rings on the surface of the nanoparticles served as gates for the storage of cargo molecules (i.e., rhodamine B) inside the nanopores of the nanoparticles under neutral conditions. At acidic pH, the cleavable imine bonds that attach the β-cyclodextrines to the particles surface were hydrolysed and the cargo released.

Besides polyamines, trymetylammonium groups and cyclodextrins, other capping molecules (such as polymers, peptides, proteins and DNA) have been used as gatekeepers in pH-triggered capped materials based in mesoporous silica (see **Table 2**).

4.2.2 Redox-responsive molecular gates

As occurred with changes in pH, the evolution of the redox potential along the gastrointestinal tract might allow the design of redox-driven gated mesoporous materials, especially for colon-targeted delivery. To date, no specific system based on naturally-occurring in redox potential changes along the GIT has been provided to modulate the delivery of bioactive molecules. However, there are a number of approaches that could be the basis for future developments.

Lai *et al.* (2003) prepared a controlled delivery system to encapsulate several pharmaceutical drug molecules and neurotransmitters inside an organically functionalized mesoporous silica framework. In particular, this nano-device was prepared using MCM-41-type mesoporous silica nanospheres as an inorganic support and cadmium sulfide (CdS) nanocrystals as chemically removable caps. Addition of disulfide-reducing molecules, such as dithiothreitol (DTT) and mercaptoethanol (ME), to the aqueous suspension of the particles triggered a rapid release of the mesopore-entrapped cargo by breaking the chemically labile disulfide linkages between the MSP and CdS nanoparticles. Also based on disulfide linkages, Liu *et al.* (2008) prepared a calcined MCM-41 support loaded with dye molecules, with the surface functionalized by the grafting of a poly(*N*-acryloxysuccinimide). The openings of the resulting hybrid material remained blocked due to the cross-linked reaction between the *N*-oxysuccimide groups along the polymer chain and the cystamine of the media. In contrast, the presence of disulfide-reducing agents, such as DTT cleavage the disulfide bond of cystamine, inducing pore opening and controlled dye release.

A different approach was published by Hernandez *et al.* (2004). These authors described the use of a MCM-41 mesoporous scaffold loaded with an iridium complex dye and functionalized with a 1,5-dioxynaphtalene derivative (DNPD) as a redox-responsive delivery system. The addition of cyclobis-(paraquat-*p*-phenylene) ($CBPQT^{4+}$) induced the formation of a pseudorotaxane on the external surface of the solid. This new non covalent supramolecular ensemble blocked pores and prevented dye delivery. When a reductive agent was added to the mixture (cyanoborohydride in this case), the reduction in DPND started a spontaneous dethreading of the $CBPQT^{4+}$ ring to allow guest release.

The evolution of that gated system was the achievement of a total reversible hybrid material capable of being open or closed on command in a reversible manner. In this case, Nguyen *et al.* (2005) firstly synthesized a [2]rotaxane-containing DNPD and a tetrathiafulvalene moiety (TTF) as a redox centre to link each other through a oliogoethylenglycol chain. Rotaxane was completed by the presence of a rigid spacer and a $CBPQT^{4+}$ as the movable molecule. Preference for $CBPQT^{4+}$ for TTF or DNPD groups as a result of the oxidation state of TTF (dependent on the addition of oxidant or reducing species) caused gate movement, which changed from a closed to an open conformation.

4.2.3 Surfactant-responsive molecular gates

The surfactant-induced molecular gates concept was introduced by Giménez *et al.* (2014). This new material consisted of nanoparticles of MCM-41 functionalized on the external surface with 1,2-dioleoyl-sn-glycero-3-phosphocholine (DOPC). The presence of DOPC created a lipid bilayer around pore outlets that inhibited cargo release. However, the system released its cargo after the addition of dodecyltrimethylammonium bromide (DTAB), a single-chain cationic surfactant whose activity is similar to phosphocholine (lecithin).

4.2.4 Enzyme-responsive molecular gates

The wide variety of enzymes present along the gastrointestinal tract, and their selective location (stomach, brush border, colon,) allows the design of very specific site release systems. One of the first examples of gated MSPs capable of delivering an entrapped cargo in the presence of saccharases was described by Bernardos *et al.* (2009). These authors designed a mesoporous silica particle capped with a covalently anchored lactose derivative. Cargo delivery from aqueous suspensions was negligible because the formation of a dense network of lactose groups linked through the hydrogen-bonding interaction around pore outlets. The addition of β-D-galactosidase enzyme (lactase) induced progressive cargo release, which was clearly related to the enzymatic hydrolysis of the glycosidic bond in disaccharide lactose. This is a clear example of the potential use of an enzyme-responsive molecular gate to hinder cargo release during food processing, storage and the first part of the digestion in the stomach, and one that is able to release the guest molecule in the small intestine in the presence of enzymes of brush border mucosa.

In line with this, the same authors functionalized the surface of a loaded MCM-41 support with three different commercially available hydrolyzed starches (Glucidex 47, 39 and 29) via the derivatization of starch with an alkoxysilane. Cargo release was achieved by enzymatic hydrolysis in the presence of pancreatin (an enzyme cocktail that contains pancreatic amylase), which showed different release kinetics according to the the degree of starch hydrolysis (**Fig 8**). The lower the hydrolysis rate of starch, the lower the delivery rate (Bernardos *et al.,* 2010).

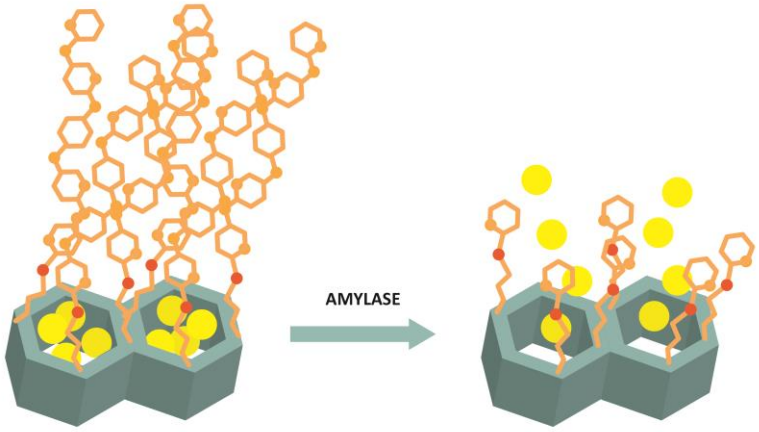

Figure 8. Schematic representation of a pH driven molecular gate-like material functionalised with hydrolysed starch.

Bein and co-workers prepared the first molecular gate opened by the presence of a protease (Schlossbauer *et al.*, 2009). Capping systems consisted in attaching avidin to a biotinylated MSP. The addition of protease trypsin induced the hydrolysis of the attached avidin and cargo release. Along the same lines, Coll *et al.* (2011) employed a click chemistry reaction to functionalize the external surface of an MSP with a peptide to develop a nanodevice capable of hampering cargo release. Delivery was observed in the presence of proteases (**Fig 9**).

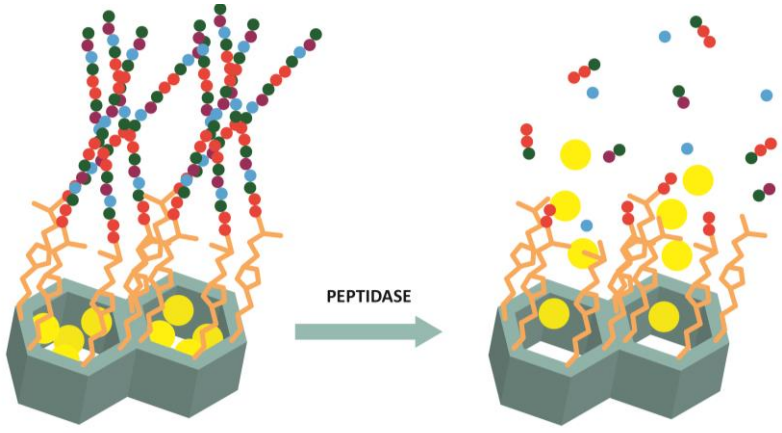

Figure 9. Schematic representation of a enzyme driven molecular gate-like material capped with a peptide.

Some examples of deoxyribonuclease-triggered delivery systems have also been reported. Zhu and coworkers presented an oligodeoxynucleotide-capped material using hollow MSPs that was opened in the presence of DNase I (Zhu *et al.*, 2011a). Zhang *et al.* (2014) reported the use of a porous material loaded with the drug colchicine and capped with oligodeoxynucleotides that was able to be uncapped also when DNase I was used.

The possibility of using enzymes secreted from colonic microflora to design smart delivery systems has been previously reported. Agostini *et al.* (2012a) described an ethylene glycol-capped hybrid material for the controlled release of a certain cargo in the presence of esterase. In the absence of an esterase enzyme, the steric hindrance imposed by bulk ester glycol moieties inhibited cargo release. Upon the addition of the esterase enzyme, cargo delivery occurred due to the hydrolysis of the ester bond. In another work, the same authors prepared MSPs loaded with Rhodamine B and functionalized with an alkylgluconamine derivative of a galacto-oligosaccharide (GOS) capable of delivering its cargo in the presence of β-galactosidase (Agostini *et al.*, 2012b). Mas *et al.* (2013) reported the synthesis of a hybrid material capped with an azopyridine derivative. This material was designed to show "zero delivery" in the absence of enzymes and to display cargo release in the presence of azo-reductases, which are usually present in the colon.

More examples of enzyme-responsive gated materials are shown in **Table 3**. The profound analysis of all the reported examples allowed a conclusion to be drawn. The most extended enzymes used as triggering stimuli are amylases, proteases, peptidases and deoxyribonucleases (which can be used for delivery in the small intestine) and reductases, esterases and ureases (which can be used for controlled cargo delivery in the colon). However, the real development of enzyme-responsive gated materials with applications in the design of site-specific delivery systems that act along the gastrointestinal tract is still in its incipient steps.

4.2.5 Dual stimuli-controlled release

One step forward in the design of gated mesoporous supports is the possibility of preparing gated materials that could be opened by using two different stimuli. For instance, Casasús *et al.* (2008) studied pH- and anion-responsive gated-like ensembles in anion complex formation terms with polyamines. This study came to the conclusion that larger anions pushed tethered polyamines toward pore openings and reduced the pore aperture. More recently, Popat *et al.* (2014) reported the use of silica nanoparticles that were responsive to multiple digestive stimuli (pH and enzymes). Their system consisted of an MCM-48-type structure loaded with sulfasalazine, and functionalized with amino groups coated with a succinylated soy protein isolate (SSPI). The resultant delivery system showed both pH and enzyme responsiveness, depending on the location of the nanoparticles in the GIT. In both the stomach and duodenum, the low environmental pH (pH 1.2 and ca. 5, respectively) restricted the release of sulfasalazine due to the capping effect of the SSPI. In contrast, when the delivery system reached the small intestine (pH 7.4) the change in pH induced the hydrolyzate destabilization, which favors protein hydrolysis by the pancreatin enzyme. The result was a controlled, slow and sustained drug release in the small intestine.

Table 2. Summary of suitable pH-driven molecular to be used in oral control delivery

Gating molecule or system	Closed	Opened	Cargo	Suitable location	delivery	Reference
Carboxylic acid	Neutral	Acid	Vancomycin	Stomach		Yang *et al.*, 2005
Chitosan	Neutral	Acid	Ibuprofen	Stomach		Popat *et al.*, 2012a
α-cyclodextrine	Neutral	Acid	Propidium iodide	Stomach		Du *et al.*, 2009
β-cyclodextrine	Neutral	Acid	Rhodamine B	Stomach		Guo *et al.*, 2010
Peptide K_8	Neutral	Acid	Doxorubicin	Stomach		Luo *et al.*, 2013
Polydopamine	Neutral	Acid	Doxorubicin	Stomach		Zheng *et al.*, 2014
Poly(dimethyldiallylammonium chloride)	Neutral/ Basic	Acid	Vancomycin	Stomach		Yang *et al.*, 2005
Poly(4-vinyl pyridine)	Neutral	Acid	Tris(bipyridine) ruthenium(II) chloride	Stomach		Liu *et al.*, 2011

Table 2. *Continuation*

Gating molecule or system	Closed	Opened	Cargo	Suitable delivery location	Reference
3-aminopropyltrimethoxysilane	Acid	Neutral	Ibuprofen	Small Intestine	Cauda *et al.*, 2010
β-lactoglobulin	Acid	Neutral	Ibuprofen	Small Intestine	Guillet-Nicolas *et al.*, 2013
Bovine serum albumin conjugated with lactobionic acid	Acid	Neutral	Doxorubicin	Small Intestine	Luo *et al.*, 2012
Hydroxypropyl methylcellulose phthalate	Acid	Neutral	Famotidine	Small Intestine	Xu *et al.*, 2009
Lysozyme	Acid	Neutral	Rhodamine B	Small Intestine	Xue *et al.*, 2012
Oligonucleotide	Acid	Neutral/ Basic	Rhodamine B	Small Intestine	Chen *et al.*, 2011
Poly(acrylic acid)	Acid	Neutral/ Basic	Salidroside	Small Intestine	Peng *et al.*, 2013
Polyamines	Acid	Neutral	Squaraine Tris(bipyridine) ruthenium(II) chloride Riboflavine Folic acid	Small Intestine	Casasús *et al.*, 2004 Casasús *et al.*, 2008 Bernardos *et al.*, 2008 Pérez-Esteve *et al.*, 2015
Trimethylammonium groups	Acid	Neutral	Sulfasalazine	Small Intestine	Lee *et al.*, 2008 Cheng *et al.*, 2011

Table 3. Summary of suitable enzyme-driven molecular to be used in oral control delivery

Gating molecule or system	Closed	Opened	Cargo	Suitable delivery location	Reference
Avidin–biotin complex	Absence of trypsin	Presence of trypsin	Fluorescein	Small intestine	Schlossbauer *et al.*, 2009
Bioactive peptide shell	Absence of thermolysin and elastase	Presence of thermolysin and elastase	Fluorescein isothiocyanate-labelled dextran	Small intestine	Thornton & Heise, 2010
β-cyclodextrin	Absence of α-amylase and lipase	Presence of α-amylase and lipase	Calcein	Small intestine	Park *et al.*, 2009
Hydrolysed starch	Absence of pancreatine	Presence of pancreatine (amylases and β-D-galactosidase)	Tris(bipyridine) ruthenium(II) chloride	Small intestine	Bernardos *et al.*, 2010
Lactose	Absence lactase (β-D-galactosidase)	Presence lactase (β-D-galactosidase)	Tris(bipyridine) ruthenium(II) chloride	Small Intestine	Bernardos *et al.*, 2009

Table 3. *Continuation.*

Gating molecule or system	Closed	Opened	Cargo	Suitable delivery location	Reference
Oligodeoxynucleotide	Absence of deoxyribonuclease	Presence of deoxyribonuclease	Fluorescein	Small intestine	Zhu *et al.*, 2011a
Peptide sequence	Absence of peptidases or acid pH	Presence of peptidases and neutral pH	Tris(bipyridine) ruthenium(II) chloride	Small Intestine	Coll *et al.*, 2011
Poly(L-lysine)	Absence of α-chymotrypsin	Presence of α-chymotrypsin	Fluorescein	Small intestine	Zhu *et al.*, 2011b
Protamine	Absence of trypsin	Presence of trypsin	Diclofenac	Small intestine	Radhakrishnan *et al.*, 2014
Single-stranded DNA	Absence of deoxyribonuclease	Presence of deoxyribonuclease	Colchicine	Small intestine	Zhang *et al.*, 2014

Table 3. *Continuation.*

Gating molecule or system	Closed	Opened	Cargo	Suitable delivery location	Reference
α-cyclodextrin included onto a polyethyleneglycol fragment	Absence of esterase	Presence of bacterial esterases	Rhodamine B	Colon	Patel *et al.*, 2008
Azobenzene-4,4'-dicarboxylic acid	Absence of azo-reductase	Presence of bacterial azo-reductase	Ibuprofen	Colon	Li *et al.*, 2014
Azopyridine derivative	Absence of azo-reductases and esterases	Presence of bacterial azo-reductases and esterases	Rhodamine B	Colon	Mas *et al.*, 2013
Choline-sulfonatocalix[4]arene [2]pseudorotaxane	Absence of urease	Presence of bacterial ureases	Rhodamine B	Colon	Sun *et al.*, 2013
Ethylene glycol	Absence of esterase	Presence of bacterial esterases	Tris(bipyridine) ruthenium(II) chloride	Colon	Agostini *et al.*, 2012a
Galacto-oligosaccharide (GOS)	Absence of β-galactosidase	Presence of β-galactosidase	Rhodamine B	Colon	Agostini *et al.*, 2012b
Sulfasalazine	Absence of bacterial azo-reductase	Presence of bacterial azo-reductase	Sulfasalazine	Colon	Popat *et al.*, 2012b

5. Benefits and potential current limitations of MSPs for their use in human food

As previously demonstrated, delivery systems based on hybrid organic-inorganic MSPs show most of the desired properties for a smart delivery system: high loading capacity, controlled release rate of a bioactive molecule at a particular site in response to a particular trigger, good biocompatibility, low-cost fabrication given its composition, easy handling, etc. Yet, given its novelty, some limitations (toxicological, technological, semantic, legal and sociological) still need to be overcome, before starting to use MSP as smart delivery systems in food and nutrition.

5.1 Toxicological: lack of conclusive studies

Despite silica not being considered harmful for humans, it is known that engineered nanomaterials are not governed by the same laws as larger particles (Pérez-Esteve *et al.*, 2013). If we bear in mind that change in size affects the functionality of particles, it could also affect people exposed to newly developed particles. In this context, in recent years, several studies have addressed the toxicological and biocompatibility properties of MSPs.

The impact of nanoparticles generally depends on certain properties, such as particle size, size distribution, shape, solubility, reactivity, mass, chemical composition, surface properties (area and charge) and aggregation state (Chau *et al.*, 2007; Athinarayanan *et al.*, 2014).

He *et al.* (2009) studied the effect of particle size (nano- and microparticles), concentration, biodegradation products, and residual surfactant on the cytotoxicity of human breast-cancer cell lines (MDA-MB-468) and African green monkey kidney cell lines (COS-7). These authors observed that 190 nm and 420 nm particles showed significant cytotoxicity at concentrations above 25 mg mL^{-1}, while microscale particles of 1220 nm showed only slight cytotoxicity due to reduced endocytosis. In line with this, in an *in vivo* study with male nude mice,

Souris *et al.* (2010) confirmed that after oral administration, silica nanoparticles located in the liver could be excreted into the intestine by the hepatobiliary excretion process. Later, Fu *et al.* (2013) demonstrated with female ICR mice that silica nanoparticles (110 nm in size) are absorbed into the body at 24 h of oral administration. Yet once absorbed, particles are transported via the portal vein to the liver and are then eliminated during a 7-day period by fecal excretion, and also through urine, without changing the kidney microstructure. These results agree with the studies done into tissue distribution and excretion kinetics of orally administered silica nanoparticles in rats carried out by Lee *et al.* (2014). These authors reported that after ingestion, particles are distributed to kidneys, liver, lungs and spleen. However, silica particles are easily decomposed and eliminated via urinary and fecal excretion after oral exposure. The smaller the particles, the more rapidly they are secreted, presumably because they are more easily decomposed.

As well as particle size, particle shape seems important when talking about potential toxicology. Tao *et al.* (2008) evaluated the effect of two types of mesoporous silica particles on mitochondrial O_2 consumption. For this purpose, the effect of SBA-15 (irregular rods of ca. 1000 nm in length and aspect ratio of 1:5) and MCM-41 (spheres of 300-1000 nm in diameter) on mitochondrial O_2 consumption (respiration) was evaluated in HL-60 (myeloid) cells, Jurkat (lymphoid) cells, and isolated mitochondria. These authors observed that while SBA-15 inhibited cellular respiration at 25-500 μg mL^{-1}, MCM-41 had no noticeable effect on the respiration rate.

Finally, surface properties also seem relevant for potential toxicology (Tang *et al.,* 2012). Specifically, van Schooneveld *et al.* (2008) reported the improved biocompatibility and pharmacokinetics of silica nanoparticles by means of a lipid coating. In their extensive study on bare and lipid-coated silica nanoparticles in mice, these authors concluded that coating porous silica with organic molecules can increase the biocompatibility and half-lives of cells by more than 10-fold compared to bare silica mesoporous supports.

Thus despite adverse effects having been observed in some cells or animals treated with different concentrations of some MSPs, other *in vitro* and *in vivo* studies have suggested that certain particles are well tolerated by both cells and superior animals. Therefore, it is hard to draw conclusive conclusions about the biocompatibility and toxicity of MSPs as a unique concept. In any case, the use of mesoporous silica microparticles functionalized on their surface with biocompatible organic molecules seems a good strategy to minimize the risks associated with using MSPs as supports to develop smart delivery systems.

5.2 Technological problems: mass production and impact of MSPS-based delivery systems on the food matrix

There is no doubt that the application of MSP-based delivery systems to the formulation of novel functional foods opens up new strategies for the food industry. However, before launching foods that contain MSPs to the market, some technological problems should be solved.

First problem is related with the mass production of MSPs. To date, processes for the synthesis, loading and functionalization of MSPs are being developed on a laboratory scale. As a result, production costs are high and mass production is practically underdeveloped.

The second technological problem is related to the compatibility of these devices with the food matrix. Generally, introducing new ingredients or additives to a food matrix can affect the physico-chemical and sensory properties of the product. However, it is considered that a delivery system suitable for a particular application should be compatible with the food or beverage matrix that it is to be incorporated into, and should cause no adverse effects on product appearance, flavor, texture, mouth feel or shelf life.

Despite the importance of this aspect, as far as we know, there is only one publication that has dealt with determining the influence of MSPs on physical properties of the food matrix to which they could be included (Pérez-Esteve *et al.,* 2014). However, since MSPs have a high load capacity and bioactive compounds

exhibit their functional properties at very low concentrations, it is assumed that the amount of support needed to release an adequate concentration of the component is very low. Thus it is foreseeable that the physicochemical features of the matrix that is to incorporate these supports should not be affected by the presence of encapsulating systems.

5.3 Semantic: Disharmonized and changing and denominations

As previously described, the MSPs concept involves structures of silicon dioxide (SiO_2) arranged in such a way that they are able to create pores of 2-50 nm. This structure on the nanoscale is the key to design molecular or supramolecular capped materials. Its design, fabrication, manipulation and characterization are possible thanks to nanotechnology. Therefore, should MSPs be considered nanomaterials? It is clear that mesoporous silica nanoparticles are nanomaterials. But what happens with mesoporous silica microparticles? By taking into account only European recommendations and regulations, denominations are disharmonized and have changed over the years.

Regulation (EC) No. 1169/2011, on the provision of food information to consumers, defined the engineered nanomaterial concept as intentionally produced materials that have one dimension or more in the order of 100 nm, or less, or is composed of discrete functional parts, either internally or on the surface, many of which have one dimension or more in the order of 100 nm, or less, including structures, agglomerates or aggregates, whose size above the order may be 100 nm, but retain characteristic properties of the nanoscale. Characteristic of the nanoscale includes: (i) those related to the large specific surface area of the materials considered; and/or (ii) the specific physico-chemical properties that differ from those of the non nanoform of the same material. According to this definition, and regardless of size, MSPs can be considered nanomaterials as they are intentionally produced to modify their physico-chemical properties and to create nanoporous structures to increase their specific surface area.

In the same year, the European Commission defined nanomaterials as natural, incidental or manufactured material that contains particles, in an unbound state, or as an aggregate or agglomerate, where for >50% of the particles in the number size distribution, one external dimension or more falls within the 1-100 nm size range (EU, 2011). This definition is in line with the opinion of the Scientific Committee on Emerging and Newly Identified Health Risks (SCENIHR), included the size distribution of a material as a defining element, and excludes other types of nanostructured materials, such as nanoporous or nanocomposite materials, since there is not enough evidence to guide what materials should be included.

These definitions, apart from being technical, affect regulatory aspects and food labeling. Thus, they are vital for the future of these systems. The NanoDefine Project (FP7) is expected to deliver an implementable test scheme for regulatory purposes to distinguish nano from non nanomaterials by 2017.

5.4 Legal: Lack of specific regulations

According to their composition (SiO_2), MSPs should be authorized for use in food. SiO_2 is "Generally Recognized as Safe" (GRAS) by FDA regulations. It is also an authorized additive in Europe and achieves the E-551 classification (Contado *et al.,* 2013). In the food industry, synthetic amorphous silica has been used for many years to clear beers and wines, as an anti-caking agent to maintain the flow properties of powder products, and as a carrier agent for flavorings and aromas, and to thicken pastes.

However when we consider their physical features, MSPs could be classified as novel food ingredients based on engineered nanomaterials. Thus in order to place a specific MSP as a food ingredient in the Community market, the applicant should submit a request to the Member State in which the product would be placed (Regulation (EC) No. 258/97). If approved, the presence of the engineered nanomaterial should be clearly indicated in the list of ingredients by writing the word "nano" in brackets (Regulation (EC) No. 1169/2011).

5.5 Sociological: in the face of the unknown, the precautionary principle

The uncertainty in purely semantic aspects and in conclusive toxicological studies has not only consequences at a regulatory level, but also influences consumers' risk perception and acceptance. Although very little research has been conducted in developing countries on consumer attitudes toward foods that contain nanostructured ingredients, recent studies point out that lack of information about the impact of nanotechnology on environmental and health consequences leads consumers to apply the precautionary principle and, therefore, to reject such products (Chau *et al.,* 2007).

For novel foods to be accepted, consumers must perceive that any potential benefits outweigh potential risks or negative effects (for example, potential for a negative impact on the environment, human and animal health, or ethical concerns, such as animal welfare or social equity) (Frewer & Fischer, 2010).

For this to happen, information about the potential benefits and potential risks should not only be accurate, but also very clear. This entails properly regulating the use of nanotechnologies in food and publishing conclusive studies about the potential risks of each type of MSP by considering all the variables that can affect their toxicity. Until this time comes, generalizations, doubts or risk perceptions will outweigh the real benefits.

6. Conclusions

Gated MSPs have the potential to encapsulate bioactive molecules and, consequently, to protect them from the environment during production, storage and digestion, to mask their odor and taste, to improve their compatibility with the food matrix, and to amend their bioaccessibility along the GIT. This review reports the most recent research into the design of gated mesoporous siliceous materials for controlled release along the GIT using physiologic stimuli. It also highlights the possibilities of naturally-occurring stimulus along the GIT that could

be used to develop new gated systems. Applications for these capped materials can be found in the design of novel functional foods.

Nevertheless, given their novelty, the incorporation of gated-MSPs into food still poses major challenges (i.e. technological, toxicological, legal, sociological...) that need to be overcome by researchers and regulatory bodies. Researchers have the task of evaluating the potential hazards of MSPs-gated systems in human health and the environment, and to design specifically designed systems to be triggered in the gastrointestinal tract. Regulatory bodies should provide specific regulations and criteria to be followed when evaluating the safety of this new smart delivery system to be used in food applications. Collaborative work from those groups will be essential in forthcoming years to generate confidence in industry and consumers. Only then will functional foods developed by this new technology be available in the food chain.

References

Agostini, A., Mondragón, L., Pascual, L., Aznar, E., Coll, C., Martínez-Máñez, R., Sancenón, F., Soto, J., Marcos, M. D., Amorós, P., Costero, A. M., Parra, M., & Gil, S. (2012). Design of enzyme-mediated controlled release systems based on silica mesoporous supports capped with ester-glycol groups. *Langmuir*, *28*(41), 14766-14776.

Agostini, A., Mondragón, L., Bernardos, A., Martínez-Máñez, R., Marcos, M. D., Sancenón, F., Soto, J., Costero, A., Manguan-García, C., Perona, R., Moreno-Torres, M., Aparicio-Sanchis, R. & Murguía, J. R. (2012). Targeted cargo delivery in senescent cells using capped mesoporous silica nanoparticles. *Angewandte Chemie International Edition*, *51*(42), 10556-10560.

Akhtar, M. J., Khan, M. A., & Ahmad, I. (2003). Identification of photoproducts of folic acid and its degradation pathways in aqueous solution. *Journal of pharmaceutical and biomedical analysis*, *31*(3), 579-588.

Arcos, D., & Vallet-Regí, M. (2013). Bioceramics for drug delivery. *Acta Materialia*, *61*(3), 890-911.

Aryee, A. N., & Boye, J. I. (2015). Current and Emerging Trends in the Formulation and Manufacture of Nutraceuticals and Functional Food Products.*Nutraceutical and Functional Food Processing Technology*, 1-52.

Athinarayanan, J., Periasamy, V. S., Alsaif, M. A., Al-Warthan, A. A., & Alshatwi, A. A. (2014). Presence of nanosilica (E551) in commercial food products: TNF-mediated oxidative stress and altered cell cycle progression in human lung fibroblast cells. *Cell Biology and Toxicology*, *30*(2), 89-100.

Aznar, E., Martínez-Máñez, R., & Sancenón, F. (2009a). Controlled release using mesoporous materials containing gate-like scaffoldings. *Expert Opinion on Drug Delivery,6*(6), 643-655.

Aznar, E., Marcos, M. D., Martínez-Máñez, R., Sancenón, F., Soto, J., Amorós, P., & Guillem, C. (2009b). pH-and photo-switched release of guest molecules from mesoporous silica supports. *Journal of the American Chemical Society*,*131*(19), 6833-6843.

Bagshaw, S. A., Prouzet, E., & Pinnavaia, T. J. (1995). Templating of mesoporous molecular sieves by nonionic polyethylene oxide surfactants.*Science*, *269*(5228), 1242-1244.

Bailey, L. B., & Gregory, J. F. (1999). Folate metabolism and requirements.*The Journal of nutrition*, *129*(4), 779-782.

Balas, F., Manzano, M., Horcajada, P., & Vallet-Regí, M. (2006). Confinement and controlled release of bisphosphonates on ordered mesoporous silica-based materials. *Journal of the American Chemical Society*, *128*(25), 8116-8117.

Bech-Larsen, T., & Grunert, K. G. (2003). The perceived healthiness of functional foods: A conjoint study of Danish, Finnish and American consumers' perception of functional foods. *Appetite*, *40*(1), 9-14.

Beck, J. S., Vartuli, J. C., Roth, W. J., Leonowicz, M. E., Kresge, C. T., Schmitt, K. D., Chu, C. T. W., Olson, D. H., & Sheppard, E. W. (1992). A new family of mesoporous molecular sieves prepared with liquid crystal templates. *Journal of the American Chemical Society*, *114*(27), 10834-10843.

Bernardos, A., Aznar, E., Coll, C., Martínez-Mañez, R., Barat, J. M., Marcos, M. D., Sancenón, F., Benito, A., & Soto, J. (2008). Controlled release of vitamin B2 using mesoporous materials functionalized with amine-bearing gate-like scaffoldings. *Journal of Controlled Release*, *131*(3), 181-189.

Bernardos, A., Aznar, E., Marcos, M. D., Martínez-Máñez, R., Sancenón, F., Soto, J., Barat, J. M. & Amorós, P. (2009). Enzyme-Responsive Controlled Release Using Mesoporous Silica Supports Capped with Lactose. *Angewandte Chemie*,*121*(32), 5998-6001.

Bernardos, A., Mondragon, L., Aznar, E., Marcos, M. D., Martínez-Máñez, R., Sancenón, F., Soto, J., Barat, J. M., Perez-Paya, E., Guillem, C., & Amorós, P. (2010). Enzyme-responsive intracellular controlled release using nanometric silica mesoporous supports capped with "saccharides". *Acs Nano*, *4*(11), 6353-6368.

Bernardos, A., Mondragón, L., Javakhishvili, I., Mas, N., de la Torre, C., Martínez-Máñez, R., Sancenón F., Barat, J. M., Hvilsted, S., Orzaez, M., Pérez-Payá, E., & Amorós, P. (2012). Azobenzene Polyesters Used as Gate-Like Scaffolds in Nanoscopic Hybrid Systems. *Chemistry-A European Journal*, *18*(41), 13068-13078.

Bernardos, A., & Kourimská, L. (2013). Applications of mesoporous silica materials in food-a review. *Czech Journal of Food Science*, *31*(2), 99-107.

Bhagiyalakshmi, M., Yun, L. J., Anuradha, R., & Jang, H. T. (2010). Utilization of rice husk ash as silica source for the synthesis of mesoporous silicas and their application to CO 2 adsorption through TREN/TEPA grafting. *Journal of hazardous materials*, *175*(1), 928-938.

Branum, A. M., Bailey, R., & Singer, B. J. (2013). Dietary supplement use and folate status during pregnancy in the United States. *The Journal of nutrition*, *143*(4), 486-492.

Burguete, P., Beltrán, A., Guillem, C., Latorre, J., Pérez-Pla, F., Beltrán, D., & Amorós, P. (2012). Pore length effect on drug uptake and delivery by mesoporous silicas. *ChemPlusChem*, *77*(9), 817-831.

Campieri, M., & Gionchetti, P. (1999). Manipulation of intestinal microflora. In: Rutgeerts, P. (Ed.), *Advances in inflammatory bowel disease* (pp. 297-300). London: Kluwer Academic.

Cao, Z., Yang, L., Yan, Y., Shang, Y., Ye, Q., Qi, D., Ziener, U., Shan, G., & Landfester, K. (2013). Fabrication of nanogel core-silica shell and hollow silica nanoparticles via an interfacial sol-gel process triggered by transition-metal salt in inverse systems. *Journal of colloid and interface science*, *406*, 139-147.

Casasús, R., Marcos, M. D., Martínez-Máñez, R., Ros-Lis, J. V., Soto, J., Villaescusa, L. A., Amorós, P., Beltrán, D., Guillem, C., & Latorre, J. (2004). Toward the development of ionically controlled nanoscopic molecular gates. *Journal of the American Chemical Society*, *126*(28), 8612-8613.

Casasús, R., Climent, E., Marcos, M. D., Martínez-Máñez, R., Sancenón, F., Soto, J, Amorós, P., Cano, J., & Ruiz, E. (2008). Dual aperture control on pH-and anion-driven supramolecular nanoscopic hybrid gate-like ensembles. *Journal of the American Chemical Society*, *130*(6), 1903-1917.

Cauda, V., Argyo, C., Schlossbauer, A., & Bein, T. (2010). Controlling the delivery kinetics from colloidal mesoporous silica nanoparticles with pH-sensitive gates. *Journal of Materials Chemistry*, *20*(21), 4305-4311.

Chau, C. F., Wu, S. H., & Yen, G. C. (2007). The development of regulations for food nanotechnology. *Trends in Food Science & Technology*, *18*(5), 269-280.

Chen, C., Pu, F., Huang, Z., Liu, Z., Ren, J., & Qu, X. (2010). Stimuli-responsive controlled-release system using quadruplex DNA-capped silica nanocontainers. *Nucleic acids research*, *39,* 1638-1644.

Chen, J. (2009). Food oral processing—a review. *Food Hydrocolloids*, *23*(1), 1-25..

Cheng, S. H., Liao, W. N., Chen, L. M., & Lee, C. H. (2011). pH-controllable release using functionalized mesoporous silica nanoparticles as an oral drug delivery system. *Journal of Materials Chemistry*, *21*(20), 7130-7137.

Cheung, R. H. F., Morrison, P. D., Small, D. M., & Marriott, P. J. (2008). Investigation of folic acid stability in fortified instant noodles by use of capillary electrophoresis and reversed-phase high performance liquid chromatography.*Journal of Chromatography A*, *1213*(1), 93-99.

Chiras, D. D. (2015). Nutrition and digestion. In: *Human biology*. (pp. 131-164). Jones & Bartlett Learning. Sudbury.

Choi, S. W., & Mason, J. B. (2002). Folate status: effects on pathways of colorectal carcinogenesis. *The Journal of nutrition*, *132*(8), 2413S-2418S.

Chourasia, M. K., & Jain, S. K. (2003). Pharmaceutical approaches to colon targeted drug delivery systems. *Journal of Pharmaceutical Sciences*, *6*(1), 33-66.

Clarke, R., Smith, A. D., Jobst, K. A., Refsum, H., Sutton, L., & Ueland, P. M. (1998). Folate, vitamin B12, and serum total homocysteine levels in confirmed Alzheimer disease. *Archives of neurology*, *55*(11), 1449-1455.

Climent, E., Marcos, M. D., Martínez-Máñez, R., Sancenón, F., Soto, J., Rurack, K., & Amorós, P. (2009). The determination of methylmercury in real samples using organically capped mesoporous inorganic materials capable of signal amplification. *Angewandte Chemie*, *121*(45), 8671-8674.

Colilla, M., González, B., & Vallet-Regí, M. (2013). Mesoporous silica nanoparticles for the design of smart delivery nanodevices. *Biomaterials Science*, *1*(2), 114-134.

Coll, C., Casasús, R., Aznar, E., Marcos, M. D., Martínez-Máñez, R., Sancenón, F., Soto, J., & Amorós, P. (2007). Nanoscopic hybrid systems with a polarity-controlled gate-like scaffolding for the colorimetric signalling of long-chain carboxylates. *Chemical Communications*, (19), 1957-1959.

Coll, C., Mondragón, L., Martínez-Máñez, R., Sancenón, F., Marcos, M. D., Soto, J., Amorós, P., & Pérez-Payá, E. (2011). Enzyme-Mediated Controlled Release Systems by Anchoring Peptide Sequences on Mesoporous Silica Supports. *Angewandte Chemie International Edition*, *50*(9), 2138-2140.

Coll, C., Bernardos, A., Martínez-Máñez, R., & Sancenón, F. (2012). Gated silica mesoporous supports for controlled release and signaling applications. *Accounts of Chemical Research*, *46*(2), 339-349.

Combs, G. F. (2008). Folates. In: Combs, G. F. (Ed.) *The vitamins* (pp. 355-380). San Diego: Elsevier Academic Press.

Contado, C., Ravani, L., & Passarella, M. (2013). Size characterization by Sedimentation Field Flow Fractionation of silica particles used as food additives. *Analytica Chimica Acta*, *788*, 183-192.

Cornel, M. C., De Smit, D. J., & De Jong-van den Berg, L. T. W. (2005). Folic acid-The scientific debate as a base for public health policy. *Reproductive Toxicology*, *20*(3), 411-415.

Drewnowski, A., & Almiron-Roig, E. (2010). Human Perceptions and Preferences for Fat-Rich Foods.In: Montmayeur, J. P., le Coutre, J. (Ed.), Fat detection: Taste, texture and post ingestive effects (pp. 265-292). Boca Ratón: CRC Press

Du, L., Liao, S., Khatib, H. A., Stoddart, J. F., & Zink, J. I. (2009). Controlled-access hollow mechanized silica nanocontainers. *Journal of the American Chemical Society*, *131*(42), 15136-15142.

Eichholzer, M., Tönz, O., & Zimmermann, R. (2006). Folic acid: a public-health challenge. *The Lancet*, *367*(9519), 1352-1361.

El Haskouri, J., de Zárate, D. O., Guillem, C., Latorre, J., Caldés, M., Beltrán, A.,Beltrán, D., Descalzo, A .B., Rodríguez-López, G., Martínez-Máñez, R., Marcos, M. D., & Amorós, P. (2002). Silica-based powders and monoliths with bimodal pore systems. *Chemical Communications*, (4), 330-331.

European Commission. (1997). Regulation (EC) No 258/97 of the European Parliament and of the Council of 27 January 1997 concerning novel foods and novel food ingredients.

European Commission. (2011). Regulation (EU) No 1169/2011 of the European Parliament and of the Council of 25 October 2011 on the provision of food information to consumers.

European Commission. (2011). Commission recommendation of 18 October 2011 on the definition of nanomaterial 2011/696/EU.

European Food Safety Authority (EFSA). 2009. ESCO report on analysis of risks and benefits of fortification of food with folic acid.

Fallingborg, J. (1999). Intralumnial pH of the human gastrointestinal tract. *Danish Med Bull, 46*, 183-196.

Fang, Z., Bhandari, B. (2012). Spray dyring, freeze drying and related processes for food ingredient and nutraceutical encapsulation. In: Garti, N., McClements, D. J., (Ed.), *Encapsulation and delivery systems for food ingredients and nutraceuticals (*pp. 73-109*)*. Cambridge: Woodhead Publishing..

Fathi, M., Mozafari, M. R., & Mohebbi, M. (2012). Nanoencapsulation of food ingredients using lipid based delivery systems. *Trends in food science & technology*, *23*(1), 13-27.

Fathi, M., Martin, A., & McClements, D. J. (2014). Nanoencapsulation of food ingredients using carbohydrate based delivery systems. *Trends in Food Science & Technology*, *39*(1), 18-39.

Frewer, L., Fischer, A. (2010). The evolution of food technology, novel foods, and the phychology of novel food acceptance. In: Chaudhry, Q., Castle, L., Watkins, R., (Ed.), *Nanotechnologies in food* (pp. 18-31). Cambridge: RSC Nanoscience & Nanotechnology.

Friend, D. R. (1992). Oral control specific drug delivery. In: Friend, D. R. (Ed.), *Structural features and function of the gastrointestinal tract* (pp. 2-23). Florida: CRC Press Inc.

Fu, C., Liu, T., Li, L., Liu, H., Chen, D., & Tang, F. (2013). The absorption, distribution, excretion and toxicity of mesoporous silica nanoparticles in mice following different exposure routes. *Biomaterials*, *34*(10), 2565-2575.

Giménez, C., Climent, E., Aznar, E., Martínez-Máñez, R., Sancenón, F., Marcos, M. D., Amorós, P., & Rurack, K. (2014). Towards Chemical Communication between Gated Nanoparticles. *Angewandte Chemie International Edition*,*53*(46), 12629-12633.

Ginting, E., & Arcot, J. (2004). High-performance liquid chromatographic determination of naturally occurring folates during tempe preparation. *Journal of agricultural and food chemistry*, *52*(26), 7752-7758.

Golding, P. H. (2014). Severe experimental folate deficiency in a human subject-a longitudinal study of biochemical and haematological responses as megaloblastic anaemia develops. *SpringerPlus*, *3*(1), 442-445.

Gregory, J. F. (2007). Vitamins. In: Damodaran, S., Parkin, K. L., Fennema, O. R. (Ed.), *Fennema's Food Chemistry, Fouth Eddition (*pp. 439-522). Boca Raton: CRC Press.

Guillet-Nicolas, R., Popat, A., Bridot, J. L., Monteith, G., Qiao, S. Z., & Kleitz, F. (2013). pH-Responsive Nutraceutical-Mesoporous Silica Nanoconjugates with Enhanced Colloidal Stability. *Angewandte Chemie International Edition*, *125*(8), 2374-2378.

Han, L., Gao, C., Wu, X., Chen, Q., Shu, P., Ding, Z., & Che, S. (2011). Anionic surfactants templating route for synthesizing silica hollow spheres with different shell porosity. *Solid State Sciences*, *13*(4), 721-728.

He, Q., Zhang, Z., Gao, Y., Shi, J., & Li, Y. (2009). Intracellular Localization and Cytotoxicity of Spherical Mesoporous Silica Nano-and Microparticles. *Small*, *5*(23), 2722-2729.

Hernandez, R., Tseng, H. R., Wong, J. W., Stoddart, J. F., & Zink, J. I. (2004). An operational supramolecular nanovalve. *Journal of the American Chemical Society*, *126*(11), 3370-3371.

Hoag, S. W., Ramachandruni, H., & Shangraw, R. F. (1996). Failure of prescription prenatal vitamin products to meet USP standards for folic acid dissolution. *Journal of the American Pharmaceutical Association 37*(4), 397-400.

Hoffbrand, A. V., & Weir, D. G. (2001). The history of folic acid. *British journal of haematology*, *113*(3), 579-589.

Hoffmann, F., Cornelius, M., Morell, J., & Fröba, M. (2006). Silica-based mesoporous organic-inorganic hybrid materials. *Angewandte Chemie International Edition*, *45*(20), 3216-3251.

Humphrey, S. P., & Williamson, R. T. (2001). A review of saliva: normal composition, flow, and function. *The Journal of Prosthetic Dentistry*, *85*(2), 162-169.

Guo, W., Wang, J., Lee, S. J., Dong, F., Park, S. S., & Ha, C. S. (2010). A General pH-Responsive Supramolecular Nanovalve Based on Mesoporous Organosilica Hollow Nanospheres. *Chemistry-A European Journal*, *16*(29), 8641-8646.

Ishii, R., Itoh, T., Yokoyama, T., Matsuura, S. I., Tsunoda, T., Hamakawa, S., Mizukami, F., & Hanaoka, T. A. (2012). Preparation of mesoporous silicas using food grade emulsifiers and its application for enzyme supports. *Journal of Non-Crystalline Solids*, *358*(14), 1673-1680.

Izquierdo-Barba, I., Sousa, E., Doadrio, J. C., Doadrio, A. L., Pariente, J. P., Martínez, A., Babonneau, F., & Vallet-Regí, M. (2009a). Influence of mesoporous structure type on the controlled delivery of drugs: release of ibuprofen from MCM-48, SBA-15 and functionalized SBA-15. *Journal of sol-gel science and technology*,*50*(3), 421-429.

Izquierdo-Barba, I., Vallet-Regí, M., Kupferschmidt, N., Terasaki, O., Schmidtchen, A., & Malmsten, M. (2009b). Incorporation of antimicrobial compounds in mesoporous silica film monolith. *Biomaterials*, *30*(29), 5729-5736.

Jang, H. T., Park, Y., Ko, Y. S., Lee, J. Y., & Margandan, B. (2009). Highly siliceous MCM-48 from rice husk ash for CO_2 adsorption. *International Journal of Greenhouse Gas Control*, *3*(5), 545-549.

Jansen, J. C., Shan, Z., Marchese, L., Zhou, W., vd Puil, N., & Maschmeyer, T. (2001). A new templating method for three-dimensional mesopore networks.*Chemical Communications*, (8), 713-714.

Kapoor, M. P., Vinu, A., Fujii, W., Kimura, T., Yang, Q., Kasama, Y., ... & Juneja, L. R. (2010). Self-assembly of mesoporous silicas hollow microspheres via food grade emulsifiers for delivery systems. *Microporous and Mesoporous Materials*, *128*(1), 187-193.

Kierys, A., Buda, W., & Goworek, J. (2010). The porosity and morphology of mesoporous silica agglomerates. *Journal of Porous Materials*, *17*(6), 669-676.

Krohn, K., Demmelmair, H., Koletzko, B. (2008) Macronutrient requirements for growth: fats and fatty acids. In: Duggan, C., Watkins, J. B., Walker, A. (Ed.) *Nutrition in paediatrics* (pp. 59-66). Ontairo: BC Decker.

Lai, C. Y., Trewyn, B. G., Jeftinija, D. M., Jeftinija, K., Xu, S., Jeftinija, S., & Lin, V. S. Y. (2003). A mesoporous silica nanosphere-based carrier system with chemically removable CdS nanoparticle caps for stimuli-responsive controlled release of neurotransmitters and drug molecules. *Journal of the American Chemical Society*, *125*(15), 4451-4459.

Lee, C. H., Lo, L. W., Mou, C. Y., & Yang, C. S. (2008). Synthesis and Characterization of Positive-Charge Functionalized Mesoporous Silica Nanoparticles for Oral Drug Delivery of an Anti-Inflammatory Drug. *Advanced Functional Materials*, *18*(20), 3283-3292.

Lee, J. A., Kim, M. K., Paek, H. J., Kim, Y. R., Kim, M. K., Lee, J. K., Jeong, J., & Choi, S. J. (2014). Tissue distribution and excretion kinetics of orally administered silica nanoparticles in rats. *International journal of nanomedicine*,*9*(Suppl 2), 251.

Levine, M. J., Reddy, M. S., Tabak, L. A., Loomis, R. E., Bergey, E. J., Jones, P. C., Cohen, R. E., Stinson, M. W., & Al-Hashimi, I. (1987). Structural aspects of salivary glycoproteins. *Journal of dental research*, *66*(2), 436-441.

Li, X., Tang, T., Zhou, Y., Zhang, Y., & Sun, Y. (2014). Applicability of enzyme-responsive mesoporous silica supports capped with bridged silsesquioxane for colon-specific drug delivery. *Microporous and Mesoporous Materials*, *184*, 83-89.

Li, Z. Z., Wen, L. X., Shao, L., & Chen, J. F. (2004). Fabrication of porous hollow silica nanoparticles and their applications in drug release control. *Journal of Controlled Release*, *98*(2), 245-254.

Liu, R., Zhao, X., Wu, T., & Feng, P. (2008). Tunable redox-responsive hybrid nanogated ensembles. *Journal of the American Chemical Society*, *130*(44), 14418-14419.

Liu, R., Liao, P., Liu, J., & Feng, P. (2011). Responsive polymer-coated mesoporous silica as a pH-sensitive nanocarrier for controlled release. *Langmuir*, *27*(6), 3095-3099.

Lubecka-Pietruszewska, K., Kaufman-Szymczyk, A., Stefanska, B., & Fabianowska-Majewska, K. (2013). Folic acid enforces DNA methylation-mediated transcriptional silencing of PTEN, APC and RARbeta2 tumour suppressor genes in breast cancer. *Biochemical and biophysical research communications*, *430*(2), 623-628.

Lucock, M. (2000). Folic acid: nutritional biochemistry, molecular biology, and role in disease processes. *Molecular genetics and metabolism*, *71*(1), 121-138.

Lucock, M., & Yates, Z. (2009). Folic acid fortification: a double-edged sword.*Current Opinion in Clinical Nutrition & Metabolic Care*, *12*(6), 555-564.

Luo, G. F., Chen, W. H., Liu, Y., Zhang, J., Cheng, S. X., Zhuo, R. X., & Zhang, X. Z. (2013). Charge-reversal plug gate nanovalves on peptide-functionalized mesoporous silica nanoparticles for targeted drug delivery.*Journal of Materials Chemistry B*, *1*(41), 5723-5732.

Luo, Z., Cai, K., Hu, Y., Zhang, B., & Xu, D. (2012). Cell-Specific Intracellular Anticancer Drug Delivery from Mesoporous Silica Nanoparticles with pH Sensitivity. *Advanced Healthcare Materials*, *1*(3), 321-325.

McClements, D. J. (2012). Requirements for food ingredient and nutraceutical delivery systems. In: Garti, N., McClements, D.J. (Ed.), *Encapsulation and delivery systems for food ingredients and nutraceuticals* (p. 3-18). Cambridge: Woodhead Publishing.

Mal, N. K., Fujiwara, M., & Tanaka, Y. (2003). Photocontrolled reversible release of guest molecules from coumarin-modified mesoporous silica. *Nature*,*421*(6921), 350-353.

Manzano, M., Aina, V., Arean, C. O., Balas, F., Cauda, V., Colilla, M., ... & Vallet-Regi, M. (2008). Studies on MCM-41 mesoporous silica for drug delivery: effect of particle morphology and amine functionalization. *Chemical Engineering Journal*, *137*(1), 30-37.

Márquez-Alvarez, C., Sastre, E., & Pérez-Pariente, J. (2004). Solid catalysts for the synthesis of fatty esters of glycerol, polyglycerols and sorbitol from renewable resources. *Topics in Catalysis*, *27*(1-4), 105-117.

Mas, N., Agostini, A., Mondragón, L., Bernardos, A., Sancenón, F., Marcos, M. D., Martínez-Máñez, R,, Costero, A. M., Gil, S., Merino-Sanjuán, M., Amorós, P., Orzáez, M., & Pérez-Payá, E. (2013). Enzyme-responsive silica mesoporous supports capped with azopyridinium salts for controlled delivery applications. *Chemistry-A European Journal*, *19*(4), 1346-1356.

Milabuer, M. N., Kam, Y., Rubinstein, A. (2010). Orally administered drug delivery systems to the colon. In: Wen, H., Park, K. (Ed.), *Oral controlled release formulation design and drug delivery* (pp. 225-243). New Jersey: Willey.

Moat, S. J., Lang, D., McDowell, I. F., Clarke, Z. L., Madhavan, A. K., Lewis, M. J., & Goodfellow, J. (2004). Folate, homocysteine, endothelial function and cardiovascular disease. *The Journal of nutritional biochemistry*, *15*(2), 64-79.

Mondragón, L., Mas, N., Ferragud, V., de la Torre, C., Agostini, A., Martínez-Máñez, R., Sancenón, F., Amorós, P., Pérez-Payá, E., & Orzáez, M. (2014). Enzyme-responsive intracellular-controlled release using silica mesoporous nanoparticles capped with ε-Poly-L-lysine. *Chemistry-A European Journal*, *20*(18), 5271-5281.

Nguyen, T. D., Tseng, H. R., Celestre, P. C., Flood, A. H., Liu, Y., Stoddart, J. F., & Zink, J. I. (2005). A reversible molecular valve. *Proceedings of the National Academy of Sciences of the United States of America*, *102*(29), 10029-10034.

Nieto, A., Balas, F., Colilla, M., Manzano, M., & Vallet-Regí, M. (2008). Functionalization degree of SBA-15 as key factor to modulate sodium alendronate dosage. *Microporous and Mesoporous Materials*, *116*(1), 4-13.

Park, C., Kim, H., Kim, S., & Kim, C. (2009). Enzyme responsive nanocontainers with cyclodextrin gatekeepers and synergistic effects in release of guests. *Journal of the American Chemical Society*, *131*(46), 16614-16615.

Patel, K., Angelos, S., Dichtel, W. R., Coskun, A., Yang, Y. W., Zink, J. I., & Stoddart, J. F. (2008). Enzyme-responsive snap-top covered silica nanocontainers. *Journal of the American Chemical Society*, *130*(8), 2382-2383.

Peng, H., Dong, R., Wang, S., Zhang, Z., Luo, M., Bai, C., Zhao, Q., Li, J., Chen, L., & Xiong, H. (2013). A pH-responsive nano-carrier with mesoporous silica nanoparticles cores and poly (acrylic acid) shell-layers: Fabrication, characterization and properties for controlled release of salidroside. *International journal of pharmaceutics*, *446*(1), 153-159.

Pérez-Esteve, E., Bernardos, A., Martínez-Máñez, R., & M Barat, J. (2013). Nanotechnology in the development of novel functional foods or their package. An overview based in patent analysis. *Recent patents on food, nutrition & agriculture*, *5*(1), 35-43.

Pérez-Esteve, É., Fuentes, A., Coll, C., Acosta, C., Bernardos, A., Amorós, P., Marcos, M. D., Sancenón, F., Martínez-Máñez, R., & Barat, J. M. (2015). Modulation of folic acid bioaccessibility by encapsulation in pH-responsive gated mesoporous silica particles. *Microporous and Mesoporous Materials*, *202*, 124-132.

Pérez-Esteve, E., Oliver, L., García, L., Nieuwland, M., de Jongh, H. H., Martínez-Máñez, R., & Barat, J. M. (2014). Incorporation of mesoporous silica particles in gelatine gels: Effect of particle type and surface modification on physical properties. *Langmuir*, *30*(23), 6970-6979.

Pitkin, R. M. (2007). Folate and neural tube defects. *The American journal of clinical nutrition*, *85*(1), 285S-288S.

Popat, A., Liu, J., Lu, G. Q. M., & Qiao, S. Z. (2012). A pH-responsive drug delivery system based on chitosan coated mesoporous silica nanoparticles.*Journal of Materials Chemistry*, *22*(22), 11173-11178.

Popat, A., Ross, B. P., Liu, J., Jambhrunkar, S., Kleitz, F., & Qiao, S. Z. (2012). Enzyme-Responsive Controlled Release of Covalently Bound Prodrug from Functional Mesoporous Silica Nanospheres. *Angewandte Chemie International Edition*, *51*(50), 12486-12489.

Popat, A., Jambhrunkar, S., Zhang, J., Yang, J., Zhang, H., Meka, A., & Yu, C. (2014). Programmable drug release using bioresponsive mesoporous silica nanoparticles for site-specific oral drug delivery. *Chemical Communications*, *50*(42), 5547-5550.

Radhakrishnan, K., Gupta, S., Gnanadhas, D. P., Ramamurthy, P. C., Chakravortty, D., & Raichur, A. M. (2014). Protamine-Capped Mesoporous Silica Nanoparticles for Biologically Triggered Drug Release. *Particle & Particle Systems Characterization*, *31*(4), 449-458.

Reynolds, E. (2006). Vitamin B12, folic acid, and the nervous system. *The lancet neurology*, *5*(11), 949-960.

Said, H. M. (2011). Intestinal absorption of water-soluble vitamins in health and disease. *Biochemical Journal*, *437*(3), 357-372.

Schlossbauer, A., Kecht, J., & Bein, T. (2009). Biotin-Avidin as a Protease-Responsive Cap System for Controlled Guest Release from Colloidal Mesoporous Silica. *Angewandte Chemie*, *121*(17), 3138-3141.

Spitzer, V. (1997). Folic acid. In: Spitzer, V (Ed.), *Vitamin Basics: The facts about vitamins in nutrition* (pp. 79-84) Waldkirch: DSM Nutritional Products.

Souris, J. S., Lee, C. H., Cheng, S. H., Chen, C. T., Yang, C. S., Ja-an, A. H., ... & Lo, L. W. (2010). Surface charge-mediated rapid hepatobiliary excretion of mesoporous silica nanoparticles. *Biomaterials*, *31*(21), 5564-5574.

Stover, P. J. (2004). Physiology of folate and vitamin B12 in health and disease. *Nutrition reviews*, *62*(1), S3-S12.

Suitor, C. W., & Bailey, L. B. (2000). Dietary folate equivalents: interpretation and application. *Journal of the American Dietetic Association*, *100*(1), 88-94.

Sun, Y. L., Zhou, Y., Li, Q. L., & Yang, Y. W. (2013). Enzyme-responsive supramolecular nanovalves crafted by mesoporous silica nanoparticles and choline-sulfonatocalix [4] arene [2] pseudorotaxanes for controlled cargo release. *Chemical Communications*, *49*(79), 9033-9035.

Talaulikar, V. S., & Arulkumaran, S. (2011). Folic acid in obstetric practice: a review. *Obstetrical & gynecological survey*, *66*(4), 240-247.

Tanev, P. T., & Pinnavaia, T. J. (1995). A neutral templating route to mesoporous molecular sieves. *Science*, *267*(5199), 865-867.

Tang, F., Li, L., & Chen, D. (2012). Mesoporous silica nanoparticles: synthesis, biocompatibility and drug delivery. *Advanced Materials*, *24*(12), 1504-1534.

Tao, Z., Morrow, M. P., Asefa, T., Sharma, K. K., Duncan, C., Anan, A.,... & Souid, A. K. (2008). Mesoporous silica nanoparticles inhibit cellular respiration.*Nano letters*, *8*(5), 1517-1526.

Thornton, P. D., & Heise, A. (2010). Highly specific dual enzyme-mediated payload release from peptide-coated silica particles. *Journal of the American Chemical Society*, *132*(6), 2024-2028.

United States Department of Agriculture (USDA). 2010. *Dietary Guidelines for Americans*. 7th ed. Whasington DC: Government Printing Office.

van Schooneveld, M. M., Vucic, E., Koole, R., Zhou, Y., Stocks, J., Cormode, D. P., ... & Mulder, W. J. (2008). Improved biocompatibility and pharmacokinetics of silica nanoparticles by means of a lipid coating: a multimodality investigation. *Nano letters*, *8*(8), 2517-2525.

Vinu, A., Hossain, K. Z., & Ariga, K. (2005). Recent advances in functionalization of mesoporous silica. *Journal of Nanoscience and Nanotechnology*, *5*(3), 347-371.

Vora, A., Riga, A., Dollimore, D., & Alexander, K. S. (2002). Thermal stability of folic acid. *Thermochimica Acta*, *392*, 209-220.

Wagner, C. (1995). Biochemical role of folate in cellular metabolism. Bailey, L.B. (Ed), *Folate in Health and Disease* (pp. 23-42). New York: Marcel Dekker.

Wang, X., Bu, X., Feng, P. (2011). Porous inorganic materials. Encyclopedia of inorganic and bioinorganic chemistry (pp1-21)

Wang, Y., Bamdad, F., Song, Y., Chen, L. (2012). Hydrogel particles and other novel protein-based methods for food ingredient and nutraceutical delivery systems. In: Garti, N., McClements, D.J. (Ed.), *Encapsulation and delivery systems for food ingredients and nutraceuticals* (pp. 412-450). Cambridge: Woodhead Publishing.

Wright, A. J., Dainty, J. R., & Finglas, P. M. (2007). Folic acid metabolism in human subjects revisited: potential implications for proposed mandatory folic acid fortification in the UK. *British Journal of Nutrition*, *98*(04), 667-675.

Wright, P. A. (2008). Families of microporous framework solids. In. Wright, P. A (Ed.), *Microporous Framework Solids* (pp. 8-78). Cambridge: The royal society of chemistry.

Xu, W., Gao, Q., Xu, Y., Wu, D., & Sun, Y. (2009). pH-Controlled drug release from mesoporous silica tablets coated with hydroxypropyl methylcellulose phthalate. *Materials Research Bulletin*, *44*(3), 606-612.

Xue, M., & Findenegg, G. H. (2012). Lysozyme as a pH-responsive valve for the controlled release of guest molecules from mesoporous silica. *Langmuir*, *28*(50), 17578-17584.

Yanagisawa, T., Shimizu, T., Kuroda, K., & Chuzo, K. (1990). The preparation of alkyltrimethylammonium kanemite complexes and their conversion to microporous silica. *Bulletin of the Chemical Society of Japan*, *63*, 988-992.

Yang, Q., Wang, S., Fan, P., Wang, L., Di, Y., Lin, K., & Xiao, F. S. (2005). pH-responsive carrier system based on carboxylic acid modified mesoporous silica and polyelectrolyte for drug delivery. *Chemistry of Materials*, *17*(24), 5999-6003.

Zhang, L., D'Acunzi, M., Kappl, M., Auernhammer, G. K., Vollmer, D., van Kats, C. M., & van Blaaderen, A. (2009). Hollow silica spheres: synthesis and mechanical properties. *Langmuir*, *25*(5), 2711-2717.

Zhang, G., Yang, M., Cai, D., Zheng, K., Zhang, X., Wu, L., & Wu, Z. (2014). Composite of Functional Mesoporous Silica and DNA: An Enzyme-Responsive Controlled Release Drug Carrier System. *ACS Applied Materials & Interfaces*, *6*(11), 8042-8047.

Zhao, D., Feng, J., Huo, Q., Melosh, N., Fredrickson, G. H., Chmelka, B. F., & Stucky, G. D. (1998a). Triblock copolymer syntheses of mesoporous silica with periodic 50 to 300 angstrom pores. S*cience*, *279*(5350), 548-552.

Zhao, D., Huo, Q., Feng, J., Chmelka, B. F., & Stucky, G. D. (1998b). Nonionic triblock and star diblock copolymer and oligomeric surfactant syntheses of highly ordered, hydrothermally stable, mesoporous silica structures. *Journal of the American Chemical Society*, *120*(24), 6024-6036.

Zhao, X. S. (2006). Novel porous materials for emerging applications. *Journal of Materials Chemistry,* 16, 623-625.

Zhao, Y. L., Li, Z., Kabehie, S., Botros, Y. Y., Stoddart, J. F., & Zink, J. I. (2010). pH-operated nanopistons on the surfaces of mesoporous silica nanoparticles. *Journal of the American Chemical Society*, *132*(37), 13016-13025.

Zheng, Q., Lin, T., Wu, H., Guo, L., Ye, P., Hao, Y., Guo, Q., Jiang, J., Fu, F., & Chen, G. (2014). Mussel-inspired polydopamine coated mesoporous silica nanoparticles as pH-sensitive nanocarriers for controlled release. *International journal of pharmaceutics*, *463*(1), 22-26.

Zhu, Y., Meng, W., & Hanagata, N. (2011). Cytosine-phosphodiester-guanine oligodeoxynucleotide (CpG ODN)-capped hollow mesoporous silica particles for enzyme-triggered drug delivery. *Dalton Transactions*, *40*(39), 10203-10208.

Zhu, Y., Meng, W., Gao, H., & Hanagata, N. (2011). Hollow mesoporous silica/poly (L-lysine) particles for codelivery of drug and gene with enzyme-triggered release property. *The Journal of Physical Chemistry C*, *115*(28), 13630-13636.

4. SCIENTIFIC CONTRIBUTION

4.1 CHAPTER 1. NUTRITIONAL APPROACH

4.1.1 Modulation of folic acid bioaccesibility by encapsulation in pH-responsive gated mesoporous silica particles

Édgar Pérez-Esteve,[a] Ana Fuentes,[a] Carmen Coll,[b,c] Carolina Acosta,[a] Andrea Bernardos,[a,b] Pedro Amorós,[d] María D. Marcos,[b,c] Félix Sancenón, [b,c] Ramón Martínez-Máñez,[b,c,*] José M. Barat[a]

[a]Grupo de Investigación e Innovación Alimentaria, Universitat Politècnica de València. Camino de Vera s/n, 46022, Spain
[b]Centro de Reconocimiento Molecular y Desarrollo Tecnológico (IDM), Unidad Mixta Universitat Politècnica de València - Universidad de Valencia. Departamento de Química Universitat Politècnica de València, Camino de Vera s/n, 46022, Valencia, Spain
[c]CIBER de Bioingeniería, Biomateriales y Nanomedicina (CIBER-BBN)
dInstitut de Ciència dels Materials (ICMUV), Universitat de València, P.O. Box 2085, 46071, Valencia, Spain

Microporous and Mesoporous Materials, ***2015****, 202, 124-132*
(Reproduced with permission of Elsevier)

Abstract

A study on the controlled release of folic acid (FA) from pH-responsive gated mesoporous silica particles (MSPs) is reported. The MCM-41 support was synthesized using tetraethyl orthosilicate (TEOS) as hydrolytic inorganic precursor and the surfactant hexadecyltrimethylammonium bromide (CTAB) as porogen species. Calcination of the mesostructured phase resulted in the starting solid. This solid was loaded with FA to obtain the initial support **S0**. Moreover, this FA-loaded material was further functionalized with N^1-(3-Trimethoxysilylpropyl)diethylenetriamine (N3) in order to obtain the gated polyamine-functionalised material **S1**. Solids **S0** and **S1** were characterized using standard solid state procedures. It was found that the functionalization process and the inclusion of FA on the pores did not modify the mesoporous structure of the starting material. FA delivery studies in water with solids **S0** and **S1** were carried out in water at pH 2 and 7.5. **S0** was not able to completely inhibit FA delivery at acidic pH yet a rapid FA release at neutral pH was observed in few minutes. In contrast, **S1** was tightly capped at pH 2 and displayed a sustained delivery of FA when the pH was switched to 7.5. In the second part of the study, FA loading and functionalization of **S1**-like supports was optimized. In particular, solids loaded with FA in phosphate buffered saline (PBS) and capped with N3 in acetate buffer at pH 2 exhibited a delivery capacity up to 95 μg FA mg^{-1} solid. Finally, FA release from the selected optimized supports was studied following an in vitro digestion procedure. The results showed that amine-capped MSP were not only able to hinder the release of the vitamin in gastric fluids (pH 2), but were also capable of deliver progressively the FA in presence of a simulated intestinal juice (pH 7.5) offering a suitable mechanism to control the bioaccessibility of the vitamin.

Keywords: Folic acid, bioaccessibility, loading optimization, controlled release, mesoporous silica particles.

1. Introduction

Folate is a generic term by which is known a group of water-soluble compounds with B9 vitamin activity and with chemical structures similar to synthetic pteroyl monoglutamic acid (PGA), commonly known as folic acid (FA). Folates are essential to numerous bodily functions, including DNA synthesis and repair, cell division and cell growth (Lucock, 2000). Main folate sources include green leafy vegetables, yeast extracts, liver, kidney, and citrus fruit. Despite this wide distribution, folate deficiency is a common finding that can be caused by a variety of factors such as malabsorption of folate from the diet, an increased utilization by the body or a significant loss up to 50% during cooking processes (Younis *et al.*, 2009). FA deficiency is such important in humans that it can cause neural tube defects in developing embryos (Czeizel *et al.*, 1992), is associated with elevated plasma homocysteine (an emerging risk factor for vascular diseases), with cognitive decline and neurodegenerative diseases such as Alzheimer and also is risk factor for certain tumours (acute lymphoblastic leukaemia, breast cancer, and gastric cancer) (Wright *et al.*, 2001; Koike *et al.*, 2012)

To prevent the occurrence of these and other diseases, food supplementation with folates is mandatory in certain countries such as USA (FDA, 1996), Canada (Health Canada, 1997) or UK (Lucock & Yates, 2009) with the objective of ensure a 400 µg intake for adults and an additional 200 µg for pregnant women (Eichholzer *et al*., 2006). To achieve this supplementation, the most employed molecule is FA, due to its high stability and bioavailability (Sanderson *et al.*, 2003).

Although there are irrefutable evidences about the benefits of FA supplementation to prevent some diseases, recent studies suggest that the margin of the benefit is very narrow, and despite the necessity of the supplementation, a massive exposition to high bioavailable FA could be a double-edged sword (Lucock & Yates, 2009). In particular it has been reported that biotransformation processes of FA are saturated at doses of 266-400 µg of FA and up to this amount unmetabolized FA is found in plasma, which could be correlated with the increase of cancer risk, insulin resistance, preneoplastic and neoplastic

lesions (Kim, 2004). In this context, the design of systems to dosage FA along the digestion and therefore modulating its bioaccessibility and bioavailability is a challenge for current nutritional science.

The bioaccessibility of a nutrient is defined as the amount of the nutrient that is released from a food matrix during digestion and made accessible for absorption into the intestinal mucosa (Hedrén *et al.*, 2002). One possibility to modulate bioaccessibility of a molecule consists of its encapsulation and later controlled release under suitable stimuli. Organic-based ensembles using lipids or carbohydrates have been reported as classical encapsulation systems (Tomiuk *et al.*, 2012). However, they have some important drawbacks, such as the difficulty for a scale production (Chen *et al.,* 2006; Fathi *et al.,* 2012), low stability of the structure during food processing and storage, difficulty of controlling the release rate and also a poor capability to protect the encapsulated substance through the harsh stomach conditions (McClemens & Li, 2010). As an alternative, systems based in polyalcohols, polyamides, celluloses (Mastromatteo *et al.*, 2010) or in mesoporous inorganic materials (Vallet-Regí *et al.*, 2004), have been recently developed as suitable systems for controlled delivery applications. In particular, mesoporous silica particles (MSP) exhibit unique features as supports for controlled release, such as high stability (Ghedini *et al.*, 2010), biocompatibility (Al Shamsi *et al.*, 2010), no apparent toxicity (Suh *et al.*, 2009), large load capacity (Coll *et al.,* 2011), and the possibility to include gate-like scaffoldings on the external surface. This last characteristic allows the design of carriers for on-command delivery in the presence of target physical (such as light, temperature) (Mal *et al.,* 2003; Aznar *et al.*, 2012), chemical (pH-changes, redox potential) (Park *et al.*, 2007; Guillet-Nicolas & Popat, 2013; Jiao *et al.*, 2013; Tian *et al.*, 2013; Zhao *et al.*, 2013) and biomolecules stimuli (enzymes, antibodies, DNA) (Patel *et al.*, 2008; Climent *et al.*, 2009; Agostini *et al.*, 2012; Li *et al.*, 2013). Of those, several gated MSP have proved to show “zero” delivery yet are able to release the cargo under digestive stimuli (Bernardos *et al.*, 2008; Bernardos *et al.*, 2011). In particular, gated ensembles based in amines have been reported to be suitable systems for cargo delivery upon pH changes.

The purpose of this study is, on one hand, to evaluate the use of MSP capped with amines as suitable pH-responsive systems capable to modulate FA delivery and bioaccessibility in *in vitro* digestion assays and on the other hand, to optimize the loading process in these materials to achieve the release of dietary reference intake of folic acid using the minimum amount of inorganic matrix. As far as we know, this is the first time that an optimization of folic acid loading in MSP and a study of *in vitro* delivery from MSP of this molecule of nutritional interest is reported.

2. Materials and methods

2.1 Chemicals

Tetraethyl orthosilicate (TEOS), n-cetyltrimethylammonium bromide (CTABr), sodium hydroxide (NaOH), triethanolamine ($TEAH_3$), the organosiloxane derivative N^1-(3-Trimethoxysilylpropyl)diethylenetriamine (N3), sodium phosphate dibasic (Na_2HPO_4), tetrabutylammonium hydrogen sulphate (TBAHS) and all chemicals for the digestive fluids were provided by Sigma-Aldrich (Poole, Dorset, UK). Folic acid was purchased from Schircks Laboratories (Jona, Switzerland). Acetonitrile HPLC grade was provided by Scharlau (Barcelona, Spain).

2.2 FA molecular structural mechanics simulations

Theoretical calculations of the structure of FA were carried out by using HyperChem 8.0.6 Molecular Modelling System (Hypercube Inc., Gainesville, FL, USA). The calculation of geometry was performed using molecular mechanics MM+ in a first step and AMBER in a second step. Full geometry optimizations were carried out in vacuum employing the Polak-Ribiere conjugate gradient method until an RMS gradient of 0.1 kcal mol^{-1} was reached. The final 3D structure was refined by optimization of the geometry using molecular dynamics methods at a simulation temperature of 300 K. QSAR properties of the vitamin were determined.

2.3 Synthesis of MCM-41

The mesoporous MCM-41 support was first synthesized using the so-called "atrane route" in which 4.68 g of CTAB were added at 118 °C to a solution of TEAH3 (25.79 g) containing 0.045 mol of a silatrane derivative (11 mL of TEOS). Next, 80 mL of water was slowly added with vigorous stirring at 70 °C. After few minutes, a white suspension was formed. This mixture was aged at room temperature overnight. The resulting powder was collected by filtration and washed with water and ethanol. Finally, the solid was dried at 70 °C. To prepare the final mesoporous material, the as-synthesized solid was calcined at 550 °C using an oxidant atmosphere for 5 h in order to remove the template phase.

2.4 Synthesis of S0 and S1

100 mg of MCM-41 and 0.035 g (0.08 mmol) of FA were suspended in 7 mL of phosphate buffered saline (PBS) inside an amber round-bottom flask in an inert atmosphere. The mixture was stirred for 24 h at room temperature to achieve the maximum loading in the pores of the MCM-41 scaffolding. The loaded solid (**S0**) was isolated by vacuum filtration, washed with 300 mL of water adjusted to pH 2, and dried at room temperature for 24 h. This loading process was optimized in further assays *(vide infra* in 2.5).

To obtain **S1**, 100 mg of S0 were suspended in 4 mL of acetonitrile and an excess of N3 (0.43 mL, 0.015 mmol) was added. The final mixture was stirred for 5.5 h at room temperature. The loaded and functionalized solid (**S1**) was isolated by vacuum filtration, washed with 300 mL of water adjusted to pH 2, and dried at room temperature for 24 h.

2.5 Folic acid release studies

To determine the effect of pH in FA release from the non-gated (**S0**) and amine-gated (**S1**) mesoporous silica particles, 10 mg of the corresponding solids (**S0** or **S1**) were placed in 25 mL of water at pH 2 and pH 7.5. At a certain times aliquot were separated, the suspension filtered and the solution analysed by HPLC.

2.6 Folic acid loading optimization

With the aim of optimize the amount of FA loaded inside the MSP, two different loading methods were tested: immersion (A) and impregnation (B). **Table 1** summarizes the 8 loading conditions assayed. Solids were synthesized by triplicate.

Table 1. Conditions employed in loading optimization assays: immersion method (A) and impregnation method (B).

Loading mechanism	Solid	MCM (mg)	Folic (mg)	PBS (mL)	C_{folic} (mg mL^{-1})	Cycles (amount of solution per cycle)
Immersion	A1	100	35	7	5	
	A2	100	35	3.5	10	
	A3	100	70	7	10	
	A4	100	70	3.5	20	
Impregnation	B1	100	10	1	10	1 (1 mL)
	B2	100	10	1	10	2 (0.5 mL)
	B3	100	15	1.5	10	3 (0.5 mL)
	B4	100	20	2	10	4 (0.5 mL)

For the immersion method (A), 100 mg of MCM-41 were immersed into a PBS solution containing 4 different amounts of FA, stirred for 24 h, filtered and washed. Then, loaded solids were functionalized with 0.43 mL of N3 in acetonitrile following the procedure described in the synthesis of **S1**. Using this method, 4 different loaded and functionalized solids were obtained (A1-4).

For the impregnation method (**B**), FA dissolved in PBS (10 mg mL^{-1}) was added to 100 mg of MCM-41 employing 4 different FA amounts and cycles of addition (see **Table 1**). After each addition cycle, solids were dried at 30 °C to eliminate water content. Then, each of the loaded solids (B1-4) were functionalized with 0.43 mL of N3 using different media; i.e. water at pH 2 (solids **BW#**), acetate buffer at pH 2 **(BB#** solids) or acetonitrile (**BA#** solids). The loaded

and functionalized solids were isolated by vacuum filtration, washed with 300 mL of water adjusted to pH 2 with HCl, and dried at room temperature for 24 h. Finally, 12 solids were obtained: 4 functionalized in water at pH 2 with HCl (**BW1-4**), 4 functionalized in acetate buffer at pH2 (**BB1-4**) and 4 functionalized in acetonitrile (**BA1-4**).

2.7 Loading efficiency evaluation

Loading efficiency of each of the 16 obtained solids was determined by quantification FA delivered in PBS after 5 h by HPLC. The "relative loading efficiency" was calculated according to the following equation:

$$\text{Relative loading efficiency (\%)} = FA_D/FA_L \times 100$$

where FAD are the mg of folic delivered per 1 mg of loaded solid and FAL are the mg of folic acid employed for the loading of 1 mg of MCM-41.

2.8 Determination of in vitro folic acid bioaccessibility

FA bioaccessibility (FA delivery from the prepared solids) was determined by simulating a human digestion in the stomach and small intestine adapting the procedure described by Versantvoort[1] *et al.* (2005) (**Fig 1**). The large intestinal track was not taken into account since *in vivo* folic acid absorption occurs throughout the jejunum (Lucock, 2000). In a typical experiment, 10 mg of the corresponding solid were suspended in 12 mL of gastric juice and incubated for 2 h at 37 °C. Finally, 12 mL of duodenal juice, 6 mL of bile, and 2 mL of bicarbonate solution (1 M) were added simultaneously. After the addition, the mixture was maintained under stirring at 37 °C for 2 h. All digestive juices were heated to 37 °C before being mixed. During this period aliquots were taken, filtered and analysed by HPLC.

[1] See composition of the fluids in appendix 3 (page 257)

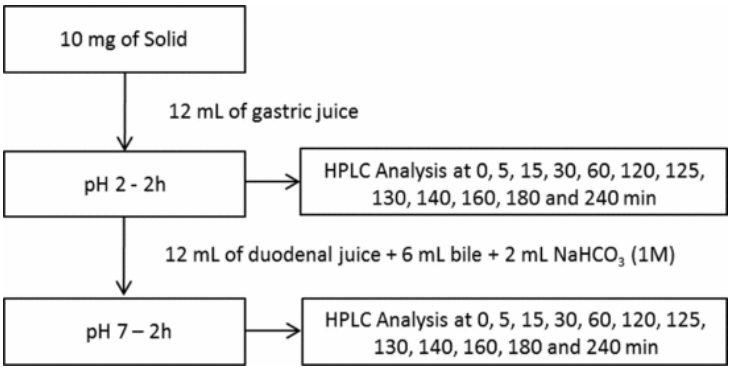

Figure 1. Schematic representation of the in vitro digestion model.

2.9 Folic acid determinations

FA was determined by reversed-phase gradient HPLC method according to the method described by Póo-Prieto *et al.* (2011) with minor modifications. The HPLC instrument consisted of a Hitachi LaChrom Elite liquid chromatograph (Hitachi Ltd., Tokyo, Japan) equipped with an auto-sampler and UV detector (model L-2400). A Kromaphase 100 C18 (250 mm × 4.6 mm i.d., 5 µm particle size analytical column) (Scharlab, Barcelona, Spain) was used for the separations. Mobile phase consisted of (A) 0.125 mM of NaH_2PO_4, 0.875 mM of Na_2HPO_4 and 0.4 mM of TBAHS in water and (B) acetonitrile-phase A 65:35 (v/v). The flow rate employed is described in **Table 2**. The wavelength of UV detector was set at 280 nm. Solutions for preparation of calibration standards were made at 1, 5, 10, 25, 50, 75, 100 µg FA mL^{-1} in PBS.

Table 2. Elution program for HPLC analysis.

Time (min)	Flow (mL min^{-1})	Mobile phase A (%)	Mobile phase B (%)
0	1.0	90	10
5	1.0	90	10
15	1.0	64	36
30	1.0	40	60
35	1.0	90	10
40	1.0	90	10

A: NaH2PO4 (0.125 mM), Na2HPO4 (0.875 mM) and TBAHS (0.4 mM) in water.

B: Acetonitrile-Phase A 65:35 (v/v)

2.10 Solids characterization

X-ray diffraction (XRD), transmission electron microscopy (TEM), N_2 adsorption-desorption isothermes and thermogravimetric analyses (TGA) were employed to characterize the synthesized materials. XRD were performed on a BrukerD8 Advance diffractometer using CuKα radiation. TEM images were obtained with a JEOL JEM-1010. The N_2 adsorption-desorption isotherms were recorded by a Micrometrics ASAP2010 automated sorption analyser. Samples were degassed at 90 °C in vacuum, overnight. The specific surface areas were calculated from the adsorption data within the low pressure range using the BET model. Pore size was determined following the BJH method. Thermogravimetric analyses were carried out on a TGA/SDTA 851e Mettler Toledo balance, using an oxidant atmosphere (air, 80 mL min^{-1}) with a heating program consisting of a heating ramp of 10 °C per minute from 393 to 1273 K and an isothermal heating step at this temperature for 30 min.

2.11 Data analysis

The results of the FA delivery from the different solids prepared were statistically processed using Statgraphics Centuriun XV (Manugistics Inc., Rockville, MD, USA). Statistical analysis on FA concentrations was made using an analysis of variance (One-Way ANOVA).

3. Results and discussion

3.1 FA molecular modelling and geometrical dimensions

Molecular dynamics calculations on FA were carried out. The molecular structure of FA is shown in **Figure 2**. As it can be seen, FA (pteroyl monoglutamic acid) consists of a pteridin ring linked to the para-amino benzoic acid (PABA) and a molecule of glutamic acid. In the larger dimension, FA exhibits a length of 1.45 nm, whereas the calculated volume is 1.16 nm^3. These calculations were used to determine the total theoretical amount of vitamin that could be encapsulated in the silica mesoporous matrix (*vide infra*).

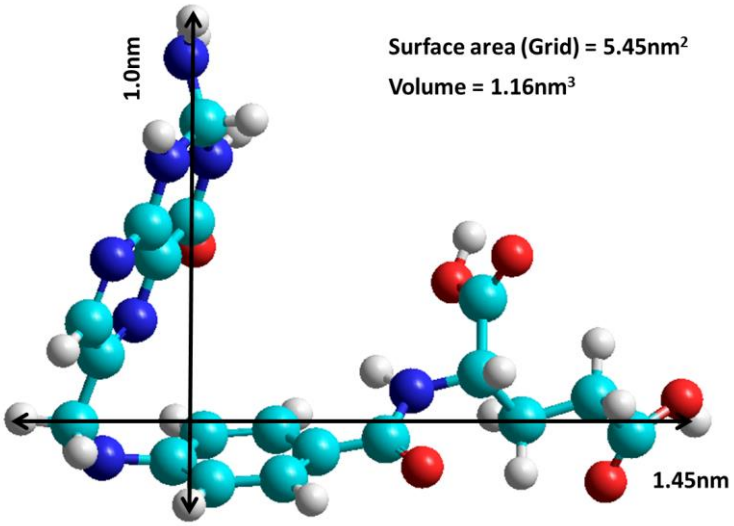

Figure 2. 3D FA molecular structure and geometrical dimensions.

3.2 Design, synthesis and characterization of the gated particles

For the design of the proposed pH-controlled and sustained release system described above MCM-41 mesoporous silica microparticles were selected as an inorganic support due to its high loading capacity, homogeneous porosity in the 2-3 nm range, high inertness, and ease of functionalization. This starting support was loaded with FA to obtain solid **S0**. Moreover, this FA-loaded material was further capped with a pH-responsive ensemble (i.e. N^1-(3-Trimethoxysilylpropyl)diethylenetriamine, N3) in order to obtain the gated polyamine-functionalised material **S1**. In this work pH was chosen as a suitable digestive stimulus for the modulation of FA release from the inner of the MCM-41 voids. In stomach, pH is very acid (pH 1-2) to help the degradation of proteins and to provide a non-specific immunity, retarding or eliminating various pathogens. In the small intestine, the duodenum provides critical pH balancing to activate digestive enzymes. The liver secretes bile into the duodenum to neutralise (pH 7-7.5) the acidic conditions from the stomach. Also the pancreatic duct empties into the duodenum, adding bicarbonate to neutralize the acidic chyme, thus creating a neutral environment. FA is known to be mainly absorbed in the small intestine (jejunum; pH 7.5) from where it is distributed to the tissues through the bloodstream and stored in the liver.

As stated above, pH has been chosen in this paper as triggering stimulus. In this particular system changes in the pH are expected to modulate FA delivery in two different ways. On the one hand, it is known that FA under neutral/basic conditions is about 1000 times more soluble than FA in an acidic environment due to protonation (acid) and deprotonation (neutral/basic) of FA in aqueous environments (Wu, 2010). On the other hand, it has been reported that MSP functionalised with the polyamine derivative N^1-(3-Trimethoxysilylpropyl)diethylenetriamine (N3) are suitable pH-responsive controlled release systems able to allow or inhibit delivery as a function of pH changes due to the transformation of amines (open gate at neutral/basic pH) to polyammonium groups (closed gate at acidic pH). These two mechanisms of action are illustrated in **Figure 3**.

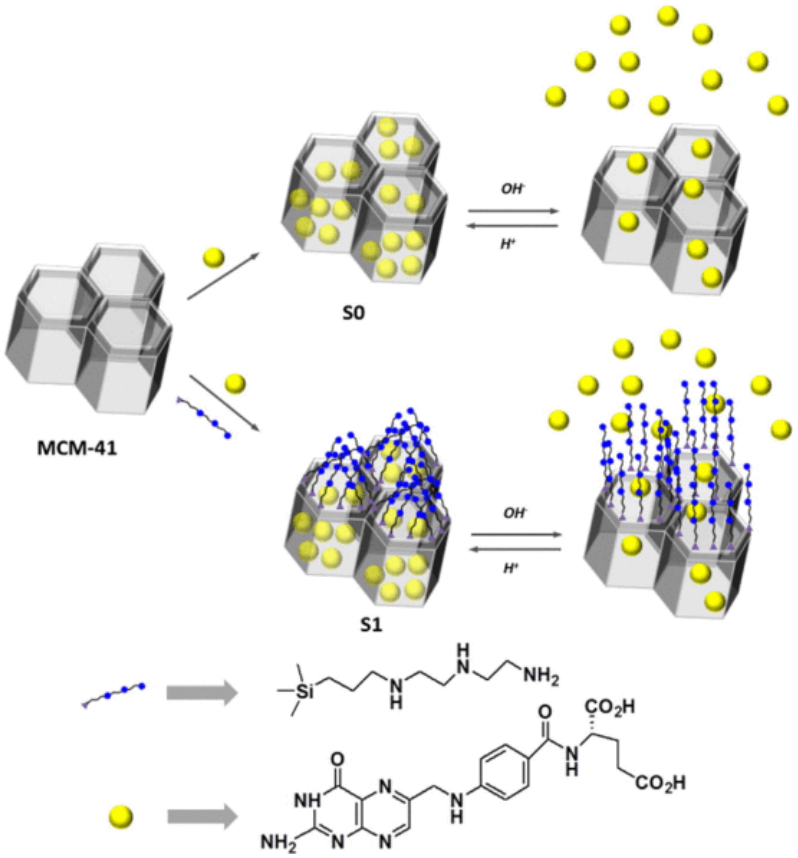

Figure 3. Illustration of the synthetic procedure for the preparation of solids **S0** and **S1**, and the mechanism of FA delivery at neutral or acidic conditions.

The different solids prepared were characterized according to standard techniques. X-ray patterns of the solids MCM-41 as synthesized (a), calcined (b), loaded with folic acid (**S0**) (c) and loaded with folic acid and functionalized with amines (**S1**) (d) are shown in **Figure 4**. Curve a shows the expected four peaks of a hexagonal ordered array indexed as (1 0 0), (1 1 0), (2 0 0) and (2 1 0) Bragg reflections. A significant shift of the (1 0 0) reflection in the XRD powder of the MCM-41 calcined sample is clearly appreciated in the curve b, corresponding to a cell contraction related to condensation of silanols during the calcination step. Curves c and d show that reflections (1 1 0), (2 0 0) and (2 1 0) are lost, most likely due to a reduced contrast that can be attributed to the presence of FA in the pore voids and the anchored N3 molecule. Nevertheless, the existence in all cases of

the (1 0 0) peak in the XRD patterns indicated that the process of pore loading with FA, and the additional functionalization with the polyamine, did not modify the typical porosity of the mesoporous MCM-41 scaffold.

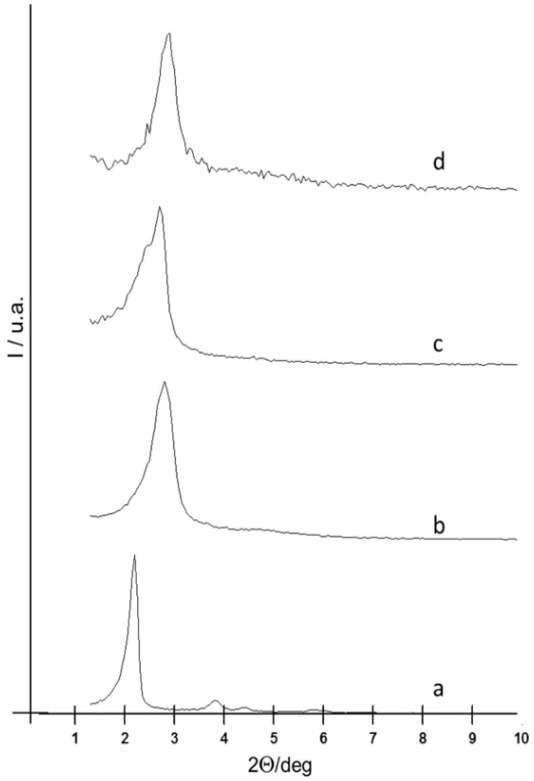

Figure 4. Powder X-ray patterns of the solids (a) MCM-41 as-synthesized, (b) MCM-41 calcined, (c) the uncapped solids containing the vitamin B9 (S0) and (d) the capped mesoporous system (**S1**).

The MCM-41 mesostructure mesostructure after loading with FA and functionalization with polyamines was also confirmed by TEM images (**Fig 5**).

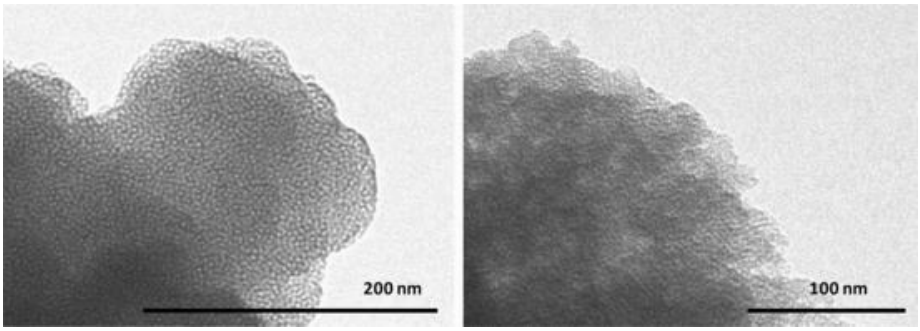

Figure 5. TEM image of (a) MCM-41 calcined and (b) solid **S1** showing the typical porosity of the MCM-41 matrix.

The N_2 adsorption-desorption isotherms of the starting MCM-41 calcined material are shown in **Figure 6**. The curve shows a well defined and sharp adsorption step at P/P_0 values between 0.1 and 0.3, corresponding to a type IV isotherm, which is typical of mesoporous materials, attributed to nitrogen condensation in the mesopore inlets. With the Barrett-Joyner-Halenda (BJH) model on the adsorption curve of the isotherm, pore diameter and pore volume were calculated to be 2.52 nm and 0.92 $cm^3\ g^{-1}$, respectively. The absence of a hysteresis loop in this interval and the narrow BJH pore distribution suggested the existence of uniform cylindrical mesopores. The application of the BET model resulted in a value of 1040 $m^2\ g^{-1}$ for the total specific surface. From the XRD, porosimetry and TEM studies, the a_0 cell parameter (3.98 nm), the pore diameter (2.52 nm), and a value for the wall thickness of 1.69 nm were calculated.

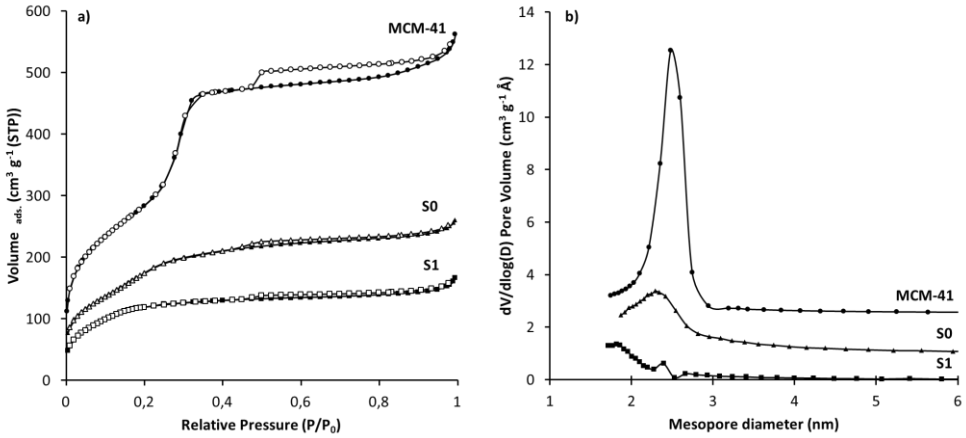

Figure 6. Nitrogen adsorption-desorption isotherms (a) and pore size distribution (b) for MCM-41 mesoporous material, **S0**, and **S1** materials.

Considering the pore size of the MCM-41 support and the FA structure (see Section 3.1), it can be stated that FA can be perfectly encapsulated in pores of 2.52 nm of diameter. Moreover, bearing in mind the volume of the FA molecule (1.16 nm^3), the specific volume of the MCM-41 (0.92 $cm^3\ g^{-1}$) and tentatively assuming that ca. 75% of the pore volume in the mesoporous support can be occupied by FA, it can be roughly established that 1 mg of MCM-41 could host as a maximum 436 µg (0.98 mmol) of FA in its porous network.

Table 3 also shows the change on the textural properties of the starting silica after the vitamin adsorption (**S0**) and the functionalization with the N3 molecule (**S1**). The incorporation of the FA leads to a decrease of ca. 37% and 46% for the BET surface area and the BJH mesopore volume, respectively. This evolution indicates that the FA molecules must be incorporated inside the mesopores. Under the pH conditions used for the drug uptake (7.5), the two carboxilate groups must be deprotonated, and consequently, the interaction with the silanol groups at the silica surface must be mediated by H^+ species. Taking into account the presence of partially filled mesopores in the solid **S0** together with the relatively large arm of the N3 molecule, the incorporation of these last species preferentially must occurs in the external surface at the mesopore entrances. As

expected, the incorporation of the N3-gates leads to an additional decrease of both the surface area as the volume of 31 and 57%, respectively. In a parallel way, the size of the mesopores decreases after FA inclusion. A large variety of FA aggregates on the silica are possible which is consistent with the wider peak observed in the pore size distribution curve. An additional mesopore size reduction occurs after functionalization with N3 groups. Hence, solid **S1** shows a wide pore size distribution with a principal peak centred at 1.82 nm and a residual signal at ca. 2.38 nm. The first peak could be associated to a majority of the mesopores well surrounded by N3 molecules and the residual peak must be attributed to a small proportion of mesopores showing some deficiencies respect to an optimum presence of N3 groups.

Table 3. Textural parameters from N^2 adsorption-desorption isotherms.

	SBET (m^2 g^{-1})	**Pore volume (cm^{-3} g^{-1})**	**Pore size (nm)**
MCM-41	1040	0.92	2.52
S0	653	0.49	2.28
S1	451	0.21	1.82 (2.38)

3.3 pH gate-like mechanism confirmation

FA delivery from the uncapped solid **S0** in acid and neutral conditions was studied. In a typical experiment 5 mg of **S0** were suspended in 25 mL of two different aqueous solutions (pH 2 and pH 7.5) in an attempt to reproduce the pH of gastric or intestinal fluids. The release profile of **S0** is shown in **Figure 7**.

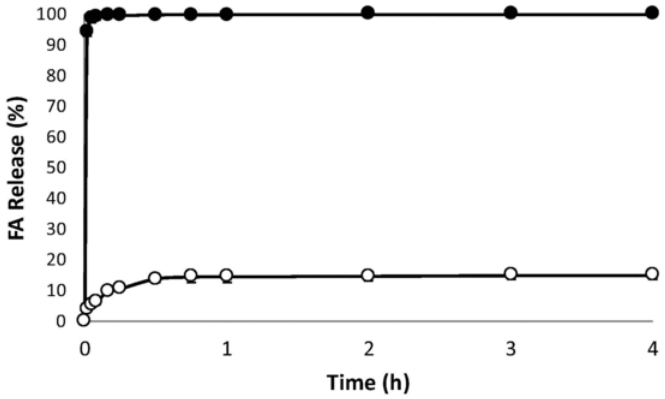

Figure 7. Release profiles of folic acid from the pores of solid **S0** in water at pH 2 (unfilled marker points) and pH 7.5 (filled marker points). Values are Means ± SD, n = 3.

As observed in the **Figure 7**, the asymptote of the release curve was achieved in the first few minutes of the delivery at pH 7.5. According to TGA experiments, the maximum delivery achieved (indicated in the figure as 100%) corresponds to 32% of the FA content in the solid. This indicated that, under the experimental conditions, not all the FA loaded was able to be released. In contrast, only a 14.9 ± 1.2% of the maximum delivery capacity was achieved at pH 2 (which corresponds to ca. 5% of the total FA content determined by TGA). Considering that the increase of FA concentration in the water phase is proportional to the delivery of the vitamin from the pores and that FA release is not inhibited by the presence of functional molecular groups on the surface of the MCM-41, the effect of solubility in FA bioaccessibility (release) is confirmed. At pH 2, FA is in the form of acid with low solubility, while at pH 7.5 folic is in the form of salt, increasing its solubility, and enhancing the delivery (Moffat, 1986) from the pore voids of **S0** to the solution. However, as it can be seen in **Figure 7** this pH-induced "solubilisation mechanism" is insufficient to modulate a sustained release of FA, a fact that would not allow a proper absorption of FA in the jejunum.

In a second study, delivery of FA from **S1** was tested using similar delivery conditions; i.e. 5 mg of **S1** were suspended in 25 mL of two different aqueous solutions at pH 2 and pH 7.5. As shown in **Figure 8**, FA delivery after 4 h at pH 2 achieved values 0.22 ± 0.03% of the maximum delivery capacity of **S1** (which corresponds to ca. 0.09% of the total FA content determined by TGA). In contrast, at pH 7.5, a progressive delivery of the vitamin was observed, achieving ca. 100% of the release capacity in the performed conditions after 1 h (which corresponds to 40% of FA content determined by TGA).

In this case, the pH-dependent release behaviour can be explained by considering the different FA solubility as a function of the pH and the presence of the gate-like ensemble based in polyamines. To explain this latter effect, it has to be taken into account that at acidic conditions (pH 2), amines anchored to the surface of the pores are fully protonated. This fact favours Coulombic repulsions between closely located polyammonium groups, so that tethered polyamines tend to adopt a rigid-like conformation that blocks the pores and practically no release occurs. At pH 7.5, a lower proportion of polyamines are expected to be protonated, favouring hydrogen bond interactions between the different amine chains. As a consequence, pores unblock and vitamin release is produced. Moreover, in amine-based gated ensembles a second cooperative anion-dependent effect occurs. In general polyamines are well-known pH-responsive molecules that can additionally complex anions via electrostatic forces and by formation of hydrogen-bonding interactions in a wide pH range. Additionally, the relative amine/ammonium ratio can control the interaction with anionic species. If electrostatic forces are taken into account (which in general are stronger than hydrogen bonding interactions) the presence of a large percentage of ammonium groups (acidic pH) will favour the interactions of the “gate” with anions in the solution resulting in an additional pore blockage that is not observed at neutral or basic pH (Casasús *et al.*, 2008).

Comparing the delivery profiles at pH 2 and 7.5 of the uncapped (**S0**) and capped (**S1**) materials it is apparent that **S0** is not able to completely inhibit FA delivery at acidic pH being the delivery very fast at neutral pH. In contrast, **S1** is tightly capped at pH 2 and displays a sustained delivery (in 1 h) when the pH is switch to 7.5. It can be concluded that the gated support **S1** might be a suitable prototype for the development of orally applicable FA delivery systems designed to block cargo delivery in the acidic conditions of the stomach (acid pH, gate closed) yet be able to display a sustained FA release at the intestine (basic pH, gate open).

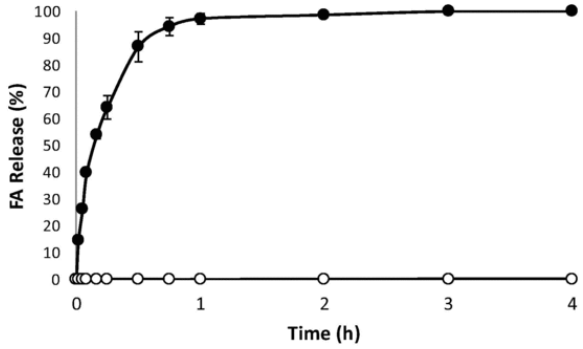

Figure 8. Release profiles of folic acid from the pores of solid **S1** in water at pH 2 (unfilled marker points) and pH 7.5 (filled marker points). Values are Means ± SD, n = 3.

Comparing the delivery profiles at pH 2 and 7.5 of the uncapped (**S0**) and capped (**S1**) materials it is apparent that **S0** is not able to completely inhibit FA delivery at acidic pH being the delivery very fast at neutral pH. In contrast, **S1** is tightly capped at pH 2 and displays a sustained delivery (in 1 h) when the pH is switch to 7.5. It can be concluded that the gated support **S1** might be a suitable prototype for the development of orally applicable FA delivery systems designed to block cargo delivery in the acidic conditions of the stomach (acid pH, gate closed) yet be able to display a sustained FA release at the intestine (basic pH, gate open).

3.4 Loading/releasing optimization process

After studying the delivery of FA from the polyamine-functionalised (**S1**) and unfunctionalised (**S0**) materials, this section deals with a detailed study of FA loading optimization for the preparation of functionalised solids (**S1**-like supports). For this purpose, 16 solids differing in the loading (immersion and impregnation) and the functionalization media used to anchor the polyamine N3 (water at pH 2, acetate buffer at pH 2 or acetonitrile) were prepared. Delivery effectiveness of each solid was evaluated by the determination of FA delivered after 5 h at pH 7.5. Moreover, the loading/delivery performance of the solids was evaluated using the "relative loading efficiency" via the determination of the ratio between the amount of FA delivered (after 5 h at pH 7.5) per mg of loaded solid and the mg of FA used for loading 1 mg of MCM-41 (see Section 2 for details).

The first block of bars of **Figure 9** shows values of FA delivered per mg of **A#** solids, solids obtained by using a traditional immersion procedure. Among them, solid **A1** was able to deliver 3.7 ± 0.2 μg of FA mg^{-1} of solid. By increasing the amount of FA present in the loading solution to 70 mg (0.016 mmol) (**A3**) the amount delivered increased to 21.2 ± 0.3 μg of FA mg^{-1} of solid. However, when the same amount of folic was loaded in the half of solvent, the release capacity decreased (**A4**) to 6.2 ± 0.2 μg of FA mg^{-1} of solid. To understand this behaviour the maximum FA amount able to be solubilized in PBS was determined, finding that above of 10 mg of FA mL^{-1} PBS, FA remains insolubilized, and thus, cannot participate in the loading process.

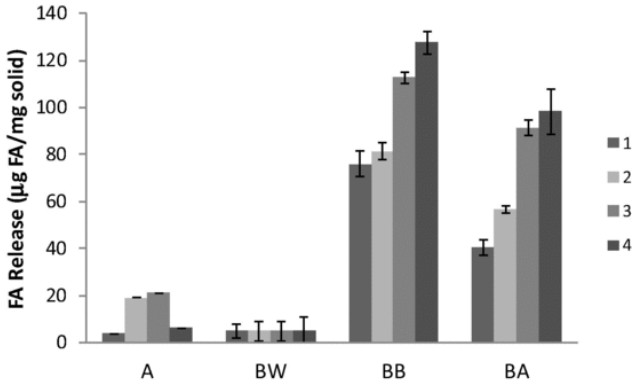

Figure 9. Maximum FA delivery (µg FA mg^{-1} solid) for different solids loaded by immersion in PBS and functionalized with N3 in acetonitrile (A# solids) or loaded by impregnation and functionalized with N3 in different solvents: water adjusted to pH 2 (BW), acetate buffer at pH 2 (BB) or acetonitrile (BA). Numbers 1-4 refers to different FA loading conditions described in **Table 1**. Values are Means ± SD, n = 3.

The same figure shows values of FA delivered by solids loaded by impregnation and functionalized in water at pH 2 (**BW#**), acetate buffer at pH 2 (**BB#**) or acetonitrile (**BA#**). As it can be seen, **BW#** solids exhibited the lowest loading capacity. In fact the 4 solids prepared using these conditions were white, strongly suggesting the presence of a very low amount of FA (pale yellow) in the pores. To understand the cause of this behaviour, it was found that pH reached values of 10 upon the addition of the amine N3 during the synthesis of the solid. At this pH FA is highly soluble and most likely leaked from the pore voids during the synthesis of the materials.

In contrast, **B** solids functionalized with N3 in aqueous acetate buffer (**BB#** solids) or acetonitrile (**BA#** solids), showed a remarkable larger FA delivery in water. In this case, the poor solubility of FA in the acetate buffer or acetonitrile during the N3 functionalization avoided the FA leakage during this step of the synthesis. When both **BA#** and **BB#** solids are compared in terms of delivery, it can be stated the **BB#** series display larger delivery ability. In particular, **BB#** solids exhibited a remarkable delivery capacity ($p<0.005$), being solid **BB4** able to release 127 ± 5 µg of FA mg^{-1} of solid (**Fig 9**). As a conclusion, the choice of the solvent

employed for the surface functionalization step is as important as the loading procedure in terms of loading efficiency. Nevertheless, the maximum loading capacity calculated in Section 3.2 has not been achieved in any of the designed solids.

From the release ability displayed by the different solids prepared and taking into account the amount of FA employed for the loading of each solid, the relative loading efficiency (RLE) was calculated. **Figure 10** shows RLE values for the 16 prepared solids. As expected, solids loaded by immersion (**A#)** were the less efficient in terms of delivery with RLE values of around 1-3%. Moreover RLE values of ca. 2.5-5%, 40-60% and 63-75% were observed for **BW#**, **BA#** and **BB#** supports. In addition, for solids **BA#** and **BB#** RLE increased significantly ($p< 0.005$) from 10 mg in 1 cycle **(#1** solids) to 15 mg in 3 cycles (**#3** solids). However, the addition of 1 extra cycle of addition (**#4** solids) did not increase RLE values indicating that, in this case, not all the FA added was loaded inside the pore voids of the mesoporous materials. According to these results, the conditions employed for preparing solid **BB3** should be considered as optimal, in terms of RLE values, for the preparation of MSP loaded with folic acid and gated with N3 moieties.

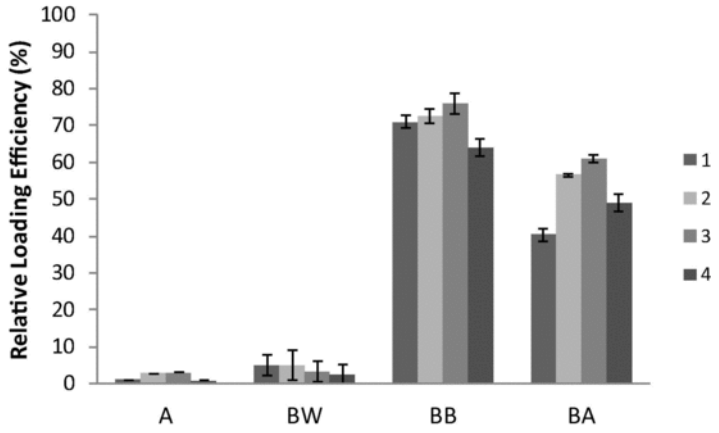

Figure 10. Relative Loading Efficiency for different solids loaded by immersion in PBS and functionalized with N3 in acetonitrile (A# solids) or loaded by impregnation and functionalized with N3 in different solvents: water adjusted to pH 2 (BW# solids), acetate buffer at pH 2 (BB# solids) or acetonitrile (BA# solids). Numbers 1-4 refers to different FA loading conditions described in **Table 1**. Values are Means ± SD, n = 3.

All these prepared solids were characterized using standard techniques. In all cases XRD patterns and TEM images (data not shown) were equivalent to those obtained for solid **S1** (Section 3.1), confirming that the mesoporous structure of the MCM-41 scaffold was maintained in spite of the different loading and functionalization process.

3.5 In vitro folic acid bioaccessibility and nutritional implications

After the loading optimization procedure described above, this section deals with the use of solid **BB3**, which exhibited the maximum RLE value, for delivery studies in a more realistic media. In particular, the aim of this part was to study FA release, and therefore FA bioaccessibility, during a simulated pass of the solid through the gastrointestinal tract. To evaluate this, a variation of the dynamic in vitro digestion protocol reported by Versantvoort *et al.* (2005) was performed. Briefly **BB3** was suspended in simulated gastric juice and incubated for 2 h at 37 °C and then duodenal juice, bile and bicarbonate solution were added to obtain a simulated intestinal fluid (see Section 2 for details). Note that in this study the pass of the solid through large intestinal track was not taken into account since in vivo folic acid absorption occurs throughout the jejunum (Lucock, 2000). At certain times aliquots were taken, filtered and analysed by HPLC. Results of FA delivery from **BB3** are shown in **Figure 11**. During the first two hours of simulated digestion, where **BB3** solid was in contact with a simulated gastric fluid, only 10.2 ± 1.4 μg of FA mg^{-1} of solid were delivered. After the addition of the simulated intestinal fluid, FA delivered increased progressively to reach a maximum value of 94 ± 9 μg of FA mg^{-1} of solid at 2 h.

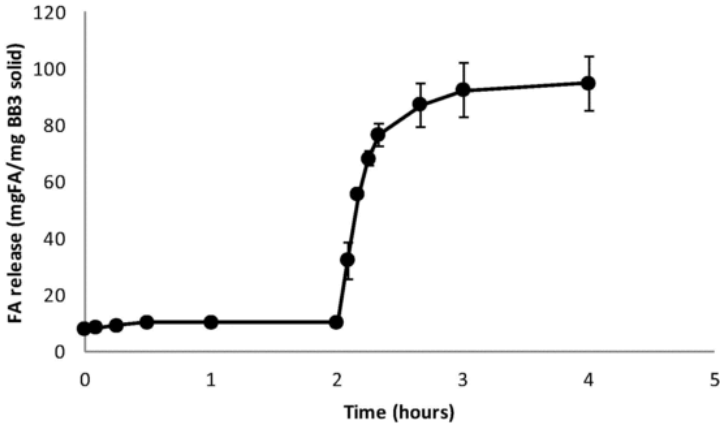

Figure 11. Release profile of FA from solid **BB3** along the simulated gastrointestinal digestion process. Time 0-2 h correspond to the simulation of stomach conditions and time from 2 to 4 h correspond with the simulation of intestinal conditions. Values are Means ± SD, n = 3.

Thus, as it can be observed in **Figure 9**, **BB3** solid is tightly capped in simulated gastric fluid yet opens and deliver the cargo when in contact with simulated intestinal fluid. Moreover, the most important thing is that 1 mg of solid **BB3** is able to release ca. 95 µg of FA during the whole simulated digestion process. This implicates that the higher dietary reference intake in human nutrition, established for pregnant woman in 600 µg per day of folates or 360 µg of synthetic PGA (1 µg of dietary folate equivalent = 0.6 µg of folic acid) (Eichholzer *et al.,* 2006), could be reached by an oral administration of only ca. 4 mg of **BB3**, which is a remarkable low amount. Moreover, based in the oral toxicological evaluation of other mesoporous silica particles carried out by Kupferschmidt *et al.* (2013) -that found that even high amounts of MSP up to 1200 mg of MSP kg^{-1} of rat administrated orally were not toxic- our less than 7 mg are very far of a toxicological effect, signifying that the optimized solid **BB3** could be safe for oral administration.

4. Conclusions

Mesoporous silica particles (MSP) have been recently proposed as smart delivery devices able to load large amounts of cargo and release the same using different triggering stimuli. In this study FA has been successfully encapsulated in mesoporous silica particles capped with N^1-(3-Trimethoxysilylpropyl)diethylenetriamine groups. A detailed study of the loading process allowed us to obtain solids with relative encapsulation efficiencies of the 75%. The simulation of an *in vitro* digestion of selected optimized gated support allowed to conclude that the developed MSP capped with amines were not only able to hinder the release of the vitamin in the presence of a simulated gastric fluid, but also were able to deliver progressively the vitamin along the time in presence of a simulated intestinal fluid, offering a mechanism to modulate the bioaccessibility of the FA vitamin during the pass across the intestine. In this study it was found that 1 mg of the optimized solid was able to release ca. 95 μg of FA indicating that maximum levels of higher dietary reference intake in human nutrition could be reached using only 4 mg of the optimized solid. Bearing additionally into account that mesoporous silica particles are non-toxic at low levels for humans, it can be stated that pH-dependent capped MSP are suitable candidates for the design of orally applicable delivery systems designed to protect FA from the acidic conditions of the stomach (acid pH, gate closed) but release the vitamin at the intestine (basic pH, gate open).

Acknowledgements

Authors gratefully acknowledge the financial support from the Ministerio de Economía y Competitividad (Projects AGL2012-39597-C02 and MAT2012-38429-C04-01) and the Generalitat Valenciana (project PROMETEO/2009/016). E.P. is grateful to the Ministerio de Ciencia e Innovación for his Grant (AP2008-00620). C.C. thanks the Generalitat Valenciana for her post-doctoral contract VALi+D.

References

Agostini, A., Mondragón, L., Bernardos, A., Martínez-Máñez, R., Marcos, M. D., Sancenón, F., Soto, J., Costero, A., Manguan-García, C., Perona, R., Moreno-Torres, M., Aparicio-Sanchis, R. & Murguía, J. R. (2012). Targeted cargo delivery in senescent cells using capped mesoporous silica nanoparticles. *Angewandte Chemie International Edition*, *51*(42), 10556-10560.

Al Shamsi, M., Al Samri, M. T., Al-Salam, S., Conca, W., Shaban, S., Benedict, S., Tariq, S., Biradar, A. V., Penefsky○, H. S., Asefa, T., & Souid, A. K. (2010). Biocompatibility of calcined mesoporous silica particles with cellular bioenergetics in murine tissues. *Chemical research in toxicology*, *23*(11), 1796-1805.

Aznar, E., Mondragón, L., Ros-Lis, J. V., Sancenón, F., Marcos, M. D., Martínez-Máñez, R., Soto, J., Pérez-Payá, E., & Amorós, P. (2011). Finely Tuned Temperature-Controlled Cargo Release Using Paraffin-Capped Mesoporous Silica Nanoparticles. *Angewandte Chemie*, *123*(47), 11368-11371.

Bernardos, A., Aznar, E., Coll, C., Martínez-Mañez, R., Barat, J. M., Marcos, M. D., Sancenón, F., Benito, A., & Soto, J. (2008). Controlled release of vitamin B2 using mesoporous materials functionalized with amine-bearing gate-like scaffoldings. *Journal of Controlled Release*, *131*(3), 181-189.

Bernardos, A., Mondragon, L., Aznar, E., Marcos, M. D., Martínez-Máñez, R., Sancenón, F., Soto, J., Barat, J. M., Perez-Paya, E., Guillem, C., & Amorós, P. (2010). Enzyme-responsive intracellular controlled release using nanometric silica mesoporous supports capped with "saccharides". *Acs Nano*, *4*(11), 6353-6368.

Casasús, R., Climent, E., Marcos, M. D., Martínez-Máñez, R., Sancenón, F., Soto, J, Amorós, P., Cano, J., & Ruiz, E. (2008). Dual aperture control on pH-and anion-driven supramolecular nanoscopic hybrid gate-like ensembles. *Journal of the American Chemical Society*, *130*(6), 1903-1917.

Chen, L., Remondetto, G. E., & Subirade, M. (2006). Food protein-based materials as nutraceutical delivery systems. *Trends in Food Science & Technology*, *17*(5), 272-283.

Climent, E., Bernardos, A., Martínez-Máñez, R., Maquieira, A., Marcos, M. D., Pastor-Navarro, N., Puchades, R., Sancenón, F., Soto, J., & Amorós, P. (2009). Controlled delivery systems using antibody-capped mesoporous nanocontainers. *Journal of the American Chemical Society*, *131*(39), 14075-14080.

Coll, C., Mondragón, L., Martínez-Máñez, R., Sancenón, F., Marcos, M. D., Soto, J., Amorós, P., & Pérez-Payá, E. (2011). Enzyme-Mediated Controlled Release Systems by Anchoring Peptide Sequences on Mesoporous Silica Supports. *Angewandte Chemie International Edition*, *50*(9), 2138-2140.

Czeizel, A. E., & Dudas, I. (1992). Prevention of the first occurrence of neural-tube defects by periconceptional vitamin supplementation. *New England Journal of Medicine*, *327*(26), 1832-1835.

Ghedini, E., Signoretto, M., Pinna, F., Crocellà, V., Bertinetti, L., & Cerrato, G. (2010). Controlled release of metoprolol tartrate from nanoporous silica matrices. *Microporous and Mesoporous Materials*, *132*(1), 258-267.

Guillet-Nicolas, R., Popat, A., Bridot, J. L., Monteith, G., Qiao, S. Z., & Kleitz, F. (2013). pH-Responsive Nutraceutical-Mesoporous Silica Nanoconjugates with Enhanced Colloidal Stability. *Angewandte Chemie International Edition*, *125*(8), 2374-2378.

Eichholzer, M., Tönz, O., & Zimmermann, R. (2006). Folic acid: a public-health challenge. *The Lancet*, *367*(9519), 1352-1361.

Fathi, M., Mozafari, M. R., & Mohebbi, M. (2012). Nanoencapsulation of food ingredients using lipid based delivery systems. *Trends in food science & technology*, *23*(1), 13-27.

Food and Drug Administration (FDA). (1996) Food labelling: health claims and food label statements; folate and neural tube defects. Federal Register, 61, 8752-8807.

Health Canada. (1997) Regulations amending the food and drug regulations (1066). *Canada Gazette*, 131, 8752-8807.

Hedren, E., Diaz, V., & Svanberg, U. (2002). Original Communications-Estimation of carotenoid accessibility from carrots determined by an in vitro digestion method. *European Journal of Clinical Nutrition*, *56*(5), 425-430.

Jiao, Y., Sun, Y., Chang, B., Lu, D., & Yang, W. (2013). Redox-and temperature-controlled drug release from hollow mesoporous silica nanoparticles. *Chemistry-A European Journal*, *19*(45), 15410-15420.

Kim, Y. I. (2004). Folate, colorectal carcinogenesis, and DNA methylation: lessons from animal studies. *Environmental and Molecular Mutagenesis*, *44*(1), 10-25.

Koike, H., Hama, T., Kawagashira, Y., Hashimoto, R., Tomita, M., Iijima, M., & Sobue, G. (2012). The significance of folate deficiency in alcoholic and nutritional neuropathies: Analysis of a Case. *Nutrition*, *28*(7), 821-824.

Kupferschmidt, N., Xia, X., Labrador, R. H., Atluri, R., Ballell, L., & Garcia-Bennett, A. E. (2013). *In vivo* oral toxicological evaluation of mesoporous silica particles. *Nanomedicine*, *8*(1), 57-64.

Li, L. L., Xie, M., Wang, J., Li, X., Wang, C., Yuan, Q., Pang, D. W., Lu, Y., & Tan, W. (2013). A vitamin-responsive mesoporous nanocarrier with DNA aptamer-mediated cell targeting. *Chemical Communications*, *49*(52), 5823-5825.

Lucock, M. (2000). Folic acid: nutritional biochemistry, molecular biology, and role in disease processes. *Molecular genetics and metabolism*, *71*(1), 121-138.

Lucock, M., & Yates, Z. (2009). Folic acid fortification: a double-edged sword.*Current Opinion in Clinical Nutrition & Metabolic Care*, *12*(6), 555-564.

Mal, N. K., Fujiwara, M., & Tanaka, Y. (2003). Photocontrolled reversible release of guest molecules from coumarin-modified mesoporous silica. *Nature*,*421*(6921), 350-353.

McClements, D. J., & Li, Y. (2010). Review of in vitro digestion models for rapid screening of emulsion-based systems. *Food & function*, *1*(1), 32-59.

Mastromatteo, M., Mastromatteo, M., Conte, A., & Del Nobile, M. A. (2010). Advances in controlled release devices for food packaging applications. *Trends in Food Science & Technology*, *21*(12), 591-598.

Moffat, A.C. (1986) Clarke's isolation and identification of drugs in pharmaceuticals, body fluids, and post-mortem material, second ed. London: The Pharmaceutical Press.

Park, C., Oh, K., Lee, S. C., & Kim, C. (2007). Controlled Release of Guest Molecules from Mesoporous Silica Particles Based on a pH-Responsive Polypseudorotaxane Motif. *Angewandte Chemie International Edition*, *46*(9), 1455-1457.

Patel, K., Angelos, S., Dichtel, W. R., Coskun, A., Yang, Y. W., Zink, J. I., & Stoddart, J. F. (2008). Enzyme-responsive snap-top covered silica nanocontainers. *Journal of the American Chemical Society*, *130*(8), 2382-2383.

Póo-Prieto, R., Alonso-Aperte, E., & Varela-Moreiras, G. (2011). Analysis of Folate Form Distribution in Spanish Beers Using Combined Affinity and Ion-Pair Chromatography. *Journal of the Institute of Brewing*, *117*(2), 188-194.

Sanderson, P., McNulty, H., Mastroiacovo, P., McDowell, I. F., Melse-Boonstra, A., Finglas, P. M., & Gregory, J. F. (2003). Folate bioavailability: UK Food Standards Agency workshop report. *British Journal of Nutrition*, *90*(02), 473-479.

Suh, W. H., Suslick, K. S., Stucky, G. D., & Suh, Y. H. (2009). Nanotechnology, nanotoxicology, and neuroscience. *Progress in neurobiology*,*87*(3), 133-170.

Tian, Y., Glogowska, A., Zhong, W., Klonisch, T., & Xing, M. (2013). Polymeric mesoporous silica nanoparticles as a pH-responsive switch to control doxorubicin intracellular delivery. *Journal of Materials Chemistry B*,*1*(39), 5264-5272.

Tomiuk, S., Liu, Y., Green, T. J., King, M. J., Finglas, P. M., & Kitts, D. D. (2012). Studies on the retention of microencapsulated L-5-methyltetrahydrofolic acid in baked bread using skim milk powder. *Food chemistry*, *133*(2), 249-255.

Vallet-Regı, M., Doadrio, J. C., Doadrio, A. L., Izquierdo-Barba, I., & Pérez-Pariente, J. (2004). Hexagonal ordered mesoporous material as a matrix for the controlled release of amoxicillin. *Solid State Ionics*, *172*(1), 435-439.

Versantvoort, C. H., Oomen, A. G., Van de Kamp, E., Rompelberg, C. J., & Sips, A. J. (2005). Applicability of an in vitro digestion model in assessing the bioaccessibility of mycotoxins from food. *Food and Chemical Toxicology*,*43*(1), 31-40.

Wright, A. J. A., Finglas, P. M., & Southon, S. (2001). Proposed mandatory fortification of the UK diet with folic acid: have potential risks been underestimated?. *Trends in Food Science & Technology*, *12*(9), 313-321.

Wu, Z., Li, X., Hou, C., & Qian, Y. (2010). Solubility of Folic Acid in Water at pH Values between 0 and 7 at Temperatures (298.15, 303.15, and 313.15) K. *Journal of Chemical & Engineering Data*, *55*(9), 3958-3961.

Younis, I. R., Stamatakis, M. K., Callery, P. S., & Meyer-Stout, P. J. (2009). Influence of pH on the dissolution of folic acid supplements. *International journal of pharmaceutics*, *367*(1), 97-102.

Zhao, Z., Meng, H., Wang, N., Donovan, M. J., Fu, T., You, M.,... & Tan, W. (2013). A Controlled-Release Nanocarrier with Extracellular pH Value Driven Tumor Targeting and Translocation for Drug Delivery. *Angewandte Chemie International Edition*, *52*(29), 7487-7491.

4.1.2 Encapsulation of folic acid in different silica porous supports: a comparative study

Édgar Pérez-Esteve,[a*] María Ruiz-Rico,[a] Cristina de la Torre,[b,c] Luis A. Villaescusa,[b] Felix Sancenón,[b,c] María D. Marcos,[b,c] Pedro Amorós,[d] Ramón Martínez-Máñez,[b,c] José Manuel Barat[a]

[a] Grupo de Investigación e Innovación Alimentaria, Universitat Politècnica de València. Camino de Vera s/n, 46022, Valencia, Spain
[b] Centro de Reconocimiento Molecular y Desarrollo Tecnológico (IDM), Unidad Mixta Universitat Politècnica de València - Universidad de Valencia. Departamento de Química Universitat Politècnica de València, Camino de Vera s/n, 46022, Valencia, Spain
[c] CIBER de Bioingeniería, Biomateriales y Nanomedicina (CIBER-BBN)
[d] Institut de Ciència dels Materials (ICMUV), Universitat de València, P.O. Box 2085, E-46071, Valencia, Spain

*Food Chemistry, **2016**, 196, 66-75*
(Reproduced with permission of Elsevier)

Abstract

Although folic acid (FA) is essential to numerous bodily functions, recent research indicates that a massive exposition to the vitamin could be a double-edged sword. In this study, the capacity of different caped mesoporous silica particles (i.e. Hollow Silica Shells, MCM-41, SBA-15 and UVM-7) to dose FA during its passage through the gastrointestinal tract has been evaluated. Results confirmed that the four capped materials were capable to hinder the delivery of FA at low pH (i.e. stomach) as well as able to deliver great amounts of the vitamin at neutral pH (i.e. intestine). Nevertheless, the encapsulation efficiency and the deliver kinetics differed among supports. While supports with large pore entrance exhibited an initial fast release, MCM-41, showed a sustained release along the time. This correlation between textural properties and release kinetics for each of the supports reveals the importance of a proper support selection as a strategy to control the delivery of active molecules.

Keywords: Folic acid, porous silica supports, smart delivery, nutrition, cell viability.

1. Introduction

Folates have been, and remain, a subject of ongoing research due to their numerous bodily functions, including DNA synthesis and repair, cell division and cell growth. Folates exist in a large variety of foods including green leafy vegetables, fruits, meat products, beans, fermented dairy products, and cereals. However, folates are sensitive to physical factors such as temperature, pressure, and exposure to light and can be affected during food processing or digestion (Nasr Hage *et al.,* 2012) so that folate deficiencies occur worldwide. Folate deficiency is of such importance to humans that it can cause neural tube defects in developing embryos, elevated plasma homocysteine, different types of cancer, Alzheimer, etc. (Nguyen & Hendrickx, 2003, Kotsopoulos *et al.*, 2012, Hinterberger & Fischer, 2013 and Lubecka-Pietruszewska *et al.*, 2013). To maintain an adequate folate status a diet supplementation with FA from fortified foods or nutritional supplements is generally recommended in many countries, especially during pregnancy.

Although there are irrefutable evidences about the benefits of FA supplementation, recent studies suggest that a massive exposition to high bioavailable FA leads to the direct appearance of untransformed FA in the systemic circulation. The presence of unmetabolized FA in blood has been lately related to certain cancer development, cardiovascular disease, anaemias… (Kotsopoulos *et al.*, 2012). In this context, encapsulation methods to prevent environmental degradation of folates as well as to control the release along the digestive tract (i.e. no delivery in the stomach -pH 2-, and a sustained release in the intestine -pH 7.5-) seems to be a convenient strategy to solve problems related to FA deficiency, while avoiding problems related with massive exposition to the vitamin.

From another point of view, the development of nanotechnology is opening new areas for exploration in the design of smart delivery systems. In particular several nanodevices have been suggested to provide a benefit to the drug delivery

scene. Among potential drug-delivery supports, mesoporous silica particles (MSPs) have been widely proposed as delivery systems in various life science fields such as medicine, nutrition, and food technology in recent years (Wang *et al.*, 2009 and Mondragón *et al.*, 2014).

Periodically ordered mesoporous silicas, created by combining surfactant micellar aggregates with reactive silica precursors, were discovered about 20 years ago by researchers at Mobil (Beck *et al.*, 1992). This first class of periodic mesoporous silicas was known as M41S phases. Since these seminal studies, fine tuning of the reaction parameters such as concentrations, pH value, chemical nature of the surfactants, temperature, and time has allowed a precise adjustment of size, morphology, and pore structure and the development of different MSPs such as MCM-41, SBA-15, UVM-7, etc. (Argyo *et al.*, 2014 and Pérez-Esteve *et al.*, 2014). MSPs are characterized by a high homogeneous porosity defined from tunable pores with size between 2 and 10 nm, which make these scaffolds ideal for hosting functional guest molecules. Moreover it has been reported that the surface of ordered silicas can be functionalised with molecular/supramolecular ensembles to develop gated-MSPs, which show "zero delivery" yet can release their cargo on-command in response to specially designed external stimuli (Aznar *et al.,* 2009). This opens the possibility to design stimuli-responsive mechanisms with spatiotemporal control of cargo release (Argyo *et al.*, 2014). In particular, polyamines are well-known pH-responsive molecules able to adopt different conformations as a consequence of changes in the pH, and this characteristic has been applied to the design of pH-responsive gated materials (Bernardos *et al.*, 2008).

In this work, encapsulation of large amounts of FA in the final delivery systems is very important to minimize the quantity of material needed to provide the dietary reference intake or a percentage of the same. Moreover, to control the FA release rate is very important to avoid absorption peaks. In this manner, the most suitable delivery system to modulate FA bioaccessibility along the gastrointestinal tract should be able to hinder FA release in the stomach, and

achieve a sustained release before arriving to the jejunum where FA is absorbed (i.e. first 2 h of the intestinal phase of the digestion) (Baker *et al.,* 1969). It is well known that in mesoporous materials both, loading efficiency as well as release rate, depend on properties of the support such as surface area, pore size, pore geometry, total pore volume, surface chemistry as well as on the loading procedure.

Based in these concepts, the aim of this work was the evaluation of different silica supports (MCM-41, SBA-15, UVM-7 and hollow silica microspheres) caped with pH-responsive molecular gates to encapsulate sufficient amount of FA and to achieve a controlled and sustained release of the vitamin under digestive conditions. To reach this goal studies on loading optimization, encapsulation capacity, release kinetics and biocompatibility of the delivery systems with different cell lines have been performed.

2. Materials and methods

2.1 Chemicals

Tetraethylorthosilicate (TEOS), N-cetyltrimethylammonium bromide (CTABr), pluronic P123 (P123), triethanolamine ($TEAH_3$), sodium hydroxide (NaOH), hydrochloric acid (HCl), acetic acid and N^1-(3-Trimethoxysilylpropyl)diethylenetriamine (N3), sodium phosphate monobasic (NaH_2PO_4), sodium phosphate dibasic (Na_2HPO_4), tetrabutylammonium hydrogen sulphate (TBAHS), deuterium oxide (D_2O), sodium deuteroxide (NaOD) and all chemicals for the digestive fluids were provided by Sigma (Sigma-Aldrich Química S.L., Madrid, Spain). Folic acid was purchased from Schircks Laboratories (Jona, Switzerland). Acetonitrile HPLC grade was provided by Scharlau (Barcelona, Spain). Hollow Silica Shells were provided by Exilica Limited (Coventry, UK). Tetraethyl ammonium bromide (>99%) was provided by Merck (Darmstadt, Germany).

For cell culture experiments, trypan blue solution (0.4%) cell culture grade and DMSO, PBS and Dulbecco's Modified Eagle's medium (DMEM) with glucose, l-glutamine and pyruvate for cell culture were provided by Sigma-Aldrich. Mc Coy's 5a Medium and Keratinocyte Serum Free Medium, Fetal Bovine Serum (FBS) and trypsin were purchased from Gibco (Life Technologies, Madrid, Spain). Cell proliferation reagent WST-1 was purchased from Roche Applied Science (Barcelona, Spain).

2.2 Mesoporous silica particles synthesis

Microparticulated MCM-41 particles (**M**) were synthesized following the so-called "atrane route", according to the method described by Bernardos *et al.* (2008). CTABr was used as the structure-directing agent. The molar ratio of the reagents was fixed to 7 $TEAH_3$:2 TEOS:0.52 CTABr:0.5 NaOH:180 H_2O. CTABr was added to a solution of $TEAH_3$ containing NaOH and TEOS at 118 °C. After dissolving CTABr in the solution, water was slowly added with vigorous stirring at 70 °C. After a few minutes, a white suspension was formed. This mixture was aged in an autoclave at 100 °C for 24 h.

SBA-15 microparticles (**S**) were synthesized following the method reported by Zhao *et al.* (1998). P123 was used as the structure-directing agent. The molar ratio of the reagents was fixed to: 0.017 P123:1.0 TEOS:6 HCl:196 H_2O. The preparation was performed by mixing an aqueous solution of P123 with HCl solution, and stirring for 2 h, after which the silica source, TEOS, was added. This final mixture was stirred for a further 24 h. The mixture was aged in an autoclave at 100 °C for 24 h.

UVM-7 particles (**U**) were synthesised following the method presented by Comes *et al.* (2009), based also on the "atrane route". The molar ratio of the reagents was fixed at 7 $TEAH_3$:2 TEOS:0.52 CTABr:180 H_2O. The TEOS/$TEAH_3$ mixture was heated to 120 °C in a Dean-Stark until no elimination of ethanol was observed. The mixture was cooled to 90 °C and CTABr was added gradually in small portions, followed by dilution with water. The mixture was aged for 24 h.

For all samples, the resulting powder was recovered by centrifugation, washed with deionised water, and air-dried at room temperature. To prepare the final mesoporous materials, the as-synthesized solids were calcined at 550 °C using an oxidant atmosphere for 5 h in order to remove the template phase.

2.3 Folic acid loading and amine functionalization

10 different FA loaded and functionalised solids were prepared for each support. In a typical synthesis, 0.5 mL of an aqueous solution of FA in phosphate buffer (PBS) (10 mg mL^{-1}) was dropped to 100 mg of the corresponding support (i.e. MCM-41, SBA-15, UVM-7 and Hollow Silica Shells) and mixed. After the impregnation, solids were dried at 30 °C to eliminate water content. The procedure was repeated as many times as needed to obtain solids with a sequential number of impregnation cycles from 1 to 10.

To obtain the final loaded and functionalised solids, 100 mg of each of the FA-loaded supports were suspended in 10 mL of an aqueous solution of acetic acid (5%) and an excess of N3 (0.43 mL, 0.015 mmol) was added. The final mixtures were stirred for 5.5 h at room temperature. The forty loaded and functionalized solids (**H1-10**, **M1-10**, **S1-10** and **U1-10**) were isolated by vacuum filtration, washed with 300 mL of water adjusted to pH 2, and dried at room temperature for 24 h.

To evaluate the efficiency of the different impregnation cycles, the “relative loading efficiency” was calculated (see Section 2.5).

2.4 Characterization

X-ray diffraction (XRD), transmission electron microscopy (TEM), field emission scanning electron microscopy (FESEM), N_2 adsorption-desorption, thermogravimetric analysis (TGA), ^1H NMR, laser diffraction and Z-potential measurements were employed to characterize the synthesized supports.

XRD were performed on a Bruker D8 Advance diffractometer (Bruker, Coventry, UK) using CuKα radiation. TEM images were obtained with a JEOL JEM-1010 (JEOL Europe SAS, Croissy-sur-Seine, France). FESEM images were acquired with a Zeiss Ultra 55 (Carl Zeiss NTS GmbH, Oberkochen, Germany) and observed in the secondary electron mode.

N_2 adsorption-desorption isotherms were recorded with a Micromeritics ASAP 2010 automated sorption analyser (Micromeritics Instrument Corporation, Norcross, USA). The samples were degassed at 120 °C in vacuum overnight. The specific surface areas were calculated from the adsorption data in the low pressure range using the BET model. Pore size was determined following the BJH method. From the XRD and porosimetry studies, the a_0 cell parameter and wall thickness of the different supports were calculated.

The theoretical maximum loading capacity in the different supports was calculated by dividing the value of pore volume of each of the supports by the value of FA molecule volume (1.16 nm^3) and assuming that in a highly efficient packaging FA could lead to a maximum occupancy of ca. 75% of the supports total pore volume (Pérez-Esteve *et al.*, 2015).

The composition of loaded and functionalised supports was determined by TGA and ^1H NMR. Thermogravimetric analyses were carried out on a TGA/SDTA 851e Mettler Toledo balance (Mettler Toledo Inc., Schwarzenbach, Switzerland), using an oxidant atmosphere (air, 80 mL min^{-1}) with a heating program consisting of a heating ramp of 10 °C per minute from 393 to 1273 K and an isothermal heating step at this temperature for 30 min. ^1H NMR spectra were recorded at RT using a Bruker AV400 spectrometer (Bruker Daltonik GmbH, Bremen, Germany) after dissolving the corresponding sample in $NaOD/D_2O$ in the presence of tetraethyl ammonium bromide as internal standard.

The particle size distribution of the different bare and functionalised MSPs was determined using a Malvern Mastersizer 2000 (Malvern Instruments, Malvern, UK). For the measurements, samples were dispersed in distilled water. Data analysis was based on the Mie theory using refractive indices of 1.33 and 1.45 for the dispersant and MSPs, respectively. An adsorption value of 0.001 was used for all samples. Variation of this adsorption value did not significantly alter the obtained distributions. Measurements were performed in triplicate.

To determine the zeta potential (ζ) of the bare and functionalised MSPs, a Zetasizer Nano ZS equipment (Malvern Instruments, Malvern, UK) was used. Samples were dispersed in distilled water at a concentration of 1 mg mL^{-1}. Before each measurement, samples were sonicated for 2 min to preclude aggregation. The zeta potential was calculated from the particle mobility values by applying the Smoluchowski model. The average of five recordings was reported as zeta potential. The measurements were performed at 25 °C. Measurements were performed in triplicate.

2.5 FA release kinetics and loading efficiency evaluation

To obtain the FA release kinetics for each of the 40 solids at different pHs, 10 mg of the corresponding solids were placed in 25 mL of water at pH 2 (simulating condition at the stomach) and pH 7.5 (simulating condition at the intestine). At a certain times aliquots were separated, the suspension filtered and the solution analysed by HPLC.

The "relative loading efficiency" for each solid was calculated according to the following equation:

$$\text{Relative loading efficiency (\%)} = FA_D/FA_L \times 100$$

where FA_D are the mg of FA delivered per 1mg of loaded solid at pH 7.5 after 4 h and FA_L are the mg of folic acid employed for the loading of 1 mg of the corresponding solid.

The FA release kinetics from pore voids of the porous silica supports were calculated using the Higuchi model where the amount of guest release, Q_t, per unit of exposed area at time *t* can then be described by the following equation:

$$Q_t = k_H \sqrt{t}$$

where k_H is the release rate constant for the Higuchi model.

2.6 Folic acid quantification

FA was quantified by reversed-phase gradient HPLC method according to the method described by Pérez-Esteve *et al.* (2015). The HPLC instrument consisted of a Hitachi LaChrom Elite liquid chromatograph (Hitachi Ltd., Tokyo, Japan) equipped with an auto-sampler and UV detector (model L-2400). A Kromaphase 100 C18 (250 mm × 4.6 mm i.d., 5 µm particle size analytical column) (Scharlau, Barcelona, Spain) was used for the separations. The mobile phase consisted of (A) 0.125 mM of NaH_2PO_4, 0.875 mM of Na_2HPO_4 and 0.4 mM of TBAHS in water and (B) acetonitrile-phase A 65:35 (v/v). The gradient program was as follows: 0-5 min, 90% A and 10% B; thereafter, the proportion of B was increased linearly to reach 36% at 15 min and 60% at 30 min. After that, decreased linearly to reach 10% at 35 min and remained in the initial conditions for 5 min.

2.7 Cell culture Conditions

HeLa human cervix adenocarcinoma and HEPG2 human liver carcinoma were grown in DMEM supplemented with 10% FBS. HCT116 human colon carcinoma cells were grown in McCoy's 5a Medium Modified supplemented with 10% FBS and HK2 homo sapiens kidney papilloma cells were grown in Keratinocyte Serum Free Medium supplemented with bovine pituitary extract (BPE) and human recombinant epidermal growth factor (EGF). All of these cells were purchased from the German Resource Centre for Biological Materials (DSMZ). Cells were maintained at 37 °C in an atmosphere of 5% carbon dioxide and 95% air and underwent passage twice a week.

2.8 WST-1 Cell viability Assay

HeLa, HCT116, HEPG2 and HK2 cells were cultured in sterile 24-well plates at a density of $2 \cdot 10^4$ cells/well for HeLa and HK2 and $2 \cdot 10^5$ for HCT116 and HEPG2 in a 1000 µL of respectively grown medium and were incubated 24 h in a CO_2 incubator at 37 °C. Then, solids in DMSO were added to cells in quadruplicate at final concentrations of 50, 100, 150 and 200 µg mL^{-1}. Control wells did not contain any solid. After 23 h, cells were washed with PBS and then 30 µL of WST-1 reagent were added to each well and were incubated during 1 h, a total of 24 h of incubation was therefore studied. Before reading the plate, cells shacked for 1 min to ensure homogeneous distribution of colour. Then the absorbance was measured at a wavelength of 450 nm and 690 nm in VICTOR X5 PerkinElmer. Results are expressed as an average of the results of three independent experiments.

2.9 Data analysis

The results of the FA delivery from the different solids prepared were statistically processed using Statgraphics Centuriun XV (Manugistics Inc., Rockville, MD, USA). Statistical analysis on FA concentrations was made using an analysis of variance (One-Way ANOVA). The LSD (least significant difference) procedure was utilised to test for differences between averages at the 5% significance level.

3. Results and discussion

3.1 Design, synthesis and characterization of the gated supports

Incorporation of gate-like ensembles into porous silica particles is a suitable approach to design devices for controlled delivery applications. The development of responsive gated materials requires selecting two components: (i) a suitable gate-like ensemble that changes one or several properties (size, shape, bulkiness, charge, etc.) upon external stimuli and (ii) the selection of the nano-structured matrix in which the gate-like scaffold is grafted. In this wok we have selected a diethylenetriamine moiety as capping ensemble due to its proved properties to control the delivery of cargo molecules from the void of mesoporous silica particles as a response of pH changes (Bernardos *et al.*, 2008, Casasús *et al.*, 2008 and Pérez-Esteve *et al.*, 2015). Moreover as inorganic support, we have selected four different porous silica supports (MCM-41, UVM-7, SBA-15 and Hollow Silica) having different size, shape and pore system. In all cases, the particle size was in the microscale. The MCM-41 support (**M**), the most popular member of the M41S family, is characterized by a regular pore system which consists of a hexagonal array of unidimensional, hexagonally shaped pores (Grün *et al.*, 1999). The UVM-7 support (**U**) can be described as bimodal porous silica constructed by the aggregation of pseudo-spherical mesoporous primary nanoparticles. The intra-nanoparticle pore system consists of regular-sized mesopores disposed in a pseudo-hexagonal disordered array, while the arrangement of the inter-particle meso/macropores exhibits xerogel-like characteristics (Pérez-Cabero *et al.*, 2012). Microparticulated SBA-15 (**S**) presents uniform hexagonal pores with a narrow pore size distribution and a tunable pore diameter between 5 and 15 nm. The thickness of the framework walls is about 3.1-6.4 nm, which gives the material a higher hydrothermal and mechanical stability (Thielemann *et al.*, 2011). Finally, Hollow Silica Shells (**H**) were employed due to their reported high storage capacity of its hollow core structure (Zhu *et al.*, 2005). According to these reported textural features, FA (which measures 1 × 1.45 nm) might be easily encapsulated in the four selected supports (Pérez-Esteve *et al.*, 2015).

Once synthesized (**M**, **S**, **U**) or acquired from the supplier (**H**), solids were characterized by using standard procedures. XRD patterns of each of the supports can be found in **Figure 1**.

Figure 1H shows the diffractogram of the commercially available Hollow Silica Shells. As observed, at low angles there were no reflections suggesting the absence of any order in the pore structure. XRD at high angles revealed a broad peak around 22 (2θ) (data not shown), indicating that employed H support presents an amorphous structure. X-ray patterns of the MCM-41, SBA-15 and UVM-7 as synthesized, calcined and loaded with FA and functionalized with amines are shown in **Figures 1M**, **1S** and **1U** respectively.

Figure 1M shows the four typical peaks of a hexagonal ordered array, indexed as (1 0 0), (1 1 0), (2 0 0) and (2 1 0) Bragg reflections, of the as-synthesised MCM-41 material. An a_0 cell parameter of 41.7 Å (d_{100} spacing = 36.1 Å) was calculated. A significant shift of the (1 0 0) reflection in the XRD powder of the MCM-41 calcined sample was clearly appreciated, corresponding to a cell contraction (5.6 Å) related to condensation of silanols during the calcination step. The loaded and capped final material showed that reflections (1 1 0), (2 0 0) and (2 1 0) were lost, most likely due to a reduced contrast that can be attributed to the presence of FA in the pore voids and the anchored polyamine molecule. Nevertheless, the existence in all cases of the (1 0 0) peak in the XRD patterns indicated that the process of pore loading with FA, and the additional functionalization with the polyamine, did not modify the typical porosity of the mesoporous MCM-41 scaffold.

Figure 1S shows a sharp peak at ca. 0.9, indexed as the (1 0 0) reflection, and two minor reflections in the 1.0-2.0 interval, indexed as (1 1 0) and (2 0 0) Bragg reflections, respectively. These peaks were indexed according to two-dimensional hexagonal p6mm symmetry, of a well-defined SBA-15 mesostructure. Hence, the obtained a_0 cell parameter was 113.47 Å (d_{100} spacing = 98.27 Å). The calcination process displaced the (1 0 0) reflection due to condensation of silanol groups,

resulting a cell contraction of 10.5 Å. The preservation of (1 0 0) in the final solid indicated that the long-range hexagonal symmetry of SBA-15 was maintained after FA loading and amine functionalization.

Finally, **Figure 1U** shows two broad low-angle reflections that could be related with a disordered hexagonal array of the mesopores in this UVM-7 support. Assuming the first peak could be indexed as the (1 0 0) reflexion, an a_0 cell parameter of 47.54 Å (d_{100} spacing = 41.18 Å) was obtained. The XRD pattern of the calcined UVM-7 solid showed a displacement of the (1 0 0) peak. It indicated a cell contraction of approximately 3.1 Å. The X-ray diffraction patterns of the FA loaded and polyamine-functionalised solid was characterized by the presence of an intense peak at ca. 2 (1 0 0 reflection) typical of a surfactant-assisted mesoporous material, indicating that neither the loading nor the functionalization induced any significant effect on the mesoporous structure of the silica matrix.

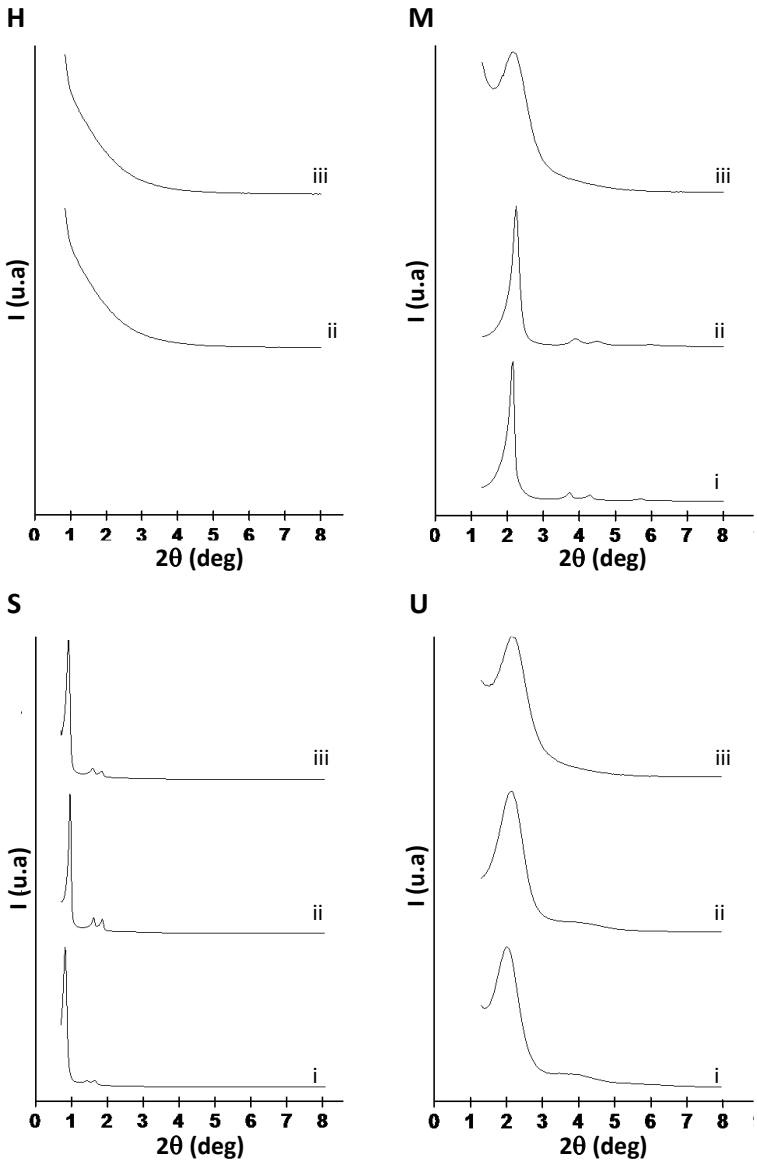

Figure 1. Powder X-ray patterns of the solids i) as synthesized, ii) after surfactant extraction and iii) after loading with folic acid and functionalisation with polyamines. Hollow Silica Shells (H), MCM-41 (M), SBA-15 (S) and UVM-7 (U).

As a complement to XRD patterns to elucidate porous structure of different supports, **Figure 2** shows FESEM and TEM images of the different silica support used in this study. By means of FESEM observation, a characterization of the shape of the particles was performed. All different supports showed sizes in the micro-scale. These pictures also confirmed that different particles exhibited diverse morphology, from completely spherical particles (**H**), to irregular shaped particles (**M**), elongated particles (**S**) or agglomeration of nanoparticles (**U**). The comparison of the pictures before and after loading with FA and functionalization with N3 for the same support allowed concluding that neither loading nor functionalization significantly modified the appearance of the external surface suggesting none deposition of FA on the surface, and thus a complete encapsulation of FA in the support.

The presence of mesostructures on **M**, **S** and **U** after loading with FA and functionalization with polyamines was confirmed by TEM images. **Figure 2** shows the typical channels of the mesoporous matrixes either as alternate black and white stripes or as pseudo hexagonal arrays of pore voids. These channels were visualised not only in the starting calcined materials but also in final FA-loaded and N3-functionalised supports, confirming the preservation of the mesopores during the preparation process. Moreover, TEM observations revealed the absence of any clear mesostructure in **H** particles.

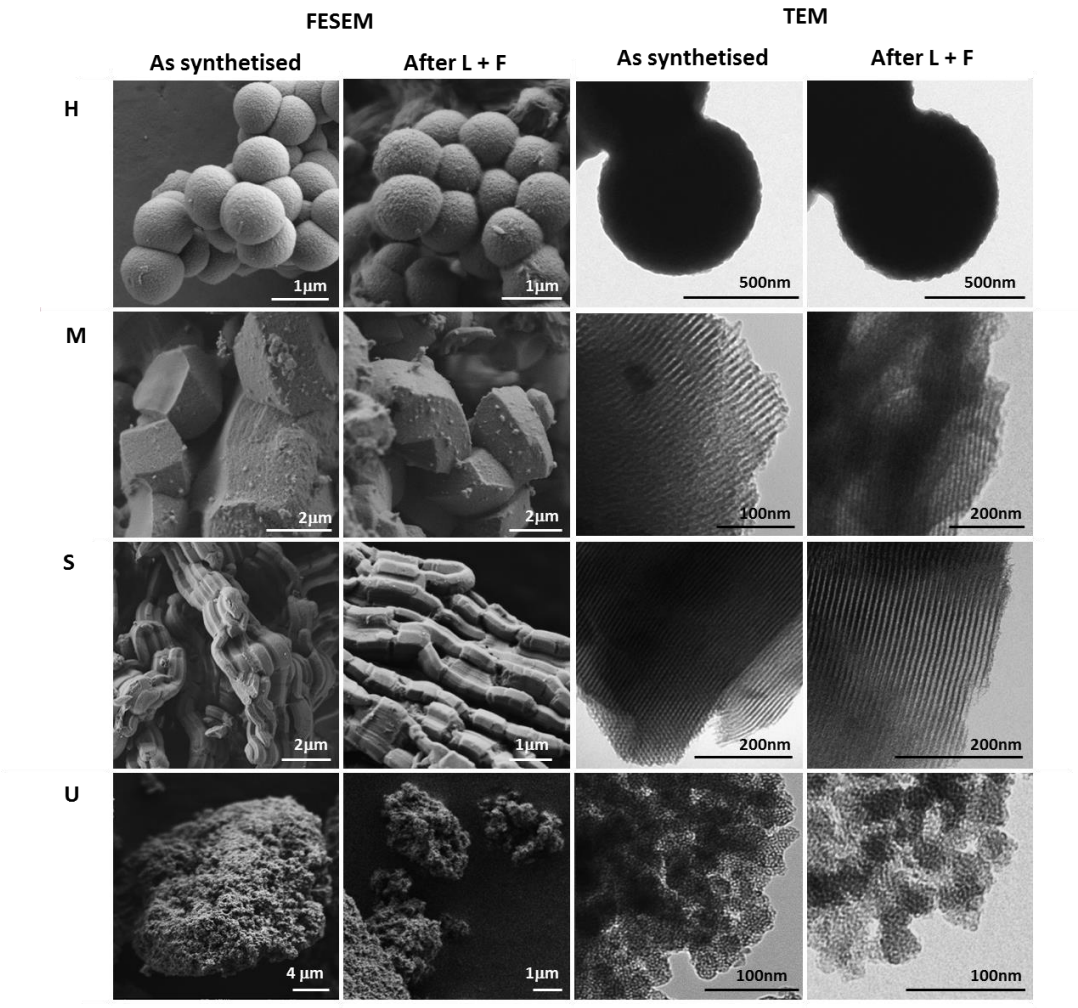

Figure 2. Characterization of particle size, particle shape and pore system by means of FESEM and TEM. Hollow Silica Shells (H), MCM-41 (M), SBA-15 (S) and UVM-7 (U).

N_2 adsorption-desorption isotherms of the starting and final silica supports are shown in **Figure 3**. **Figure 3H** shows the N_2 adsorption-desorption isotherms of Hollow Silica Shells. No capillary condensation was detected in the isotherms, confirming the absence of mesopores suggested by XRD and microscopy observations. Nevertheless, the high loading capacity exhibited by this material (see Section 3.2) made us think that the sample might have accessible microcavities where FA can be clearly entrapped.

Figures 3M and **3U** show the isotherms of the MCM-41 and UVM-7 systems, respectively. In both cases the starting materials exhibited a sharp and well defined adsorption step at relative pressure values between 0.2 and 0.6, attributed to nitrogen condensation in the mesopore inlets. The absence of a hysteresis loop in this interval and the narrow BJH pore distribution suggested the existence of uniform cylindrical mesopores. The difference between **M** and **U** was that the curve of **U** showed two steps. The first, as commented, was originated from the capillarity condensation of N_2 into the mesopores, whereas the second, at higher relative pressures, was related to the filling of textural interparticle pores typical of the **U** scaffolding. According to IUPAC definition, both isotherms are type IV, characteristic of mesoporous materials with narrow pore size distributions. Finally, **Figure 3S** shows a type IV isotherm with adsorption step at relative pressure around 0.6, typical of **S** particles with well-defined channel-like mesopores. Moreover, we have applied the Barrett-Joyner-Halenda (BJH) model on the adsorption curves of the isotherms to calculate pore diameter and pore volume of all solids. In addition, the application of the Brunauer, Emmett and Teller (BET) model allowed the calculation of total specific surface. Calculated values for different supports are shown in **Table 1**. **M** and **U** have a similar surface area of ca. 1000 $m^2\ g^{-1}$ and a mesoporous size of ca. 2.6 nm. In contrast, **S** has lower surface area but a larger pore size of ca. 8 nm. Surface of Hollow Silica Shells was very low compared with the other supports due to the confirmed absence of mesoporosity.

For all supports, a change on the N_2 adsorption-desorption isotherms for the corresponding FA-loaded and N3-functionalized supports was observed. In particular, isotherms showed no remarkable steps at low-intermediate relative pressure indicating a decrease of surface area and volume after FA loading and amine functionalization (**Fig 3**).

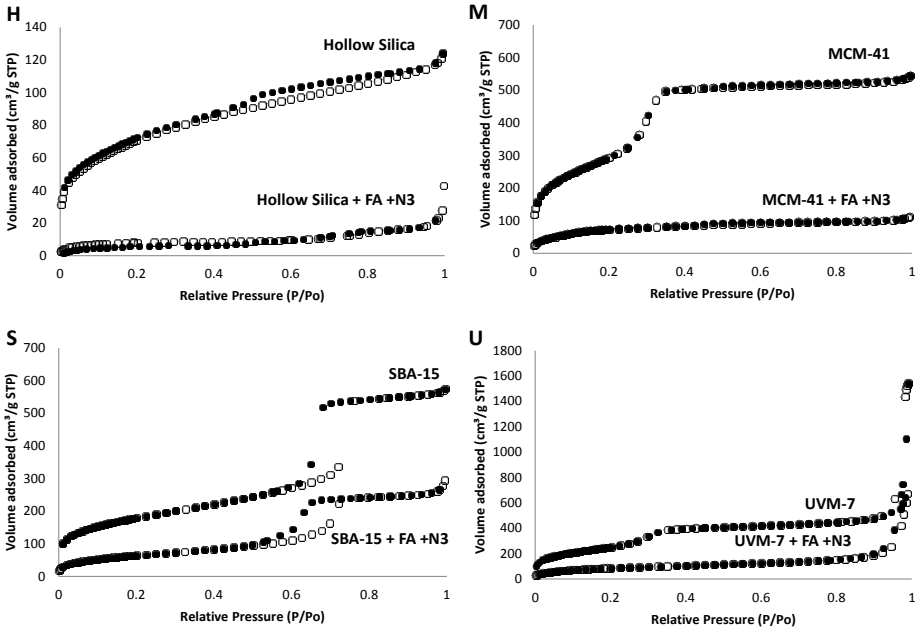

Figure 3. Nitrogen adsorption(○)-desorption(●) isotherms for (a) Hollow Silica Shells, (b) MCM-41, (c) SBA-15 and (d) UVM-7.

Table 1. Textural properties of calcined silica matrixes: Hollow Silica Shells (H), MCM-41 (M), SBA-15 (S) and UVM-7 (U).

Silica Support	Area[a] ($m^2\ g^{-1}$)	Mesopore (P/P_0<0,6)		Textural pore (P/P_0>0,6)		[c] (nm)	dw[d] (nm)	TMLC[e] ($\mu g\ mg^{-1}$)
		Pore volume[b] ($c^3\ g^{-1}$)	Pore size[b] (nm)	Pore volume[b] ($c^3\ g^{-1}$)	Pore size[b] (nm)			
H	258	-	-	-	-	[f]	[f]	-
M	1074	0.91	2.61	-	-	4.54	1.93	431
S	649	0.92	7.89	-	-	10.54	2.64	436
U	919	0.75	2.65	1.10	54.80	4.75	2.10	355

a. BET specific surface values calculated from the N_2 adsorption branch of the isotherms.
b. Pore volumes and pore sizes (diameter) calculated from the N_2 adsorption-desorption isotherms for selected materials.
c. Cell parameter. $a_{0=}2d_{100} \cdot (\sqrt{3})^{-1}$
d. Wall thickness. $dw = a_0 - d_p$, where d_p is the mesopore pore diameter
e. Theoretical maximum loading capacity
f. Without available data from XRD.

Textural properties of different supports calculated from nitrogen adsorption-desorption isotherms and XRD are summarized in **Table 1**. **Table 1** also shows the calculated theoretical maximum loading capacity for **M**, **S** and **U**.

Particle size is important when designing devices for oral control release. It is well known that nanoparticles' cellular uptake is size-dependant. In particular it has been reported that nanoparticles larger than 600-1000 nm exhibit a notable lower transport across the follicle-associated epithelium when compared with smaller particles (He *et al.*, 2012). According to these data, all the final supports are suitable for oral delivery purposes and are not expected to be absorbed in the digestive tract. Size distribution of the four supports in all the stages of their preparation, from the bare particles to the particles loaded with FA and functionalised with the N3 polyamine is shown is **Figure 4**. Three of the supports (**H**, **M** and **S**) did not change significantly their grain size as a function of the loading and functionalization. However, **U** grains which are composed of an

agglomeration of porous nanoparticles changed dramatically its size after the functionalization with the polyamine. This change was attributed to the deflocculant effect of the functionalization process. During functionalization process the vigorous stirring provoked grain desegregation. The subsequent functionalization with amines increases the stability of desegregated grains by adding positive charges to the surface (Pérez-Esteve *et al.*, 2014). This cooperative effect results in the reduction of **U** grain size, also detected in FESEM observations (**Fig 1U**). In this manner, after the loading and functionalization process, all the solids exhibited a particle size of ca. 0.6-1 μ.

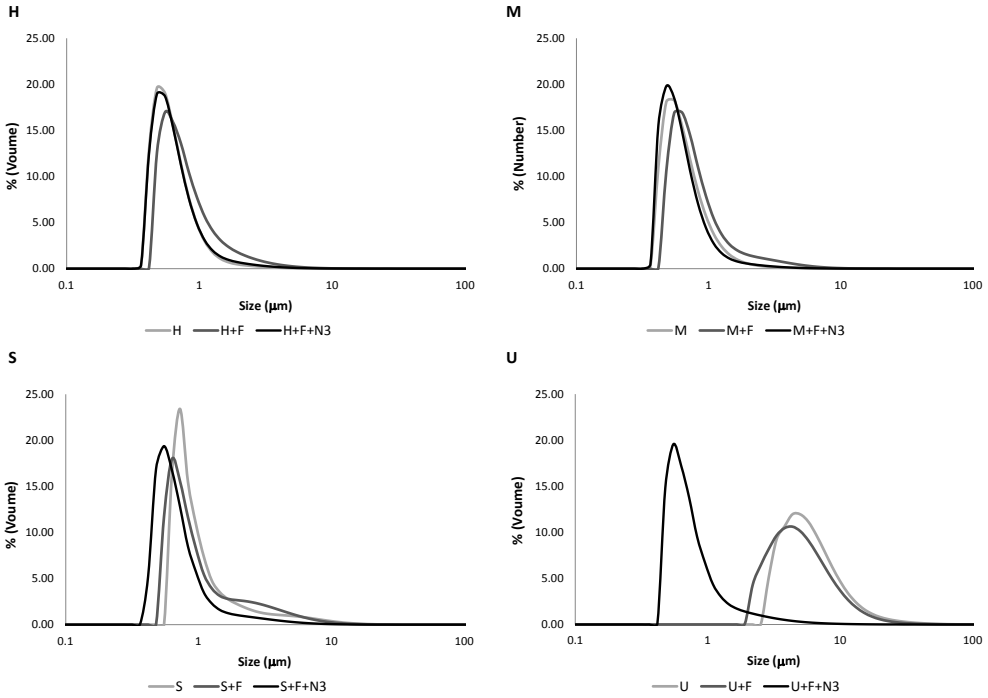

Figure 4. Size distribution of different bare particles (#), particles loaded with FA (#+F) and particles loaded with FA and functionalised with N3 (#+F+N3).

Finally, the efficiency of functionalization was tested by zeta potential determinations. It is generally accepted that mesoporous silica is negatively charged above the isoelectric point (pH 2-3). These values agree with those measured for all the four starting particles. As it can be seen in **Figure 5**, unloaded **H**, **M**, **S**, **U** exhibited negative zeta potential values in the -50 mV to -30 mV range. The loading of the supports with FA did not modify significantly zeta potential values. However, the functionalization of the loaded supports with the polyamine N3 transformed the zeta potential from negative to positive (ca. +30 mV), confirming that the functionalization successfully occurred in all cases. Moreover we also found that the number of loading cycles (*vide infra*) did not cause remarkable changes on final zeta potential values for the different particles.

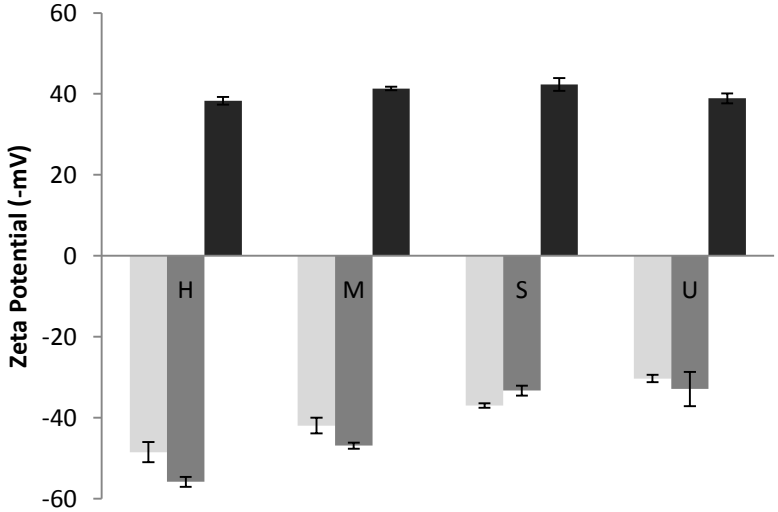

Figure 5. Zeta potential values (Mean ± SD) of unloaded supports (light grey), supports loaded with FA (dark grey) and supports loaded with FA and functionalised with N3 (black) dispersed in distilled water. Hollow Silica Shells (H), MCM-41 (M), SBA-15 (S) and UVM-7 (U).

3.2 Loading efficiency evaluation

With the objective of evaluating the loading capacity of the silica supports with FA, different experiments were carried out. For each of the supports, 10 solids impregnated from 1 to 10 times with 0.5 mL of an aqueous solution of FA in PBS (10 mg mL^{-1}) were prepared.

FA content in prepared solids was determined by TGA and ^{1}H NMR. **Table 2** shows content of organic matter (α) in solids impregnated 10 times as well as in those with the highest (FA released): (FA employed in the loading of the support) ratio, called optimized solids (vide infra). For all the supports, the higher the impregnation cycles, the higher the content in FA. N3 content was larger for solids **S** and **U**, than for **H** and **M**. For the same support, content of N3 (expressed in mg N3 mg^{-1} SiO_2) did not change as a function of the number of loading cycles.

Table 2. Content (α) of FA and N3 in optimized solids and in solids loaded 10 times. Hollow Silica Shells (H), MCM-41 (M), SBA-15 (S) and UVM-7 (U)

Support	Optimized		Loaded 10 times	
	αFA (mg g_{solid}^{-1})	αN3(mg g_{solid}^{-1})	αFA(mg g_{solid}^{-1})	αN3(mg g_{solid}^{-1})
H	125	71	272	59
M	99	75	249	63
S	77	106	264	89
U	95	142	257	118

Comparing the calculated theoretical maximum loading capacity (**Table 1**) with real FA content it was shown that **M** and **S** were able to reach after 10 impregnation cycles ca. 60% of the maximum content, while **U** incorporated ca. 70%. These results point that the loading procedure employed for FA loading (i.e. impregnation) is very efficient.

Release effectiveness of each solid was also evaluated by determining the maximum amount of FA delivered at pH 7.5. **Figure 6** shows FA delivered (μg FA mg^{-1} solid) from each of the 40 solids prepared after reaching the equilibrium (2 h). As it can be seen, for each of the different supports, the more impregnation cycles employed, the more FA delivery was achieved. In no case a saturation of the loading capacity seems to be achieved, since the slope described by the bars for each of the impregnation cycles does not reach the horizon. These data confirm that the theoretical maximum loading capacity was not achieved in any of the supports.

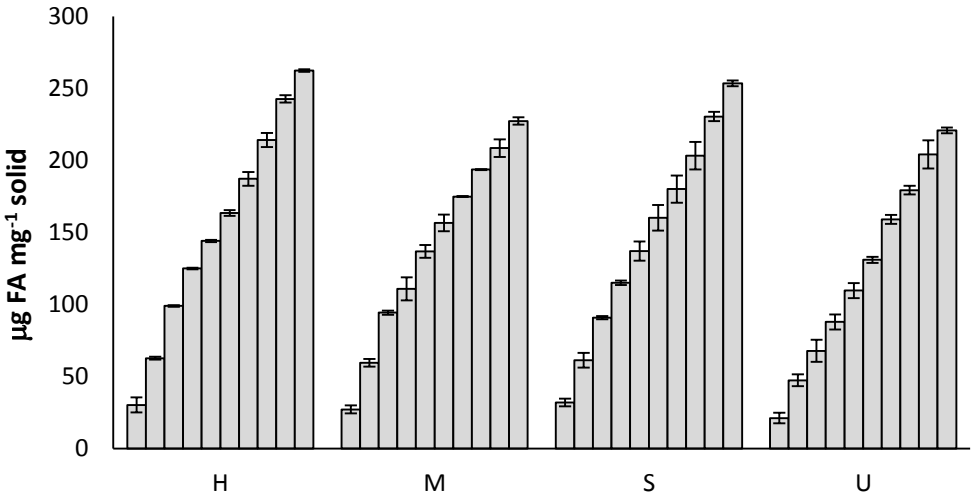

Figure 6. Maximum FA delivery (μg FA mg^{-1} solid) for different solids impregnated from 1 to 10 times (ordered sequentially) and functionalized with N3. Hollow Silica Shells (H), MCM-41 (M), SBA-15 (S) and UVM-7 (U). Values are Means ± SD, n=3.

Comparing the maximum amount of FA delivered for the different supports after 10 loadings, it can be seen how Hollow Silica Shells (**H**) was the support that exhibited the maximum FA delivery (262 μg FA mg^{-1} solid) followed by **S** (ca. 252 μg FA mg^{-1} solid), **M** (227 μg FA mg^{-1} solid) and **U** (220 μg FA mg^{-1} solid). These values represent a percentage of release of 96%, 91%, 95% and 85% of the loaded FA for **H**, **M**, **S** and **U** supports, respectively. These high values indicate that the release of FA from the voids of the studied supports is very efficient, probably due

to a very low interaction among FA (charged negatively at pH 7.5) and the inner surface of the supports (also charged negatively at pH 7.5).

Finally and with the objective of determine the relative loading/delivery performance of the solids from a technological efficiency point of view the "relative loading efficiency" (RLE) was calculated. This parameter was calculated by determining the ratio between the amount of FA delivered (after 4 h at pH 7.5) per mg of loaded solid and the mg of FA used for loading 1 mg of the support (see Section 2.5 for details).

Figure 7 shows RLE values for different solids impregnated from 1 to 10 times with FA and functionalized with N3. As observed, each support exhibited a different behaviour according to the relative loading efficiency. **S** was the support with larger RLE, probably due to its higher pore size and pore volume. **H** also exhibited a high RLE, similar to **M** in the first impregnation cycles. Besides, **U** was the support with lower RLE values, most likely because FA tend to remain in the textural pore of the UVM-7 structure in the loading process and was removed during the washing process.

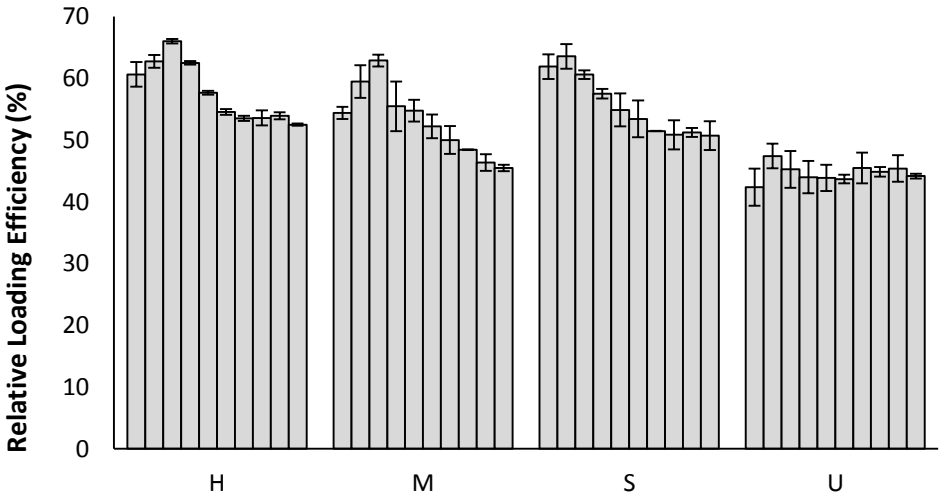

Figure 7. Relative Loading Efficiency for different solids impregnated from 1 to 10 times (ordered sequentially) and functionalized with N3. Hollow Silica Shells (H), MCM-41 (M), SBA-15 (S) and UVM-7 (U). Values are Means ± SD, n=3.

On the other hand, a comparison of RLE values among different impregnation cycles for each support indicated that **H** and **M** increased RLE until the third impregnation cycle and then decreased. **S** exhibited the highest RLE value in the second loading cycle. Finally, no significant statistical differences were found for **U** among different impregnation cycles. According to these results, we considered **H3**, **M3**, **S2** and **U2** as the optimised solids. Those solids were employed in subsequent release and toxicological experiments.

3.3 FA pH-driven controlled release

In order to evaluate the feasibility of different supports to control the bioaccessibility of FA in gastric and intestinal conditions, delivery studies of FA from optimised solids (i.e. **H3**, **M3**, **S2** and **U2**) were carried out at pH 2 (gastric) and pH 7.5 (intestinal). FA concentrations in the solutions were monitored by HPLC. **Figure 8** shows the release behaviour of the four supports loaded with FA and functionalised with N3. For all four supports, a nearly flat baseline was found at pH 2, indicating that FA remained in the voids of the particles without release. It confirmed the capability of the four proposed supports to hinder the release of the vitamin during pass through the stomach. As observed in previous works (Bernardos *et al.*, 2008, Casasús *et al.*, 2008 and Pérez-Esteve *et al.*, 2015), there are three mechanisms that favour this zero release: solubility of FA, conformation of polyamines in the gate-like ensemble and the interaction of polyammonium groups with anionic species. At acid pH FA is in its acidic form, exhibiting a very low solubility that hampers FA delivery from the pores (Pérez-Esteve *et al.*, 2015). On the other hand, at low pH values (i.e. pH 2) polyamines are transformed to polyammonium groups. This molecular change favours Coulombic repulsions between closely located chains. Tethered polyammonium moieties tend to adopt a rigid-like conformation that pushes them away towards pore openings, blocking the pores and inhibiting completely or partially the release of the vitamin. Moreover, polyammonium groups have the ability to coordinate anions. At pH 2, anions present in the sample (phosphates) interact with the protonated gate-like

ensemble creating a superstructure that collaborates to pore blocking. The last two mechanisms are closely interconnected and it is not easy to measure their individual contributions (Bernardos *et al.*, 2008).

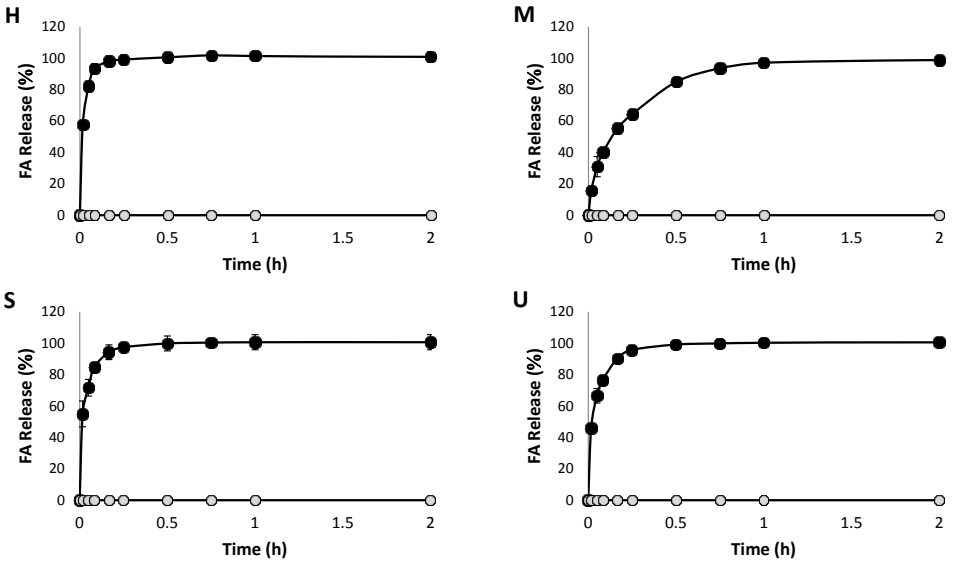

Figure 8. Release profile for different solids in water adjusted at pH 2 (○) and 7.5 (●). Hollow Silica Shells (H), MCM-41 (M), SBA-15 (S) and UVM-7 (U).

In contrast, at pH 7.5 (pH of the small intestine), a progressive delivery of FA was observed for all four supports. This different and remarkable behaviour at pH 7.5, when compared to that of pH 2, was due to the effect of pH on both, the solubility of FA and on the conformation of the polyamines. At pH 7.5 FA is in the form of salt, increasing its solubility, and enhancing the delivery from the pore voids to the solution (Zhou & García-Bennett, 2010). Meanwhile polyamines are, at neutral pH, less protonated and their interaction with anions is weaker, favouring pore unblockage. As a consequence, FA was able to be released. This overall behaviour (i.e. no FA delivery at acidic pH and FA delivery at neutral pH) pointed towards the suitability of the designed solids for a selective and controlled delivery of FA in the gastrointestinal tract. At acidic conditions

(stomach) the molecular gates would be closed, and therefore no release will be performed. In contrast, after passing to the duodenum the chime could be neutralized as a consequence of the bile and bicarbonate secretion from the pancreatic duct. This neutralization would favour the delivery of the vitamin from the voids, improving the bioaccessibility in the jejunum (pH 7.5), where folic acid is absorbed by a saturable, carrier-mediated, pH and energy-dependent transport mechanism (Wright *et al.*, 2007).

3.4 Release kinetics

Besides achieving a remarkable pH-triggered release of FA, we also aimed to evaluate the capability of those systems to control the delivery of the vitamin along time. With this purpose, data from the release kinetics at pH 7.5 were fitted to the Higuchi model. This simple model has been widely, and satisfactorily, applied for describing drug release kinetics from insoluble porous carrier matrixes (Guo *et al.,* 2014). It is based on Fickian diffusion processes taking into account the hypotheses that initial drug concentration in the matrix is much higher than drug solubility, that drug diffusion takes place in only one dimension and that drug diffusivity is constant (Dash *et al.,* 2010). **Figure 9** shows the good fitting of the model to data taken in the first minutes of the delivery, suggesting that in these conditions the delivery of the FA from the pores of different solids is basically a diffusive process. After these times a certain deviation from linearity was found (data not shown).

To facilitate interpretation of the data, the release Higuchi rate constant (kH) of FA from the **H3**, **M3**, **S2** and **U2** supports was calculated. The highest kH constant was observed for **H3** (kH = 19). **S2** and **U2** exhibited kH of 18 and 17 respectively. The lowest kH value (13) was exhibited by **M3**, being the support that allows a more sustained delivery, and thus the most convenient for modulating FA bioaccessibility along the pass through the small intestine.

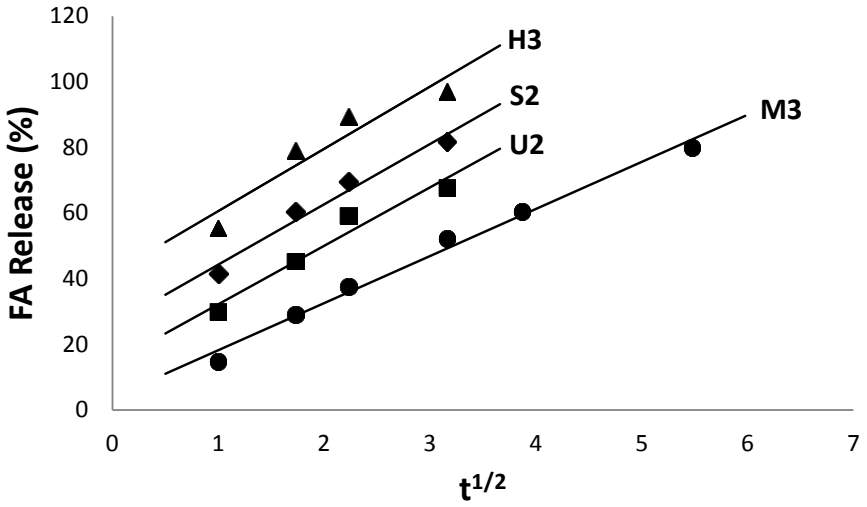

***Figure 9**. Higuchi release profile of FA delivered from solids H3, M3, S2 and U2 in aqueous media at pH 7.5*

Higuchi constant has been reported to depend, among other factors, on the diffusivity and solubility of the cargo in the solvent, the tortuosity of the system, the porosity of the matrix and the total amount of compound present in the matrix (Bernardos *et al.*, 2008). In this work the cargo as well as the solvent were the same, and thus, different values were only due to the inorganic support. Having in mind that **H** is the support with the highest kH, coinciding with the larger cavity, and that **S**, **U**, and **M** are ordered according to its pore size, the effect of pore size seems to be important to modulate the release kinetics of FA from different supports. The bigger the pore diameter, the easier the entrance of the solution to voids (or main cavity in the case of **H**), and thus the lower the diffusional problems of FA to escape from the entrapping support.

Figure 9 also allows observing that, with the exception of **M3**, three of the solids presented a y-interception very superior to 0 value. This phenomenon, called burst release, has been referred to an initial massive release occurring immediately upon placement the delivery system in the release medium. It has been observed in a number of capped mesoporous silica based delivery systems (Bhattacharyya *et al.*, 2012 and Radhakrishnan *et al.*, 2014). Burst release can be

favourable in some applications (i.e. encapsulation of aromas, targeted release). However, it is undesired when a sustained release is needed. Having this in mind, M is the support that allows controlling the release of FA during more time and avoids initial burst release.

In previous works, some authors have tried to understand the underlying mechanisms of this effect. Potential reasons that may lead to this behaviour are surface characteristics of the host material, sample geometry, host-cargo interaction, morphology and porous structure of dry material among others (Huang & Brazel, 2001). Although the importance of this phenomenon, conclusions are still rare. Thus we have tried to elucidate why different supports with different textural properties exhibited different burst release.

Intuitively, it is reasonable to assume that the amount of FA that is delivered during the initial burst release must be dependent on the FA surface directly exposed to the media once the molecular gate was opened at pH 7.5. The practically zero release at pH 2 and the relatively high density of N^1-(3-Trimethoxysilylpropyl)diethylenetriamine groups (preferentially anchored on the external surface of our solids) allows us to propose that the amount of FA on the external surfaces could be practically discarded. Then, under this last consideration, the FA species must be favourably located inside the pores or cavities present in our silicas. So, in the case of the **M** support, the initial exposed surface must correspond to the cross-section of the mesopore entrances. Taking into account that the morphology of this **M** sample is based on the existence of large micrometric particles, a relatively low number of mesopore entrances, and consequently a low initial FA/media interface is expected. In fact, the **M** support shows the smaller burst release. In a rough way, the **U** support could be viewed as a nano-version of the MCM-41, with respect to the particle size. This difference strongly affect the average length of the mesopores (although the mesopore sizes are similar, (i.e. their cross-sections). While micrometric mesopore lengths are expected for **M** supports, pores of nanometric length exist in the **U** sample. Hence, for a similar mass of support the number of mesopore entrances for the **U**

material must be higher than the entrances present in **M** support. So, as expected, a higher burst release is detected for **U** when compared to **M** support.

Although the comparison between **M** and **S** supports could be straightforward (similar particle size for both solids, but larger mesopore size for the **S**), the fact that under the impregnation conditions we have used, the mesopores in the **S** support remain partially filled with FA (according to N_2 adsorption-desorption measurements), make complicated a direct comparison between both solids. In fact, a larger FA surface must be exposed for **S** support (associated not only to the mesopore entrances but also to the internal mesopore surfaces partially covered by FA). In consequence, as a larger FA/media surface is expected, a more pronounced burst release occurs.

Among all supports, is precisely H the one that has a more singular morphology, which is markedly different from the rest of the mesoporous supports. In fact, there is not mesopores in the H support. Once the gate is opened, the invasion of the reaction media inside the internal microcavity must be a very quick process. Due to the fact that the FA should be considered as deposited on the internal cavity but not confined inside pores, a large contact surface is expected, with the subsequent large burst release.

3.5 In vitro biocompatibiliy tests

In addition to the FA loading and release properties of the different supports, it was also in our aim to assess the biocompatibility of the developed FA carriers. Therefore studies with solids **H3**, **M3**, **S2** and **U2** were performed using HeLa, HTC116, HEPG2 and HK2 cell lines to exclude any toxic effect of the microparticles. Cells were treated with the corresponding capped support for 24 h at final solid concentrations of 50, 100, 150 and 200 μg mL^{-1}. After that time, a cell viability assay using WST-1 was performed. The WST-1 assay is based on the measurement of the absorbance of the stable tetrazolium salt WST-1. This salt is transformed to a soluble formazan derivative by a complex cellular mechanism

that occurs primarily at the cell surface. This bio-reduction is largely dependent on the glycolytic production of NAD(P)H in viable cells. Therefore, the amount of formazan dye formed directly correlates to the number of metabolically active cells in the culture. Tetrazolium salts are cleaved to formazan by the succinate-tetrazolium reductase system which belongs to the respiratory chain of the mitochondria, and which is only active in metabolically intact cells.

WST-1 cell viability assay indicated that all the cell lines exhibited a high level of cell viability (ca. 100% cell proliferation) after 24 h upon treatment with solids **H3**, **M3**, **S2** and **U2** up to a concentration of 200 µg mL^{-1} (**Fig 10**). The assay suggested that the developed supports loaded with folic and functionalized with N3 were well tolerated by the cells.

Similar levels of biocompatibility of functionalised porous silicas have been reported by other authors (Yuan *et al.*, 2011, Mas *et al.*, 2013 and Feng *et al.*, 2013). This high biocompatibility is most likely related with both, the particle size employed and the surface functionalization. He *et al.* (2009) studied the cytotoxic effect of spherical mesoporous particles and observed that 190 nm and 420 nm particles showed significant cytotoxicity at concentrations above 25 mg mL^{-1}, while micro-scale particles of 1220 nm showed only slight cytotoxicity due to decreased endocytosis. Moreover, the interaction of silanol groups (ca 6% of total surface) with biological molecules, such as cellular membrane lipids and proteins that may strongly interact and eventually modify the structure of these molecules was prevented in our case by the functionalization with organic molecules. In fact, it has been reported that the surface coating of porous silica with organic molecules can increase the biocompatibility and half-lives of cells by more than 10 times compared to bare silica mesoporous supports (Tang *et al.*, 2012).

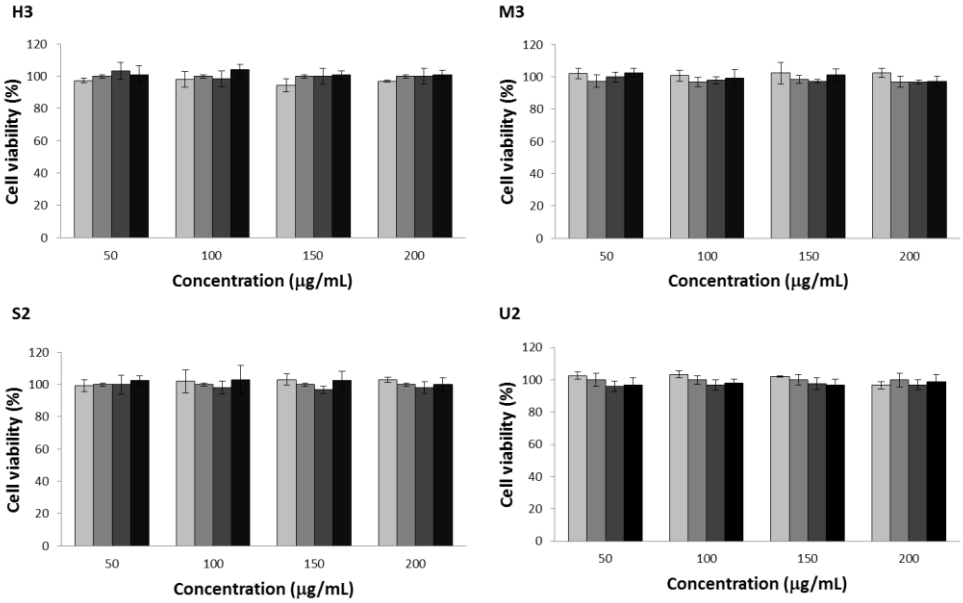

Figure 10. WST-1 cell viability assay. HCT116 (light grey), HEPG2 (medium grey), HK2 (dark grey) and HeLa (black) cells treated with optimized solids at concentrations of 25, 50, 100 and 200 µg mL^{-1} for 24 h. Cells were incubated for 24h with optimized solids at the concentrations stated before and cell viability was quantified using the WST-1 reagent.

4. Conclusions

We have reported herein the use of four different porous silica supports for the design of gated materials able to encapsulate FA, remaining closed at acidic pH (for instance the stomach) yet delivering efficiently the cargo in a neutral pH (for instance in the intestine). Despite the fact that all the designed supports presented a high loading capacity, that all were capable to control the FA release as a function of the pH and that none of them exhibited unspecific toxicity for four different cell lines, one of the supports stands out for showing remarkable advantages in controlling FA bioaccessibility. Concretely, results reported herein confirm that microparticulated MCM-41 capped with a simple pH-responsive gate based on polyamines was the only support able to sustain the cargo release for at least one hour. This sustained release is essential to modulate the bioaccessibility of the vitamin before absorption in the jejunum and thus to avoid problems related to FA absorption peaks that lead into the appearance of untransformed FA in blood. Thus, election of a proper support seems to be essential when planning the design of a smart delivery system.

Acknowledgements

Authors gratefully acknowledge the financial support from the Ministerio de Economía y Competitividad (Projects AGL2012-39597-C02-01, AGL2012-39597-C02-02 and MAT2012-38429-C04-01) and the Generalitat Valenciana (project PROMETEO/2009/016). E.P. and M.R are grateful to the Ministerio de Ciencia e Innovación for their grants (AP2008-00620, AP2010-4369). Electron Microscopy Service of the UPV is also acknowledged.

References

Argyo, C., Weiss, V., Bräuchle, C., & Bein, T. (2013). Multifunctional mesoporous silica nanoparticles as a universal platform for drug delivery.*Chemistry of Materials*, *26*(1), 435-451.

Aznar, E., Martínez-Máñez, R., & Sancenón, F. (2009). Controlled release using mesoporous materials containing gate-like scaffoldings. *Expert Opinion on Drug Delivery, 6*(6), 643-655.

Baker, H., Thomsom, A. D., Feingold, S., & Frank, O. (1969). Role of the jejunum in the absorption of folic acid and its polyglutamates. *The American journal of clinical nutrition*, *22*(2), 124-132.

Beck, J. S., Vartuli, J. C., Roth, W. J., Leonowicz, M. E., Kresge, C. T., Schmitt, K. D., Chu, C. T. W., Olson, D. H., & Sheppard, E. W. (1992). A new family of mesoporous molecular sieves prepared with liquid crystal templates. *Journal of the American Chemical Society*, *114*(27), 10834-10843.

Bernardos, A., Aznar, E., Coll, C., Martínez-Mañez, R., Barat, J. M., Marcos, M. D., Sancenón, F., Benito, A., & Soto, J. (2008). Controlled release of vitamin B2 using mesoporous materials functionalized with amine-bearing gate-like scaffoldings. *Journal of Controlled Release*, *131*(3), 181-189.

Bhattacharyya, S., Wang, H., & Ducheyne, P. (2012). Polymer-coated mesoporous silica nanoparticles for the controlled release of macromolecules. *Acta Biomaterialia*, *8*(9), 3429-3435.

Casasús, R., Climent, E., Marcos, M. D., Martínez-Máñez, R., Sancenón, F., Soto, J, Amorós, P., Cano, J., & Ruiz, E. (2008). Dual aperture control on pH-and anion-driven supramolecular nanoscopic hybrid gate-like ensembles. *Journal of the American Chemical Society*, *130*(6), 1903-1917.

Comes, M., Aznar, E., Moragues, M., Marcos, M. D., Martínez-Máñez, R., Sancenón, F., Soto, J., Villaescusa, L. A., Gil, L., & Amorós, P. (2009). Mesoporous hybrid materials containing nanoscopic "binding pockets" for colorimetric anion signaling in water by using displacement assays. *Chemistry-A European Journal*, *15*(36), 9024-9033.

Dash, S., Murthy, P. N., Nath, L., & Chowdhury, P. (2010). Kinetic modeling on drug release from controlled drug delivery systems. *Acta Poloniae Pharmaceutica67*(3), 217-23.

Feng, W., Zhou, X., He, C., Qiu, K., Nie, W., Chen, L., Wang, H., Mo, X., & Zhang, Y. (2013). Polyelectrolyte multilayer functionalized mesoporous silica nanoparticles for pH-responsive drug delivery: layer thickness-dependent release profiles and biocompatibility. *Journal of Materials Chemistry B*, *1*(43), 5886-5898.

Grün, M., Unger, K. K., Matsumoto, A., & Tsutsumi, K. (1999). Novel pathways for the preparation of mesoporous MCM-41 materials: control of porosity and morphology. *Microporous and Mesoporous Materials*, *27*(2), 207-216.

Guo, W., Yang, C., Cui, L., Lin, H., & Qu, F. (2013). An Enzyme-Responsive Controlled Release System of Mesoporous Silica Coated with Konjac Oligosaccharide. *Langmuir*, *30*(1), 243-249.

He, C., Yin, L., Tang, C., & Yin, C. (2012). Size-dependent absorption mechanism of polymeric nanoparticles for oral delivery of protein drugs.*Biomaterials*, *33*(33), 8569-8578.

He, Q., Zhang, Z., Gao, Y., Shi, J., & Li, Y. (2009). Intracellular Localization and Cytotoxicity of Spherical Mesoporous Silica Nano-and Microparticles. *Small*, *5*(23), 2722-2729.

Hinterberger, M., & Fischer, P. (2013). Folate and Alzheimer: when time matters. *Journal of Neural Transmission*, *120*(1), 211-224.

Huang, X., & Brazel, C. S. (2001). On the importance and mechanisms of burst release in matrix-controlled drug delivery systems. *Journal of controlled release*, *73*(2), 121-136.

Kotsopoulos, J., Kim, Y. I., & Narod, S. A. (2012). Folate and breast cancer: what about high-risk women?. *Cancer Causes & Control*, *23*(9), 1405-1420.

Lubecka-Pietruszewska, K., Kaufman-Szymczyk, A., Stefanska, B., & Fabianowska-Majewska, K. (2013). Folic acid enforces DNA methylation-mediated transcriptional silencing of PTEN, APC and RARbeta2 tumour suppressor genes in breast cancer. *Biochemical and biophysical research communications*, *430*(2), 623-628.

Mas, N., Agostini, A., Mondragón, L., Bernardos, A., Sancenón, F., Marcos, M. D., Martínez-Máñez, R,, Costero, A. M., Gil, S., Merino-Sanjuán, M., Amorós, P., Orzáez, M., & Pérez-Payá, E. (2013). Enzyme-responsive silica mesoporous supports capped with azopyridinium salts for controlled delivery applications. *Chemistry-A European Journal*, *19*(4), 1346-1356.

Mondragón, L., Mas, N., Ferragud, V., de la Torre, C., Agostini, A., Martínez-Máñez, R., Sancenón, F., Amorós, P., Pérez-Payá, E., & Orzáez, M. (2014). Enzyme-responsive intracellular-controlled release using silica mesoporous nanoparticles capped with ε-Poly-L-lysine. *Chemistry-A European Journal*, *20*(18), 5271-5281.

Hage, C. N., Jalloul, M., Sabbah, M., & Adib, S. M. (2012). Awareness and intake of folic acid for the prevention of neural tube defects among Lebanese women of childbearing age. *Maternal and Child Health Journal*, *16*(1), 258-265.

Nguyen, M. T., Indrawati, and, & Hendrickx, M. (2003). Model studies on the stability of folic acid and 5-methyltetrahydrofolic acid degradation during thermal treatment in combination with high hydrostatic pressure. *Journal of agricultural and food chemistry*, *51*(11), 3352-3357.

Pérez-Cabero, M., Hungría, A. B., Morales, J. M., Tortajada, M., Ramón, D., Moragues, A., El Haskouri, J., Beltrán, A., Beltrán, D., & Amorós, P. (2012). Interconnected mesopores and high accessibility in UVM-7-like silicas. *Journal of Nanoparticle Research*, *14*(8), 1-12.

Pérez-Esteve, É., Fuentes, A., Coll, C., Acosta, C., Bernardos, A., Amorós, P., Marcos, M. D., Sancenón, F., Martínez-Máñez, R., & Barat, J. M. (2015). Modulation of folic acid bioaccessibility by encapsulation in pH-responsive gated mesoporous silica particles. *Microporous and Mesoporous Materials*, *202*, 124-132.

Pérez-Esteve, E., Oliver, L., García, L., Nieuwland, M., de Jongh, H. H., Martínez-Máñez, R., & Barat, J. M. (2014). Incorporation of mesoporous silica particles in gelatine gels: Effect of particle type and surface modification on physical properties. *Langmuir*, *30*(23), 6970-6979.

Radhakrishnan, K., Gupta, S., Gnanadhas, D. P., Ramamurthy, P. C., Chakravortty, D., & Raichur, A. M. (2014). Protamine-Capped Mesoporous Silica Nanoparticles for Biologically Triggered Drug Release. *Particle & Particle Systems Characterization*, *31*(4), 449-458.

Tang, F., Li, L., & Chen, D. (2012). Mesoporous silica nanoparticles: synthesis, biocompatibility and drug delivery. *Advanced Materials*, *24*(12), 1504-1534.

Thielemann, J. P., Girgsdies, F., Schlögl, R., & Hess, C. (2011). Pore structure and surface area of silica SBA-15: influence of washing and scale-up. *Beilstein journal of nanotechnology*, *2*(1), 110-118.

Wang, S. G., Wu, C. W., Chen, K., & Lin, V. S. Y. (2009). Fine-Tuning Mesochannel Orientation of Organically Functionalized Mesoporous Silica Nanoparticles. *Chemistry-An Asian Journal*, *4*(5), 658-661.

Wright, A. J., Dainty, J. R., & Finglas, P. M. (2007). Folic acid metabolism in human subjects revisited: potential implications for proposed mandatory folic acid fortification in the UK. *British Journal of Nutrition*, *98*(04), 667-675.

Yuan, L., Tang, Q., Yang, D., Zhang, J. Z., Zhang, F., & Hu, J. (2011). Preparation of pH-responsive mesoporous silica nanoparticles and their application in controlled drug delivery. *The Journal of Physical Chemistry C*,*115*(20), 9926-9932.

Zhao, D., Huo, Q., Feng, J., Chmelka, B. F., & Stucky, G. D. (1998). Nonionic triblock and star diblock copolymer and oligomeric surfactant syntheses of highly ordered, hydrothermally stable, mesoporous silica structures. *Journal of the American Chemical Society*, *120*(24), 6024-6036.

Zhou, C., & Garcia-Bennett, A. E. (2010). Release of folic acid in mesoporous NFM-1 silica. *Journal of nanoscience and nanotechnology*, *10*(11), 7398-7401.

Zhu, Y., Shi, J., Shen, W., Chen, H., Dong, X., & Ruan, M. (2005). Preparation of novel hollow mesoporous silica spheres and their sustained-release property. *Nanotechnology*, *16*(11), 2633.

4.1.3 Stability of different mesoporous silica particles during an in vitro digestion

Édgar Pérez-Esteve[a*], María Ruiz-Rico[a], Cristina de la Torre[b,c], Empar Llorca[d], Félix Sancenón[b,c], María D. Marcos[b,c], Pedro Amorós[e], Ramón Martínez-Máñez[b,c,], José Manuel Barat[a]

[a]Grupo de Investigación e Innovación Alimentaria, Universitat Politècnica de València. Camino de Vera s/n, 46022, Spain
[b]Centro de Reconocimiento Molecular y Desarrollo Tecnológico (IDM), Unidad Mixta Universitat Politècnica de València - Universidad de Valencia. Departamento de Química Universitat Politècnica de València, Camino de Vera s/n, 46022, Valencia, Spain
[c]CIBER de Bioingeniería, Biomateriales y Nanomedicina (CIBER-BBN)
[d]Grupo de Microestructura y Química de Alimentos. Departamento de Tecnología de Alimentos, Universitat Politècnica de València. Camino de Vera s/n, 46022, Valencia, Spain
[e]Institut de Ciència dels Materials (ICMUV), Universitat de València, P.O. Box 2085, 46071, Valencia, Spain

Submitted to Langmuir

Abstract

Mesoporous silica materials have the ability to entrap drugs, nutrients and functional biomolecules creating smart delivery systems capable to control and target the release of their cargo in a particular part of the gastrointestinal tract when administrated orally. The aptness of these encapsulation supports in *in vivo* oral controlled release relies on their chemical stability through the whole digestive tube. In this study, we evaluate the stability of four different mesoporous silica particles frequently used as encapsulating support during an *in vitro* digestion process comprising buccal, stomach and intestinal phases. Results showed that after 4 h of digestion, the textural properties of silica supports based on nanoparticles (MCM-41 nanoparticles and UVM-7) were lost in varying degrees. Porous structure of silica supports based in microparticles (MCM-41 microparticles and SBA-15) endure better the digestion process. Moreover, the protective effect of surface functionalization with *N*[1]-(3-trimethoxysilylpropyl)diethylenetriamine, an organic moiety commonly used in the preparation of pH-responsive mesoporous silica particles, improved the stability of the supports. In this manner, the same process that allows obtaining gated silica particles for controlled release purposes improves the stability of the inorganic supports during a human digestion process.

Keywords: mesoporous silica particles, *in vitro* digestion, stability, amine-functionalization

1. Introduction

Mesoporous Silica Particles (MSPs) are receiving great attention in the field of oral controlled release due to their capability for improving drug solubility and stability in the gastrointestinal tract, as well as to release the cargo along the time (sustained controlled release) specific places of the gastrointestinal tract (GIT) (targeted controlled release) (Agostini *et al*., 2012; Popat *et al.*, 2012). These reported features that render MSPs unique smart delivery systems are due to their large loading capacity (Coll *et al*., 2011), low toxicity (Suh *et al.*, 2009) and the fact that their surface can be functionalized with molecular/supramolecular ensembles. This last feature allows the development of gated-MSPs showing "zero delivery", and capability of releasing their cargo on-command in response to specifically designated external stimuli (Mondragón *et al.*, 2014).

Drug delivery/formulation technologies that can improve bioavailability, drug stability and subsequently increase drug effectiveness are much desired in the pharmaceutical sciences. In food technology, encapsulation of bioactive molecules (e.g. vitamins, antioxidants, phytochemicals, etc.) may improve their biological stability, facilitate components handling, mask unpleasant sensorial properties and modulate the bioaccessibility of the molecule of interest along the GIT (Pérez-Esteve *et al.*, 2015).

Besides a high loading capacity, controlled release and biocompatibility, the suitability of these MSPs in oral controlled release in *in vivo* applications depend on the chemical stability of the supports though the whole digestive tube. However, it is known that, due to the metastability of MSPs, silica can be biodegraded into silicic acids, including monomeric silicic acid and various polysilicic acids with different polymerization degrees, under harsh environments provoking a collapse of the porous structures (He *et al.*, 2009). In this line, Cauda, Schlossbauer & Bein (2010) studied the biodegradation of colloidal mesoporous silica nanoparticles (50 nm) in simulated body fluid of bare, globally functionalized, and surface poly(ethylene glycol)-coated colloidal mesoporous

silica nanoparticles in simulated body fluid (pH 7.4) for a period of 1 month at 37 °C. After this month, the textural properties of the mesoporous system were lost and pores were blocked because the precipitation of inorganic components from the simulated body solution. Particles stability increased by surface functionalization with poly(ethylene glycol). The degradation behaviour of surfactant-extracted mesoporous silica in simulated body fluid was also evaluated by He and co-workers (He *et al*., 2010), who proposed a three-stage degradation process comprising a fast bulk degradation on an hour-scale, a silicon concentration decrease stage due to the deposition of calcium/magnesium silicate layer, and a later continuous sustained diffusion over a period of days. The same year, Lin, Abadeer & Haynes (2011), evaluated the stability of small mesoporous silica nanoparticles (<50 nm) functionalised with poly(ethylene glycol) in H_2O, phosphate buffer solution (PBS) (pH 7.5), and Dulbecco's modified Eagle's medium (DMEM) with 10% fetal bovine serum (FBS) (pH ca. 7.5). These particles exhibited long term stability in all these media at both, room and physiological temperature. In a different attempt, El Mourabit *et al.* (2012) studied the stability of mesoporous silica under acidic conditions. In their work, the loss of textural properties of silicas under acid solutions was observed. However, it was stated that the degradation rate depends of the nature of the acidic media (phosphoric acid have stronger impact than hydrochloric or sulphuric) and also the type of silica.

Most of these studies evaluated the stability of mesoporous silica nanoparticles. However, MSPs can be fabricated with a controlled size from 50 nm to a few microns. When preparing smart delivery systems based on MSPs, particle size is very important since it conditions the distribution and behaviour of particles in living systems. In general, small MSPs can cross epitheliums and can be distributed in the body to be non-specifically internalized by certain cells (Arcos & Vallet-Regí, 2013). In contrary, oversized particles (microparticles) cannot easily cross physical membranes in the body, and thus large particle sizes are preferred for developing orally administrated controlled release devices (Pérez-Esteve *et al*., 2016). Having in mind the importance of particle size in oral administration,

studies of stability of mesoporous silica particles should also be done with particles in the micro size. However, as far as we know, the stability of large MSPs has not yet been studied. Moreover, there are no available studies about the effect of saliva (pH 7.5), gastric (pH 1.2-2), or intestinal fluids (pH 7.8-8) on the stability of the small and large MSPs. Thus, notwithstanding these works a lack of information about the degradability/stability of MSPs with different sizes during a whole digestion is still unavailable.

The aim of this study was to evaluate the stability of different bare and functionalised mesoporous silica particles differing in particle size, particle shape and pore structure (pore size and wall thickness) during a simulated *in vitro* digestion. With this purpose, a detailed evaluation of the stability of textural properties of MSPs during the *in vitro* digestion has been performed. Descriptive studies were completed with the assessment of potential cytotoxicity of digested particles or their degradation products.

2. Materials and methods

2.1 Chemicals

Tetraethylorthosilicate (TEOS), *N*-cetyltrimethylammonium bromide (CTABr), Pluronic P123 (P123), triethanolamine ($TEAH_3$), sodium hydroxide (NaOH), hydrochloric acid (HCl), N^1-(3-trimethoxysilylpropyl)diethylenetriamine (N3), and all chemicals for the digestive fluids were provided by Sigma-Aldrich (Poole, Dorset, UK). HPLC grade acetonitrile was provided by Scharlau (Barcelona, Spain). Rhodamine B was acquired from Fluka (Missouri, USA).

For cell culture experiments, trypan blue solution (0.4%) cell culture grade and dimethyl sulfoxide (DMSO), phosphate buffered saline (PBS) and Dulbecco's Modified Eagle's medium (DMEM) with glucose, L-glutamine and pyruvate for cell culture were provided by Sigma-Aldrich (Poole, Dorset, UK). Mc Coy's 5a Medium and Keratinocyte Serum Free Medium, Fetal Bovine Serum (FBS) and trypsin were purchased from Gibco (Life Technologies, Madrid, Spain). Cell proliferation reagent WST-1 was purchased from Roche Applied Science (Barcelona, Spain).

2.2 Mesoporous silica particles synthesis

Synthesis of microparticulated MCM-41 (**M**) was carried out following the so-called "atrane route", using CTABr as the structure-directing agent and a molar ratio fixed to $7TEAH_3$:2TEOS:0.52CTABr:0.5NaOH:$180H_2O$. The procedure consisted in adding CTABr to a solution of $TEAH_3$ and NaOH containing TEOS at 118 °C. After dissolving CTABr in the liquor, water was slowly added with vigorous stirring at 70 °C to form a white suspension. This mixture was aged at room temperature overnight (Bernardos *et al*., 2008).

Nanoparticulate MCM-41 (**N**) was synthesized using the following procedure: NaOH was added to the CTABr solution, followed by adjusting the solution temperature to 95 °C. TEOS was then added dropwise to the surfactant solution. The mixture was allowed to stir for 3 h to give a white precipitate (Bernardos *et al.*, 2010).

UVM-7 (**U**) was synthesised using, once again, the "atrane route". The molar ratio of the reagents in the mother liquor was fixed at $7TEAH_3$:2TEOS:0.52CTABr:$180H_2O$. The TEOS/$TEAH_3$ mixture was heated to 120 °C until no elimination of ethanol was observed. The mixture was cooled to 90 °C and the CTABr was added gradually in small portions, followed by water. The mixture was aged for 24 h (Comes *et al.*, 2009).

The SBA-15 (**S**) sample was synthesized using P123 as the structure-directing agent with the reactant molar ratios: 0.017P123:1.0TEOS:6HCl:$196H_2O$. The preparation was carried mixing an aqueous solution of P123 with HCl solution, and stirring for 2 h, after which the silica source, TEOS, was added. This final mixture was stirred for a further 20 h (Zhao *et al.*, 1998).

After the synthesis, the different solids were recovered, washed with deionised water, and air-dried at room temperature. The as-synthesized solids were calcined at 550 °C using an oxidant atmosphere for 5 h in order to remove the template phase.

The surface of the four types of particles was functionalised with N^1-(3-trimethoxysilylpropyl)diethylenetriamine (N3) according to the procedure described by Pérez-Esteve *et al.* (2014). Concretely, 1 g of the different MSPs were suspended in 40 mL of acetonitrile and an excess of N3 (4.3 mL, 15.0 mol g^{-1}) was then added. Final mixtures were stirred for 5.5 h at room temperature. Finally, the solids were filtered off, washed with 30 mL of deionised water, and dried at room temperature.

2.3 Simulated digestion procedure

An *in vitro* digestion model consisting of mouth, gastric and intestinal phases described by Versantvoort *et al.* (2005) was used to simulate the typical chemical composition, pH and residence time periods of each of the three main compartments of the GIT. A schematic representation of the *in vitro* digestion model is presented in **Figure 1**. The pH values of the digestive juices were checked and, if necessary, adjusted to the appropriate interval with NaOH (1 M) or HCl (37% w/w).

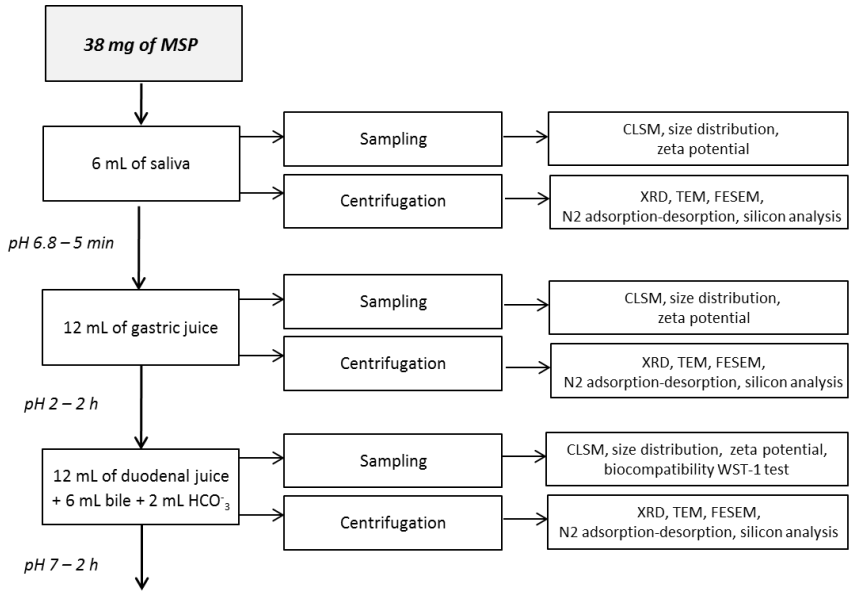

Figure 1. Schematic representation of the *in vitro* digestion process. The *in vitro* digestion model describes a three-step procedure simulating the digestive processes in mouth, stomach and small intestine. In each compartment, the matrix is incubated at 37 °C for a time relevant for the compartment. The digestion is initiated by addition of artificial saliva to the material. Subsequently, gastric juices and intestinal fluids are added to simulate the digestive processes in stomach and small intestine, respectively. See composition of the fluids in appendix 3 (page 257).

2.4 Mesoporous silica particles characterization

All materials, as synthetized and after suffering a simulated digestion process, were characterized by standard procedures: X-ray diffraction (XRD), N_2 adsorption-desorption isotherms, transmission electron microscopy (TEM), field emission scanning electron microscopy (FESEM), confocal laser scanning microscopy (CLSM), particle size distribution and zeta potential measurements.

XRD were performed on a Bruker D8 Advance diffractometer (Bruker, Coventry, UK) using CuKα radiation. N_2 adsorption-desorption isotherms were recorded with a Micromeritics ASAP 2010 automated sorption analyser (Micromeritics Instrument Corporation, Norcross, USA). The samples were degassed at 120 °C in vacuum overnight. The specific surface areas were calculated from the adsorption data in the low pressure range using the BET model. Pore size was determined following the BJH method.

The effect of digestion on single particle surface and morphology was evaluated through electron microscopy observations. TEM images were obtained with a JEOL JEM-1010 (JEOL Europe SAS, Croissy-sur-Seine, France). FESEM images were acquired with a Zeiss Ultra 55 (Carl Zeiss NTS GmbH, Oberkochen, Germany***)*** and observed in the secondary electron mode.

To determine the changes of MSPs structures and aggregation state along the whole *in vitro* digestion procedure, confocal laser scanning microscopy (CLSM) micrographs were taken. Three aliquots were taken from the digestion solution at 5 min, 2 and 4 h, just after finishing the mouth, stomach and intestine steps respectively. Samples were stained with 20 µL of rhodamine B solution (2 g L^{-1}). The observations were made 10 min after the dyes were added. Pictures were acquired using a Nikon Eclipse E800 microscope (Nikon, Tokyo, Japan). An Ar laser line (488 nm) was used to excite the rhodamine B. The images were obtained and stored at a 1,024 × 1,024-pixel resolution using the microscope software (EZ-C1 v.3.40, Nikon, Tokyo, Japan).

Microscopic studies were completed by determining the particle size distribution, and surface charge at the interface of different MSPs during the *in vitro* digestion process. To avoid interference of organic components (sugars, enzymes, etc.) in measured values, digestive fluids addressed for determination of size distribution and zeta potential were prepared with only the inorganic components (Peters *et al*., 2012). The size distribution of MSPs in each of the digestion steps (mouth, stomach and intestine) was measured with a Malvern Mastersizer 2000 (Malvern Instruments, Malvern, UK). For data evaluation, an optical model based on the Mie theory was created using the instrumental software assuming 1.45 as the real and 0 as the imaginary part of the refractive index of the particles. The surface charge at the interface of the MSPs or zeta potential (ζ) after each of the *in vitro* digestion steps, was measured at 25 °C in a Zetasizer Nano ZS equipment (Malvern Instruments, Malvern, UK). The zeta potential was calculated from the particle mobility values by applying the Smoluchowski model. The average of five recordings was reported as zeta potential. The measurements were performed at 25 °C. Zeta potential distributions were obtained by averaging 3 measurements.

2.5 Quantification of silicon content in digestion fluids

For determination of the free silicon generated during the digestion process samples, digestion juices were centrifuged (9500 rpm; 10 min) to separate digested MSPs from the aqueous solution. The degraded silicon concentration in the supernatant was determined by inductively coupled plasma optical emission spectrometry (ICP-OES) using a Horiba Jobin Yvon ULTIMA 2 spectrometer (Longjumeau, France). Before the analysis the recovered supernatants were chemically digested with nitric acid under reflux.

2.6 WST-1 Cell viability Assays

HeLa human cervix adenocarcinoma and HEPG2 human liver carcinoma were grown in DMEM supplemented with 10% FBS. HCT116 human colon carcinoma cells were grown in McCoy's 5a Medium Modified supplemented with 10% FBS and HK2 homo sapiens kidney papilloma cells were grown in Keratinocyte Serum Free Medium supplemented with bovine pituitary extract (BPE) and human recombinant epidermal growth factor (EGF). All of these cells were purchased from the German Resource Centre for Biological Materials (DSMZ). Cells were maintained at 37 °C in an atmosphere of 5% carbon dioxide and 95% air and underwent passage twice a week.

Cells were placed in 96-well plates at a density of 1000 cells per well. After 24 h, plates were incubated with the digestion fluids containing MSPs at different concentrations at 37 °C for 24 h. After removing the digestive medium containing the MSPs, MTT solution (200 mL, 1 mg mL^{-1}) was added and the cells were incubated for another 3 h. Upon removal of the MTT solution, the purple formazan crystals were solubilized with DMSO (200 mL) and measured at 560 nm on a microplate reader (SPECTRAmax plus, Molecular Devices, Sunnyvale, CA). The cytotoxicity was expressed as the percentage of cell viability.

3. Results and discussion

3.1 Preparation and characterization of the mesoporous silica supports

Four different mesoporous silica particles differing in size, shape, and pore structure were prepared following the procedures described by previous reports. **M** are porous irregular-shaped particles of ca. 1 μm with 2D-hexagonal arrangement whose pore size is in the range of 2-3 nm. With the same porous structure, **N** are spherical particles of ca. 100 nm. **U** supports are porous nanoparticles organized in the form of clusters creating a bimodal system of pores (mesopores and structural micropores). Finally, **S** are elongated particles of ca. 1 μm with a well-defined hexagonal distribution of mesopores ranging from 5-15 nm (Pérez-Esteve *et al.*, 2014). These particles were used as models to evaluate the effect of human digestion on the stability of MSPs as well as to assess the cytotoxicity of digested MSPs in four different cell lines.

After the synthesis, different MSPs were characterised using standard procedures. The mesostructure of different supports was characterised by X-Ray diffraction. As expected, the four mesoporous supports exhibited the typical properties of their family of material. **Figure 2a** and **2b** show the diffractogram of micro (a) and nanoparticles (b) of MCM-41. Curves (i) for both particles display the hexagonal ordered array of the MCM-41 family characterized by the presence of four typical peaks, indexed as (1 0 0), (1 1 0), (2 0 0) and (2 1 0) Bragg reflections (Bernardos *et al.*, 2008; Bernardos *et al.*, 2010). Similarities between the two curves confirm that the change in the particle size (nano or micro) does not have any influence in the porous structure of the particles. Moreover, the functionalization of particles' surface with N3 does not modify the typical porosity of the mesoporous MCM-41 scaffold (iii), since the (1 0 0) peak is present in both cases.

Likewise, **Figures 2c** and **2d** show typical diffractograms of bare (i) and functionalized (iii) **S** and **U** (Pérez-Esteve *et al.*, 2016). On the one hand, **Figure 2c** shows a different reflection pattern characterised by a sharp peak at 1.0 2θ, indexed as the (1 0 0) reflection, and two minor reflections in the 1.0-2.0 interval, indexed as (1 1 0) and (2 0 0) Bragg reflections, respectively. These peaks were indexed according to two-dimensional hexagonal ***p6mm*** symmetry, of a well-defined **S** mesostructure. On the other hand, **Figure 2d** presents two broad low-angle reflections that could be related with a disordered hexagonal array of the mesopores in this **U** support. Again, the presence of at least the (1 0 0) reflection peak in (iii) curves confirm that the functionalization process does not have any influence in the porous structure.

Characterization of textural properties was complemented by performing N_2 adsorption-desorption isotherms. **Table 1** list BET specific surface values, pore volumes, and pore sizes of the particles object of study. As observed, before the digestion process, all the synthetized bare particles exhibited large pore volumes and large surface area provided by the channels that cross the particles.

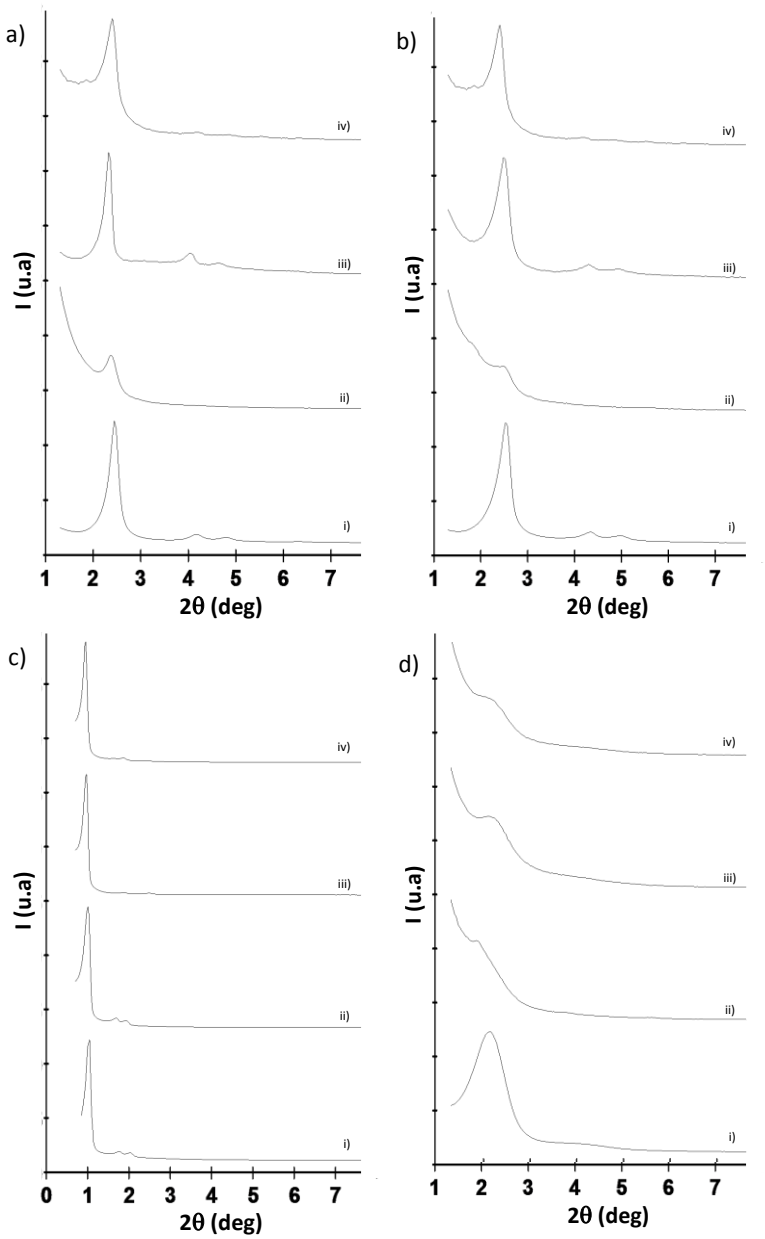

Figure 2. Powder X-ray patterns of as-synthesised MSPs before (i) and after the *in vitro* digestion (ii) as well as amine-functionalised MSPs before (iii) and after (iv) the *in vitro* digestion. MCM-41 microparticles (a), MCM-41 nanoparticles (b), SBA-15 (c) y UVM-7 (d) supports.

Table 1. BET specific surface values, pore volumes and pore sizes calculated from the N_2 adsorption-desorption isotherms for selected materials. MCM-41 micro (M), MCM-41 nano (N), SBA-15 (S) and UVM-7 (U).

	Particle size	S_{BET} (m^2 g^{-1})	Pore volume[a] (cm^3 g^{-1})	Pore size[a,b] (nm)	Wall thickness[c] (nm)
M	1.1 ± 0.2	1063	0.95	2.65	2.05
N	0.09 ± 0.02	1070	0.92	2.53	1.91
S	1.2 ± 0.2	642	0.93	7.82	2.56
U	1.2 ± 0.3	981	0.72	2.62	2.22

a. Pore volumes and pore sizes are only associated with intraparticle mesopores.
b. Pore size estimated by using the BJH model applied on the adsorption branch of the isotherm.
c. Wall thickness was estimated as cell parameter taken from the XRD minus pore size.

3.2 Effect of in vitro digestion in microstructure of bare particles

To test the effect of human digestion on bare MSPs stability, different as-synthesised particles followed a typical *in vitro* digestion procedure (**Figure 1**). After the digestion process, particles were washed with water, recovered by centrifugation and characterized by XRD, TEM, FESEM, and N_2 adsorption-desorption isotherms.

The XRD diffractogram (**Fig 2**) revealed a loss of the order in all bare digested particles (ii) characterized by a decreased intensity of (1 0 0) Bragg reflexion and a loss of almost the rest of reflexions when compared with undigested ones (i). According to the loss of intensity, the particle that exhibited a more pronounced one was **N** (wall thickness = 1.91), closely followed by **M** (wall thickness = 2.05) and **U** (wall thickness = 2.22). The differences in wall thickness among **N** (less than 2 nm) and **M** and **U** (more than 2 nm) might be due to the synthesis route. **N** and **U** follow the atrane route of synthesis, a procedure that provides wide framework walls.

For its part, **S** with a wall thickness of 2.56 nm seemed to be the particle that better conserve the hexagonal structure of the particle. In fact, diffractogram of digested **S** was very similar than that of the undigested particle meaning that mesoporous arrangement is preserved during the whole *in vitro* digestion procedure.

Nitrogen sorption data (**Fig 3**) show a reduction of the adsorbed N_2 volume in all the solids, what means that the digestion procedure provokes a loss of specific surface area and porous volume. This reduction is more marked in the case of **N** and **U** that in **M** and **S** in consonance with XRD patterns. This loss of total surface area and pore volume as a consequence of the contact with biological media has also been observed by other authors (Cauda *et al.*, 2010; El Mourabit *et al.*, 2012). In these works, the loss of textural properties of silicas is associated with a progressive elimination of the porosity by dissolution of the silica, with a pore blockage by precipitation of inorganic compounds onto the surface of the porous silica or with their combination.

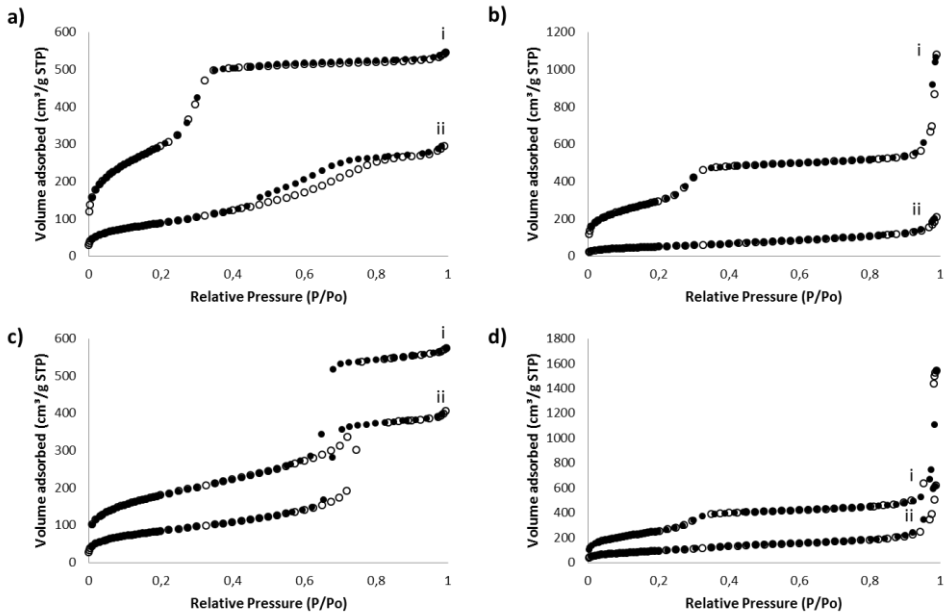

Figure 3. Nitrogen adsorption-desorption isotherms for microparticulate MCM-41 (a), nanoparticulate MCM-41 (b), SBA-15 (c) and UVM-7 (d) before (i) and after (ii) the *in vitro* digestion procedure.

To further understand which of these mechanisms are involved in the digestion-induced silica degradation, in parallel with XRD and N_2 absorption-desorption isotherms experiments, TEM and FESEM observations of the four silica supports were carried out. **Figure 4** shows FESEM and TEM pictures of different bare particles before and after the *in vitro* digestion process. This figure allows observation of not only the particle size and shape of the single particle, but also particle porosity.

After the digestion, two particles did not change their appearance (FESEM) and pore integrity (TEM). These particles are **M** and **S**, those with single particle size in the microscale. This implies that for these particles the loss of order observed in XRD was not provoked by a collapse of the mesostructure, but probably by the formation of a small volume fraction of "gel" consisting mostly of $(SiOH_2)_n$ (El Mourabit *et al.*, 2012) or the adsorption of calcium and phosphate ions present in the digestion fluids on the silica surface forming a hydroxyapatite phase (Ohtsuki, Kokubo & Yamamuro, 1992; Cho *et al*., 1998; Radim, Falaize, Lee & Ducheyne, 2002; Cauda *et al*., 2010).

In contrast, supports based on nanoparticulated materials, **N** and **U** biodegraded with a modification of the appearance of both, surface and pore structure, as a consequence of the digestion procedure. The most affected supports were **N**. After the whole digestion process, these particles lost the uniformity of pore structure (TEM) and despite keeping their particle size and shape, altered the structure of its surface (FESEM). In those cases, besides the pore closure provoked by the apparition of new phases, the decrease of the mesostructure observed by XRD and N_2 adsorption-desorption isotherms was originated by pore collapse.

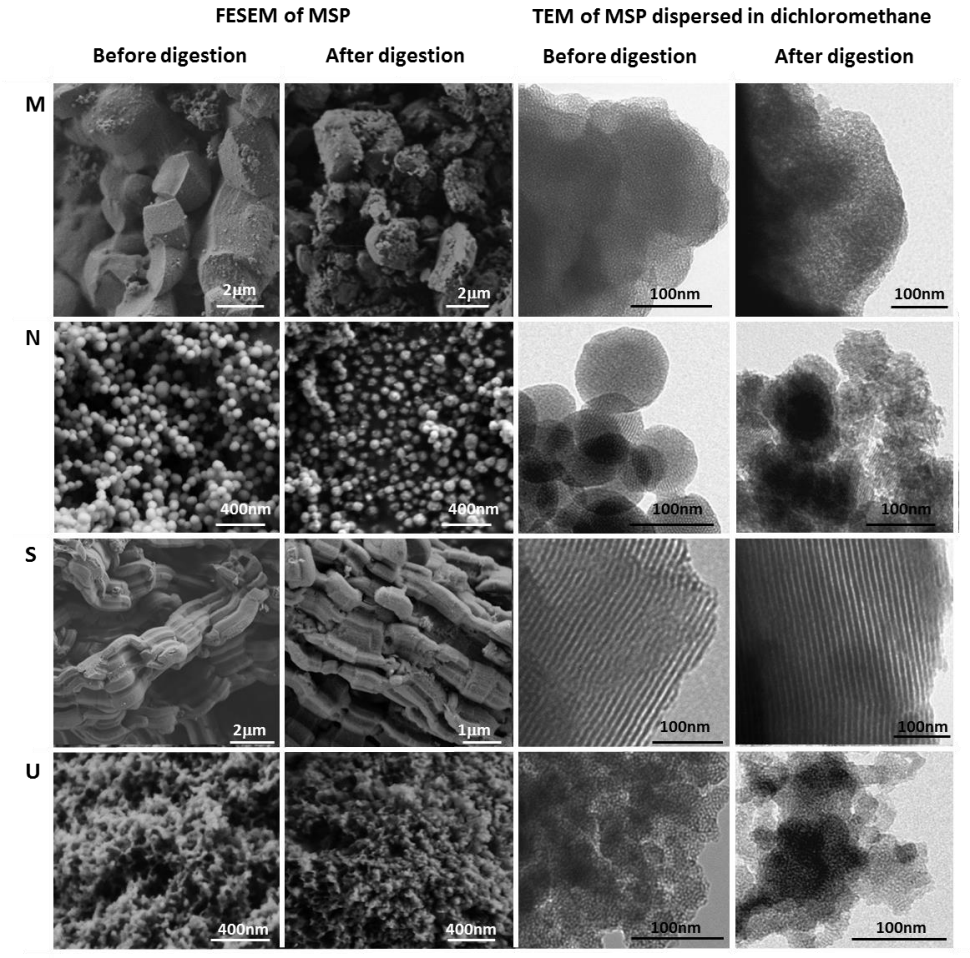

Figure 4. Characterization of particle size, particle shape and pore system of bare MSPs before and after the *in vitro* digestion procedure (IDP). MCM-41 (M), MCM-41 nano (N) SBA-15 (S) and UVM-7 (U).

Having in mind these results, it is stated that all the studied MSPs are altered as a consequence of the *in vitro* digestion process. However, the degradation degree depends on the type and size of the particles. In this context, El Mourabit *et al.* (2012) studied the structure alteration of several porous silica differing in particle size, particle shape, pore-size distribution, specific surface area, pore volume and average of pore diameter caused by immersion in acid solutions and found that the degradation of the supports was not obviously influenced by textural properties of the particles. Nevertheless, in our study, it seems to be clear that particle size and wall thickness seem to be the characteristics that condition the degradation.

In order to correlate the impact of each of the phases of the digestion with the steps of the particle's degradation, a further experiment was done. For this detailed experiment MCM-41 nanoparticles were selected given that it was the most affected support by the whole digestion process. For this purpose, **N** was put in contact with water over 4 h. In parallel, a typical *in vitro* digestion process (4 h) was performed. After each of these steps, samples were washed and observed with TEM. **Figure 5** shows TEM micrographs of **N** after 4 h in contact with water (a) and after each of the phases of the *in vitro* digestion process: buccal (b), gastric (c) and intestinal (d). As observed, particle size (ca. 100 nm) did not vary during the digestion suggesting that particle structure remains unaltered after the whole digestion process. Moreover, surface and porosity of MCM-41 remained unchanged after 4 h in water, meaning that particles do not collapse easily in water solution. Particles are also intact after the 5 min of contact with simulated saliva. However, particles change dramatically their conformation after the 2 h of gastric phase. Concretely, after this digestion step, particles lose their clearly spherical shape and ordered porous conformation and become irregular shaped spheres with disordered porosity. Little differences among particles observed after gastric and after both, gastric and intestinal phases are shown. Therefore, it is thought that once the digestive solution is neutralized by the addition of intestinal juices, the degradation process is stopped.

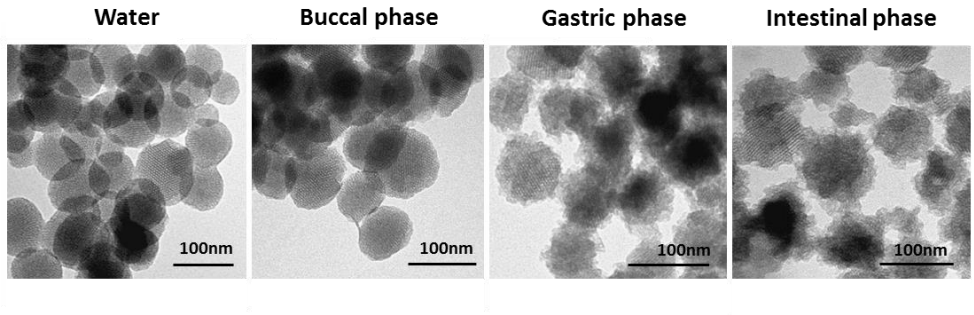

Figure 5. TEM images showing particle size, particle shape and pore system of bare MCM-41 nanopaticles after 4 h in water, and buccal, gastric and intestinal phases of the *in vitro* digestion procedure.

These findings confirm that gastric phase (pH 2) is the responsible for particle's degradation. The role of acids in porous silica degradation has previously been described (El Mourabit *et al*., 2012). These authors realised that protons play a role in the acidic alteration process of the silica. Moreover, they pointed out that in acidic conditions, anions (i.e. SO_4^{2-}, Cl^-, PO_4^{3-}) present in the media can act as nucleophilic catalyst accelerating the degradation reactions. Having in mind the composition of the two fluids comprising gastric phase of the digestion (i.e. saliva and gastric juice) it can be stated that all these degradative species (i.e. $NaSO_4$, NaH_2PO_4, HCl, NaCl, KCl, $CaCl_2$ and NH_4Cl) are present.

3.3 Effect of in vitro digestion in microstructure of amine-functionalised particles

To investigate if functionalization of particles surface with organic molecules acting as molecular gates has any influence on the preservation of the structure during the *in vitro* digestion, the four particles of study were functionalised with N^1-(3-trimethoxysilylpropyl)diethylenetriamine. This polyamine is one of the most common organic molecules used to fabricate capped mesoporous silica particles able to modulate the release of payload molecules in response to pH changes (Casasús *et al.*, 2004). After functionalization, particles were subjected to digestion process described in **Figure 1**. Digested particles were washed with water, dried and characterized by XRD, TEM and FESEM.

Figure 2 shows XRD patterns of amine-functionalized particles before (ii) and after (iv) the *in vitro* digestion process. In contrast to bare particles, functionalised particles showed the same diffraction peacks before and after the digestion, which indicate a preservation of the porous structure after the digestion procedure. The structure preservation was confirmed by microscopic analysis. As can be observed in **Figure 6**, morphology, particle size and porous structure of different amine-functionalized supports is the same before and after the in vitro digestion procedure. These determinations point out the role of amines in the protection of porous silica, especially those with nanosize (**N** and **U**), during the attack by the acids and chemical species present in the digestive juices. The prevention of silica degradation after organic functionalization has also been observed by other authors. Lin *et al.* (2011) observed that degraded Si amounts from 42 nm diameter silica nanoparticles were greater than that from the equivalent pegylated nanoparticles after both 10 days in deionized water and PBS at room temperature and 37 °C. Cauda *et al.* (2010) also observed that the attachment of a poly(ethylene glycol)-layer on the outer surface of colloidal mesoporous silica stabilizes the particles by reducing the rate of degradation in simulated body fluid at 37 °C for 1 month. The preventive effect of functional groups attached to the surface of the silica supports on the degradation of porous silica could be attributed to the capability of these molecules to interfere with the corrosion caused by acids and catalytic anions as well as to prevent the adsorption of calcium/phosphate cations and the reordenation of silicon species on a new "gel" fraction on the walls of the mesoporous silica particles. In our case, amine groups attached to particle's surface are also able to locally neutralize the acidic environment created by HCl, counteracting the corrosive effect of the acid.

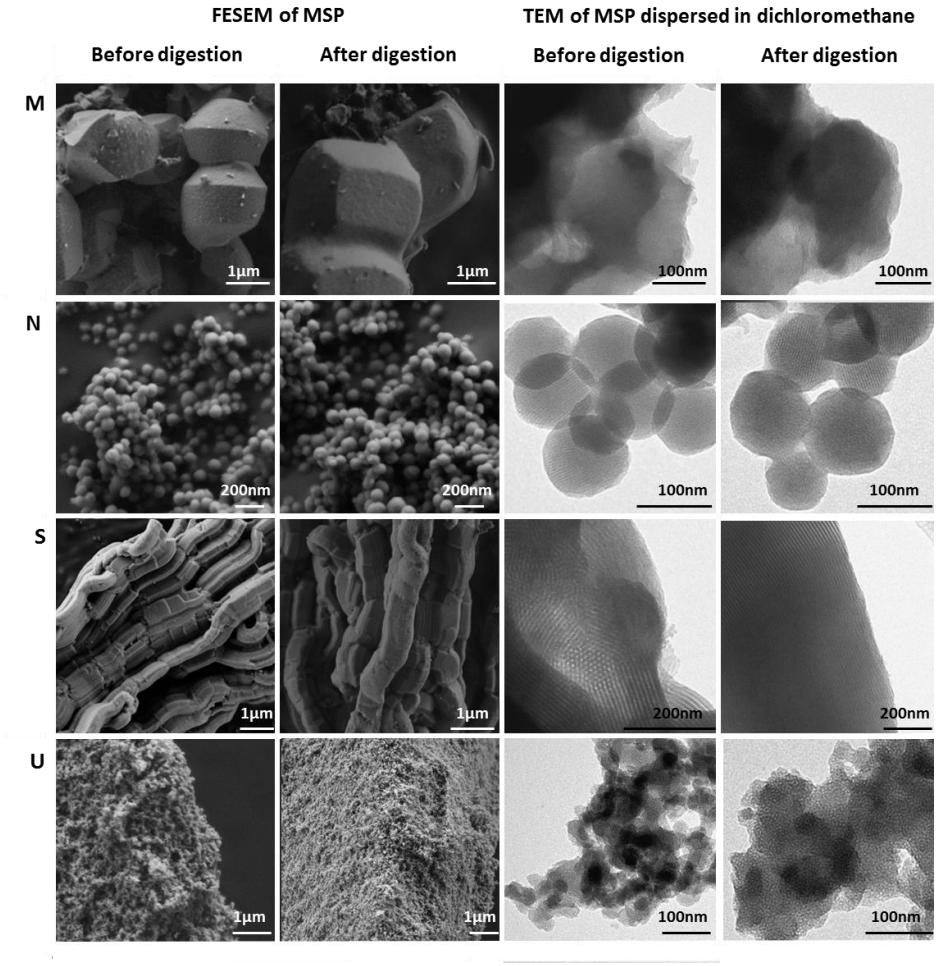

Figure 6. Characterization of particle size, particle shape and pore system of amine-functionalised MSPs before and after the *in vitro* digestion procedure. MCM-41 (M), MCM-41 nano (N) SBA-15 (S) and UVM-7 (U).

3.4 Effect of in vitro digestion in macroscopic structure

To understand the effect of each of the digestion steps on the particle size and aggregation tendency, particles were observed by CLSM in each of the artificial digestion mixtures (**Fig 7**). This analysis revealed that in water solution, all the particles tended to form aggregates. This trend to form large aggregates, especially observed in **N** and **U**, in accordance with results previously reported (Pérez-Esteve *et al.*, 2014). **Figure 7** also allows observing that for each of the particles the gastric phase provokes an enlargement of particles aggregates, and that in none of the cases digestion triggered the loss of macroscopic particle structure.

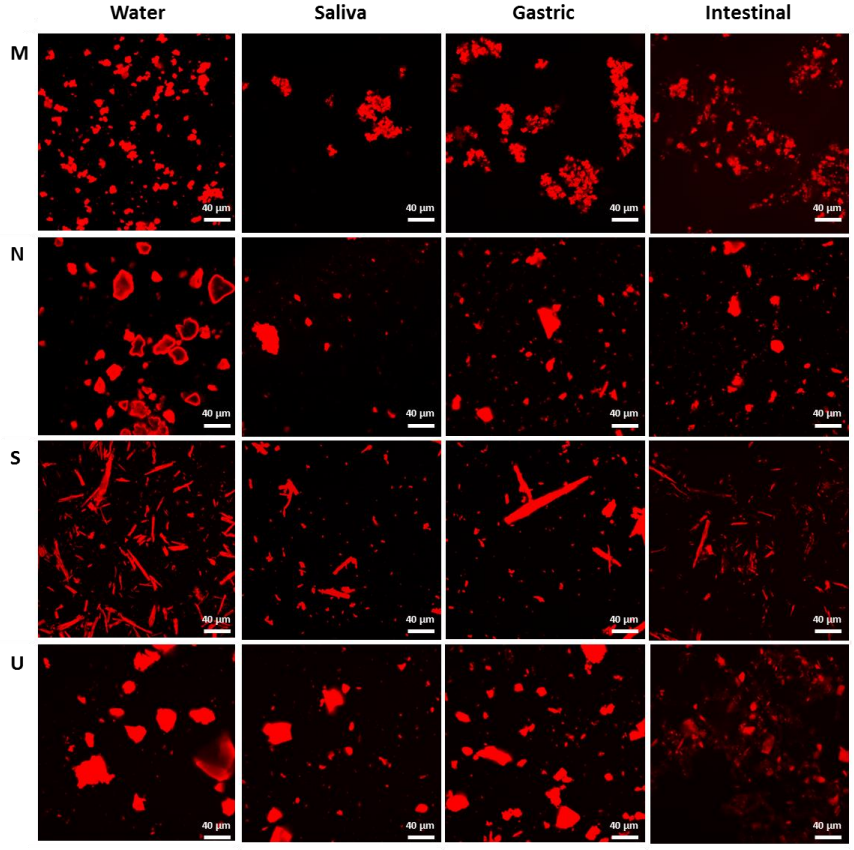

Figure 7. Characterization of particle size and particle shape of bare MSPs before and after the *in vitro* digestion procedure. MCM-41 micro (M), MCM-41 nano (N), SBA-15 (S) and UVM-7 (U).

Aggregation tendency observed in gastric phase for all the particles was confirmed by particle size distribution measurements. As shown in **Figure 8**, according to particles' grain size in different digestive media, two different groups of particles can be distinguished. On the one hand, **S** and **M** microparticles, exhibited a size distribution in the range 0.5-2 μm, while size distribution of **N** and **U** ranged from 5 up to 40 μm. Differences between single particle size and size exhibited when suspended in aqueous media suggest the formation of particle clusters.

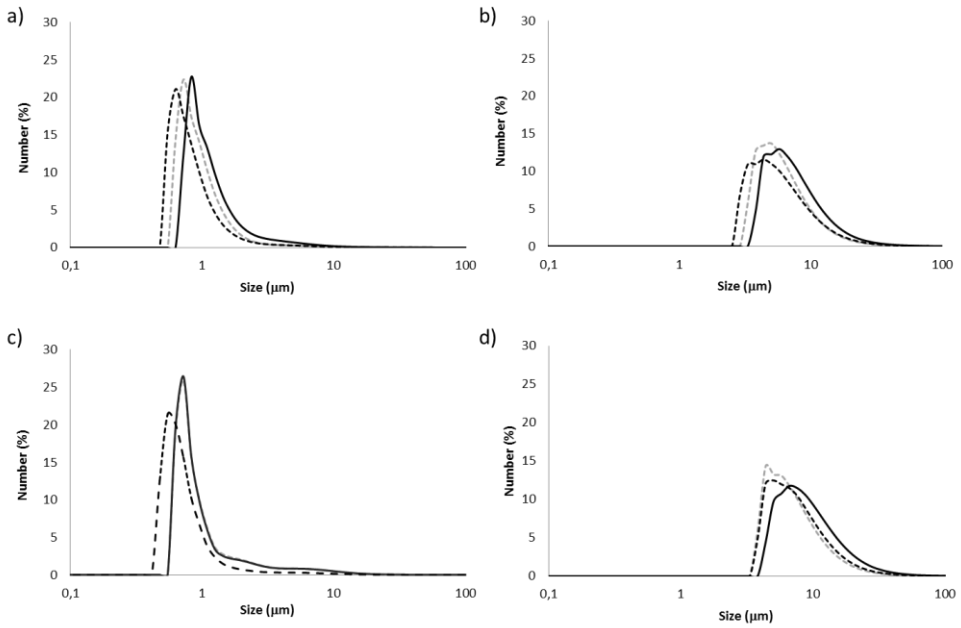

Figure 8. Hydrodynamic size distribution of MCM-41 micro (a), MCM-41 nano (b), SBA-15 (c) and UVM-7 (d) expressed as number percentage. Discontinuous gray line (buccal), continuous black line (gastric) and discontinuous black line (intestinal).

Zeta Potential analysis of particles was performed at the end of each of the three steps of the digestive process (saliva, grastric and intestinal media) to assess the influence of the digestion phase on the surface charge of the particles. As observed in **Figure 9**, particles exhibited a negative zeta potential (ca. -30 mV) in the presence of saliva (neutral pH and changed dramatically during gastric phase (ca. +10 mV) due to the protonation of silanolates at the pH of the stomach (pH 2), where silica has the isoelectric point (Kosmulski, 1998). However, after neutralization of pH in the intestinal phase, zeta potential reached negative values of ca -20 or -30 mV. Generally it is considered that particles exhibiting a zeta potential in the range from +30 to -30 mV tend to aggregate (Duman & Tunç, 2009). As expected, changes in zeta potential could be the reason for aggregation tendency in the gastric environment.

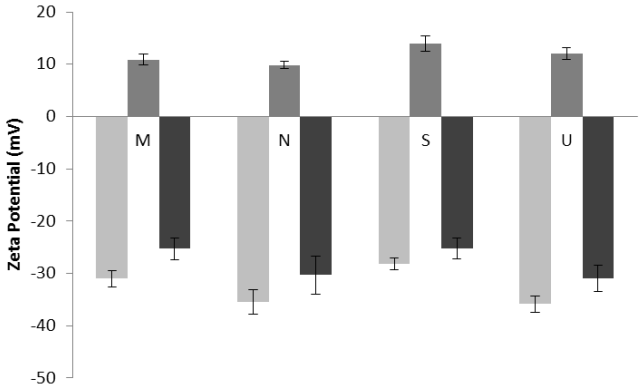

Figure 9. Zeta potential values (mean ± SD) of MSPs after oral phase (light gray), gastric phase (dark gray) and intestinal phase (black). MCM-41 micro (M), MCM-41 nano (N), SBA-15 (S) and UVM-7 (U).

3.5 Quantification of silica degradation and degree of silica network condensation

In previous sections it has been concluded that bare particles, especially **N** and **U**, lose part of their textural properties as a consequence of the *in vitro* digestion process. It was also stated by TEM and FESEM pictures that stomach phase was the responsive of the structural changes of the porous systems and the surface appearance. To better understand the degradation process it was our aim to quantify the amount of free silicic acid formed during the digestion quantified as free silicon by ICP-OES, since it is a clear indicator of silica degradation (Lin *et al.*, 2011). As observed in **Table 2**, amounts of silicon species in the digestive juice after the 4 h of digestion process was very similar for all the particles (20-25 mg Si L^{-1} of digestive fluid) and surface functionalization with polyamines did not influence this value. These amounts of free silicon are equivalent to 4-5% of the silicon present in the MSPs, depending on the support. Thus, as previously suggested, the degradation of porous structure of bare porous silica is not due to a simple dissolution of the silica provoking a collapse of the particle, but by a transformation of the silica in a new disordered phase. In addition, determination of free silicon formed in the three phases of the digestion of bare MCM-41 nanoparticles revealed that only 0.4% of the silicon was dissolved during the buccal phase of digestion. Percentage of dissolved silicon reached values of 2% in the stomach phase and continued increasing until 4% at the end of the intestinal phase.

Table 2. Free silicon formed during the *in vitro* digestion procedure (4 h) of MCM-41 microparticles (M), MCM-41 nanoparticles (N), SBA-15 (S) and UVM-7 (U).

Free silicon (mg L^{-1})	**M**	**N**	**S**	**U**
Bare	20 ± 2	19 ± 2	21 ± 2	25 ± 3
N3-functionalised	19 ± 1	22 ± 1	21 ± 1	23 ± 2

3.6 Biocompatibility of particles after the in vitro digestion

Finally, the biocompatibility of bare and functionalized particles subjected to the digestion process was tested through WST-1 test. In previous works, we have studied the cytotoxicity of the four particles object of study loaded with folic acid and functionalized with N^1-(3-trimethoxysilylpropyl)diethylenetriamine (Pérez-Esteve *et al., 2016*). The study concluded that functionalised **M**, **N**, **S** and **U** particles did not induce significant cell death upon 200 mg mL^{-1} for 24 h. However, it has been recently reported that biodegradation of silica into silicic acids including monomeric silicic acid and various polysilicic acids with different polymerization degrees could cause cytotoxicity via adsorbing and binding enzymes and substrate proteins (He et *al.*, 2009).

In previous sections, it has been demonstrated that MSPs were attacked during the digestion procedure, and that during the attack free silicon is formed. Thus, with the purpose of evaluating potential side effects of digested supports and their degradation products on human cells we aimed in this section the evaluation of the cytotoxicity of digestive fluids containing different concentrations of MSPs. To test the cytotoxicity, human colon carcinoma cells (HCT116), human liver carcinoma cells (HEPG2), human kidney epithelial cells (HK2), and human cervix carcinoma cells (HeLa) cells were chosen to test the toxicity of the products of bare and amine-functionalised **M**, **N**, **S** and **U** particles after the *in vitro* digestion procedure described above.

The results in **Figure 9** and **Figure 10** show that the viability of none of the cell lines was compromised even exposure at a relatively high particle concentration (200 mg mL^{-1}). It is considered that polysilicic acids developed during silica degradation could cause cytotoxicity via adsorbing and binding enzymes and substrate proteins. In contrast, monomeric silicic acid would not bind proteins and therefore had no cytotoxicity (He *et al.*, 2009). Having this in mind, results of this study implies that a) the formation of silicic species is very low or b) the biodegradation products of the different MSPs are mainly monomeric and oligomeric silicic acids rather than cytotoxic polysilicic acids with high polymerization degree.

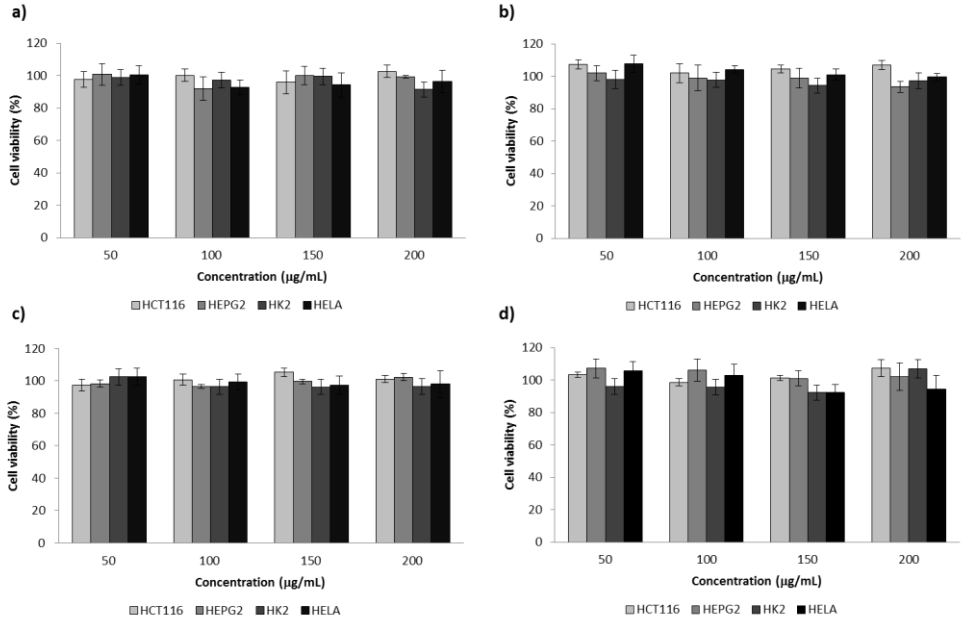

Figure 9. WST-1 cell viability assay. HCT116 (light grey), HEPG2 (medium grey), HK2 (dark grey) and HeLa (black) cells treated with digestion fluids containing bare MSPs at concentrations of 50, 100, 150 and 200 µg mL^{-1} for 24 h. Cells were incubated for 24h with optimized solids at the concentrations stated before and cell viability was quantified using the WST-1 reagent. MCM-41 microparticles (a), MCM-41 nanoparticles (b), SBA-15 (c) and UVM-7 (d).

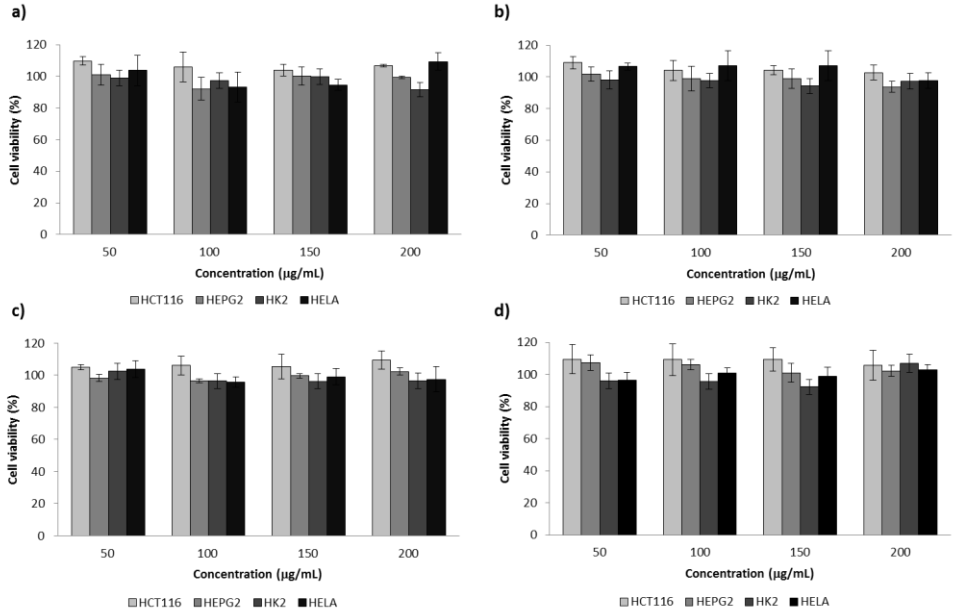

Figure 10. WST-1 cell viability assay. HCT116 (light grey), HEPG2 (medium grey), HK2 (dark grey) and HeLa (black) cells treated with digestion fluids containing amine-functionalized MSPs at concentrations of 50, 100, 150 and 200 µg mL^{-1} for 24 h. Cells were incubated for 24h with optimized solids at the concentrations stated before and cell viability was quantified using the WST-1 reagent. MCM-41 microparticles (a), MCM-41 nanoparticles (b), SBA-15 (c) and UVM-7 (d).

4. Conclusions

The present work demonstrates the effect of an *in vitro* digestion process on the stability of bare and amine-functionalized mesoporous silica particles. Results showed that bare SBA-15 and MCM-41 microparticles were very stable against degradation. However, supports based on nanoparticles (i.e. MCM-41 nanoparticulated and UVM-7) exhibited an evident degradation of its structure characterized by a loss of pore order and surface attack. In the degradation process, only ca. 5% of the silicon present in the sample was dissolved in the digestion fluids, confirming that the degradation process is not caused by the loss of matter, but in the chemical transformation of the SiO_2 in other silicic phases. This degradation was avoided by the functionalization of the external surface of the particles with N^1-(3-trimethoxysilylpropyl)diethylenetriamine. These findings

evidence the importance of particle size and surface modification on the degradation behaviour during an *in vitro* digestion process. In addition, despite the formation of free silicon during the different phases of the digestion, neither the digested particles nor the biodegradation products show any toxicity to HCT116, HEPG2 HK2 and HeLa cells. In accordance to these results, the utilization of mesoporous silica microparticles, and over all, amine-functionalized mesoporous silica microparticles in the design of oral delivery systems guarantees the chemical stability of the supports through the whole digestive tube.

Acknowledgements

Authors gratefully acknowledge the financial support from the Ministerio de Economía y Competitividad (Projects AGL2012-39597-C02-01, AGL2012-39597-C02-02 and MAT2012-38429-C04-01) and the Generalitat Valenciana (project PROMETEO/2009/016). E.P. and M.R are grateful to the Ministerio de Ciencia e Innovación for their grants (AP2008-00620, AP2010-4369). Electron Microscopy Service of the UPV is also acknowledged.

References

Agostini, A., Mondragón, L., Pascual, L., Aznar, E., Coll, C., Martínez-Máñez, R., Sancenón, F., Soto, J., Marcos, M. D., Amorós, P., Costero, A. M., Parra, M., & Gil, S. (2012). Design of enzyme-mediated controlled release systems based on silica mesoporous supports capped with ester-glycol groups. *Langmuir*, *28*(41), 14766-14776.

Arcos, D., & Vallet-Regí, M. (2013). Bioceramics for drug delivery. *Acta Materialia*, *61*(3), 890-911.

Bernardos, A., Aznar, E., Coll, C., Martínez-Mañez, R., Barat, J. M., Marcos, M. D., Sancenón, F., Benito, A., & Soto, J. (2008). Controlled release of vitamin B2 using mesoporous materials functionalized with amine-bearing gate-like scaffoldings. *Journal of Controlled Release*, *131*(3), 181-189.

Bernardos, A., Mondragon, L., Aznar, E., Marcos, M. D., Martínez-Máñez, R., Sancenón, F., Soto, J., Barat, J. M., Perez-Paya, E., Guillem, C., & Amorós, P. (2010). Enzyme-responsive intracellular controlled release using nanometric silica mesoporous supports capped with “saccharides”. *Acs Nano*, *4*(11), 6353-6368.

Casasús, R., Marcos, M. D., Martínez-Máñez, R., Ros-Lis, J. V., Soto, J., Villaescusa, L. A., Amorós, P., Beltrán, D., Guillem, C., & Latorre, J. (2004). Toward the development of ionically controlled nanoscopic molecular gates. *Journal of the American Chemical Society*, *126*(28), 8612-8613.

Cauda, V., Schlossbauer, A., & Bein, T. (2010). Bio-degradation study of colloidal mesoporous silica nanoparticles: effect of surface functionalization with organo-silanes and poly (ethylene glycol). *Microporous and Mesoporous Materials*, *132*(1), 60-71.

Cho, S. B., Miyaji, F., Kokubo, T., Nakanishi, K., Soga, N., & Nakamura, T. (1998). Apatite formation on silica gel in simulated body fluid: effects of structural modification with solvent-exchange. *Journal of Materials Science: Materials in Medicine*, *9*(5), 279-284.

Comes, M., Aznar, E., Moragues, M., Marcos, M. D., Martínez-Máñez, R., Sancenón, F., Soto, J., Villaescusa, L. A., Gil, L., & Amorós, P. (2009). Mesoporous hybrid materials containing nanoscopic "binding pockets" for colorimetric anion signaling in water by using displacement assays. *Chemistry-A European Journal*, *15*(36), 9024-9033.

Coll, C., Mondragón, L., Martínez-Máñez, R., Sancenón, F., Marcos, M. D., Soto, J., Amorós, P., & Pérez-Payá, E. (2011). Enzyme-Mediated Controlled Release Systems by Anchoring Peptide Sequences on Mesoporous Silica Supports. *Angewandte Chemie International Edition*, *50*(9), 2138-2140.

Duman, O., & Tunç, S. (2009). Electrokinetic and rheological properties of Na-bentonite in some electrolyte solutions. *Microporous and Mesoporous Materials*, *117*(1), 331-338.

He, Q., Shi, J., Zhu, M., Chen, Y., & Chen, F. (2010). The three-stage in vitro degradation behavior of mesoporous silica in simulated body fluid. *Microporous and Mesoporous Materials*, *131*(1), 314-320.

He, Q., Zhang, Z., Gao, Y., Shi, J., & Li, Y. (2009). Intracellular Localization and Cytotoxicity of Spherical Mesoporous Silica Nano-and Microparticles. *Small*, *5*(23), 2722-2729.

El Mourabit, S., Toquer, G., Cambedouzou, J., Goettmann, F., & Grandjean, A. (2012). Stability of mesoporous silica under acidic conditions. *RSC Advances, 2,* 10916-10924.

Kosmulski, M. (1998). Positive electrokinetic charge of silica in the presence of chlorides. *Journal of colloid and interface science*, *208*(2), 543-545.

Lin, Y. S., Abadeer, N., & Haynes, C. L. (2011). Stability of small mesoporous silica nanoparticles in biological media. *Chemical Communications*, *47*(1), 532-534.

Mondragón, L., Mas, N., Ferragud, V., de la Torre, C., Agostini, A., Martínez-Máñez, R., & Orzáez, M. (2014). Enzyme-Responsive Intracellular-Controlled Release Using Silica Mesoporous Nanoparticles Capped with ε-Poly-L-lysine. *Chemistry-A European Journal*, *20*(18), 5271-5281.

Ohtsuki, C., Kokubo, T., & Yamamuro, T. (1992). Mechanism of apatite formation on CaO SiO 2 P 2 O 5 glasses in a simulated body fluid. *Journal of Non-Crystalline Solids*, *143*, 84-92.

Pérez-Esteve, É., Fuentes, A., Coll, C., Acosta, C., Bernardos, A., Amorós, P., Marcos, M. D., Sancenón, F., Martínez-Máñez, R., & Barat, J. M. (2015). Modulation of folic acid bioaccessibility by encapsulation in pH-responsive gated mesoporous silica particles. *Microporous and Mesoporous Materials*, *202*, 124-132.

Pérez-Esteve, E., Oliver, L., García, L., Nieuwland, M., de Jongh, H. H., Martínez-Máñez, R., & Barat, J. M. (2014). Incorporation of mesoporous silica particles in gelatine gels: Effect of particle type and surface modification on physical properties. *Langmuir*, *30*(23), 6970-6979.

Pérez-Esteve, É., Ruiz-Rico, M., de la Torre, C., Villaescusa, L. A., Sancenón, F., Marcos, M. D., Amorós, P., Martínez-Máñez, R., & Barat, J. M. (2016). Encapsulation of folic acid in different silica porous supports: A comparative study. *Food Chemistry*, *196*, 66-75.

Peters, R., Kramer, E., Oomen, A. G., Herrera Rivera, Z. E., Oegema, G., Tromp, P. C., Fokkink, R., Rietveld, A., Marvin, H. J., Weigel, S., Peijnenburg, A. A., & Bouwmeester, H. (2012). Presence of nano-sized silica during *in vitro* digestion of foods containing silica as a food additive. *ACS nano*,*6*(3), 2441-2451.

Popat, A., Jambhrunkar, S., Zhang, J., Yang, J., Zhang, H., Meka, A., & Yu, C. (2014). Programmable drug release using bioresponsive mesoporous silica nanoparticles for site-specific oral drug delivery. *Chemical Communications*, *50*(42), 5547-5550.

Radin, S., Falaize, S., Lee, M. H., & Ducheyne, P. (2002). In vitro bioactivity and degradation behavior of silica xerogels intended as controlled release materials. *Biomaterials*, *23*(15), 3113-3122.

Suh, W. H., Suslick, K. S., Stucky, G. D., & Suh, Y. H. (2009). Nanotechnology, nanotoxicology, and neuroscience. *Progress in neurobiology*, *87*(3), 133-170.

Versantvoort, C. H., Oomen, A. G., Van de Kamp, E., Rompelberg, C. J., & Sips, A. J. (2005). Applicability of an in vitro digestion model in assessing the bioaccessibility of mycotoxins from food. *Food and Chemical Toxicology*, *43*(1), 31-40.

Zhao, D., Huo, Q., Feng, J., Chmelka, B. F., & Stucky, G. D. (1998). Nonionic triblock and star diblock copolymer and oligomeric surfactant syntheses of highly ordered, hydrothermally stable, mesoporous silica structures. *Journal*
Society, *120*(24), 6024-6036.

4.2 CHAPTER 2. TECHNOLOGICAL APPROACH

4.2.1 Incorporation of mesoporous silica particles in gelatin gels: effect of particle type and surface modification on physical properties

Édgar Pérez-Esteve[1,2], Laura Oliver[3,4], Laura García[1], Maaike Nieuwland[3,5], Harmen H. J. de Jongh[3,6], Ramón Martínez-Máñez[2,7], José Manuel Barat[1]

[1.] Grupo de Investigación e Innovación Alimentaria, Departamento de Tecnología de Alimentos, Universitat Politècnica de València, Camino de Vera s/n., 46022 Valencia, Spain

[2.] Centro de Reconocimiento Molecular y Desarrollo Tecnológico, Unidad Mixta Universitat Politècnica de València-Universitat de València, Camino de Vera s/n, 46022, Valencia, Spain

[3.] Top Institute Food & Nutrition, P.O. Box 557, 6700 AN, Wageningen, The Netherlands

[4.] NIZO Food Research B.V., P.O. Box 20, 6710 BA, Ede, The Netherlands

[5.] TNO, PO Box 360, 3700 AJ Zeist, The Netherlands

[6.] Wageningen University & Research Center, Food Physics Group, P.O. Box 17, 6700 AA Wageningen, The Netherlands

[7.] CIBER de Bioingeniería, Biomateriales y Nanomedicina (CIBER-BBN), Spain

*Langmuir, **2014,** 30(23), 6970-6979*

(Reproduced with permission of American Chemical Society)

Abstract

The aim of this work was to investigate the impact of mesoporous silica particles (MSPs) on the physicochemical properties of filled protein gels. We have studied the effect of the addition of different mesoporous silica particles, either bare or functionalised with amines or carboxylates, on the physical properties of gelatine gels (5% w/v). Texture properties of the filled gels were investigated by uniaxial compression, while optical properties were investigated by turbidity. The MSPs were characterised with the objective of correlate particle features with its impact on the corresponding filled gel properties. The addition of MSPs (both with and without functionalization) increased the stiffness of the gelatine gels. Furthermore, functionalised MSPs showed a remarkable increase in the strength of the gels and a slight reduction of the brittleness of the gels, in contrast with non-functionalised MSPs which showed no effect on these two properties. Turbidity of the gels was also affected by the addition of all tested MSPs, showing that the particles that formed smaller aggregates resulted in a higher contribution to turbidity. MSPs are promising candidates for the development of functional food containing smart delivery systems, being also able of modulating the functionality of protein gels.

Keywords: Mesoporous silica particles, smart delivery systems, gelatine, texture properties, turbidity.

1. Introduction

The design of new functional food with nutritional and/or health declarations often requires the encapsulation, controlled release, or protection of suitable bioactive agents (Weiss *et al.*, 2006). To achieve this goal, novel smart delivery systems based on emulsions (Anton *et al*., 2010), liposomes (An *et al.*, 2013), polymeric hydrogels (Chaturvedi *et al.*,, 2013) and various inorganic particles (Bernardos *et al.*, 2008; Barat *et al.*,2011) have been reported recently.

Among them, mesoporous silica particles (MSPs) have been studied as smart delivery systems in various life science fields such as medicine, nutrition, and food technology (Pérez-Esteve *et al.*,2013). Their unique properties (e.g., an ordered and uniform pore network, an adjustable pore size (from 2.0 to 50 nm), a high surface area (>700 m^2 g^{-1}) (Vallet-Regí *et al.*, 2007) and the possibility of modify their surface with organic molecules that act as bioresponsive molecular gates (Aznar *et al.*, 2009) favor the development of promising biomedical applications related to encapsulation, protection, and the controlled delivery of bioactive agents.

Different MSPs have in common that their composition is based on a SiO_2 network, a mesostructure, and the presence of silanol groups on the surface. Some differ from each other in size, shape, porous size and volume, specific surface area, and density of silanol groups on the surface providing different surface charge. Despite the fact that the most studied mesoporous silica-based material is MCM-41, (Aznar *et al*., 2009; Zhao *et al.*, 1996) both as nanoparticles (Salonen *et al*., 2005) and microparticles, (Trewyn *et al.*, 2007) other MSPs with different shapes and porous systems (e.g., SBA-15 (Rahmat *et al.*, 2010; Song *et al.*, 2005) and UVM-7 (El Haskouri *et al*., 2002, Comes *et al*., 2009)) have also been employed as molecular carriers.

MSPs possess most of the desired features for a smart delivery system designed to be incorporated into a food product, such as the capability to encapsulate a large amount of bioactive molecules, the possibility to control release within the gastrointestinal tract, (Bernardos *et al*., 2008; Song *et al*., 2005) and the ability to be highly stable and biocompatible (Asefa & Tao, 2012; Mamaeva *et al.*, 2013; Moon & Lee, 2009). However, to the best of our knowledge, there is no information in the literature about the effect of the incorporation of MSP on product appearance, texture, mouth feel, flavor, and shelf life of the final food or beverage matrixes in which they potentially could be incorporated.

One way to integrate the MSPs in food systems is to incorporate them as fillers in protein gel matrixes. The mechanical properties of emulsion filled gels or composite gels for food applications have been studied (Lorenzo & Zaritzky, 2013; Sala *et al.*, 2009a; Sala *et al.*, 2009b). These studies show that the mechanical properties of filled gels depend not only on the physicochemical characteristics of the gel matrix or the size, shape, spatial distribution, and volume fraction of the filler but also on the strength of the interaction between the filler and the gel matrix (van Vliet, 1988). Depending on the nature of this interaction, the fillers are, at the extremes, mechanically connected to the gel network and then increase the gel elastic modulus (“active”) or remain inert from the gel matrix and thereby weaken the gel by acting as a hindering steric contribution during gel formation (“inactive”) (Ring & Stainsby, 1982).

Bearing in mind the lack of information on studies on the interaction of silica mesoporous particles on (protein) gels, this article evaluates the effect of the incorporation of MSPs differing in particle size and shape and bearing different surface functionalization on the physical properties of gelatine gels, one of the most common model food systems.

2. Materials and methods

2.1 Chemicals

Porcine skin gelatine (type A, 300 bloom, average molecular weight 50-100 kDa, and isoelectric point pI = 7.0-9.0) was purchased from Sigma. For the synthesis of the mesoporous silica particles, tetraethylorthosilicate (TEOS), *N*-cetyltrimethylammonium bromide (CTABr), pluronic P123 (P123), triethanolamine (TEAH3), sodium hydroxide (NaOH), chloride acid (HCl), acetic acid, and N^1-(3-Trimethoxysilylpropyl)diethylenetriamine (N3) were provided by Sigma (Sigma-Aldrich Química S.L., Madrid, Spain), while *N*-3-(trimethoxysilyl)propyl ethylenediamine triacetic acid trisodium salt (C3) was provided by Fluorochem (Hadfield, UK).

2.2 Sample preparation

2.2.1 Mesoporous silica particles synthesis

Microparticulated MCM-41 particles (**M**) were synthesized following the so-called atrane route (Cabrera *et al.*, 2000) according to the method described by Barat *et al.* (2011). N-Cetyltrimethylammonium bromide (CTABr) was used as the structure-directing agent. The molar ratio of the reagents was fixed to 7 $TEAH_3$:2 TEOS:0.52 CTABr:0.5 NaOH:180 H_2O. CTABr was added to a solution of triethanolamine ($TEAH_3$) containing sodium hydroxide (NaOH) and tetraethylorthosilicate (TEOS) at 118 °C. After CTABr was dissolved in the solution, water was slowly added with vigorous stirring at 70 °C. After a few minutes, a white suspension was formed. This mixture was aged at room temperature overnight.

Nanoparticulated MCM-41 particles (**N**) were synthesized using the procedure described by Bernardos *et al.* (2011) The molar ratio of the reagents was fixed at 1 TEOS:0.1 CTABr:0.27 NaOH:1000 H_2O. NaOH was added to the CTABr solution, followed by adjusting the solution temperature to 95 °C. TEOS was then added dropwise to the CTABr solution. The mixture was allowed to stir for 2 h, yielding a white precipitate.

SBA-15 particles (**S**) were synthesized following the method reported by Zhao *et al.* (1998). P123 was used as the structure-directing agent. The molar ratio of the reagents was fixed at 0.017 P123:1.0 TEOS:6 HCl:196 H_2O. The preparation was performed by mixing an aqueous solution of P123 with HCl solution and stirring for 2 h, after which the silica source, TEOS, was added. This final mixture was stirred for another 20 h.

UVM-7 particles (**U**) were synthesized following the method presented by Comes *et al.* (2009) which was also based on the atrane route. The molar ratio of the reagents was fixed at 7 $TEAH_3$:2 TEOS:0.52 CTABr:180 H_2O. The TEOS/$TEAH_3$ mixture was heated to 120 °C until no elimination of ethanol was observed. The mixture was cooled to 90 °C, and CTABr was added gradually in small portions, followed by dilution with water. The mixture was aged for 24 h.

For all samples, after the synthesis, the resulting powder was recovered by centrifugation, washed with deionized water, and air dried at room temperature. To prepare the final mesoporous materials, the as-synthesized solids were calcined at 550 °C using an oxidant atmosphere for 5 h in order to remove the template phase.

2.2.2 Mesoporous silica particles functionalization

The surfaces of the four types of particles (**#**) were functionalized with *N*-(3-trimethoxysilylpropyl) diethylenetriamine (N3) or with *N*-[3-(trimethoxysilyl)propyl]ethylenediamine triacetic acid trisodium salt (C3) to add positive and negative charges, respectively. To obtain **#-N3** particles, 1 g of MSPs was suspended in 40 mL of acetonitrile, and an excess of N3 (4.3 mL, 15.0 mmol g^{-1}) was then added. To obtain **#-C3** particles, 1 g of MSPs was suspended in 30 mL of water, and an excess of C3 (5.5 mL, 15.0 mmol g^{-1}) was then added. Final mixtures were stirred for 5.5 h at room temperature. Finally, the solids were filtered off, washed with 30 mL of deionized water, and dried at room temperature.

2.2.3 Filled gelatine gels preparation

Gelatine gels containing 5% (w/w) gelatine in the aqueous phases were prepared with the four types of particles (**M**, **N**, **U**, and **S**) both bare (**#**) and functionalized with carboxylates **(#-C3**) and amines (**#-N3**) at different concentrations (0, 0.1, 0.25, 0.5, 0.75, and 1% w/w).

A stock solution of gelatine in 0.2 M acetate buffer (pH 5.5) (10% w/v) was prepared by allowing the gelatine to hydrate for 2 h under gentle stirring at room temperature. The gelatine was subsequently dissolved by holding at 60 °C for 30 min.

MSPs were dispersed, at a known volume fraction, in acetate buffer (pH 5.5) and sonicated gently to reduce particle aggregates. The required amount of the selected MSP dispersion was then mixed with the gelatine solution. For large deformation analysis, the mixture was transferred into 20 mL plastic syringes (internal diameter 20 mm) coated with a thin film of paraffin oil. For turbidity measurements, the gels were prepared in 1 cm plastic cuvettes. In both cases, the samples were left to gel and age for 22 ± 2 h at 20 °C.

2.3 Determination of particle size distribution and zeta-potential

The particle size distribution of the different bare and functionalized MSPs was determined using a Malvern Mastersizer 2000 (Malvern, UK). For the measurements, samples were dispersed in acetate buffer. Data analysis was based on the Mie theory using refractive indices of 1.33 and 1.45 for the dispersant and MSP, respectively. An adsorption value of 0.001 was used for all samples. The variation of this adsorption value did not significantly alter the obtained distributions. Measurements were performed in triplicate.

To determine the zeta potential (ζ) of the bare and functionalized MSPs, a Zetasizer Nano ZS (Malvern Instruments, UK) was used. Samples were dispersed in acetate buffer at concentration of 1 mg mL^{-1}. Before each measurement, samples were sonicated for 2 min to preclude aggregation. The zeta potential was calculated from the particle mobility values by applying the Smoluchowski model. The average of five recordings is reported as the zeta potential. Measurements were performed at 25 °C in triplicate.

2.4 Determination of functionalization degree

The degree of functionalization of different particles was determined by thermogravimetric analyses. Determinations were carried out on a TGA/SDTA 851e Mettler Toledo balance, with a heating program consisting of a heating ramp of 10° per minute from 273 to 373 °C followed by an isothermal heating step at this temperature for 60 min under a nitrogen atmosphere (80 mL min^{-1}). Then, the program continued with a dynamic heating segment from 373 to 1273 °C using an oxidant atmosphere (air, 80 mL min^{-1}) and an isothermal heating step at this temperature for 30 min.

2.5 Transmission electron microscopy (TEM)

For transmission electron microscopy (TEM) analysis, MSPs were dispersed in dichloromethane and sonicated for 2 min to preclude aggregates, and the suspension was deposited onto copper grids coated with a carbon film (Aname SL, Madrid, Spain). Imaging of the MSP samples was performed using a JEOL JEM-1010 (JEOL Europe SAS, France) operating at an acceleration voltage of 80 kV. The single-particle size was estimated by averaging the measured size values of 50 particles.

2.6 Confocal laser scanning microscopy (CLSM

The morphologic analysis of bare and functionalized MSP particles dispersed in acetate buffer and also incorporated into gelatine was performed by confocal laser scanning microscopy after staining the samples with rhodamine B (0.2%). CSLM images were recorded on a Leica TCS SP confocal laser scanning microscope (Leica Microsystems CMS GmbH., Manheim, Germany) equipped with an inverted microscope (model Leica DM IRBE) used in single-photon mode with an Ar/Kr visible light laser. The excitation wavelength was set at 540 nm. Digital image files were acquired in the format of 1024 pixel × 1024 pixel resolution.

2.7 Large deformation experiments

Uniaxial compression tests were performed using a texture analyzer (TA.XT.plus Texture Analyser, Stable Micro Systems, Godalming, Surrey, United Kingdom), employing a plate probe (diameter: 75 mm). The plates were lubricated with a thin layer of paraffin oil. The gels were removed from the syringe and cut to obtain cylinders of 20 mm of diameter and 20 mm of height. The measurements were performed at a constant deformation speed of 1 mm s^{-1} and up to a compression strain of 90%.

The relative deformation at a certain stage is expressed as a true or Hencky strain, (ε_H), which is defined as:

$$\varepsilon_H = \int_{H_0}^{H_t} \frac{1}{H} dH = ln\left(\frac{H_t}{H_0}\right), \quad (1)$$

where H_0 is the initial specimen height (m), and H is the actual height after certain deformation time t (m). For compression, the Hencky strain is negative, but it will be expressed as a positive figure. The average true or Hencky stress, $\sigma(t)$ (Pa), in the test piece at a certain deformation at time t is given by:

$$\sigma(t) = \frac{F(t)}{A(t)}, \quad (2)$$

where F(t) is the measured force after a deformation time t (N), and A(t) is the cross-sectional area of the sample (m^2). The true stress accounts for the continuous change in the cross-sectional area assuming no change in cylindrical shape and constant volume during the compression. The apparent Young's modulus, *E* (Pa), of the sample was defined as the initial slope within the linear region of the true stress versus true strain curve. The Young's modulus is representative of the stiffness of the gel. Fracture stress and strain are defined as strength and brittleness of the gel, respectively.

2.7 Turbidity measurement

The turbidity (τ) of the gels was measured using a JASCO V-630 Spectrophotometer (JASCO Analitica Spain S.L, Madrid, Spain) at 550 nm against acetate buffer and expressed as % of transmittance. Measurements were performed in duplicate.

2.8 Statistical analysis

All tests were carried out for at least three times and data were subjected to multifactorial analysis of variance (ANOVA) using Statgraphics Centuriun XV (Manugistics Inc., Rockville, MD, USA). Results followed by the same letter in the same column are not significantly different between means ($p<0.005$).

3. Results and discussion

3.1 MSPs characterization

A morphologic analysis of different synthesized MSPs was performed by transmission electron microscopy (TEM). The first column of **Figure 1** shows the evident differences in particle size, shape, and porosity. Nanoparticulate MCM-41 particles (**N**) are spherical nanoparticles with an apparent pore size in the range of 2 to 3 nm. UVM-7 particles (**U**) are organized in the form of clusters of pseudospherical mesoporous nanoparticles. Microparticulate MCM-41 particles (**M**) look like porous irregularly shaped particles whose pore size is in the range of 2 to 3 nm. Finally, SBA-15 (**S**) particles are elongated with a well-defined hexagonal mesoporous distribution.

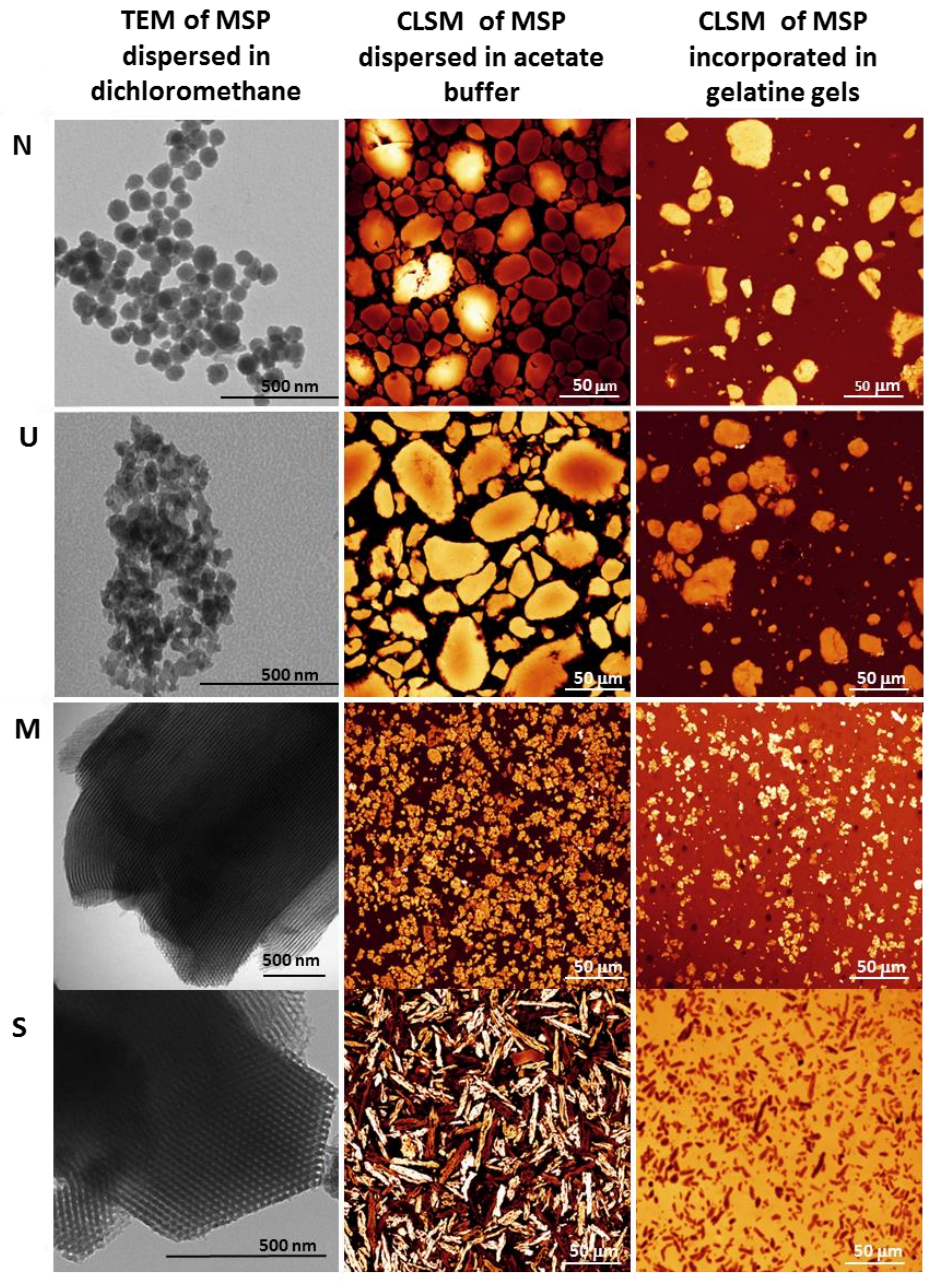

Figure 1. TEM (left) and CLSM images of different MSPs stained with Rhodamine B dispersed in acetate buffer (middle) or incorporated in gelatine gels (right). N: Nanoparticulated MCM-41; U: UVM-7; M: Microparticulated MCM-41; S: SBA-15

Besides the shape, this morphological analysis allowed the determination of the single-particle size of different MSPs. Size oscillated from ca. 100 nm of **N** to ca. 1-1.5 µm of **M** or **S**. **U** clusters had different sizes, being the average next to the microscale. Size values are summarized in Table 1.

Table 1. Size (Mean±SD) of different bare and functionalised MSP determined by TEM (dry) or Light Diffraction (dispersed in acetate buffer). N: Nanoparticulated MCM-41; U: UVM-7; M: Microparticulated MCM-41; S: SBA-15

MSP	Bare (Dry) Single particle size (µm)	Bare (Acetate) d(0.5)* (µm)	COO^- (Acetate) d(0.5)* (µm)	NH_3^+ (Acetate) d(0.5)* (µm)
N	0.09 ± 0.02^c	4.79 ± 0.04^c	2.36 ± 0.06^b	0.86 ± 0.01^b
U	0.87 ± 0.25^b	6.19 ± 0.04^b	3.38 ± 0.03^c	2.62 ± 0.08^c
M	1.2 ± 0.3^a	0.82 ± 0.01^a	0.74 ± 0.01^a	0.55 ± 0.00^a
S	1.3 ± 0.2^a	0.78 ± 0.00^a	0.78 ± 0.02^a	0.63 ± 0.01^a

*Maximum particle diameter below which 50% of the sample exists. Values with different letters in the same column are significantly different at p-value $p<0.001$. N, nanoparticulate MCM-41; U, UVM-7; M, microparticulate MCM-41; S, SBA-15.

As the particles were incorporated into gelatine gels in a buffered aqueous dispersion, the size distribution and zeta potential of the particles were also determined in acetate buffer (pH 5.5). **Figure 2a** shows the size distribution of the four bare particles. A direct visual inspection allows us to distinguish two different groups of particles according to their size in water. On one hand, **S** and **M** exhibited a size distribution in the range 0.5-10 µm, while the size distribution of **N** and **U** ranged from 5 to 20 µm. When the single-particle size obtained by TEM and the size distribution obtained by the Mastersizer were compared (**Table 2**), it was stated that the particle size remained in the same range for **S** and **M**. However, the size increased dramatically in the case of **N** and **U**, passing from the nanoscale to the microscale. The size of different MSPs was also checked by CLSM, confirming that the particle size in a water suspension was in accordance with the size distribution measured by light diffraction (**Fig 1**, middle).

The size distribution of functionalized MSPs was also determined**. Figure 2b,c** shows the size distributions of **#-C3** and **#-N3** particles, respectively. For all MSPs, both types of functionalization resulted in a decrease in the particle size. This difference was more significant for **N** and **U** and more pronounced in the case of the functionalization with amines

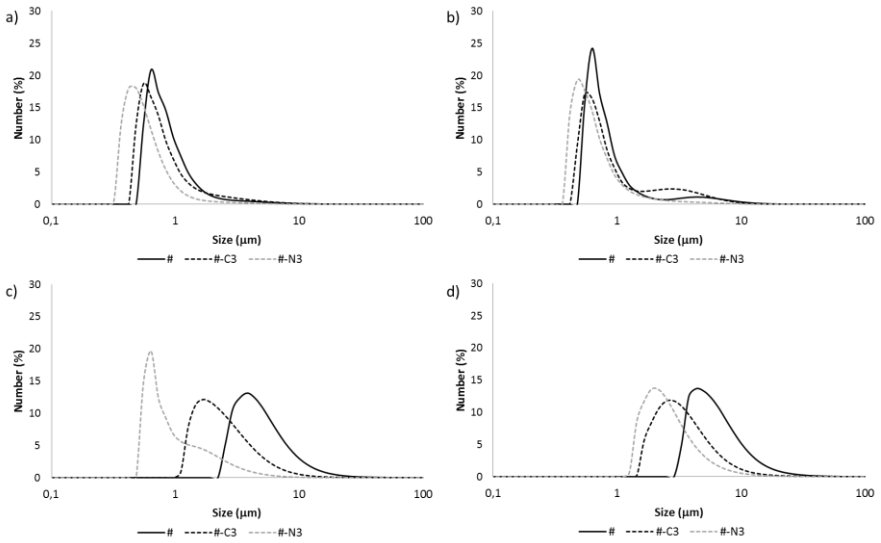

Figure 2. Size distribution of different MSPs dispersed in acetate buffer at pH 5.5. a) Microparticulated MCM-41. b) SBA-15. c) Nanoparticulated MCM-41. d) UVM-7. #: Bare particle. #-C3: Carboxylate functionalised particle. #-N3: Amine functionalised particle.

Finally, the morphology of bare and functionalized particles after being incorporated in gelatine gels was also characterized by CLSM. The third column of **Figure 1** shows how the interaction of MSP with gelatine did not modify the size or shape of the particles, in comparison to the same particle in a buffer dispersion (**Fig 1**, middle).

3.2 Functionalization characterization

The degree of functionalization of solids **#-C3** and **#-N3** was determined by thermogravimetric analysis **(Table 2**). As can be seen, similar functionalization was observed for the different materials when functionalized with N3 or C3. However, for a given material if C3 and N3 functionalization are compared, it is apparent from the data that the amount of N3 anchored to the particles (ca. 400 mg g^{-1} SiO_2) is greater than the amount of C3 (ca. 300 mg g^{-1} SiO_2). This was somehow expected and can be explained by taking into account that C3 is a bulkier molecule than N3.

Table 2. Content of organic molecules anchored to the particles after functionalization.

MSP	Carboxylate functionalised (mg C3 g^{-1} SiO_2)	Amine functionalised (mg N3 g^{-1} SiO_2)
N	322	403
U	347	442
M	354	432
S	332	425

The efficiency of functionalization was also tested by zeta potential determinations. **Figure 3** shows the zeta potential values of different MSPs suspended in acetate buffer. For bare particles, two groups could be distinguished. On one hand, **S** and **M** particles exhibited a zeta potential close to -30 mV. On the other hand, **U** and **N** showed zeta potential values next to -10 mV. After functionalization with carboxylates, zeta potential values became more negative for all types of particles. In contrast, the zeta potential changed from negative to positive values after functionalization with amines, confirming the effect of the functionalization on the surface charge. For both kinds of functionalization, the zeta potential achieved a value of -30 or +30 mV.

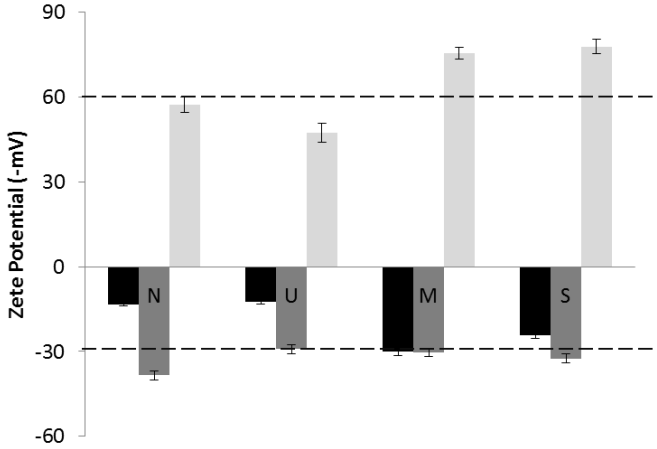

Figure 3. Zeta potential values (Mean ± SD) of different bare (black), carboxylate functionalised (dark grey) and amine functionalised (light grey) MSP dispersed in acetate buffer (pH 5.5). N: Nanoparticulated MCM-41; U: UVM-7; M: Microparticulated MCM-41; S: SBA-15.

Zeta potential measurements also explain the changes or preservation of particle size after functionalization. The general dividing line between stable and unstable suspensions is taken at either +30 or -30 mV. Particles with zeta potentials more positive than +30 mV or more negative than -30 mV are normally considered to be stable (Duman & Tunç, 2009). This fact explain why bare **N** and **U** (particles that exhibited a zeta potential of ca. -10 mV) increased its size dramatically from the nanoscale to the microscale in an aqueous suspension as a consequence of particle aggregation, while the particle distributions of **S** and **M** (zeta potential value of ca. -30 mV) remained in the same order. Values of the zeta potential also allowed us to explain why **N** and **U** decreased its size after functionalization with amines or carboxylates due to stability improvement.

3.3 Effect of MSP on large deformation properties of the gelatine gel matrix

The effect of the incorporation of different MSPs on the texture properties of gelatine gels was studied by a comparison of the modulus and fracture properties of gelatine gels containing different percentages of MSPs with those gels without particles.

3.3.1 Effect on the Young's Modulus

Figure 4 shows the Young's modulus of gels containing different concentrations of bare and functionalized MSPs. The addition of the four types of bare MSPs (**Fig 4a**) did not modify the Young's modulus significantly ($p>0.5$) at the concentrations studied. Although silicate species have been shown to interact through both electrostatic and hydrogen bonding interactions with some poly(amino acids) and proteins (Fernandes *et al.*, 2011), the interactions with the polymeric matrix are ineffective at acidic pH (Coradin *et al.*, 2004). Thus, because the gels under investigation were prepared at pH 5.5, interactions between bare MSP and gelatine are expected to be very weak.

The same behavior was found for **#-C3** particles (**Fig 4b**). However, when **M-N3**, **N-N3**, and **S-N3** were incorporated into the gel matrix, a significant increase in the Young's modulus ($p<0.05$) was observed. The Young's modulus of gels filled with U-N3 did not increase significantly.

To be able to compare the effect of the kind of particle on the stiffness of the gels, values of the Young's modulus of gels containing 0.75% of particles are plotted in **Figure 4d**. The figure shows no significant differences between gels filled with **#** and **#-C3** particles. However, when gels were filled **#-N3** particles, the effect of particle type was significant for **M**-, **N**-, and **S**-type particles.

From these results, it could be concluded that neither the MSP type nor functionalization are able to affect the stiffness of the gels by themselves. However, when functionalization is able to decrease the size of a particle cluster, the particle type and amine or carboxylate functionalization become relevant to the final gel stiffness. This is in agreement with Fu *et al.* (2008) who described that there are three decisive factors determining the elastic modulus of a filled-polymer gel: the elastic modulus of the filler and the matrix (the higher the elastic modulus of the filler, the higher the elastic modulus of the composite), the filler concentration, and the aspect ratio of the filler. Next to that, the interaction of

the filler with the matrix is an important factor, determining if the filler is active or inactive (Ring & Stainsby, 1982). In this particular case, the Young's modulus of SiO_2 is much higher than that of gelatine; however, the concentration of particles was not enough to raise the Young's modulus. The most important factors were the size of the filler and the aspect ratio, justifying why **M**, **N**, and **S** made different contributions to the increase in the Young's modulus.

In neither case, the gel strength was negatively affected by the presence of the particles, indicating that the particles act as active filler. Especially for the **#-N3** particles, the interaction between particles and the gel matrix is expected to be strong.

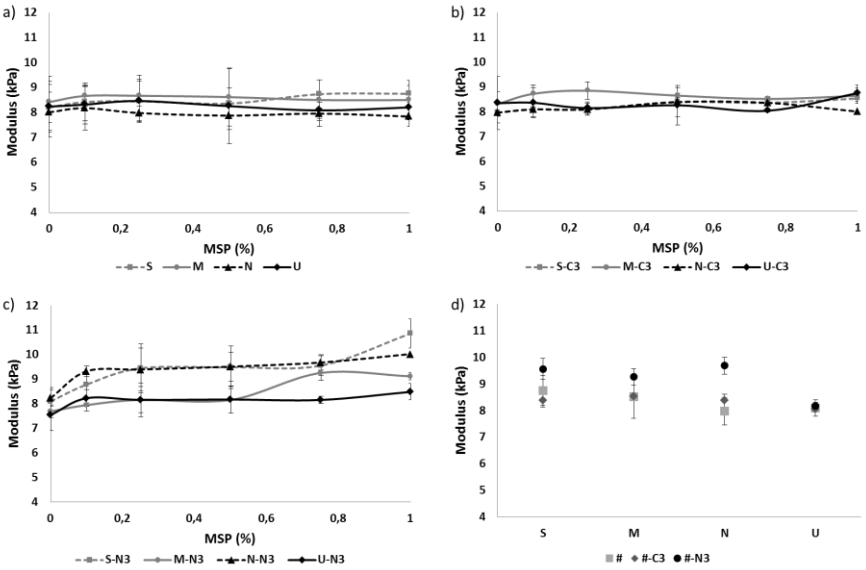

***Figure 4**. Effect of MSPs concentration on the Young's Modulus of gelatine gels. a) Bare MSP, b) MSP functionalised with carboxylates. c) MSPs functionalised with amines, d) Comparison of values of Young's Modulus at the concentration of 0.75%. N: Nanoparticulated MCM-41; U: UVM-7; M: Microparticulated MCM-41; S: SBA-15. #: Bare particle. #-C3: Carboxylate functionalised particle. #-N3: Amine functionalised particle.*

3.3.2 Effect on fracture stress

The effect of MSPs content on fracture stress is shown in **Figure 5**. Bare MSPs (**Fig 5a**) did not modify the values of fracture stress and thus did not affect the gel strength. However, when particles were functionalized with carboxylates or with amines (**Fig 5b,c**), particles contributed to the increase in the final gel strength proportionally with concentration. In spite of the functionalization, **U** was the particle that contributed to the gel strength in a less pronounced manner. In contrast, **N** contributed the most to fracture stress values. Bearing in mind that **U** formed large aggregates that did not significantly modify their size as a consequence of the functionalization and that **N** aggregates decreased noticeably the size after functionalization, the importance of particle size on fracture stress values is confirmed. **Figure 5** also displays the dependence of particle concentration on gel strength since for each particle a minimum concentration is needed to vary the value of fracture stress significantly.

According to these results, it could be stated that the particle size, particle concentration, and organic functionalization are the three parameters that affect the strength of the filled gels.

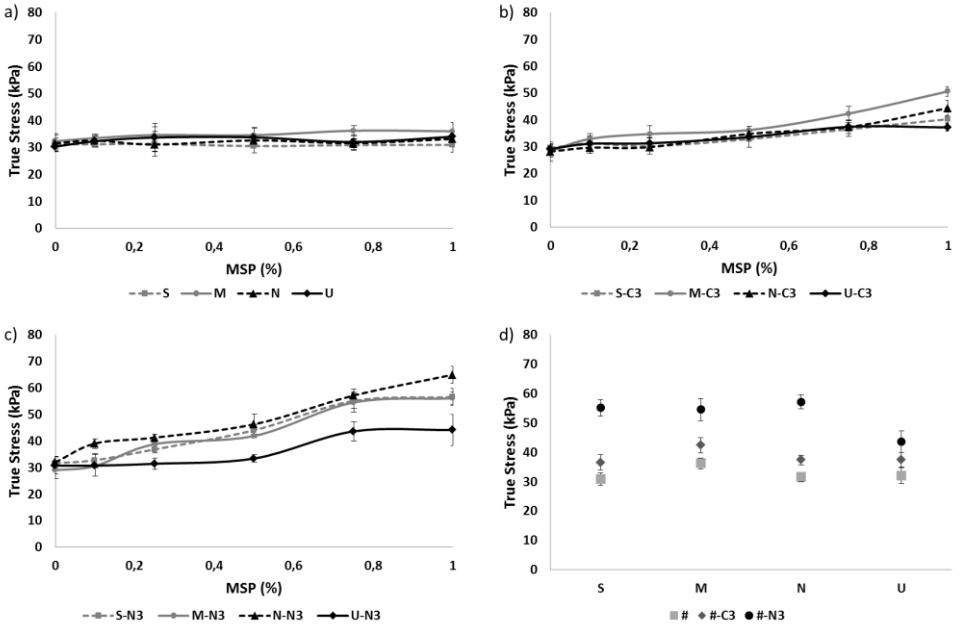

Figure 5. Effect of MSP concentration on the Fracture Stress of gelatine gels. a) Bare MSP, b) MSP functionalised with carboxylates. c) MSP functionalised with amines, d) Comparison of values of Young's Modulus at the concentration of 0.75%. N: Nanoparticulated MCM-41; U: UVM-7; M: Microparticulated MCM-41; S: SBA-15. **#**: Bare particle. **#-C3**: Carboxylate functionalised particle. **#-N3**: Amine functionalised particle.

3.3.3 Effect on fracture strain

Figure 6 shows the effect of MSPs concentration on the fracture strain of gelatine gels. As occurred for the Young's modulus and fracture strain, the addition of different concentrations of the four types of bare MSPs did not provoke significant changes in fracture strain values. Instead, gels filled with functionalized MSPs exhibited a significant increase ($p<0.005$) in the fracture strain in comparison to the control gel. The presentation of values of fracture strain for gels filled with different bare and functionalized particles on the same graph (**Fig 6d**) confirmed that the highest fracture strain values are apparent in gels filled with particles functionalized with amines, followed by gels filled with particles functionalized with carboxylates. Accordingly, it could be concluded that the functionalization is more important than the particle size or shape for fracture stress.

This improvement of the strain at the fracture of a polymer network by the incorporation of hybrid nanofillers (inorganic nanoparticles with organic surface) has also been reported by other authors (Tjong, 2006) and is related to a better filler-matrix interaction, increasing the integrity and stability of the gel and thus making it withstand more deformation before energy dissipates via (micro-) fracture events.

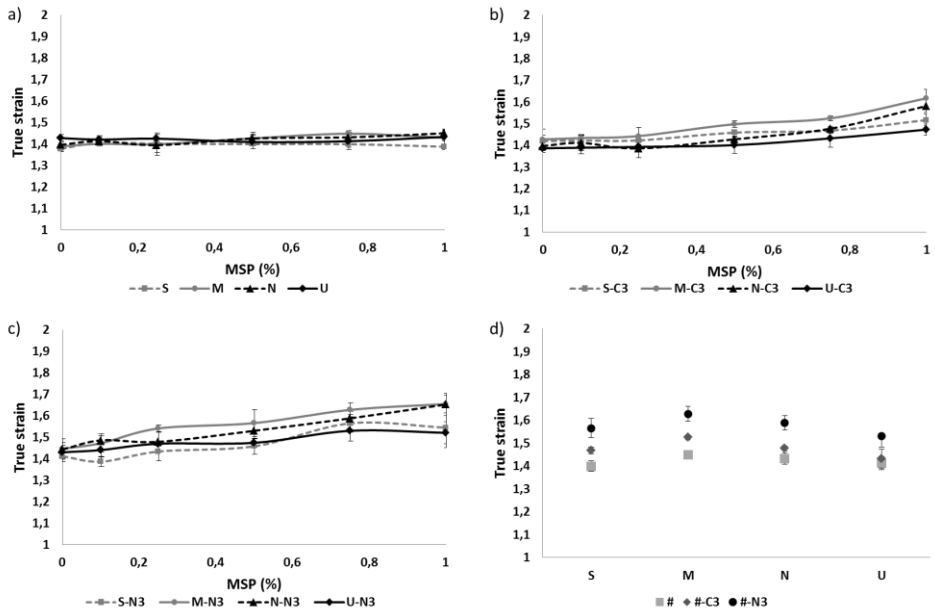

Figure 6. Effect of MSPs concentration on Fracture Strain of gelatine gels. a) Bare MSPs, b) MSPs functionalised with carboxylates. c) MSPs functionalised with amines, d) Comparison of values of Young's Modulus at the concentration of 0.75%. N: Nanoparticulated MCM-41; U: UVM-7; M: Microparticulated MCM-41; S: SBA-15. **#**: Bare particle. **#-C3**: Carboxylate functionalised particle. **#-N3**: Amine functionalised particle.

3.3.4 Effect of particle size and surface modification on the filler-matrix interaction

Two ideas are clear after evaluating the effect of the addition of **#**, **#-C3**, and **#-N3** particles at concentrations from 0 to 1% on the textural properties of gelatine gels. On one hand, organic functionalization is needed to improve the Young's modulus and fracture properties, while on the other hand, a minimum concentration of particles (different for each kind or particle) should be achieved to observe this phenomenon.

Figure 7 tries to explain graphically the influences of particle size, shape, and surface modification on the filler-matrix interaction. Bare particles that are next to the instable zone tend to aggregate. Moreover, at acidic pH, interactions between bare MSP and gelatine are expected to be very weak (**Fig 7a**). After carboxylate and amine functionalization, particles add organic molecules to their surface and achieve a zeta potential that is able to stabilize the particle, reducing the aggregation tendency. These organic molecules also improve the compatibility between the particle and the protein matrix and generate an interfacial area in the surroundings of the particles (**Fig 7b**). The interfacial area consists of immobilized proteins whose structure and properties change because of the interaction with the particles (Pitsa & Danikas, 2011; Tjong, 2006).

Large particles or small concentration will result in a small absolute number of particles embedded in the matrix. A small number of particles implies that the relative distance between them is too large and the interfacial area of each particle remains isolated from the rest (**Fig 6b**). For small particles or high volume fractions, the interfacial areas of each particle start to overlap (**Fig 7c**), resulting in an intensification of the interactions (Vaia & Wagner, 2004) and reinforcing the protein network and thus increasing both the Young's modulus and fracture properties.

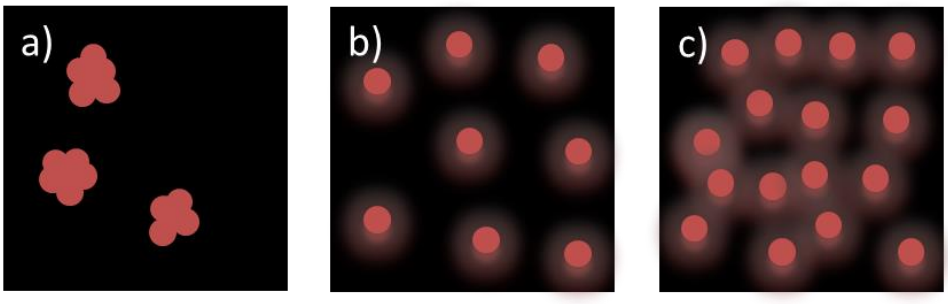

Figure 7. a) Scheme of the structure of a filled gel: bare MSPs (red spheres). b) Interfacial area formation (diffuse layer in particle surroundings) under low concentration of functionalised particles (large distance between interfacial areas). c) Interfacial area formation under high concentration of functionalised particles (overlap of interfacial areas, increase of bounding between layers).

3.4 Effect of MSPs on gel turbidity of the gelatine gel matrix

The effect of bare and functionalized MSPs at different concentrations on the turbidity of filled-gelatine gels expressed as the percentage of transmittance is shown in **Fig 8**. Nonfilled gels exhibited values of transmittance of 92 ± 2%. The subsequent addition of bare or functionalized MSPs decreased the transmittance of the sample as a function of particle concentration, thereby increasing the turbidity of the gel. At low concentrations (0.1 and 0.25%), **Fig 8** allows us to evaluate most explicitly the different contribution of each particle to the final turbidity. This is consistent with light-scattering theory, which states that for moderately dilute suspensions of particles there is an exponential decrease in transmitted light with particle concentration (Gregory, 1998). However, from concentrations of up to 0.5% particles, the turbidity dramatically increases to achieve transmittance values close to 0.

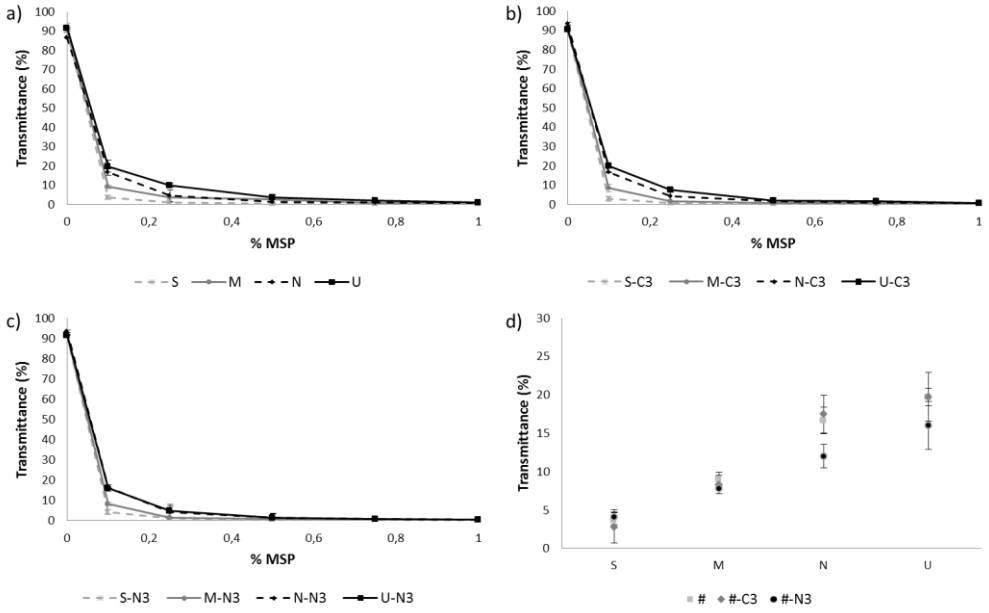

Figure 8. Effect of MSPs concentration on gel turbidity expressed as % of transmittance. a) Bare MSPs, b) MSPs functionalised with carboxilates. c) MSPs functionalised with amines, d) Comparison of transmittance at the concentration of 0.1%. N: Nanoparticulated MCM-41; U: UVM-7; M: Microparticulated MCM-41; S: SBA-15. **#**: Bare particle; **#-C3**: Caroxylate functionalised particle; **#-N3**: Amine functionalised particle

To understand the effect of particle size, shape, and functionalization on gel turbidity, values of the turbidity of gels filled with 0.1% particles have been plotted separately in **Figure 8d**. This figure shows that gel turbidity is related to the particle size determined with the Mastersizer so that the contribution of small particles to final turbidity is higher than that of large particles. A greater absolute number of particles provokes a larger decrease in transmitted light. Since the gelatine gels are prepared based on the mass concentration of the MSP, for the same mass concentration there are more small particles and the transmitted light decreases more drastically.

This effect is corroborated by the fact that particles that did not alter their size significantly as a function of functionalization (**S** and **M**) maintained turbidity values independent of the functionalization. Gels filled with particles that changed their size by functionalization (**N** and **U**) exhibit a different turbidity when the particles are functionalized with amines and thereby reduced their size significantly.

Thus, the incorporation of MSPs into gelatine gels affects the gel turbidity as a function of particle size and concentration, providing gel opacity at concentrations of up to 0.5% MSP present. To obtain transparent filled gels, a lower particle concentration would be needed.

4. Conclusions

In this study, four different MSPs have been successfully functionalized, characterized, and incorporated into gelatine gels. The characterization process stated that particles experience a significant change in their aggregation tendency after carboxylate or amine functionalization, therefore modifying their particle/cluster size. Particle functionalization also creates an organic layer on the surface of the particle that improves the filler-matrix interaction. This causes an increase in the Young's modulus, fracture stress and fracture strain, more or less pronounced depending on the type of particle, functionalization and concentration. Gelatine gels filled with bare particles at concentrations between 0 and 1% maintain their textural properties. The most affected property is turbidity, which increases with the addition of both bare and functionalized MSPs. These findings lead us to conclude that the mechanical properties of the filled gels remain or improve with the addition of MSPs and that although not being suitable for transparent systems, MSPs are promising delivery systems able to be incorporated in foodlike products.

Acknowledgements

Authors gratefully acknowledge the financial support from the Ministerio de Economía y Competitividad (Projects AGL2012-39597-C02-01, AGL2012-39597-C02-02 and MAT2012-38429-C04-01) and the Generalitat Valenciana (project PROMETEO/2009/016). E.P. is grateful to the Ministerio de Ciencia e Innovación for his grant (AP2008-00620). Saskia de Jong (NIZO food research) is acknowledged for assistance during CLSM observations and rheology interpretation.

References

An, X., Zhan, F., & Zhu, Y. (2013). Smart photothermal-triggered bilayer phase transition in AuNPs-liposomes to release drug. *Langmuir*, *29*(4), 1061-1068.

Anton, N., Mojzisova, H., Porcher, E., Benoit, J. P., & Saulnier, P. (2010). Reverse micelle-loaded lipid nano-emulsions: new technology for nano-encapsulation of hydrophilic materials. *International journal of pharmaceutics*, *398*(1), 204-209.

Asefa, T., & Tao, Z. (2012). Biocompatibility of mesoporous silica nanoparticles. *Chemical research in toxicology*, *25*(11), 2265-2284.

Aznar, E., Martínez-Máñez, R., & Sancenón, F. (2009). Controlled release using mesoporous materials containing gate-like scaffoldings. *Expert Opinion on Drug Delivery, 6*(6),643-655.

Barat, J., Pérez-Esteve, É., Bernardos, A., & Martínez-Mañez, R. (2011). Nutritional effects of folic acid controlled release from mesoporous materials. *Procedia Food Science*, *1*, 1828-1832.

Bernardos, A., Aznar, E., Coll, C., Martínez-Mañez, R., Barat, J. M., Marcos, M. D., Sancenón, F., Benito, A., & Soto, J. (2008). Controlled release of vitamin B2 using mesoporous materials functionalized with amine-bearing gate-like scaffoldings. *Journal of Controlled Release*, *131*(3), 181-189.

Bernardos, A., Mondragon, L., Aznar, E., Marcos, M. D., Martínez-Máñez, R., Sancenón, F., Soto, J., Barat, J. M., Perez-Paya, E., Guillem, C., & Amorós, P. (2010). Enzyme-responsive intracellular controlled release using nanometric silica mesoporous supports capped with “saccharides”. *Acs Nano*, *4*(11), 6353-6368.

Cabrera, S., El Haskouri, J., Guillem, C., Latorre, J., Beltrán-Porter, A., Beltrán-Porter, D., Marcos, M. D. & Amoros, P. (2000). Generalised syntheses of ordered mesoporous oxides: the atrane route. *Solid State Sciences*, *2*(4), 405-420.

Chaturvedi, K., Ganguly, K., Nadagouda, M. N., & Aminabhavi, T. M. (2013). Polymeric hydrogels for oral insulin delivery. *Journal of controlled release*, *165*(2), 129-138.

Comes, M., Aznar, E., Moragues, M., Marcos, M. D., Martínez-Máñez, R., Sancenón, F., Soto, J., Villaescusa, L. A., Gil, L., & Amorós, P. (2009). Mesoporous hybrid materials containing nanoscopic "binding pockets" for colorimetric anion signaling in water by using displacement assays. *Chemistry-A European Journal*, *15*(36), 9024-9033.

Coradin, T., Bah, S., & Livage, J. (2004). Gelatine/silicate interactions: from nanoparticles to composite gels. *Colloids and Surfaces B: Biointerfaces*, *35*(1), 53-58.

Duman, O., & Tunç, S. (2009). Electrokinetic and rheological properties of Na-bentonite in some electrolyte solutions. *Microporous and Mesoporous Materials*, *117*(1), 331-338.

El Haskouri, J., de Zárate, D. O., Guillem, C., Latorre, J., Caldés, M., Beltrán, A.,Beltrán, D., Descalzo, A .B., Rodríguez-López, G., Martínez-Máñez, R., Marcos, M. D., & Amorós, P. (2002). Silica-based powders and monoliths with bimodal pore systems. *Chemical Communications*, (4), 330-331.

Fernandes, F. M., Manjubala, I., & Ruiz-Hitzky, E. (2011). Gelatin renaturation and the interfacial role of fillers in bionanocomposites. *Physical Chemistry Chemical Physics*, *13*(11), 4901-4910.

Fu, S. Y., Feng, X. Q., Lauke, B., & Mai, Y. W. (2008). Effects of particle size, particle/matrix interface adhesion and particle loading on mechanical properties of particulate-polymer composites. *Composites Part B: Engineering*, *39*(6), 933-961.

Gregory, J. (1998). Turbidity and beyond. *Filtration & separation*, *35*(1), 63-67.

Mamaeva, V., Sahlgren, C., & Lindén, M. (2013). Mesoporous silica nanoparticles in medicine-Recent advances. *Advanced drug delivery reviews*, *65*(5), 689-702.

Lorenzo, G., Zaritzky, N., & Califano, A. (2013). Rheological analysis of emulsion-filled gels based on high acyl gellan gum. *Food Hydrocolloids*, *30*(2), 672-680.

Moon, D. S., & Lee, J. K. (2012). Tunable synthesis of hierarchical mesoporous silica nanoparticles with radial wrinkle structure. *Langmuir*, *28*(33), 12341-12347.

Pérez-Esteve, E., Bernardos, A., Martínez-Máñez, R., & M Barat, J. (2013). Nanotechnology in the development of novel functional foods or their package. An overview based in patent analysis. *Recent patents on food, nutrition & agriculture*, *5*(1), 35-43.

Pitsa, D., & Danikas, M. G. (2011). Interfaces features in polymer nanocomposites: a review of proposed models. *Nano*, *6*(06), 497-508.

Rahmat, N., Abdullah, A. Z., & Mohamed, A. R. (2010). A review: Mesoporous Santa Barbara Amorphous-15, types, synthesis and its applications towards biorefinery production. *American Journal of Applied Sciences*, *7*(12), 1579.

Ring, S., & Stainsby, G. (1982). Filler reinforcement of gels. *Progress in Food and Nutrition Science*, 6, 355-361.

Sala, G., Van Vliet, T., Stuart, M. C., Van de Velde, F., & Van Aken, G. A. (2009a). Deformation and fracture of emulsion-filled gels: Effect of gelling agent concentration and oil droplet size. *Food hydrocolloids*, *23*(7), 1853-1863.

Sala, G., Van Vliet, T., Stuart, M. A. C., Van Aken, G. A., & Van de Velde, F. (2009b). Deformation and fracture of emulsion-filled gels: effect of oil content and deformation speed. *Food Hydrocolloids*, *23*(5), 1381-1393.

Salonen, J., Laitinen, L., Kaukonen, A. M., Tuura, J., Björkqvist, M., Heikkilä, T., Vähä-Heikkilä, K., Hirvonen, J., Lehto, V. P. & Lehto, V. P. (2005). Mesoporous silicon microparticles for oral drug delivery: loading and release of five model drugs. *Journal of Controlled Release*, *108*(2), 362-374.

Song, S. W., Hidajat, K., & Kawi, S. (2005). Functionalized SBA-15 materials as carriers for controlled drug delivery: influence of surface properties on matrix-drug interactions. *Langmuir*, *21*(21), 9568-9575.

Tjong, S. C. (2006). Structural and mechanical properties of polymer nanocomposites. *Materials Science and Engineering: R: Reports*, *53*(3), 73-197.

Trewyn, B. G., Slowing, I. I., Giri, S., Chen, H. T., & Lin, V. S. Y. (2007). Synthesis and functionalization of a mesoporous silica nanoparticle based on the sol-gel process and applications in controlled release. *Accounts of Chemical Research*, *40*(9), 846-853.

Vallet-Regí, M., Balas, F., & Arcos, D. (2007). Mesoporous materials for drug delivery. *Angewandte Chemie International Edition*, *46*(40), 7548-7558.

Vaia, R. A., & Wagner, H. D. (2004). Framework for nanocomposites. *Materials today*, *7*(11), 32-37.

Van Vliet, T. (1988). Rheological properties of filled gels. Influence of filler matrix interaction. *Colloid and Polymer Science*, *266*(6), 518-524.

Weiss, J., Takhistov, P., & McClements, D. J. (2006). Functional materials in food nanotechnology. *Journal of food science*, *71*(9), R107-R116.

Zhao, D., Huo, Q., Feng, J., Chmelka, B. F., & Stucky, G. D. (1998). Nonionic triblock and star diblock copolymer and oligomeric surfactant syntheses of highly ordered, hydrothermally stable, mesoporous silica structures. *Journal of the American Chemical Society*, *120*(24), 6024-6036.

Zhao, X. S., Lu, G. Q., & Millar, G. J. (1996). Advances in mesoporous molecular sieve MCM-41. *Industrial & Engineering Chemistry Research*, *35*(7), 2075-2090.

4.2.2 Enrichment of stirred yoghurts with folic acid encapsulated in pH-responsive mesoporous silica particles: Bioaccessibility modulation and physico-chemical characterization

Édgar Pérez-Esteve[1*], María Ruiz-Rico[1], Ana Fuentes[1], María Dolores Marcos[2-3], Félix Sancenón[2-3], Ramón Martínez-Máñez[2-3], José Manuel Barat[1]

[1]*Grupo de Investigación e Innovación Alimentaria, Universidad Politécnica de Valencia. Camino de Vera s/n, 46022, Spain*

[2]*Centro de Reconocimiento Molecular y Desarrollo Tecnológico (IDM). Departamento de Química Universidad Politécnica de Valencia, Camino de Vera s/n, 46022, Valencia, Spain*

[3]*CIBER de Bioingeniería, Biomateriales y Nanomedicina (CIBER-BBN)*

E-mail: edpees@upv.es

Submitted to LWT- Food Science and Technology

Abstract

In this work, we have studied the ability of a mesoporous silica support loaded with folic acid and functionalized with amines (**S1)** to modulate the bioaccessibility of the vitamin after its incorporation in stirred yoghurts with different fat content. Due to the novelty of using mesoporous silica supports in food matrixes, the influence of **S1** addition on the physicochemical, rheological and lactic acid bacteria viability of these yoghurts during 21 days of refrigerated storage at 4°C has also been evaluated. The *in vitro* digestion procedure showed that **S1** was capable of inhibiting the release of folic acid in acidic solution at pH 2 (stomach) and controllably release their contents in neutral pH (intestine), thereby modulating the bioaccessibility. Moreover, the physicochemical and microbiological assays revealed that enrichment generally does not alter the physicochemical properties (pH, colour, syneresis and rheology) of either type of yoghurt and does not cause any effect on lactic acid bacteria survival.

Keywords: Folic acid, enrichment, yoghurt, smart delivery system, bioaccessibility.

1. Introduction

Folate status of women all over the world is a public-health challenge. Folate deficiencies during pregnancy are the cause of birth defects such as neural tube defects. In other stages of life, folates are responsible for lowering the homocystein-level as well having an impact on preventig cardiovascular diseases (Lucock, 2000; Choi & Mason, 2002; Pitkin, 2007), Alzheimer (Clarke *et al.*, 1998), arteriosclerotic disease (Hoag *et al*., 1997), or a disruption of the nucleotide biosynthesis which can result in colon and colorectal cancer (Choi & Mason, 2002; Stover, 2004).

In spite of the public-health campaigns in recent years, a sizeable proportion of women of reproductive age remain unaware of the need to take folic acid (FA) periconceptionally. The most vulnerable groups are women who have unplanned pregnancies, young people and less-educated people. The only way to reach this group of women might be through fortification or enrichment of foods with FA (Eichholzer*et al.*, 2006). The incorporation of this vitamin into general accepted and consumed products could lead to improvements in vulnerable groups.

Although there are irrefutable evidences about the benefits of FA supplementation to prevent some diseases, recent studies suggest that massive exposure to high bioavailable FA is a double-edged sword. Humans have a reduced dihydrofolate reductase activity and a poor ability to reduce FA. Thus, oral doses of FA of about 260-280 μg (589-634 nmol) have been reported to lead to the direct appearance of untransformed FA in the systemic circulation. This is related to a possible role in certain cancer development (Lucock &Yates 2009).

In this context, as an alternative to traditional free FA supplementation, we recently presented a system based on the encapsulation of FA in a mesoporous silica support functionalized with amines to dose FA along a simulated digestion process (Pérez-Esteve *et al.*, 2015). The FA loaded and amine functionalised support, not only was able to hinder the release of the vitamin during the passage

across the stomach (simulated gastric fluid), but also was able to deliver progressively the vitamin when reaching the jejunum (simulated intestinal fluid), where it is completely absorbed (Sculthorpe *et al.*, 2001; Younis *et al.*, 2009), using a minimal quantity of the encapsulating support. Mesoporous silica supports are considered potential colloidal carriers with many unique features that make them excellent candidates for a broad range of biomedical applications, and have very good *in vivo* biocompatibility and biodegradability (Hamam & Al-Remawi, 2014).

Of all kinds of food, dairy products such as yoghurts and other fermented milks are great candidates to be enriched with FA. On the one hand, it is well known that dairy products and fermented milks are highly recommended during pregnancy, as they are a great source of vitamins A, B, D and E, protein and calcium (FAO, 2013). However, FA content in these products is negligible. On the other hand, dairy products have very good qualities to become enriched and/or fortified foods, since incorporation of nutrients is very simple, and hence the large number of functional dairy products have been developed to date (Estrada *et al*., 2011; Vélez-Ruiz *et al.*, 2013; Perna *et al*., 2014).

Among dairy products, yoghurt, produced by symbiotic cultures of *Streptococcus thermophilus* and *Lactobacillus delbrueckii* ssp. *bulgaricus*, is the most popular and consumed due to its association with good health (Ramírez-Sucre & Vélez-Ruiz, 2013; Wang *et al*., 2014; Tripathi & Giri, 2014). Moreover, stirred yoghurts, in which their structure is disintegrated by shearing processes before packing, facilitates the incorporation of new ingredients such us fruits, fibers and others relevant compounds. Finally, its pH close to 4, which makes it an appropriate matrix to incorporate porous matrices with molecular gates that respond to pH changes.

A significant body of research has focused on the evaluation of the influence of the addition different ingredients (minerals, dietary fiber, flavours, etc.) on the physicochemical properties of yoghurt (Achanta *et al.,* 2006; Ramirez-Santiago *et al.*, 2010; Ramirez-Sucre & Vélez-Ruiz, 2013). However, as far as we know, there are no studies dealing with the incorporation of smart delivery systems based on mesoporous silica supports on food matrixes. Thus, no data about the maintenance of controlled release efficiency after incorporation in real systems, as well as data related to the effect of MSPs on the physico-chemical properties of dairy products or on lactic acid bacteria viability are available.

The objective of the present work was to evaluate the ability of the smart delivery system (**S1**) to modulate the bioaccessibility of FA once incorporated in different fat containing yoghurts, as well as to study the influence of **S1** addition on the physicochemical and microbial quality of yoghurts during cold storage.

2. Materials and methods

2.1 Materials

Tetraethylorthosilicate (TEOS), triethanolamine (TEAH3), *N*-cetyltrimethylammonium bromide (CTABr), sodium hydroxide (NaOH), the organosiloxane derivative N^1-(3-Trimethoxysilylpropyl)diethylenetriamine (N3), acetic acid, sodium phosphate monobasic, sodium phosphate dibasic, tetrabutylammonium hydrogen sulphate (TBAHS) and acetic acid were provided by Sigma-Aldrich (Poole, Dorset, UK). Folic acid (FA) was purchased from Schircks Laboratories (Jona, Switzerland). Acetonitrile HPLC grade was provided by Scharlau (Barcelona, Spain).

Two types of stirred yoghurts, low-fat (LF) and full-fat (FF) (Senoble, Ocaña, Spain) were used as raw material. Yoghurts were acquired in a local supermarket in 500 mL containers. The expiry date was superior to 21 days in all the cases. In LF and FF yoghurts the protein, carbohydrate and fat content were 4.7-4.1%, 12.2-5.3%, and 3.4-0.1% respectively.

2.2 MSPs preparation and characterization

Microparticulated MCM-41 particles were synthesized following the so-called "atrane route", according to the method described by Pérez-Esteve *et al*. (2015). The route is based on the use of triethanolamine ligands as hydrolytic inorganic precursors and surfactants as porogen species. In a typical synthesis, 9.36 g of CTABr were added at 118 °C to a solution of $TEAH_3$ (52.4 g) containing 0.98 g of NaOH in 2 mL of water. Formerly, 0.098 mol of a silatrane derivative (22 mL of TEOS) was added at 70 °C to the mixture. Finally, 180 mL of deionised water were added while being vigorously stirred at 70 °C. After a few minutes of stirring, a white suspension was formed. This mixture was aged in an autoclave at 100 °C for 24h. Using filtration, the resulting powder was collected and then it was washed with water and ethanol. The solid was dried at 70 °C. To prepare the final porous material **(S0)**, the as-synthesised solid was calcined at 550 °C for 5 h to remove the template phase.

FA was loaded in support **S0** by the impregnation method described by Pérez-Esteve *et al.* (2015). For this purpose, 15 mg of FA dissolved in 1.5 mL of phosphate buffer solution (PBS) were added to 100 mg of MCM-41 employing 3 cycles of addition (0.5 mL per cycle). After each addition cycle, solid was dried at 30 ºC to eliminate water content.

The loaded solid was functionalized with N3. In a typical synthesis, 100 mg of the solid were suspended in 10 mL of a solution of acetic acid 5%, where an excess of N3 (0.43 mL, 0.015 mmol) was added. The mixture was stirred for 5.5 h at room temperature. The final loadead and amine-gated solid (**S1**) was isolated by vacuum filtration, washed with 300 mL of acetic acid solution, and dried at 30 °C for 24 h.

The characterization of the different mesoporous solids (**S0** and **S1**) was made by powder X-ray diffraction (XRD), transmission electron microscopy (TEM), field emission scanning electron microscopy (FESEM), particle size distribution and zeta potential determinations. XRD was performed on a D8 Advance diffractometer (Bruker, Coventry, UK) using CuKα radiation. TEM images were obtained with a JEM-1010 (JEOL Europe SAS, Croissy-sur-Seine, France). FESEM images were acquired with a Zeiss Ultra 55 (Carl Zeiss NTS GmbH, Oberkochen, Germany) and observed in the secondary electron mode. The particle size distribution was determined using a Malvern Mastersizer 2000 (Malvern Instruments, Malvern, UK). For the measurements, samples were dispersed in distilled water. Data analysis was based on the Mie theory using refractive indices of 1.33 and 1.45 for the dispersant and particle, respectively. An adsorption value of 0.001 was used for all samples. Variation of this adsorption value did not significantly alter the obtained distributions. Measurements were performed in triplicate. A Zetasizer Nano ZS (Malvern Instruments, Malvern, UK) was used to determine the zeta potential (ζ). Samples were dispersed in distilled water at concentration of 1 mg mL^{-1}. The zeta potential was calculated from the particle mobility values by applying the Smoluchowski model. The measurement was performed at 25°C. Measurements were performed in triplicate. The composition of **S1** was determined by thermogravimetrical analysis (TGA) and ^{1}H NMR. Thermogravimetric analyses were carried out on a TGA/SDTA 851e Mettler Toledo balance, using an oxidant atmosphere (air, 80 mL min^{-1}) with a heating program consisting of a heating ramp of 10 ºC per minute from 393 to 1273 K and an isothermal heating step at this temperature for 30 min. ^{1}H NMR spectra were recorded in at RT using a Bruker AV400 spectrometer after dissolving the sample in $NaOD/D_2O$ in the presence of tetraethyl ammonium bromide as internal standard.

2.3 Folic acid release study

To determine the effect of pH in FA release from the amine-gated mesoporous silica particles (**S1**), 10 mg of the corresponding solid were placed in 25 mL of water at pH 2 (adjusted with HCl), pH 4 (adjusted with HCl and with lactic acid) and pH 7.5 (PBS). At a certain times aliquots were separated, filtered and analysed by HPLC to quantify the amount of FA.

The maximum release capacity of the solid **S1** was determined by quantifying the amount of FA released after reaching the equilibrium (2h at pH 7.5). This released FA amount was used to quantify the amount of solid **S1** needed to provide the dietary reference intake (DRI) of FA in the population most in need of this nutrient (360 μg of synthetic FA per day in pregnant women) (Eichholzer *et al.*, 2006).

2.4 Sample preparation

Three different batches of samples were prepared for low-fat (LF) and full-fat (FF) yoghurts. Yoghurts without enrichment were considered control samples (C). Enriched yoghurts containing the 100% of the DRI of FA by addition of free FA were called E_F (enriched with free FA). Yoghurts containing the amount of **S1** needed to release 100% of the DRI of FA were called E_E (enriched with encapsulated FA in **S1**). After addition of free FA or **S1**, yoghurts were stirred for 1 min. In C yoghurts the same stirring procedure was performed to standardize conditions. Samples were then stored at 4 °C until they were analysed (0, 7 and 21 days). The sample preparation procedure is schematically shown in **Figure 1**.

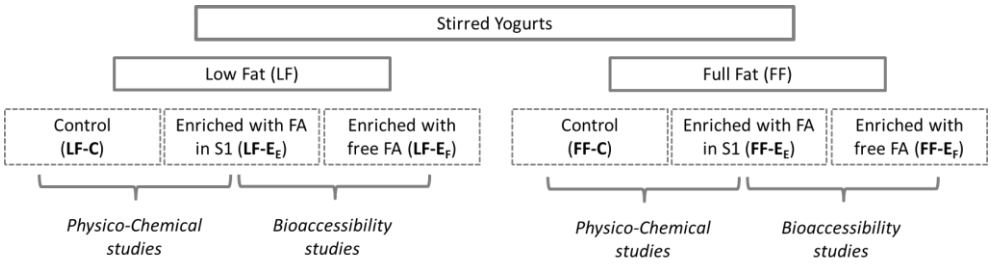

Figure 1. Scheme of sample preparation.

2.5 Yoghurts in vitro digestion and FA bioaccessibility determination

FA bioaccessibility from E_F and E_E yoghurts was determined by simulating a human digestion in mouth, stomach and small intestine adapting the procedure described by Versantvoort *et al.* (2005)[1]. The large intestinal track was not taken into account since *in vivo* FA absorption occurs throughout the jejunum (Younis *et al.*, 2009). In a typical experiment, 5 g of the corresponding yoghurt were suspended in 6 mL of saliva and incubated for 5 min at 37 °C. Then, 12 mL of gastric juice were added. The mixture was incubated for 2 h. Finally, 12 mL of duodenal juice, 6 mL of bile, and 2 mL of bicarbonate solution (1M) were added simultaneously. After the addition, the mixture was maintained under stirring at 37 ^{o}C for 2 h. All digestive juices were heated to 37 ^{o}C before being mixed. During this period, aliquots were taken, filtered using nylon filters with 0.45 μm pore size (Scharlab, Barcelona, Spain) and analysed by HPLC to determine the amount of FA (*vide infra*). All chemicals for the digestive fluids were provided by Sigma-Aldrich (Poole, Dorset, UK).

[1] See composition of the fluids in appendix 3 (page 257)

2.6 Folic acid quantification

FA was quantified by reversed-phase HPLC according to the method described by Pérez-Esteve *et al.* (2015). The HPLC instrument consisted of a Hitachi LaChrom Elite liquid chromatograph (Hitachi Ltd., Tokyo, Japan) equipped with an auto-sampler (modul L-2200) and UV detector (modul L-2400). A column Kromaphase 100 C18 (250 mm x 4.6 mm i.d., 5 μm particle size analytical column) (Scharlab, Barcelona, Spain) was used for the separations. Mobile phase consisted of (A) 0.125 mM of NaH_2PO_4, 0.875 mM of Na_2HPO_4 and 0.4 mM of TBAHS in water and (B) acetonitrile-phase A 65:35 (v/v). The gradient program was as follows: the mobile phase was run isocraticaly for the first 5 min with 90% A and 10% B. The percentage of B was increased linearly to reach 36% at 15 min and 60% at 30 min. After that, percentage of B decreased linearly to the original composition in 5 min and remained in the initial conditions for 5 min. The wavelength of the UV detector was established at 280 nm. FA was quantified according to the external standard method using a calibration curve of the peak area against concentration of the compound.

2.7 Physicochemical analysis

2.7.1 pH, syneresis and colour determinations

The pH measurements were performed using a pH meter (Crison Basic 20 +, Crison Instruments SA, Barcelona, Spain) with puncture electrode. pH measurements were taken directly on yoghurt samples in triplicate.

For syneresis determinations, 20 g of yoghurt were centrifuged at 8000 rpm and 4 ^{o}C for 10 min in a 5804 Eppendorf centrifuge (Eppendorf, Hamburg, Germany). After centrifugation, the released serum was poured off, weighed and recorded as percentage of weight to the original weight of yoghurt in triplicate.

Colour values were obtained by measuring the reflection spectrum (Minolta, CM 3600D, Tokyo, Japan). CIE Lab uniform colour space was selected to calculate colour parameters L^* (brightness), a^* (red-green), b^*(yellow-blue) using a 10° observer and D65 illuminant. The total colour differences between C and E_E yoghurts were calculated using Eq 1. Five replicates were carried out for each sample.

$$\Delta E = \sqrt{\Delta L^{*2} + \Delta a^{*2} + \Delta b^{*2}} \quad (1)$$

2.7.2 Rheological determinations

The rheological analyses were carried out on a controlled stress rheometer (RheoStress, Thermo Haake, Karlsruhe, Germany). The flow curves and the oscillatory assays were performed using concentric cylinder (6 cm diameter; 1 mm gap). The yoghurts were loaded on the inset plate and the temperature was maintained at 4 ± 0.1 °C during the tests. All trials were carried out in triplicate.

The flow curves were determined by performing shear rate sweeps from 0 to 300 s^{-1}. Three consecutive rising and falling cycles were made in order to evaluate and eliminate the effect of thixotropy. The thixotropic behaviour of the samples was evaluated by estimating the hysteresis loop area (A_{up} - A_{down}) between the upward (A_{up}) and downward (A_{down}) flow curves using the program RheoWin Data Manager (version 3.61, Thermo Haake). The experimental data obtained in the third down sweep were adjusted to the Herschel-Bulkley model for non-Newtonian fluids (Eq 2).

$$\sigma = \sigma_0 + K\gamma^n \quad (2)$$

where σ_0 is yield shear stress (Pa), K the consistency index (Pa s^n), γ the deformation rate (s^{-1}), and n the flow behaviour index (dimensionless). The yield stress value used in Herschel-Bulkley's model was previously obtained by fitting the experimental data to the Casson model (Eq 3) (Tárrega & Costell, 2007). All measurements were carried out in triplicate.

$$\sigma^{0.5} = \sigma_0^{0.5} + K\gamma^{0.5} \quad (3)$$

2.8 Determinations of microbial viability

To evaluate the effect of solid **S1** addition on the viability of lactic acid bacteria naturally present in the yoghurts (i.e. *Lactobacillus delbrueckii* ssp. *bulgaricus* and *Streptococcus thermophilus*) viable cell counts were performed in control (LF-C and FF-C) and enriched with **S1** yoghurts (LF-E_E and FF-E_E). 1 mL of yoghurt was diluted in 9 mL of 0.15% sterile buffered peptone water (Scharlau, Barcelona, Spain). The mixtures were thoroughly stirred and serial dilutions were prepared and plated on selective agar in duplicate. These selective media were Man, Rogosa, and Sharpe agar (MRS) (Scharlau, Barcelona, Spain) and 0.5% lactose M-17 media (Sigma-Aldrich, Poole, Dorset, UK) for enumeration of *L. delbrueckii* and *S. thermophilus*, respectively. The inoculated plates were incubated at 30 °C for 48 h in anaerobic conditions for the growth of *L. delbrueckii* ssp. b*ulgaricus* by introducing the plates in anaerobic jars with gas pack AnaeroGen (Oxoid, Cambridge, UK). The plates with selective media for *S. thermophilus* were incubated in aerobic conditions at 37 °C for 48 h. Results were expressed as log colony-forming units (CFU) mL^{-1}.

2.9 Statistical analysis

The differences between the samples due to the type of yoghurt, the addition of particles and the time of storage were determined by analysis of variance (ANOVA multifactorial), with a confidence level of 95% LSD ($p<0.05$). The statistical program used was Statgraphics Centurion XV (Manugistics Inc., Rockville, MD, USA).

3. Results

3.1 Support S1. Synthesis and characterization

In a first step, MCM-41 support was synthesised following well-known procedures using *N*-cetyltrimetylammonium (CTABr) as a structure director agent and tetraethylorthosilicate (TEOS) as a silica source. After removal the surfactant by calcination the starting MCM-41 support was obtained. Then, the pores of the MCM-41 support were loaded with FA. Finally, the FA-loaded support was reacted with N^1-(3-Trimethoxysilylpropyl)diethylenetriamine resulting the capped mateial **S1**.

The prepared solids were characterized according to standard techniques. **Figure 2** shows the powder X-ray diffraction (XRD) patterns of the solids MCM-41 as synthesised, MCM-41 calcined (**S0**) and the final mesoporous solid loaded with FA and functionalized with N3 (**S1**). The XRD of MCM-41 as-synthesised (curve a) shows the typical low-angle reflections of a hexagonal ordered array indexed as (1 0 0), (1 1 0), (2 0 0) and (2 1 0) Brag peaks. In curve b, corresponding to the MCM-41 calcined sample, a significant shift of the reflections in the XRD is clearly observed. This displacement is consistent with a cell contraction of ca. 5.5 Å and attributed to the condensation of silanol groups during the calcination step. The reflections of the **S1** were practically lost due to the presence of FA in the pores. However, the permanence of the (1 0 0) peak indicate that the process of pore loading with FA, and the additional functionalization with the polyamine, did not modify the typical porosity of the mesoporous MCM-41 scaffold.

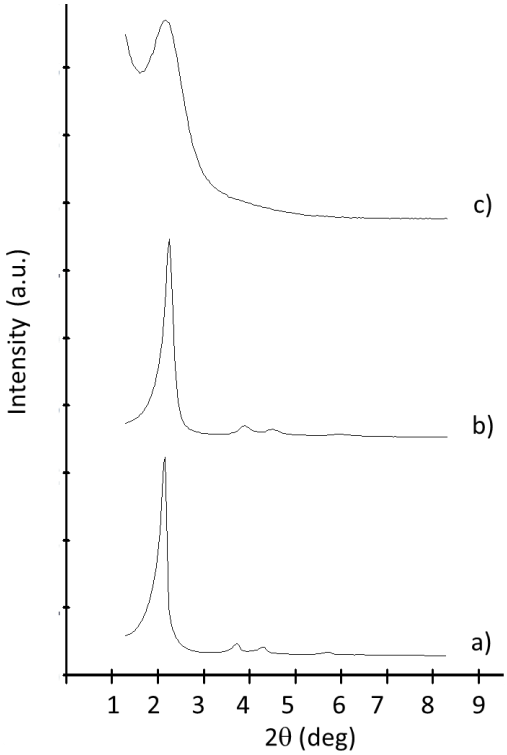

Figure 2. Powder X-ray patterns of the solids (a) MCM-41 as-synthesized, (b) MCM-41calcined **(S0)**, and (c) MCM-41 loaded with FA and functionalised with N3 (**S1**).

A morphologic analysis of both, **S0** and **S1**, was performed by TEM and FESEM studies. **Figure 3** shows that MCM-41 supports are irregular-shaped microparticles (**Fig 3a**) with porous in the range 2-3 nm (**Fig 3b**). **Figures 3c** and 3d revealed the preservation of morphology and the mesoporous structure in the final **S1** solid. The particle size was confirmed by particle size analysis. **S0** exhibited a particle size diameter (dv90) of 0.98 μm. An average particle size of 0.90 μm was observed for solid **S1**.

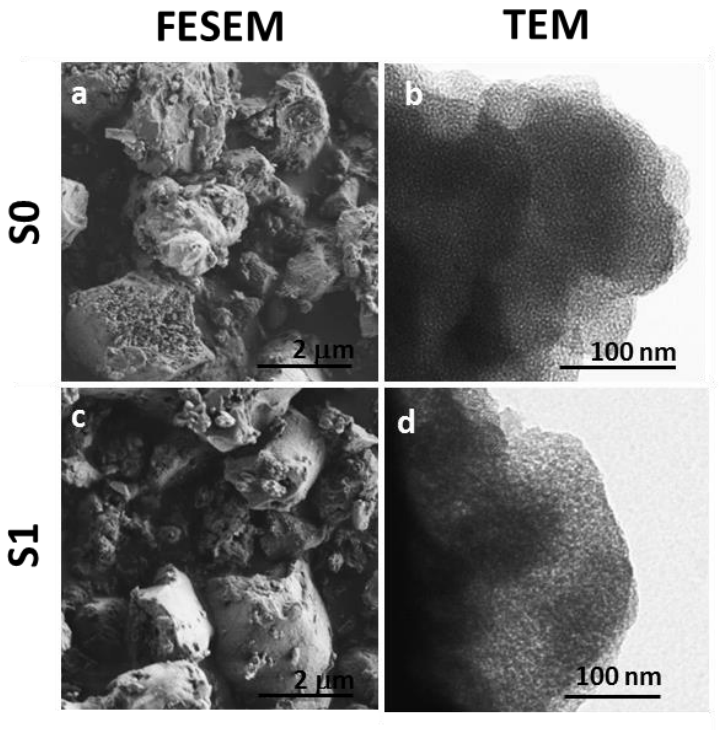

Figure 3. FESEM and TEM images of solids **S0** (a,b) and S1 (c,d).

The different prepared solids were also characterised by zeta potential determinations. **Figure 4** shows zeta potential values of **S0**, **S0** loaded with FA and the final **S1** solid. For both, **S0** and **S0** loaded with FA, zeta potential achieved negative values of ca. -40 mV. After functionalization with amines, zeta potential changed from negatively to positively values (ca. 40 mv), confirming the effect of the functionalization on the surface charge. Content of organic matter obtained from elemental and thermogravimetric analysis revealed that 1 g of **S1** contains 97 mg of FA and 63 mg of N3, confirming the efficiency of FA loading as well as N3 functionalization.

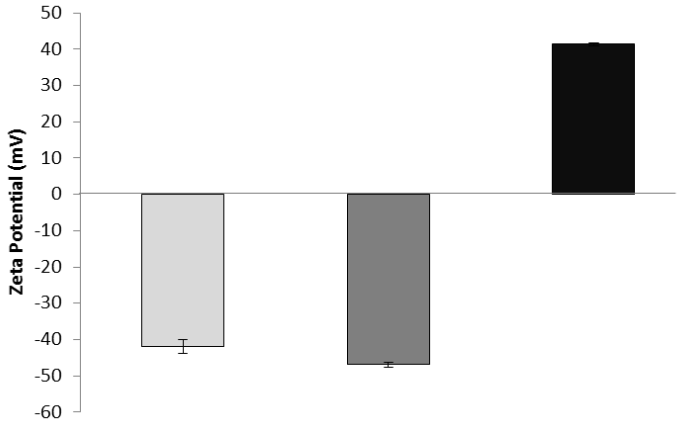

Figure 4. Zeta potential values (Mean ± SD) of **S0** (light grey), **S0** loaded with FA (dark grey) and **S1** (black).

3.2 S1 delivery profile at different pH and maximum FA delivery calculations

In order to confirm the feasibility of the FA-loaded N3-functionalised solid **S1** to modulate FA release as a function of the pH of the medium, several release experiments were carried out. FA release profiles from **S1** at different pH values (pH 2 and 4 adjusted with HCl, 4 adjusted with lactic acid and PBS at pH 7.5) are shown in **Figure 5**. At pH 2 (stomach pH) a maximum release of 1 μg mg^{-1} of FA (1.10 % of the maximum delivery) was reached at 4 h confirming that FA delivery was hindered by the effect of the low solubility of FA at acidic conditions and by the effect of the amines anchored to the surface of the silica support. At low pH, polyamines are transformed to polyammonium groups which favoured Coulombic repulsions among closely located polyammonium groups. These adopt a rigid-like conformation that block the pores and avoid the release of the vitamin (Bernardos *et al*., 2008).

When the release was performed in water adjusted to pH 4 with HCl a slight delivery of FA from the pores was observed. However it is well known that large anions are able to interact with the protonated polyamines forming strong complexes which increased pore blockage and enhanced the inhibition of the cargo release (Casasús *et al.*, 2008). Having this in mind a release assay from **S1** was also performed in water solution adjusted at pH 4 with lactic acid. In these conditions, delivery was almost zero (ca. 2%). This experiment confirmed that the gate-like superstructure based in polyamine/polyammonium groups was additionally closed by a cooperative effect of pH and the presence in the solution of bulky anions such as lactate (Bernardos *et al.*, 2008).

At pH 7.5 a sustained delivery of FA was achieved in the first 2 h. The amount released in these conditions (i.e. 94 $\mu g\ mg^{-1}$) was considered 100% of the FA that could be released from **S1**. The mechanism that allows this sustained release of FA from **S1** at neutral pH has been previously described by Pérez-Esteve *et al.* (2015). At pH 7.5 amines are less protonated and Coulombic repulsion between them and affinity for anions is significantly reduced. The overall effect results in a less effective pore blockage and in a FA delivery. On the other hand, it is known that at neutral pH, FA increases its solubility and this helps its delivery from the pores (Pérez-Esteve *et al.*, 2015).

This overall behaviour of FA release from **S1** as a function of pH would modulate the bioavailability of FA along the digestive tract. Under yoghurt and stomach conditions (acidic pH) amines are protonated preventing delivery of the vitamin. However when the yoghurt reach the intestine, molecular gates would open by effect of pH changes and FA would escape from **S1** in a sustained manner throughout the intestinal tract avoiding peaks of FA concentration. This mechanism would protect FA from the harsh conditions of the stomach, yet would favour a controlled release in the intestine.

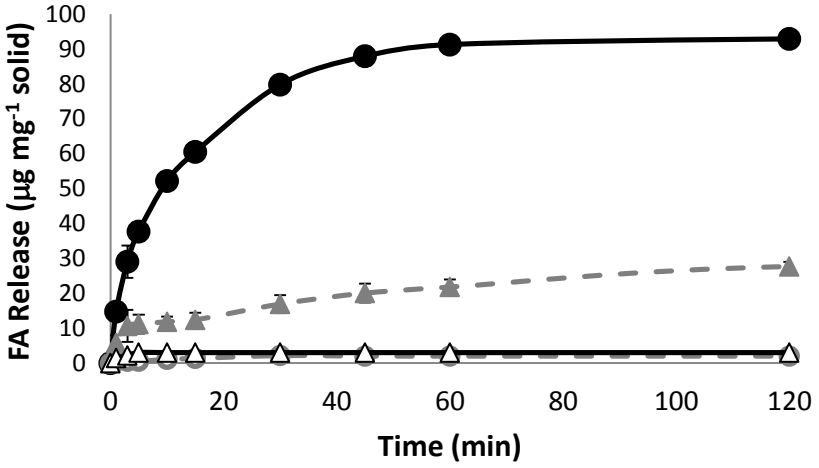

Figure 5. Release profiles of **S1** in water adjusted at pH 2 with HCl (- -o- -), at pH 4 with HCl (- -▲- -), at pH 4 with lactic acid (—**Δ**—) and PBS at pH 7.5 (—●—). Values are Means ± SD. n=3

The maximum amount of FA released from **S1** was calculated from the release profile at pH 7.5 (**Fig 5**) via the determination of FA concentration after reaching maximum delivery (4 h). At this time, 1 mg of solid **S1** releases 94 µg of FA. In USA, the DRI for FA is stablished in 400 µg folate day^{-1} in adults and 600 µg folate per day in pregnant woman (USDA, 2010). In Europe, the European Food Safety Authority (EFSA) recommends a daily intake of 200-400 µg folate per day for adults and additional 400 µg folate per day in pregnant woman (ESFA, 2009). Taking into account that the bioavailability of synthetic FA is approximately twice that of folate found in food, the dietary folate equivalent (DFE) establishes the relation between dietary folate and FA from supplements. One DFE is defined as 1 µg of dietary folate, 0.6 µg of FA supplement, or 0.5 µg of FA taken without food (Suitor & Bailey, 2000). Therefore to provide 360 µg FA (i.e. 600 µg of DFE) in only one standard portion of yoghurt (125 g), 3.8 mg of **S1** should be added to prepare enriched yoghurts with FA with controlled bioaccessiblity.

3.3 Bioaccessibility of FA during yoghurts in in vitro digestion

In order to evaluate the effect of FA encapsulation to control the bioaccessibility of the vitamin, the release behaviour of yoghurts enriched with free FA (LF-E_F and FF- E_F) were compared with yoghurts enriched with an equivalent amount of FA encapsulated in **S1** (LF-E_E and FF- E_E).

Figure 6 shows that in the four samples a very low amount of FA was detected during the first two hours of digestion, corresponding with the oral and stomach phase. The oral phase is too short to solubilize and extract FA entrapped in the yoghurt matrix. This explains why FA was no detected in saliva neither in yoghurts containing free nor encapsulated FA. Besides during the gastric phase FA remained mainly insoluble and thus bioinaccessible (Pérez-Esteve *et al.*, 2015).

After the addition of the intestinal juices (2 h), two different release behaviours were observed. Yoghurts containing free FA showed a fast increase of the bioaccessibility after the addition of intestinal juices that would provoke absorptions peaks. In contrast, samples containing encapsulated FA in **S1** exhibited a sustained release of the vitamin along the digestion time. This modulation of the bioaccessibility would control the bioavailability, favouring the metabolization of FA before reaching the bloodstream. This experiment confirms the suitability of the **S1** for modulating the bioaccessibility of FA in real food matrixes. The mechanism of action of the novel smart delivery system is schematised in **Figure 7**.

No differences on FA bioaccessibility between LF and FF yoghurts were observed. Moreover, no statistically significant differences were found in the release behaviour of yoghurts with different storage times, confirming the stability of solid **S1** in the yoghurt matrix.

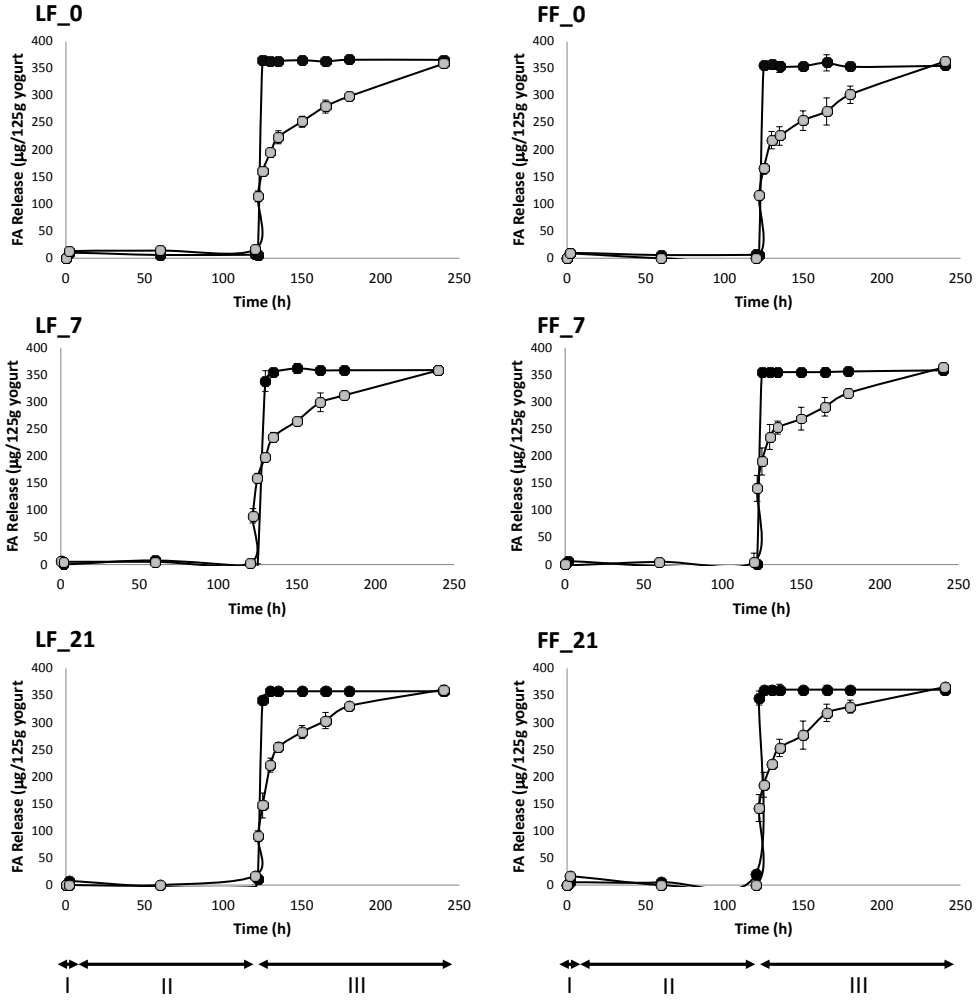

Figure 6. Bioaccessibility of FA during an *in vitro* digestion procedure in low-fat (LF) and full-fat yoghurts (FF) at 0, 7 and 21 days of storage. E_F yoghurts are represented with black dots; E_E yoghurts with grey dots. I: oral phase; II: gastric phase; III: small intestine phase. n=3

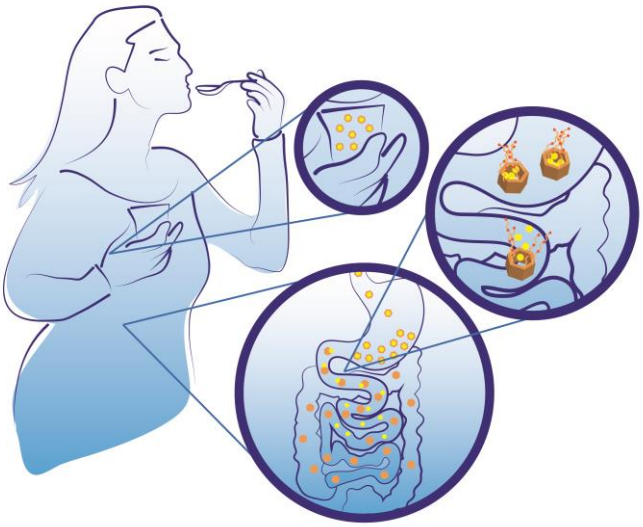

Figure 7. Illustration of the mechanism of action of the smart delivery system **S1** when included in yoghurts and ingested

3.4 Effect of S1 addition on the physicochemical properties of yoghurt during refrigerated storage

The effect of the incorporation of **S1** on the physicochemical properties of yoghurts was also studied. pH, syneresis, colour and rheology values of yoghurts containing **S1** (LF-E_E and FF-E_E) were compared with those of yoghurts without gated mesoporous particles (LF-C and FF-C).

3.4.1 pH, syneresis and colour

pH values ranged from 4.08 to 4.35 in LF yoghurts and from 4.2 to 4.5 in FF yoghurts along the 21 days of refrigerated storage. These values are similar to those reported by other authors for LF and FF yoghurts (Al-Sheraji *et al.*, 2012; Cruz *et al.*, 2013) and suggest a poor post-acidification process, a desirable characteristic in a modern yoghurt industry. This fact is related to the choice of the metabolism of lactic culture used (Cruz *et al.*, 2013). The addition of **S1** did not affect pH in neither of both LF or FF yoghurts.

Syneresis values of different yoghurts are shown in **Figure 8.** C samples exhibited syneresis values of ca. 47 and ca. 52 for LF and FF yoghurts, respectively. These values are similar to those reported by other authors (Brennan & Tudorica, 2008; Ramirez-Sucre & Vélez-Ruiz, 2013). For each type of yoghurt, the lowest syneresis values were found in samples analysed on the day 0 of storage and then increased throughout the storage process. It means that storage caused a loss of the three dimensional network of protein in both types of yoghurt. The increase of syneresis as a consequence of storage was lower in FF yoghurts. It was probably due to the presence of fat globules that difficult casein aggregation and prevents contraction and reorganization of the three dimensional network of protein. The result is a higher capacity of FF yoghurts to retain serum in the gel structure (Fox *et al*., 2000). No significant differences between C and E_E samples at each of the storage times were found, suggesting that the presence of **S1** support do not have any influence on synereris at the concentrations employed.

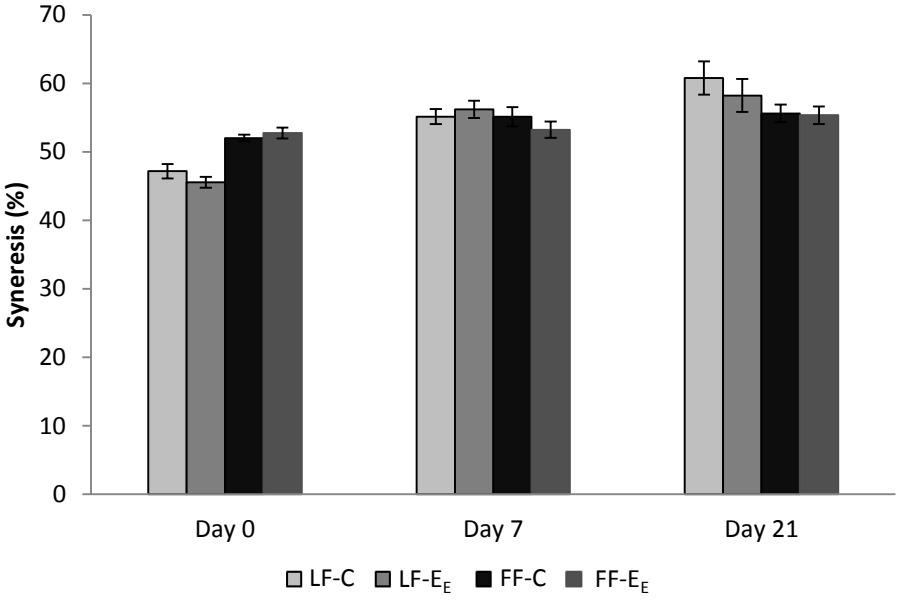

Figure 8. Syneresis values (mean ± SD) of low-fat control yoghurts (LF-C), low-fat yoghurts enriched with FA encapsulated in **S1** support (LF-E_E), full-fat control yoghurts (FF-C) and full-fat yoghurts enriched with FA encapsulated in **S1** support (FF-E_E).

The colour coordinates (L^*, a^*, b^*) of control and enriched yoghurts along a storage period of 21 days are shown in **Table 2**. Both control samples (LF-C and FF-C) showed high luminosity (L*≈92) and a yellowish hue (h°≈100), being these features characteristic of fermented milks (Ramirez-Sucre & Vélez-Ruiz, 2013). This similarity between the two types of yoghurts may be due to the trend in the industry to bring the whole products and those with reduced calories (low-fat) the same sensory properties. Despite the similarities, **Table 4** shows how FF yoghurts exhibited significantly higher values for all colour coordinates than LF yoghurts. **Table 2** also shows colour variations due to the FA enrichment through **S1** incorporation. As it can be seen, despite fortification and storage influenced significantly some colour parameters (**Table 4**), the total colour differences among C and E_E samples for the same type of yoghurt (LF or FF) and the same day of storage (0, 7 or 21) are lower than ΔE=0.5. Having in mind that ΔE values between 0-1 normally mean invisible differences for the human eye, it can be concluded that the enrichment of yoghurts with **S1** did not alter the visual perception of the colour.

3.4.2 Rheological properties

Considering the rheological behaviour described by the flow curves, all the samples showed non-Newtonian behaviour and time dependence (thixotropy). Such behaviour is in agreement with previous studies by other authors in semisolid yoghurts and dairy desserts (Tárrega & Costell, 2007, Cruz *et al.*, 2013). Nevertheless, the rheograms of control yoghurts with different fat content (LF-C and FF-C) were different, indicating the importance of fat in the rheological behaviour of a sample (Ramirez-Sucre &Vélez-Ruiz, 2013).

All the analysed samples showed an hysteresis area between the curves up and down in one cycle. FF-C yoghurts showed greater hysteresis area than LF-C yoghurts (data not shown). This hysteresis area is related to the degree of breakdown of the structure occurred during shearing.

From the third up and down cycles the hysteresis area decreased dramatically and it was considered that from this moment rheological behaviour was independent of time. Thus, up curves of the third cycle were fitted to Herschel-Bulkley model. R^2 values were greater than 0.99 in all samples confirming the adequacy of the model to model the rheological behaviour.

Table 3 shows rheological parameters obtained using the Herschel-Bulkley model for control and enriched yoghurts at 0, 7 and 28 days of refrigerated storage. Values of the flow behaviour index (n) clearly indicates that both kind of control yoghurts (LF-C and FF-C) have a pseudoplastic behaviour ($0<n<1$). These results are in agreement with previous studies carried out by Ramirez-Sucre & Vélez Ruiz (2013). The flow index was statistically significantly higher in FF-C yoghurts than LF-C yoghurts. Neither the yoghurt fortification nor the storage period had an influence in this parameter (**Table 4**).

All the samples exhibited yield stress (σ_o), suggesting that all the samples had an initial resistance to flow (**Table 3**). Values of yield stress were higher in LF-C yoghurts. For both types of yoghurt, LF-C and FF-C, σ_o values decreased significantly along the storage period. However, no significant differences were observed between control and enriched yoghurts.

The consistency index was higher in case of LF-C yoghurts. Again, for all yoghurt types, k decreased significantly along the storage period and no significant differences were observed between control and enriched yoghurts.

According to these results, addition of **S1**, to low fat and full fat yoghurt, did not provoke any modification of the rheological properties.

Table 2. Colour coordinates and total colour differences of control and enriched yogurts at 0, 7 and 28 days of refrigerated storage.

Sample	L*			a*			b*			ΔE		
	0	7	21	0	7	21	0	7	21	0	7	21
LF-C	91.6±0.6	91.9±0.2	92.0±0.3	-2.48±0.06	-2.64±0.03	-2.64±0.02	9.9±0.2	10.9±0.1	11.0±0.1	-	-	-
LF-E_E	91.7±0.3	91.8±0.2	92.0±0.3	-2.46±0.04	-2.58±0.05	-2.61±0.02	10.4±0.4	11.0±0.1	11.2±0.1	0.40±0.08	0.11±0.06	0.14±0.07
FF-C	92.6±0.2	92.7±0.2	92.6±0.2	-1.67±0.02	1.61±0.05	-1.66±0.03	10.34±0.07	10.7±0.1	11.0±0.4	-	-	-
FF-E_E	92.5±0.2	92.6±0.2	92.5±0.1	-1.61±0.05	-1.61±0.04	-1.61±0.01	10.5±0.2	10.8±0.1	10.94±0.07	0.21±0.04	0.16±0.07	0.12±0.02

Mean values (± standard deviation). L^*=brightness. a^*=red-green. b^*=yellow-blue. ΔE=Total colour difference

Table 3. Rheological parameters obtained using the Herschel-Bulkley model for control and enriched yogurts at 0, 7 and 28 days of refrigerated storage.

Sample	σ_o (Pa)			K (Pa s^n)			n		
	0	7	21	0	7	21	0	7	21
LF-C	9.5±0.4	7.9±0.3	7.9±0.2	1.15±0.04	1.00±0.03	1.00±0.02	0.647±0.002	0.656±0.002	0.657±0.002
LF-E_E	8.9±0.3	8.22±0.06	8.1±0.8	1.09±0.04	1.022±0.006	1.07±0.08	0.651±0.001	0.655±0.001	0.654±0.001
FF-C	3.9±0.5	3.8±0.7	3.4±0.9	0.71±0.06	0.69±0.06	0.62±0.09	0.76±0.01	0.74±0.03	0.77±0.02
FF-E_E	4.2±0.1	3.6±0.1	3.5±0.9	0.71±0.01	0.66±0.05	0.642±0.009	0.758±0.003	0.75±0.03	0.75±0.02

Mean ± standard deviation. σ_o = yield stress, k = consistency index, n = flow behavior index.

3.5 Effect of S1 addition on viable counts on Lactobacillus delbrueckii ssp. bulgaricus and Streptococcus thermophilus during refrigerated storage

Initial count of *L. delbrueckii* ssp. *bulgaricus* and *S. thermophiles* were 9.10 ± 0.03 and 9.07 ± 0.09 log CFU g^{-1} in LF-C yoghurt and 9.10 ± 0.03 and 9.11 ± 0.11 log CFU g^{-1} in FF-C yoghurt (**Fig 9**) with no significant variability between both types of samples. These values are in agreement with those reported by other authors (Ibrahim & Carr, 2006*;* Al-Sheraji *et al., 2012*). It is generally recommended that yoghurt or fermented milk should contain at least 10^8 CFU per serving (EFSA, 2010), which represents approximately one million viable cells per gram at the time of consumption. Initial microbial counts in all samples were in line with this recommendation. We did not find significant differences due to **S1** addition to samples indicating that **S1** do not affect microbial growth.

Recent studies suggest that biocompatibility of mesoporous silica with human cells and tissues is very high. Moreover it has been reported that toxicity of mesoporous silica is minimized or eliminated by using microparticles and by functionalizing them with certain organic molecules (He *et al.*, 2012; Tang, Li & Chen, 2012). Nevertheless, as far as we know, there are few studies evaluating the biocompatibility of mesoporous silica particles with acid lactic bacteria (LAB).

In yoghurt and fermented milks it is important not only to control initial LAB population but also to maintain these numbers. In this sense, it is essential to follow viability during yoghurt storage. To specifically analyse the effect of **S1** addition on the survival of LAB during storage process, the viability of both microorganisms, *L. delbrueckii* ssp. *bulgaricus* and *S. thermophiles,* in **S1** free yoghurts (LF-C and FF-C) and in **S1** containing yoghurts (LF-E_E and FF-E_E) was followed during 21 of cold storage. As it can be observed, the number of CFU g^{-1} decreased significantly ($p<0.001$ **Table 4**) along the storage in both yoghurt types (**Fig 7a** and **7b**); however, this effect was independent of the presence or absence of **S1** (**Table 4**). Thus, **S1** support is biocompatible with the yoghurt microflora at the concentrations needed to provide the 100% of the DRI of FA.

These results confirm that the **S1** do not have any effect in the viable LAB population. Microbial growth continues during storage and the number of viable microorganisms is a critical factor in the final product in terms of the nutritional health benefits attributed to yoghurt starters as probiotics (EFSA, 2010). The yoghurt nutritional content, physical properties, appearance and texture are important aspects for consumer acceptability. Note that if the amount of **S1** to provide 100% of DRI did not provoke any change in viable counts, yoghurts prepared to cover 25, 50 or 75% of this DRI should not experience any affection.

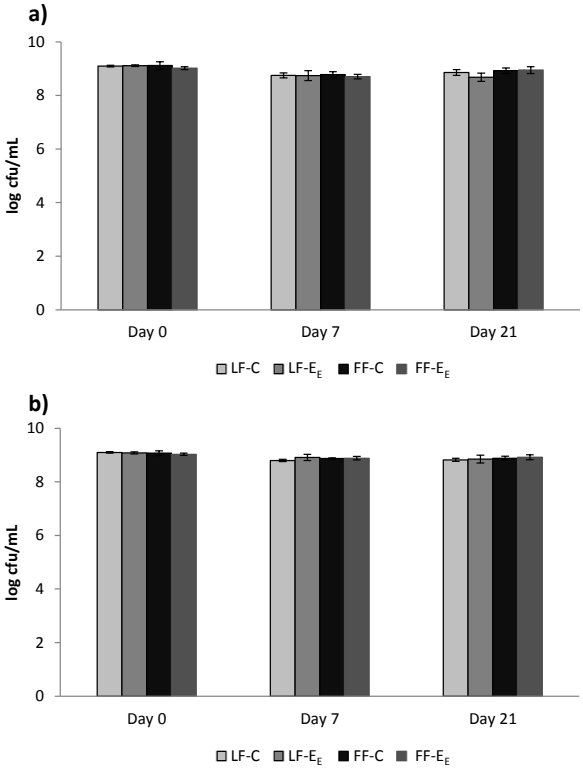

Figure 9. Viability of a) *L. delbrueckii* ssp. *bulgaricus* and b) *S. thermophilus* in control (C) and encriched (E) low-fat (LF) and full-fat (FF) yoghurts during 21 days of refrigerated storage at 4°C.

Table 4. ANOVA F-ratio for each of the parameters and its interactions.

	Main effects			Binary interations			Tertiary interactions
Parameter	**Y**	**E**	**S**	**Y*E**	**Y*S**	**E*S**	**Y*E*S**
pH	396.0***	1.83ns	539.17***	0.4168ns	0.4783ns	0.1447ns	0.8813ns
Syneresis	3.53ns	1.91ns	9.21***	0.17ns	0.83ns	0.72ns	1.62ns
L*	139.43***	0.29ns	2.86 ns	0.71ns	2.47ns	0.39ns	0.21ns
a*	1043.49***	15.53***	21.79***	0.11ns	31.46***	0.40ns	3.15*
b*	0.26ns	8.33**	99.85***	1.80ns	12.56***	2.94***	1.05ns
C*	60.92***	16.50***	18.50***	0.71ns	29.51***	1.32ns	1.51ns
h*	11265.65***	64.63***	35.04***	0.67ns	1.53ns	5.48**	1.32ns
σ_0	779.69***	0.09ns	12.38***	0.01ns	2.87ns	0.21ns	1.08ns
K	728.24***	0.46ns	15.37***	0.68ns	3.97ns	1.90ns	1.70ns
n	406.00***	0.60ns	0.88ns	0.82ns	1.47ns	0.76ns	0.64ns
V.L	1.76ns	2.64ns	38.74***	0.02ns	3.87ns	0.87ns	2.27ns
V.S.	0.63ns	1.07ns	43.34***	0.87ns	2.32ns	1.91ns	0.72ns

Y = yoghurt, E = enrichment, S = storage. σ_o = yield stress, k = consistency index, n = flow behavior index, V.L. = Viability of *Lactobacillus delbrueckii* ssp. *bulgaricus* , V.S. = Viability of *Streptococcus thermophilus.* Significance level (α): *** ($p<0.001$). ** ($p<0.01$). * ($p<0.1$). ns (no significant).

4.Conclusions

A novel preparation of FA-enriched yoghurts with controlled bioaccessibility is reported. pH-responsive mesoporous silica particles functionalised with polyamines and loaded with FA were able to modulate the release kinetics of FA during the *in vitro* digestion. Sensory analysis were not performed because mesoporous silica particles have not been yet declared as an authorised food ingredient or recognized as "Generally Recognized As Safe products" by the FDA. Nevertheless, physico-chemical characterization of enriched yoghurts with **S1** particles, suggest that **S1** addition did not have any impact neither in pH, syneresis, colour or rheology. Moreover, the addition of **S1** to yoghurts did not have any significant impact on the survival of starting cultures of yoghurts during refrigerated storage. We believe that the results obtained in this work should be easily extrapolated to other bioactive molecules and put forward that encapsulation of bioactive components in mesoporous silica carriers opens new opportunities for the development of novel functional dairy products with added value.

Acknowledgements

Authors gratefully acknowledge the financial support from the Ministerio de Economía y Competitividad (Projects AGL2012-39597-C02-01, AGL2012-39597-C02-02 and MAT2012-38429-C04-01) and the Generalitat Valenciana (project PROMETEO/2009/016). E.P.E. and M.R.R. are grateful to the Ministerio de Ciencia e Innovación for their grants (AP2008-00620, AP2010-4369). Electron Microscopy Service of the UPV is also acknowledged.

References

Achanta, K., Aryana, K. J., & Boeneke, C. A. (2006) Fat free plain set yogurts fortified with various minerals. *LWT Food Science and Technology, 40*, 424-429.

Al-Sheraji, S.H., Ismail, A., Manap, M.Y., Mustafa, S., & Yusof, R.M. (2012) Viability and activity of bifidobacteria during refrigerated storage of yoghurt containing Mangifera pajang fibrous polysaccharides. *Journal of Food Science, 77*, M624-630.

Bernardos, A., Aznar, E., Coll, C., Martínez-Mañez, R., Barat, JM., Marcos, M.D., Sancenón, F., Benito, A., & Soto, J. (2008) Controlled release of vitamin B2 using mesoporous materials functionalized with amine-bearing gate-like scaffoldings. *Journal of Controlled Release, 131*, 181-189.

Brennan C., & Tudorica. C.M (2008) Carbohydrate-based fat replacers in the modification of the rheological, textural and sensory quality of yoghurt: comparative study of the utilisation of barley beta-glucan, guar gum and inulin. *International Journal of Food Science & Technology, 43,* 824-833.

Casasús, R., Climent, E., Marcos, M.D., Martínez-Mañez, R., Sancenón, F., Soto, J., Amoros, P., Cano, J., & Ruiz, E. (2008) Dual Aperture Control on pH- and Anion-Driven Supramolecular Nanoscopic Hybrid Gate-like Ensembles. *Journal of the American Chemical Society, 130,* 1903-1917.

Choi, S.W., & Mason, J.B. (2002) Folate status: effects on pathways of colorectal carcinogenesis. *Journal of Nutrition, 132*, 2413S-2418S.

Clarke, R., Smith, A. D., Jobst, K. A., Refsum, H., Sutton, L. &. Ueland, P.M. (1998) Folate, vitamin B12 and serum total homocysteine levels in confirmed alzheimer disease. *Archives of neurology, 55,* 1449-1455.

Cruz, A.G., Cavalcanti, R.N., Guerreiro, L.M.R., Sant'Ana, A.S., Nogueira, L.C., Oliveira, C.A.F., Deliza, R., Cunha, R.L., Faria, J.A.F., & Bolini, H.M.A. (2013) Developing a prebiotic yogurt: Rheological, physic-chemical and microbiological aspects and adequacy of survival analysis methodology. *Journal of food engineering, 114,* 323-330.

Eichholzer, M., Tonz, O., & Zimmermann, R. (2006) Folic acid: a public-health challenge. *Lancet, 367,* 1352-1361.

Estrada, J.D., Boeneke, C., Bechtel, P., & Sathivel, S. (2011) Developing a strawberry yogurt fortified with marine fish oil. *Journal of Dairy Science, 94,* 5760-5769.

European Food and Safety Agency (EFSA) ESCO report prepared by the EFSA Scientific Cooperation Working Group on Analysis of Risks and Benefits of Fortification of Food with Folic Acid. [accessed on January 30, 2015]. Available online: http://www.efsa.europa.eu/en/scdocs/scdoc/3e.htm.

EFSA Panel on Dietetic Products, Nutrition and Allergies (NDA); Scientific Opinion on the substantiation of health claims related to Yoghurt cultures and improving lactose digestion (ID 1143, 2976) pursuant to Article 13(1) of Regulation (EC) No 1924/2006. EFSA Journal 2010;8(10):1763. [18 pp.]. doi:10.2903/j.efsa.2010.1763. Available online: www.efsa.europa.eu/efsajournal.htm

Food and Agriculture Organization of the United Nations (FAO). Milk and dairy products in human nutrition. Rome, 2013.

Fox, P. F., McSweeney, P. L. H., Cogan, T. M., & Guinee T. P., 2000, Fundamentas of Cheese Science. (1st ed.). New York: Springer

Hamam, F., & Al-Remawi, M. (2014) Novel delivery system of curcumin through transdermal route using sub-micronized particles composed of mesoporous silica and oleic acid. *Journal of Functional Foods, 8,* 87-99.

He, C., Yin, L., Tang, C., & Yin, C. (2012) Size-dependent absorption mechanism of polymeric nanoparticles for oral delivery of protein drugs. *Biomaterials, 33*, 8569-8578.

Hoag, S.W., Ramachandruni, H. & Shangraw R.F. (1997) Failure of prescription prenatal vitamin products to meet USP standards for folic acid dissolution. *Journal of the American Pharmaceutical Association, 37*, 397-400.

Ibrahim, S.A., & Carr J.P. (2006) Viability of bifidobacteria in commercial yogurt products in North Carolina during refrigerated storage. International Journal of Dairy Technology, 59, 272-277

Lucock M. (2000) Folic Acid: Nutritional biochemistry, molecular biology and role in disease processes. *Molecular Genetics and Metabolism, 71*, 121-138.

Lucock, M., & Yates, Z. (2009) Folic acid fortification: a double-edged sword. *Current Opinion in Clinical Nutrition & Metabolic Care, 12*, 555-564.

Pérez-Esteve, E., Fuentes, A., Coll, C., Acosta, C., Bernardos, A., Amorós, P., Marcos, M.D., Sancenón, F., Martínez-Máñez, R., & Barat, J.M. (2014) Modulation of folic acid bioaccesibility by encapsulation in pH-responsive gated mesoporous silica particles. *Microporous & Mesoporous Materials, 15*, 124-132.

Perna, A., Intaglietta, I., Simonetti, A., Gambacorta, E. (2014) Antioxidant activity of yogurt made from milk characterized by different casein haplotypes and fortified with chestnut and sulla honeys. *Journal of Dairy Science, 97*, 6662-6670.

Pitkin, R.M. (2007) Folate and neural tube defects. *The American Journal of Clinical Nutrition, 85*, 285S-288S.

Ramirez-Santiago, C., Ramos-Solis, L., Lobato-Calleros, C., Peña-Valdivia, C., & Vernon-Carter, E. J. (2010). Enrichment of stirred yogurt with soluble dietary fiber from Pachyrhizus erosus L. urban: effect on syneresis, microstructure and rheological properties. *Journal of Food Engineering, 101*, 229-235.

Ramírez-Sucre, M.O., & Vélez-Ruiz J.F. (2013) Physicochemical, rheological and stability characterization of a caramel flavored yogurt. *LWT - Food Science and Technology, 51*, 233-241.

Sculthorpe, N.F., Davies, B., Ashton, T., Allison, S., McGuire, D.N & Malhi, J.S (2001) Commercially available folic acid supplements and their compliance with the British Pharmacopoeia test for dissolution. *Journal of Public Health Medicine, 23*, 195-197.

Stover P. J. (2004) Physiology of Folate and Vitamin B12 in health and disease. *Nutrition Reviews, 62*, 3-12.

Suitor, C.W., & Bailey, L.B. (2000) Dietary folate equivalents: interpretation and application. *Journal of the American Dietetic Association*, 100, 88-94.

Tang, F., Li L., & Chen, D. (2012) Mesoporous silica nanoparticles: Synthesis, biocompatibility and drug delivery. *Advanced Materials*, 24, 1504-1534.

Tripathi, M.K., Giri, S.K. (2014) Probiotic functional foods: Survival of probiotics during processing and storage. *Journal of functional foods*, 9, 225-241.

Tárrega, A., & Costell, E. (2007) Colour and consistency of semi-solid dairy desserts: Instrumental and sensory measurements. *Journal of Food* Engineering, 78(2), 655-661.

United States Department of Agriculture (USDA) (2010) Dietary Guidelines for Americans (7th ed.). Washington. DC: Government Printing Office.

Younis, I. R., Stamatakis, M. K., Callery, P. S., &. Meyer-Stout, P. J. (2009): Influence of pH on the dissolution of folic acid supplements. *International Journal of Pharmaceutics, 367*, 97-102.

Vélez-Ruiz, J., Hernandez-Carranza, P., & Sosa-Morales, M. (2013) Physicochemical and flow properties of low-fat yogurt fortified with calcium and fibre. *Journal of Food Processing and Preservation, 37*, 210-221.

Wang, H., Troy, L.M., Rogers, G.T., Fox, C.S., McKeown, N.M., Meigs, J.B., Jacques, P.F. (2014) Longitudinal association between dairy consumption and changes of body weight and waist circumference: The Framingham Heart Study. *International Journal of Obesity, 38*, 299-305.

5. GENERAL DISCUSSION

The general objective of the present PhD thesis was to design, fabricate and evaluate different porous silica supports, capped with molecular gates responsive to changes in pH, to act as smart delivery systems capable of modulating the bioaccessibility of folic acid (FA) during a digestion procedure when incorporated into food matrices. The findings of all the studies carried out to assess this general objective have been discussed in detail in one review paper and in five original research papers. They all pursue the same ultimate goal. However, being divided into independent articles can lead to the thread of the argument being lost. Therefore, this section aims to holistically and comprehensively discuss all the results obtained in this thesis.

FA is an essential vitamin for numerous bodily functions and is especially indispensable in pregnancy. Although there is irrefutable evidence for the benefits of FA supplementation, recent studies have suggested that massive exposure to high bioavailable FA is a double-edged sword. Thus controlling FA dosage and modulation of FA bioavailability (e.g. by adjusting its bioaccessibility along the gastrointestinal tract) are apparently vital for maintaining positive effects of fortification, while avoiding massive exposure-related problems.

Mesoporous silica materials have proved remarkably potential in the design of efficient smart delivery systems for biomedical, agriculture and food sciences. The surface of MSPs presents a high concentration of structural defects in the form of silanol (Si-OH) groups, which can easily react with trialkoxysilane derivatives to allow the possibility of generating organic–inorganic hybrid materials. One appealing concept in this area is the development of “molecular gates”. The gastrointestinal tract (GIT) offers a wide variety of stimuli that can be used to design capped MSPs for controlled release purposes triggered by digestive stimuli. Specifically, changes in pH along the GIT seem an easy way to trigger FA release along the GIT.

An extensive review of the possibilities of mesoporous silica particles for designing smart delivery systems is provided in the **Introduction**. The human gastrointestinal tract offers many possibilities for developing controlled delivery systems in response to digestive trigger stimuli, such as pH, ionic strength, redox potential or enzyme activity. Controlled release in the stomach might be based on the action of acid-responsive molecules, and also on food components sensitive to proteases and lipases. Controlled delivery in the small intestine may combine (neutral or basic) pH with the presence of emulsifier molecules and a wide variety of digestive enzymes (saccharidases, peptidases and lipases). Finally, specific delivery in the colon should address the use of materials that respond to the action of the enzymes delivered by colonic bacteria or to the particular redox potential in the colon. The conclusions of this review were the basis used to plan the following studies of Chapters 1 and 2. Among the various possibilities of inorganic supports and molecular gates, we selected four different silica supports (MCM-41, Hollow Silica, SBA-15 and UVM-7) as inorganic carriers and pH as a triggering stimulus.

Chapter 1 examines FA encapsulation by a nutritional (or even physiological) approach. In a first step, FA was encapsulated in the commonest mesoporous silica particle (i.e. MCM-41). The efforts made in these first studies (***Article 1***) focused on optimising loading efficiency. The literature offers a wide variety of MSPs loaded with different dies or bioactive molecules. However, most works are shown as proof of concept. Thus the amount of final solid needed to accomplish the function is not that important. Contrarily in this thesis, reducing the amount of solid needed to release 100% of the RDI of FA was our priority. The more FA delivered by a unit of mass of solid, the less solid required to provide the RDI. The less solid used, the lower the cost, the less marked the toxicological effect and, thus, fewer technological problems associated with adding encapsulating systems to real matrices appear.

To ensure that folic acid is encapsulated in the voids of different silica supports, molecular dynamics calculations on FA were done. On a larger dimension, FA exhibited a length of 1.45 nm, whereas the calculated volume was 1.16 nm^3. These calculations were used to determine the total theoretical amount of vitamin that could be encapsulated in all the different silica supports employed in ***Articles 1*** and ***2***.

Having proved the theoretical feasibility of FA to be entrapped in the voids of MCM-41 (pore size 2.5 nm and pore volume 0.9 $cm^3\ g^{-1}$), different loading conditions were tested. The results showed that the best loading efficiency was achieved by an impregnation procedure. Besides the loading conditions, the subsequent functionalisation method with the molecular gate seemed important to avoid pore emptying in this step. According to the results found in these sections, the most efficient conditions to load FA in MCM-41 were impregnation of the solid with the FA dissolved in PBS (10 mg mL^{-1}) in 3 cycles (0.5 mL per cycle) and functionalising the solid in acetic solution media.

In order to evaluate the efficacy of *N*^{1}-(3-Trimethoxysilylpropyl)diethylenetriamine (N3) as a molecular gate able to control FA release according to pH, two different solids with and without N3 anchored to the outer surface of the solid were prepared. A comparison of the delivery kinetics from both solids at two different pH values led to the conclusion that the bare solid was able to hinder FA release, but not very efficiently at an acid pH given the lack of solubility of FA under acidic conditions, but could deliver its content very quickly at pH 7.5 given the solubilisation of FA. In contrast, the solid that contained the molecular gate was tightly capped at pH 2 and displayed sustained delivery when pH was switched to 7.5. This confirms the efficacy of amines to control the transport of mass from support voids according to pH.

In another step, the efficiency of the developed smart delivery system, based on FA encapsulated in an MCM-41 support functionalised with amines to modulate the bioaccessibility of the vitamin in a more real context, was evaluated by simulating a human digestion procedure. The FA delivery results obtained under these conditions confirmed that vitamin release was hindered during the simulated pass through the stomach. In contrast, after adding the simulated intestinal fluid, FA delivery increased progressively to a maximum value of 94 μg of FA mg^{-1} of solid at 4 h of digestion. The most important point was that 1 mg of solid BB3, the release of ca. 95 mg of FA during the whole simulated digestion process was possible. This means that higher recommended dietary intakes in human nutrition, established for pregnant woman as 600 μg per day of folates or 360 μg of synthetic PGA (1 μg of dietary folate equivalent = 0.6 μg of folic acid), could be achieved by orally administering only ca. 4 mg of the smart delivery system, which is a remarkably small amount.

Bearing in mind that by tuning the synthesis conditions of mesoporous silica particles, different silica supports with various particle sizes, shapes and porous structures can be obtained. The main objective of ***Article 2*** was to compare different silica supports (MCM-41, SBA-15, UVM-7 and Hollow Silica Shells) in FA loading efficiency and release kinetics terms. In all cases, the capping system consisted in polyamines (N3) anchored to the external surface of silica supports.

The four capped materials were capable of hindering FA delivery at a low pH (i.e. stomach), whereas FA release was found at a neutral pH (i.e. small intestine). Data from the release kinetics at pH 7.5 were fitted to the Higuchi model to obtain Higuchi constants (k_H). This analysis showed that k_H increased in this order: MCM-41 < UVM-7 < SBA-15 < Hollow Silica Shells: which indicates that MCM-41 was the inorganic support that reached the most sustained delivery and was, thus, the most appropriate one to modulate FA bioaccessibility.

The complete characterisation of hybrid materials was carried out to correlate the physical features of the supports with their loading capacity and release kinetics. Bearing in mind that Hollow Silica is the support with the highest k_H, which coincides with the larger cavity, and that SBA-15, UVM-7, and MCM-41 were ordered according to their pore size, the pore size effect seems important for modulating the release kinetics of FA from different supports. The bigger the pore diameter, the easier the solution enters voids (or the main cavity for H). Thus there are fewer diffusional problems of FA escaping from the entrapping support.

In this study, the cell viability assays on HCT116, HEPG2, HK2 and HeLa cells indicated that all the cell lines exhibited a high level of cell viability (ca. 100% cell proliferation) after 24 h upon treatment with the four FA-loaded capped silica supports, with a concentration of up to 200 $\mu g\ mL^{-1}$. Although this study has shown that the developed particles did not cause acute toxicity in cell cultures, further research is necessary to evaluate the more extensive chronic toxicity of these studies.

Beyond its loading efficiency, and its capacity to modulate the bioaccessibility or biocompatibility, the suitability of MSPs to be used in oral controlled release in *in vivo* applications relies on the chemical stability of the supports through the whole digestive tube. It is well-known that silica can be biodegraded into silicic acids, including monomeric silicic acid and various polysilicic acids at different degrees of polymerisation. Yet as far as we know, hardly any attempts have been made to understand the degradation of MSPs in biologic fluids. Based, therefore, on the objective of understanding the effect of saliva, gastric or intestinal fluids on the stability of different porous materials, the experiments reported in ***Article 3*** were run.

In this work, apart from evaluating the stability of the particles used in previous experiments (MCM-41 micro, SBA-15, UVM-7), the nanoparticulated MCM-41 support was included. MCM-41 micro and MCM-41 nano share the same porous structure, but their morphology and size differ. The comparison of both

particles enabled the evaluation of the influence of particle size on greater or lesser degradation tendency. The hollow silica particles were not included because it was a commercial particle that proved unaffordable at the time this work was completed.

The results showed that bare MCM-41 microparticulated and SBA-15 were very stable against degradation. However, the structure of the supports based on nanoparticles (i.e. MCM-41 nanoparticulated and UVM-7) only slightly degraded, while functionalisation with N3 resulted in greater particle stability in all cases.

To conclude the first chapter, it can be stated that MCM-41, Hollow Silica, UVM-7 and SBA-15 loaded with FA and functionalised with amines (N3) exhibited good properties for the encapsulation and controlled release of FA. Specifically, all the designed supports presented good properties to develop smart delivery systems: a) they all exhibited good loading capacity; b) all the supports were able to hinder FA release at an acid pH (i.e. in the stomach) and to efficiently deliver the cargo at a neutral pH (i.e. in the intestine); c) none of them exhibited non-specific toxicity; d) after functionalisation, they were all very stable against degradation.

However when comparing the release profile of the four supports, the MCM-41 capped with polyamines should be considered the support with the best capability to release FA in a more controlled manner. This sustained release is essential for modulating the bioaccessiblity of the vitamin before its absorption in the jejunum and to, thus, avoid problems related to FA absorption peaks, which lead to untransformed FA appearing in blood. By considering these results, the development of the final food product that contains FA encapsulated in MSPs (**Article 5**) was based on using MCM-41 microparticles as an encapsulating support.

Based on the results obtained in **Chapter 1**, there is very little doubt that MSP-based delivery systems open up new alternatives to food supplementation with FA. This new formulation of novel functional foods also offers novel strategies for the food industry at the same time. Yet before proposing foods that contain MSPs as novel foods, the influence of adding supports on the physico-chemical properties of the final food should be evaluated. The general introduction of new ingredients or additives to a food matrix can affect the product's physico-chemical and sensory properties. However, a delivery system is considered suitable for a particular application if it is compatible with the food or beverage matrix that it is to be incorporated into, and when it has no adverse effects on product appearance, flavour, texture, mouth feel or shelf life. Indeed evaluating the use of MSP-based delivery systems by a technological approach was the aim of **Chapter 2** (the technological approach).

Article 4 studied the effect of adding different mesoporous silica particles (MCM-41 nano and micro, UVM-7 and SBA-15), either bare or functionalised with amines or carboxylates, on the physical properties of gelatine gels (5% w/v). The effect of incorporating different MSPs on the texture properties of gelatine gels was studied by comparing the modulus and fracture properties of the gelatine gels that contained different percentages of MSPs with those gels without particles.

The incorporation of bare MSPs had no influence on mechanical properties. However with functionalised MSPs, the strength of the gels remarkably increased and their brittleness slightly diminished. This effect was attributed to an organic layer being created on the surface of the particle, which improved the filler-matrix interaction. Turbidity of gels was also affected by the addition of all the tested MSPs, and the particles that formed smaller aggregates greatly contributed to turbidity. Given these findings, it can be stated that despite the addition of MSPs not worsening the physico-chemical properties of gels, the smaller the amount of the smart delivery system needed to provide a percentage of the RDI of a bioactive molecule, the slighter the effect on matrix properties.

Finally, the MCM-41 support was selected for the final work because MCM-41 was the support that best displayed the capacity to modulate FA delivery with time. Nor was this support affected by digestive fluids, and it was one of the supports that least affected the physico-chemical properties of the matrix. Along these lines, ***Article 5*** achieved the final thesis goal: preparing functional food enriched with FA encapsulated in a pH-responsive porous silica support capable of modulating the bioaccessibility of the vitamin along the gastrointestinal tract without altering the properties of yoghurt.

In the first part of this work, the ability of the MCM-41 microparticle loaded with FA and functionalised with amines to modulate the bioaccessibility of FA after its incorporation into two types of stirred yogurt (low-fat and full-fat) was evaluated. The results of the *in vitro* digestion procedure showed that the proposed smart delivery system was capable of inhibiting the release of FA in acidic solution at pH 2 (stomach) and of controllably releasing its contents at a neutral pH (intestine) to thus modulate bioaccessibility.

In the second part of this work, the influence of adding FA encapsulated in the MCM-41 support on the physico-chemical, rheological and lactic acid bacteria viability of these yogurts during 21-day refrigerated storage (4°C) was evaluated. The physico-chemical and microbiological assays revealed that enrichment with this support neither altered the physico-chemical properties (pH, colour, syneresis and rheology) of both types of yogurt nor caused any effect on lactic acid bacteria survival.

In conclusion, this thesis presents the design of a controlled delivery system that has been optimised specially for a food application, and includes studies into the loading optimisation, encapsulation capacity, release kinetics, toxicology assessments and evaluation of the influence of the encapsulating matrix on the properties of the food matrix. This global approach seems a suitable procedure to improve encapsulation efficiency and to ensure the compatibility of the delivery system with both the final consumer's food and organism.

6. CONCLUSIONS AND PERSPECTIVES

CONCLUSIONS AND FUTURE PERSPECTIVES

Different smart delivery systems for controlled FA release have been successfully prepared. These systems were based on using several MSPs with different morphologies and porous systems (MCM-41, Hollow Silica, SBA-15 and UVM-7) loaded with FA and functionalized with amines. A loading optimization process allowed us to obtain a system capable of delivering 100% of FA DRI with a very small amount of the delivery system (ca. 4 mg).

All the developed systems were tightly capped at pH 2 and displayed sustained FA delivery when pH was switched to 7.5. This sustained release is essential for modulating the bioaccessiblity of the vitamin before its absorption in the jejunum, and to thus avoid problems related to FA absorption peaks, which lead to untransformed FA appearing in blood.

The WST-1 cell viability assay indicated that all the cell lines exhibited a high level of cell viability (ca. 100% cell proliferation) after 24 h upon treatment with solids up to a concentration of 200 $\mu g\ mL^{-1}$. This assay suggested that the developed supports loaded with FA and functionalized with N3 were well-tolerated by cells.

Bare MCM-41 microparticulated and SBA-15 remained very stable during a digestion procedure. However, the structure of the supports based on nanoparticles (i.e. MCM-41 nanoparticulated and UVM-7) exhibited slight degradation. Nevertheless, functionalization with N3 resulted in the increased stability of particles.

The incorporation of the different MSPs into gelatine gels allowed us to conclude that bare MSPs have no influence on mechanical properties. However after the functionalization with amines, particles were able to create an organic layer on the particle surface that improved the filler-matrix interaction. This led to an in increase in Young's modulus, fracture stress and fracture strain, which was more or less pronounced depending on the kind of particle, functionalization and concentration.

Of all the supports, one stood out for showing remarkable advantages in controlling FA bioaccessiblity. Specifically, microparticulated MCM-41 capped with polyamines was the only support able to sustain cargo release for at least 1 h. Thus MCM-41 was the support selected for preparing enriched yoghurts.

MCM-41, microparticulated and loaded with FA and functionalized with polyamines, was able to modulate the release kinetics of FA after being added to two different yoghurts (low-fat and full-fat) during in vitro digestion. The physico-chemical characterization of yoghurts enriched with the particles suggested that their addition had no impact on pH, syneresis, color or rheology. Moreover, the addition of particles to yoghurts had no significant impact on the survival of the starting cultures of yoghurts during refrigerated storage.

In summary, it can be concluded that gated MSPs have the potential to act as FA-based smart delivery systems. This strategy can avoid problems related to overexposure of the vitamin, while maintaining food fortification advantages. Moreover, its addition to real food matrices did not provoke any undesired change in the physico-chemical properties. This new encapsulation approach offers new opportunities for the development of novel functional food. We also hope that the results obtained in this thesis will inspire the future design of new advanced hybrid materials for nutritional applications.

7. APPENDICES

Appendix I. Abbreviations and Acronyms

ANOVA	Analysis of variance
BET	Brunauer, Emmett and Teller Model
BJH	Barret, Joyner and Halenda Model
BPE	Bovine Pituitary Extract
C3	N^1-3-(trimethoxysilyl)propyl ethylenediamine triacetic acid trisodium salt
CFU	Colony-Forming Unit
CTAB	Hexadecyltrimethylammonium bromide
D2O	Deuterium oxide
DMEM	Dulbecco's Modified Eagle's medium
DMSO	Dimethyl sulfoxide
DSMZ	German Resource Centre for Biological Material
DNA	Deoxyribonucleic acid
DRI	Dietary Reference Intake
dv90	90th percentile of the size distribution
EGF	Epidermal Growth Factor
FA	Folic acid
FBS	Fetal Bovine Serum
FESEM	Field Emission Scanning Electron Microscopy
FF	Full Fat
FSM	Folded Sheet Mesoporous Materials
GI	Gastro Intestinal
GRAS	Generally Recognized As Safe
HCT116	Human colon carcinoma cells
HeLa	Human cervix carcinoma cells
HEPG2	Human liver carcinoma cells
HMS	Hexagonal Mesoporous Silica
HK2	Human kidney epithelial cells
^{1}H NMR	Proton nuclear magnetic resonance
HPLC	High liquid performance chromatography

IUPAC	International Union of Pure and Applied Chemistry
K_H	Higuchi constant
LF	Low Fat
LSD	Least Significant Difference
MCM	Mobil Crystalline Material
MSU	Michigan State University Material
MSPs	Mesoporous Silica Particles
N3	N^1-(3-trimethoxysilylpropyl)diethylenetriamine
NAD(P)H	Nicotinamide adenine dinucleotide phosphate
NaOD	Sodium deuteroxide
NaOH	Sodium hidroxyde
PBS	Phosphate Buffer Solution
PMOs	Periodic Mesoporous Organosilicas
RLE	Relative Loading Efficiency
RT	Room Temperature
SBA	Santa Barbara Amorphous Material
SEM	Scanning Electron Microscopy
TEAH3	Triethanolamine
TEM	Transmission Electron Microscopy
TEOS	Tetraethylorthosilicate
P123	Pluronic 123
SiO_2	Silicon Dioxide
TUD	Technische Universiteit Delft material
UVM	Universidad Valencia Material
XRD	X-ray diffraction

Appendix II. Key definitions

Bioactive compound

Compound that has an effect on a living organism, tissue or cell.

Bioactivity

Beneficial or adverse effects of a bioactive compound on living matter. Bioactivity includes events linked to how the is transported and reaches the target tissue, how it interacts with biomolecules, the metabolism or biotransformation that it may undergo, and the generation of a biomarker and the physiologic response it causes.

Bioaccessibility

Fraction of a compound that is released from its matrix in the gastrointestinal tract and thus becomes available for intestinal absorption. Bioaccessibility includes the entire sequence of events that take place during the digestive transformation of food into material that can be assimilated by the body, the absorption/assimilation into the cells of the intestinal epithelium, and lastly, the presystemic metabolism (both intestinal and hepatic).1mismo que bioactivity

Bioavailability

Fraction of a given nutrient (or bioactive compound) in a given food or diet ingested that is available for use in physiologic functions or to be stored. The therm bioavailabity is thus a sum of bioaccessibility and bioactivity.

Controlled release

Process of releasing an encapsulated component with a specific concentration-time profile at the site of action. The release process may follow a number of different profiles, including:

- Burst release: rapid release of most of the encapsulated component over a short time.
- Sustained release: prolonged release of the encapsulated component at a relatively constant rate.
- Triggered release: release of the encapsulated component in response to a specific environmental trigger (e.g., pH, ionic strength, enzyme activity, temperature).
- Targeted release: release of the encapsulated component at a specific location (e.g., mouth, stomach, small intestine, colon).

Delivery system

Formulation or system designed to encapsulate, deliver and release one or more active components after targeting specific areas of the body.

Dietary Reference Intake

Daily intake level of a nutrient that is considered to be sufficient to meet the requirements of 97-98% of healthy individuals in every demographic in the United States (where it was developed, but has since been used in other places).

Encapsulation

Process of entrapping a specific component (the “active”) within some kind of matrix (the “encapsulant”).

Folate

Generic term for a water-soluble group of B vitamins including folic acid and naturally occurring folates.

Folic acid

Synthetic folate compound used in vitamin supplements and fotified food because of tits increased stability. Folic acid , chemically pteroylglutamuic acid, consist of a pteridine ring system, p-aminobenzoic acid and one molecule of of glutamic acid.

Food fortification

The process of addition micronutrients to foodstuffs, during or after processing, to bring micronutrient levels over and above amounts in the original food product. An example is adding C vitamin to an orange juice after the pasterization process.

Food enrichment

The process of addition of micronutrients to foodstuffs, during of after processing, that were not originally in the food. An example is adding vitamin D to milk.

Functional food

Food or food ingredient that may provide a health benefit beyond the nutrients it contains.

Mesoporous materials

A mesoporous material is a material containing pores with diameters between 2 and 50 nm. Porous materials are classified into several kinds by their size. According to the International Union of Pure and Applied Chemistry (IUPAC) notation, microporous materials have pore diameters of less than 2 nm and macroporous materials have pore diameters of greater than 50 nm; the mesoporous category thus lies in the middle.

Mesoporous Silica Particle (Mesoporous Silica Support)

Partices form of silica with porous in the range from 2-50 nm recent developed by nanotechnology. The most common types of mesoporous nanoparticles are MCM-41 and SBA-15. Research continues on the particles, which have applications in catalysis, drug delivery and imaging.

Molecular gate

Nanoscopic supramolecular-based devices, attached to certain solid supports, in which mass transport can be triggered by a target external stimulus that can control the state of the gate (closed or open) at will.

Nanotechnology

Manipulation of matter on an atomic, molecular, and supramolecular scale.

Rheology

Study of the flow of matter, primarily in a liquid state, but also as 'soft solids' or solids under conditions in which they respond with plastic flow rather than deforming elastically in response to an applied force

Supplementation

Provision of nutrients either via a food ar as a tablet, capsule, syrup, or poder to boost the nutrional conten of the diet.

Appendix III. Constituents and concentrations of the various synthetic juices of the in vitro digestion model

	Saliva	Gastric juice	Duodenal juice	Bile juice
Inorganic solution	10 ml KCl 89.6 g L^{-1}	15.7 ml NaCl 175.3 g L^{-1}	40 ml NaCl 175.3 g L^{-1}	30 ml NaCl 175.3 g L^{-1}
	10 ml KSCN 20 g L^{-1}	3.0 ml NaH_2PO_4 88.8 g L^{-1}	40 ml $NaHCO_3$ 84.7 g L^{-1}	68.3 ml $NaHCO_3$ 84.7 g L^{-1}
	10 ml NaH_2PO_4 88.8 g L^{-1}	9.2 ml KCl 89.6 g L^{-1}	10 ml KH_2PO_4 8 g L^{-1}	4.2 ml KCl 89.6 g L^{-1}
	10 ml $NaSO_4$ 57 g L^{-1}	18 ml $CaCl_2 \cdot 2H_2O$ 22.2 g L^{-1}	6.3 ml KCl 89.6 g L^{-1}	150 µl HCl 37% g g^{-1}
	1.7 ml NaCl 175.3 g L^{-1}	10 ml NH_4Cl 30.6 g L^{-1}	10 ml $MgCl_2$ 5 g L^{-1}	
	20 ml $NaHCO_3$ 84.7 g L^{-1}	6.5 ml HCl 37% g g^{-1}	180 µl HCl 37% g g^{-1}	
Organic solution	8 ml urea 25 g L^{-1}	10 ml glucose 65 g L^{-1} 10 ml glucuronic acid 2 g L^{-1} 3.4 ml urea 25 g L^{-1} 10 ml glucoseamine hydrochloride 33 g L^{-1}	4 ml urea 25 g L^{-1}	10 ml urea 25 g L^{-1}
Add to mixture organic + inorganic solution	290 mg α-amylase	1 g BSA	9 ml $CaCl_2 \cdot 2H_2O$ 22.2 g L^{-1}	10 ml $CaCl_2 \cdot 2H_2O$ 22.2 g L^{-1}
	15 mg uric acid	2.5 g pepsin	1 g BSA	1.8 g BSA
	25 mg mucin	3 g mucin	9 g pancreatin 1.5 g lipase	30 g bile
pH	6.8 ± 0.2	1.30 ± 0.02	8.1 ± 0.2	8.2 ± 0.2

The inorganic and organic solutions are augmented to 500 mL with distiled water. After mixing of the inorganic and organic solutions, some further constituents are added and disolved. If necessary, the pH of the juices is adjusted to the appropiate interval. **Source:** Versantvoort, C. H., Oomen, A. G., Van de Kamp, E., Rompelberg, C. J., & Sips, A. J. (2005). Applicability of an in vitro digestion model in assessing the bioaccessibility of mycotoxins from food. *Food and Chemical Toxicology*, *43*(1), 31-40.

Apendix IV. List of Publications object of this thesis

Pérez-Esteve, É., Oliver, L., García, L., Nieuwland, M., de Jongh, H. H., Martínez-Máñez, R., & Barat, J. M. (2014). Incorporation of mesoporous silica particles in gelatine gels: Effect of particle type and surface modification on physical properties. *Langmuir*, *30*(23), 6970-6979.

Pérez-Esteve, É., Fuentes, A., Coll, C., Acosta, C., Bernardos, A., Amorós, P., Marcos, M.D., Sancenón, F., Martínez-Máñez, R., & Barat, J.M. (2014) Modulation of folic acid bioaccesibility by encapsulation in pH-responsive gated mesoporous silica particles. *Microporous & Mesoporous Materials, 15*, 124-132.

Pérez-Esteve, É., Ruiz-Rico, M., Martínez-Máñez, R., & Barat, J. M. (2015) Mesoporous silica based supports for controlled and targeted release of bioactive molecules in the gastrointestinal tract. *Journal of Food Science.* DOI: 10.1111/1750-3841.13095.

Pérez-Esteve, É., Ruiz-Rico, M., de la Torre, C., Villaescusa, L. A., Sancenón, F., Marcos, M. D., Amorós, P., Martínez-Máñez, R., Barat, & J. M. (2016) Encapsulation of folic acid in different silica porous supports: a comparative study. *Food Chemistry, 196,* 66-75*.*

Pérez-Esteve, É., Ruiz-Rico, M., Fuentes, A., Marcos, M. D., Sancenón, F., Martínez-Máñez, R., & Barat, J. M. Enrichment of stirred yoghurts with folic acid encapsulated in pH-responsive mesoporous silica particles: Bioaccessibility modulation and physico-chemical characterization. *Submitted to LWT- Food Science and Technology.*

Pérez-Esteve, É., Ruiz-Rico, M., de la Torre, C., Llorca, E., Sancenón, F., Amorós, P., Martínez-Máñez, R., Marcos, M. D., & Barat, J. M. Stability of different mesoporous silica particles during an in vitro digestion. *Submitted Langmuir.*

Apendix V. Other scientific publications

Ruiz-Rico, M., Daubenschüz, H., **Pérez-Esteve, É**., Marcos, M. D., Amorós, P., Martínez-Máñez, R., & Barat, J. M. Enhancing stability of folates and folic acid through encapsulation in mesoporous silica particles. *Submitted to Food Science*.

Pérez-Esteve, É., Lerma-García, M., Palomares, C., Fuentes, A., & Barat, J. M. Control of undeclared flavouring of cocoa powders by the determination of vanillin and ethylvanillin by HPLC. *Submitted to Food Research International.*

Bernardos, A., Álvarez, S., **Pérez-Esteve, É.**, Kloucek, P., Martínez-Máñez, R., Lhotka, M., Frankova, A., Pulkrabek, J., & Kourimska, L. The efficacy of essential oil components loaded into hydrophilic bentonite nanoclays against *Aspergillus niger* and *Staphylococcus aureus*. *Submitted to Journal of Pest science.*

Ruiz-Rico, M., Fuentes, C., **Pérez-Esteve, É.**, Jiménez-Belenguer, A. I., Quiles, A., Marcos, M. D., Martínez-Máñez, R., & Barat, J. M. (2015). Bactericidal activity of caprylic acid entrapped in mesoporous silica nanoparticles. *Food Control, 56,* 77-85.

Bernardos, A., Marina, T., Žáček, P., **Pérez-Esteve, É.**, Martínez-Mañez, R., Lhotka, M., Kouřimská, L., Pulkrábek, J., & Klouček, P. (2014) Antifungal effect of essential oil components against Aspergillus niger when loaded into silica mesoporous supports. *Journal of the Science of Food and Agriculture*, 95(14), 2824-2831.

Acosta, C., **Pérez-Esteve, É.**, Benedetti, S., Fuenmayor, C. A., Cosio, M. S., Soto, J., Sancenón, F., Marcos, M. D., Mannino, S., Barat, J. M., & Martínez-Mañez, R. (2014) Polymer composites containing gated mesoporous materials for on-command controlled reléase. *ACS Applied Materials and Interfaces, 6*(9), 6453-60.

Pérez-Esteve, É., Fuentes, A., Grau, R., Fernández-Segovia, I., Masot, R., Alcañiz, M., & Barat, J. M. (2014). Use of impedance spectroscopy for predicting freshness of sea bream (Sparus aurata). *Food Control*, *35*(1), 360-365.

Perez-Esteve, É., Barat, J. M., & Martínez-Máñez, R. (2013) Controlled release of 5-methyltetrahydrofolate encapsulated in mesoporous silica supports capped with "saccharides" under gastrointestinal stimulus. *Annals of Nutrition & Metabolism, 63*(1), 1708-1709.

Barat, J. M., **Pérez-Esteve, É**., Aristoy, M. C., & Toldrá, F. (2013). Partial replacement of sodium in meat and fish products by using magnesium salts. A review. *Plant and soil*, *368*(1-2), 179-188.

Pérez-Esteve, É., Bernardos, A., Martínez-Máñez, R., & M Barat, J. (2013). Nanotechnology in the development of novel functional foods or their package. An overview based in patent analysis. *Recent patents on food, nutrition & agriculture*, *5*(1), 35-43.

Salinas, Y., Agostini, A., **Pérez-Esteve, É.**, Martínez-Máñez, R., Sancenón, F., Marcos, M. D., Soto, J., Costero, A. M., Gil, S., Parra, M., & Amorós, P. (2013) Fluorogenic detection of Tetryl and TNT explosives using nanoscopic-capped mesoporous hybrid materials. *Journal of Materials Chemistry A, 1*, 3561-3564.

Barat, J., **Pérez-Esteve, É**., Bernardos, A., & Martínez-Mañez, R. (2011). Nutritional effects of folic acid controlled release from mesoporous materials. *Procedia Food Science*, *1*, 1828-1832.

Perez-Esteve, É., Bernardos, A., Martínez-Máñez, R., & M Barat, J. (2011). Recent Patents in Food Nanotechnology. *Recent patents on food, nutrition & agriculture*, *3*(3), 172-178.

Apendix VI. Book chapters

Pérez-Esteve, É., Ruiz-Rico, M., Martínez-Máñez, R., & Barat, J. M. Mesoporous silica particles as encapsulation and delivery systems for food ingredients and nutraceuticals. In: Pathak, Y. (Ed.) Nanotechnology in Nutraceuticals: production to consumption. CRC press. *In press.*

Ruiz-Rico, M., **Pérez-Esteve, É.**, & Barat, J. M. Use of nanotechnology as an antimicrobial tool in the food sector. In: Dhawan, A., Shanker, R., Singh, S., Kumar, A. (Ed.) Nanobiotechnology: Human Health and the Environment. CRC Press, *In press*.

Ruiz-Rico, M., **Pérez-Esteve, É**., Jiménez-Belenguer, A., Ferrús, M. A., Martínez-Mañez, R., & Barat, J. M. (2015) Bactericidal effect of encapsulated caprylic acid on Listeria monocytogenes. In: Méndez-Vilas, A. (Ed.). *Multidisciplinary Approaches for Studying and Combating Microbial Pathogens*. Brown Walker Press (pp. 63-67).